THIN GLASS SANDWICH PANEL DESIGNED FOR VISUAL COMFORT

Designing the core of the panel to dynamically enhance the visual comfort of the façade

Grianne van der Ham
14 April 2024

T̃U Delft

THIN GLASS SANDWICH PANEL DESIGNED FOR VISUAL COMFORT

Designing the core of the panel to dynamically enhance the visual comfort of the façade

Grianne van der Ham

MSc. Building Engineering

4678230

14 April 2024

Prof.dr.ir. P.C. (Christian) Louter

Civil Engineering and Geosciences, Applied Mechanics

Dr. ing. A. (Alessandra) Luna Navarro

Architecture and the Built Environment, Architectural Technology

Dr. J. (Jun) Wu

Industrial Design Engineering, Materials and Manufacturing

Dr.ir. H.R. (Roel) Schipper

Civil Engineering and Geosciences, Applied Mechanics

TUDelft

Delft University of Technology

Faculty of Civil Engineering and Geosciences

ACKNOWLEDGEMENTS

ABSTRACT

The main focus of this thesis is on a thin glass sandwich panel combined with a three-dimensional printed core pattern. The core pattern provides stiffness to the panel, but it also influences the daylight transmission. The goal of this research is to design a façade system which can dynamically improve the daylight performance, effectively control the illuminance inside the building together with preventing disturbing glare.

The research first evaluates the theory behind thin glass, the structural sandwich structure and how the design of a façade panel correlates with its visual comfort. The properties of existing dynamic systems are evaluated, together with exploring other possible dynamic systems that can be integrated in the panel.

The resulting system, a hexagonal core pattern with integrated inflatables, is evaluated on its structural performance and daylight performance using analyses executed in the grasshopper model. This is further expanded by studying the structural performance of more complex core geometry using Diana Finite Element analyses. From the results of these evaluations, a design strategy is created which is able to find the optimal properties of the inflatable façade system.

This design strategy is then applied to a case study, to show both the design of a single façade panel, as well as the full façade system of the whole building. The final result is the design strategy for the dynamic inflatable façade system.

Keywords: Thin glass, Sandwich structure, Dynamic façade, Daylight, Glare

TABLE OF CONTENTS

1 RESEARCH PLAN

1.1 Introduction

Thin glass, with a thickness ranging from 0.5 to 2 *mm*, is mainly used in the electronics industry to manufacture displays for devices like smartphones and tablets. This type of glass is preferred because of its high strength, scratch resistance, impact resistance, optical quality, and low weight. These desirable features have the potential to be used in the construction industry for innovative glazing solutions. However, thin glass is typically too flexible to replace conventional window glazing without experiencing excessive deformations and vibrations.

Using thin glass for façade panels offers ecological benefits by reducing the amount of material used. Since glass requires a significant amount of energy to manufacture, limiting its use leads to lighter and more energy-efficient panels. The addition of a 3D-printed polymer core to the thin glass makes the panel rigid, resulting in a thin glass composite façade panel based on the sandwich theory.

The composition of the polymer core determines not only the stiffness of the panel but also its performance in building physics. The main properties that determine this performance include structural performance, thermal insulation, sound insulation, moisture resistance, optical performance, and fire safety.

Previous research has focused on the structural performance and for example on the thermal performance of the thin glass sandwich panel, but little research has been done on the optical performance. Since the 3D-printed part of the panel blocks the view, it influences the transparency of the façade. Furthermore, it influences the daylight that can enter through the façade panel.

The core in the thin glass sandwich panel mostly functions as a way to increase the stiffness of the panel. However, this does not require much material, together with many possible core patterns that can be used. This allows for many possibilities in designing the core, like optimising it for daylight performance.

The daylight performance of a thin glass panel is not expected to perform differently from a normal-thickness glass façade panel. However, the 3D-printed core does offer further possibilities to influence this performance. For example, a dynamic system can be integrated in the panel that can respond to the angle and intensity of the sun at a given moment. This way the transparency, amount of direct light, glare and solar heat gain of the façade panel can be controlled and adjusted for the desired outcome.

1.2 State of the art

1.2.1 Previous research

This thesis builds on previous research done on thin glass panels with 3D-printed cores for architectural and structural applications. Below, some recent MSc theses at the TU Delft on this topic are shown.
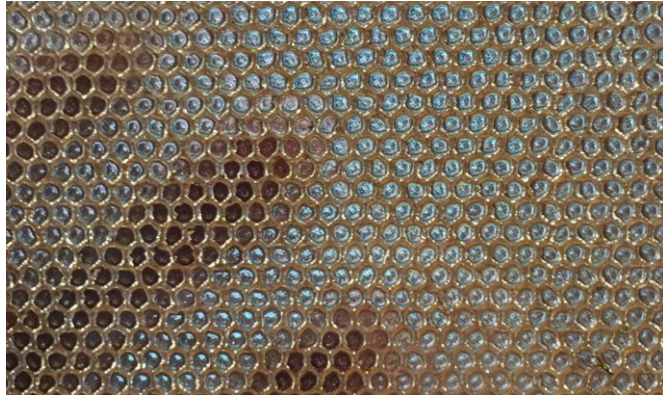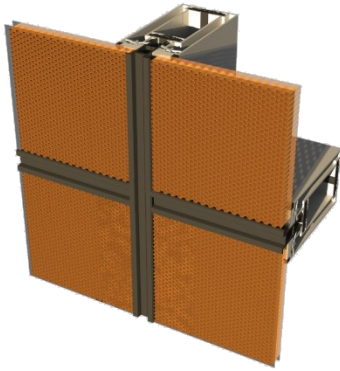
Figure 1 Lightweight insulating thin glass façade panel with honeycombed aramid core (van der Weijde, 2017)

The MSc thesis of van der Weijde (2017) uses a thin glass sandwich panel, where the core is an aramid honeycomb, see Figure 1. This setup creates a façade panel with a substantially reduced weight while providing integrated sun shading, sufficient insulation (U-value of 1.4 W/m^2K) and light transmission. The testing results of this thesis looked at different configurations of the design, starting with just a glass panel, to a fully sandwiched panel. The results show that the bottom panel will break first in bending tests due to the tensile forces acting here. The bending stiffness and flexural strength of a panel can be increased by adding an additional sheet of glass, or by providing an interlayer. The sandwich panels show a much larger bending stiffness than the tests with single- and stacked glass sheets.

The research also showed that chemically strengthened glass can withstand a much larger stress than annealed glass. During the tests, the chemically strengthened glass had not yet broken under a significantly larger load. The sandwich structure also holds the glass in place, resulting in a safer failure scenario.

Figure 2 Thin glass composites, based on a structural efficiency increasing design strategy (Neeskens, 2018)

The MSc thesis of Neeskens (2018) focused on the combined use of thin glass and a 3D-printed spacer pattern, which is designed using gradient mapping based on a structural analysis. This creates a Voronoi pattern that represents the structural shape, see Figure 2 for the three final prototypes that were used for testing.

2

The testing results show that for deformation, the top of the panel shows the normal pattern of deflection in plates, with local deflections in the cells. The back of the panel has an evenly spread deformation pattern, which shows that the core element is giving resistance to the deflection of the plate. The testing results compared randomly designed panels with panels designed specifically for the calculated structural analysis. It showed an improved resistance against bending of -2.7 %. It also shows that the stresses in the material rise when the cells become bigger. Lastly, the connecting method used also contributes to the stiffness of the panel, where the panel using a UV curing adhesive was 6.6 times stronger, ignoring the effect of core type.

Figure 3 Ultra-thin composite panel: A research on the durability and stiffness of a composite panel of (thin) glass and recycled PET (Saleh, 2019)

Next is the MSc thesis of Saleh (2019) who added a 3D-printed core made from recycled PET. This helps further reduce the environmental footprint of the panel, due to the materials used and a reduction of 71.9 % of weight compared to a normal double glazed window panel. This research also showed that using 3D-printed recycled PET reduces the mechanical properties. Compared to the PET filament, the Young's modulus of 3D-printed PET decreases with a factor 2.70 and the maximum strength (tensile strength) with a factor 1.56.

In the testing phase, the durability of the panel was evaluated on UV radiation, elevated temperatures and fire. Exposing the panel to UV radiation made the recycled PET change into a yellowish colour and the Young's modulus degrade with 50%, making it more brittle. At an elevated temperature of 80 ºC, recycled PET loses its stiffness and strength and cannot carry forces when exposed. Recycled PET has a melting temperature starting from 200 ºC and during a fire, temperatures could reach up to 1000 ºC. This allows the core element to melt fully during a fire.

Interesting about the final design (the two images on the right in Figure 3), is that the centre of the panel has relatively low shear stresses. Therefore, the density of the core in the centre can be reduced or even removed completely, while the panel still performs well structurally. This is particularly interesting when the middle is for example placed at eye-level, thereby allowing people to look through the window without the view being obstructed.
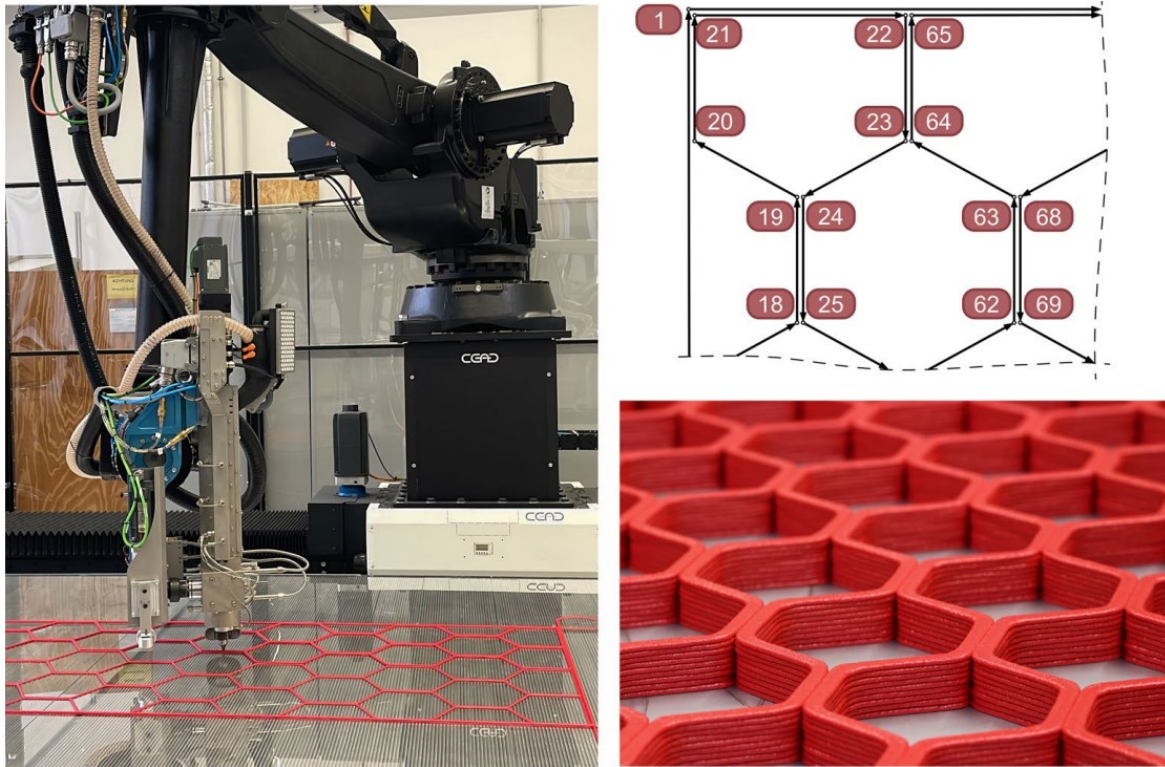
Figure 4 Thin glass sandwich panel with a honeycomb pattern with a single line toolpath (Pfarr & Louter, 2023)

Aside from these theses, a recent paper developed a thin glass panel with a hexagonal 3D-printed pattern, as shown in Figure 4. This pattern was used in the paper by Pfarr and Louter (2023) to explore how digital techniques can be used in the design and manufacturing of a composite façade panel consisting of an additively manufactured polymer core and adhesively bonded thin glass outer sheets. The composite panel designed here has a very efficient design, resulting in a potential reduction of up to 80% of the glass used in a façade panel (Pfarr & Louter, 2023).
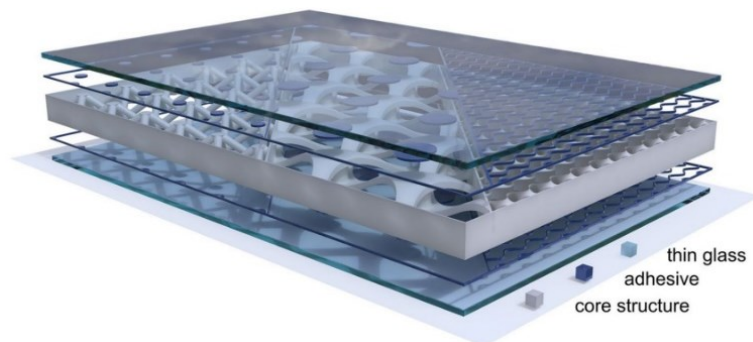
Figure 5 Rendering of the composite panel with thin glass as a cover layer, an adhesive bonding and an additively manufactured core structure (Pfarr & Louter, 2023)

The composite panel is built up with thin glass as a cover layer, an adhesive bonding and a core structure, see Figure 5. Each layer can be designed in such a way to maximise the benefits of its properties. To design the full panel, first the desired properties should be determined. The panel should be structurally sound, but also perform well in building physics properties, like shading, light control, insulation, glare protection and sound insulation. Finding the balance between these aspects is part of the challenge of designing a panel.

Mechanical properties can be estimated using finite element analysis (FEA) or even analytical calculations. Also, Solar radiation studies, sightline analyses, and sunlight hours modelling can estimate the visual comfort level of the composite panel.

The thin glass panes serve as the cover layer of the sandwich panel, functioning as protection from environmental influences, like providing good scratch resistance. The adhesive layer contributes to the strength properties of the panel. The adhesive joint is under shear stress, which makes stiffer adhesives advantageous for designing such a panel (Pfarr & Louter, 2023). In connection with the transparent material glass, transparent adhesives are also favourable to ensure a high visual quality.

The core structure is considered to be the form-giving layer of the composite panel, it can influence almost all properties. For this purpose, the form-finding process can be divided into the following four design categories: structural design, functional design, aesthetic design and manufacturing design. Each of these categories may have different objectives, which may result in different topologies (Pfarr & Louter, 2023).

1.2.2 Visual comfort

In this thesis, the focus needs to not only be on the structural design but also on the other aspects. The design of the core is responsible for most aspects since it provides both its structural strength and influences the building's physical properties. For the designs in this thesis, the focus will be on the visual comfort provided by the façade panels, like illuminance levels in the room and glare control. Research on existing systems with standard thickness glass is used to further explore how visual comfort can be achieved and to see whether this can be applied to thin glass panels as well.

For determining the visual comfort level in a room, many different methods that analyse various aspects are available. The variable aspects of lighting quality include quantity, distribution, glare, spectral power distribution, daylight, directionality, and dynamics (Kruisselbrink et al., 2018). The core of a façade panel can influence some of these aspects drastically and thereby influence the occupants' perceptions of daylight distribution in the room. Assessing the performance of the façade and its effect on the environment it encloses include luminance and vertical eye illuminance as key variables (Kruisselbrink et al., 2018).

The placement of the core influences all these aspects of visual comfort, but when the design is fully static, it cannot respond to the changing brightness and angle of the incoming sunlight. By designing the core to have different angles which reflect light differently based on the direction of the incoming light, the visual comfort can be improved. One example of this is seen in the OKAfree panel of BASF 3D Printing Solutions GmbH (2021), see Figure 6. This product is a 3D-printed insert for insulating glass units, which are optimised for daylight performance. Here each panel can be uniquely designed for the preferred open-closed ratio at that location.
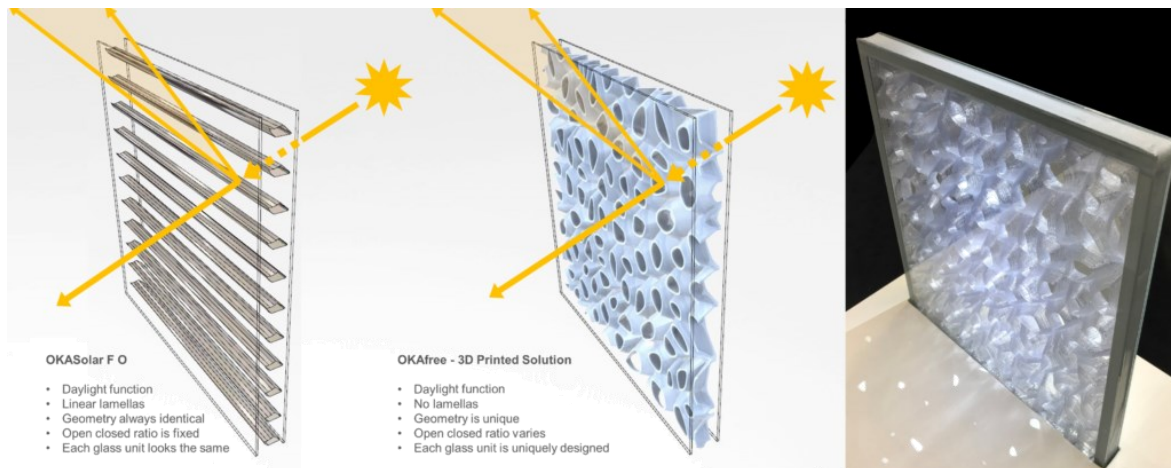
Figure 6 OKAfree 3D-printed panel for effective daylight usage in a panel (BASF 3D Printing Solutions GmbH, 2021)

The design of each panel here influences the open-close ratio of the panel itself, but you can also change the overall perception of the panels together. This is shown in Figure 7, where the density of the pattern is changed, to be able to create more privacy in a room, but also keeping it open to allow people to look through the pattern.
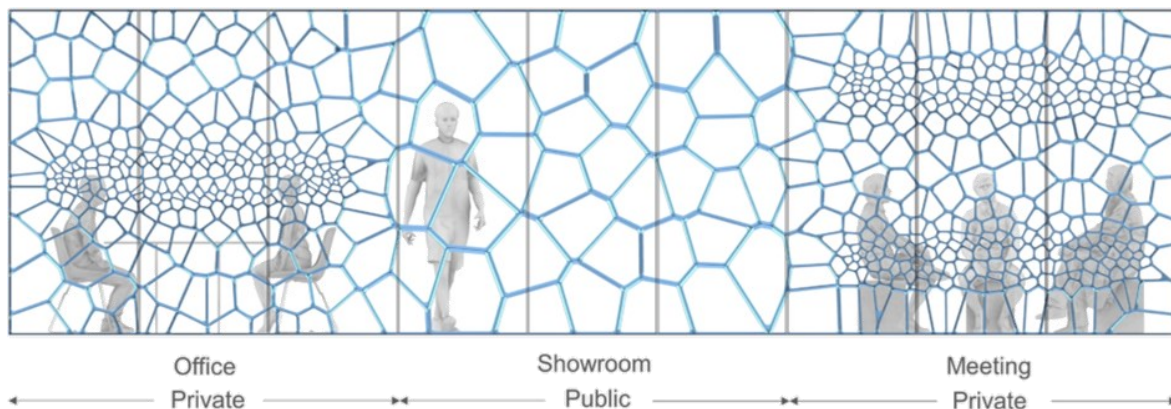
Figure 7 Providing different privacy levels along a single-floor façade (BASF 3D Printing Solutions GmbH, 2021)

These designs still have one big downside, which is that it is a static panel, it cannot respond to the environment and change its open close ratio or respond to sunlight. Introducing a dynamic aspect to the panel, which can respond to the light circumstances, would be ideal. When a panel can change the open-close ratio depending on the environment, it can increase the daylight performance of this panel. A panel like this could also be made controllable, so the amount of light coming in can be changed when needed.

Common solutions currently available are usually placed on the inside or outside of the panel. For example, curtains, lamellas or sunshades can be added to a façade. This could also be applied to the thin glass panel with the designed core. However, the design of the core could be used in itself to control the daylight quality of the panel, instead of having to install an additional element. When the panel itself has a good daylight performance, it makes additional measures abundant.

1.2.3 Concept 1: inflatable soft robotics

As seen with the OKAfree panel from BASF 3D Printing Solutions GmbH (2021) a 3D-printed core could be created to get the wanted open-close ratio, while still providing the

panel with its structural needs. However, this solution is static it cannot actively respond. To be able to control the amount of sunlight able to enter through a façade panel, the percentage of area covered should be made dynamic. To find a suitable solution, it should still fit within the two glass panels, while being able to change shape. Here a few ideas are presented that can potentially be integrated in the panel.

Firstly, a solution could be to add inflatables to the core, which can be enlarged on demand. Here inspiration is taken from soft material robotics, which use materials which can expand and shrink depending on the desired result. One example is based on the highly deformable soft robot as seen in Figure 8. This design is a bioinspired actuator capable of achieving a large volumetric change. Inspired by the changes in body shape seen in the euglena during its characteristic locomotion, a novel soft pneumatic actuator has been designed that exploits the hyper elastic properties of elastomers (Digumarti et al., 2017).
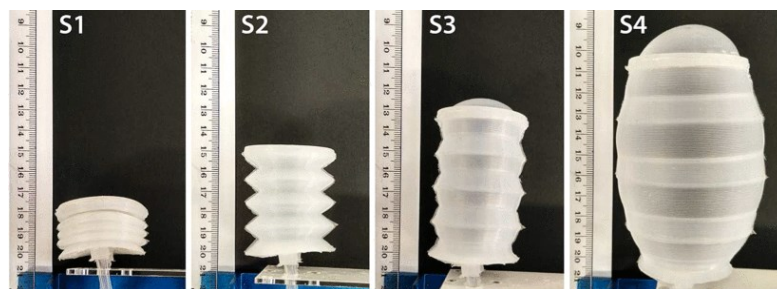
Figure 8 The four states of the actuator, where S2 is the neutral state (Digumarti et al., 2017)

For the façade panel, such a highly deformable soft robot could be used to change the open-close ratio of the panel. As seen in Figure 8, the way the shape of the actuator changes can be controlled by how the actuator is designed. As a first concept, this principle is applied in Figure 9. Here the main hexagonal pattern is inspired by Pfarr and Louter (2023), which is then combined with round 'balloons'. These balloons can be shaped to fit inside the hexagons when inflated, and then almost disappear when vacuumed. The result is a panel which can partly open and close on demand, therefore being able to respond to direct sunlight.
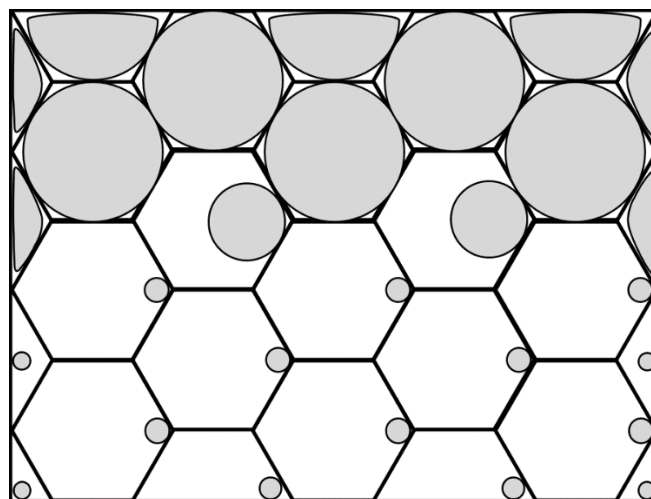
Figure 9 Concept fluid activated actuator in a sandwich panel with hexagonal pattern

To be able to inflate and deflate the system, a tube system needs to be installed, connecting all the balloons. Here a logical connection pattern should be decided on, to be able to open only part of the panel, as shown in the figure. A possible third option could

be explored, where the balloons are not fully inflated, making them only cover part of the cell. This could further customise the open-close ratio.

This system would need to respond to the amount of daylight and therefore requires a mechanism that can analyse this. A solution would be to add sensors to the panel, which can then send a signal to inflate/activate certain cells in the panel.

1.2.4 Concept 2: shape memory material

Another solution could be found by taking inspiration from flowers. They unfold during the day, increasing the area they cover. During nighttime they collapse inward, making themselves much smaller. Something similar has been developed in soft robotics, where a shape memory material is used. Based on the actuator, the material can change its shape. In Figure 10 a device is used with an electrical actuation, where the actuator can bend based on the electrical input. The bending angle almost linearly decreases with increasing electrical power, and the maximum change in bending angle of 147° (from 180° to 33°) can be achieved with a power of 0.106 $W\ cm^{-2}$ (operating at 5.1 V) (Cai et al., 2019).
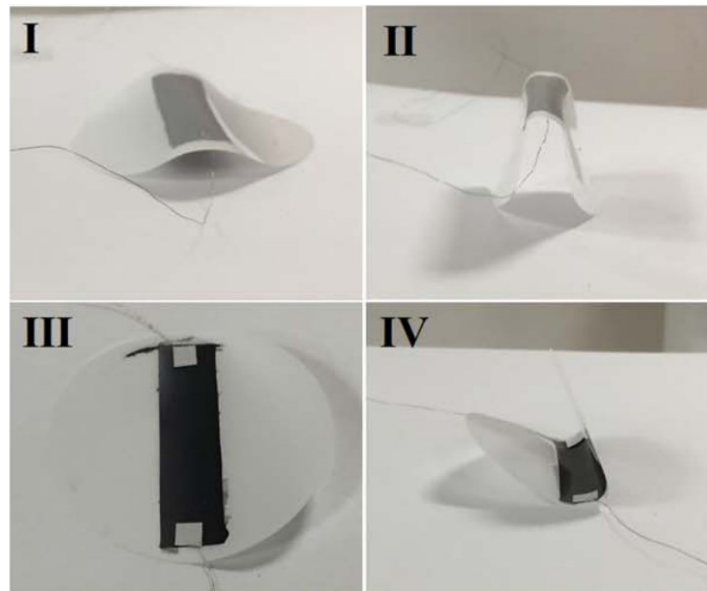
Figure 10 Electricity-responsive capability of the MXCC/PC bilayer-structured actuator (power off for I and III, and power on for II and IV) (Cai et al., 2019)

There are many different examples of actuators, where the location of the bending part and the type of actuator can be changed. The paper of Kim et al. (2020) evaluates many different types of actuators and how these perform. Interesting examples include actuators with cellulose inclusion. Figure 11 shows a schematic illustration of the representative IPMC bending mechanism used in the electrical actuators. Initially, the ions are randomly distributed in a solid electrolyte matrix. After applying a voltage, the ion migration triggers a macroscopic bending response in the material (Kim et al., 2020).
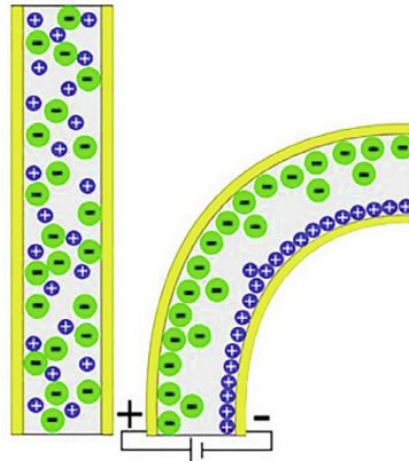
Figure 11 Schematic illustration of a representative IPMC bending mechanism (Kim et al., 2020)

The example above uses an electrical actuation, but light, temperature or other actuators could be used as well. There are many different shapes possible, which can be designed based on the required results. Figure 12 shows a few examples of different shapes that can be created, collected by Kim et al. (2020).
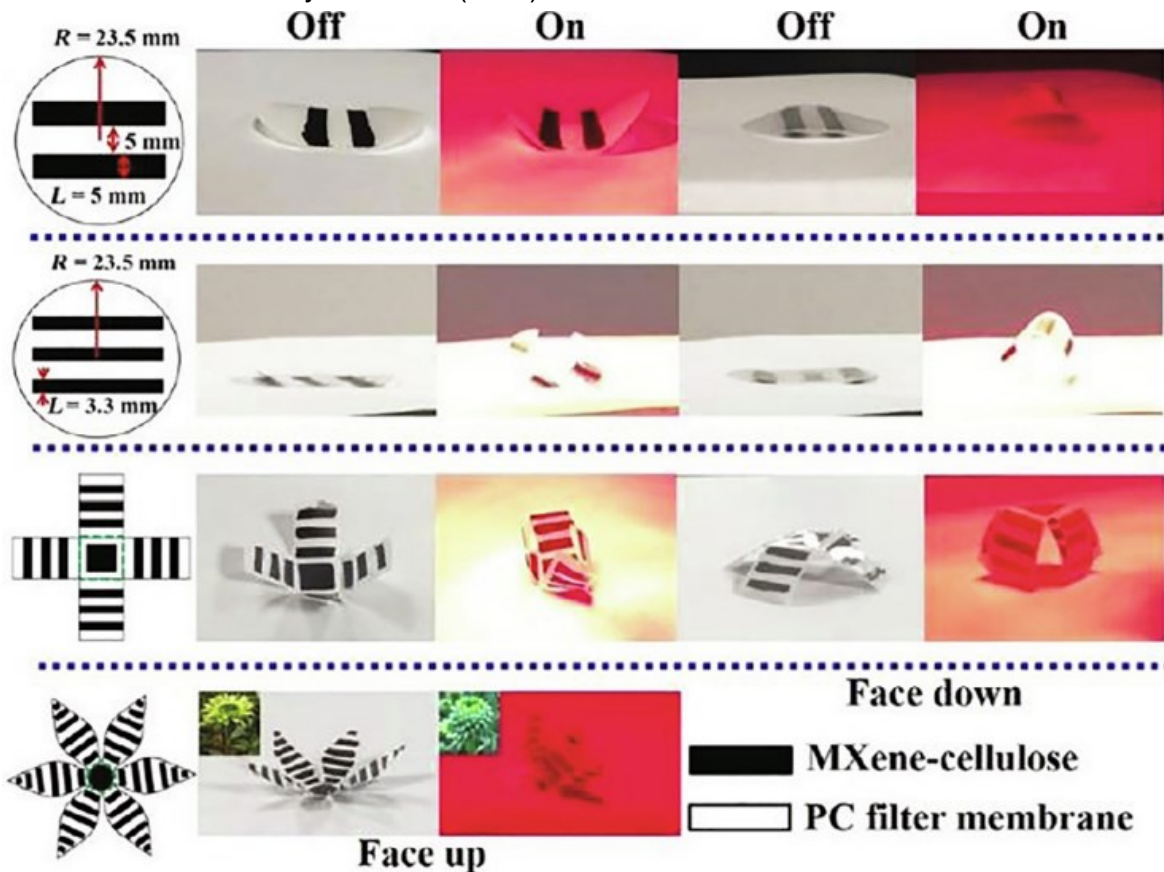
Figure 12 Examples of photothermal actuation of an MXCC–PC bilayer film. The shape change can be controlled by programming hinges, as illustrated (Kim et al., 2020)

Based on this mechanism, a first concept is made using the hexagonal pattern again, but now with a shape memory material added, see Figure 13. Here each side of the hexagon has a triangular-shaped actuator attached, which can then be controlled to either close or open. This way the open-close ratio of the panel can be controlled. Finding the right way to bend, curl or fold the material so that it fits within the panel, will need to be thoroughly

researched. When looking at the research about the different types of actuators, many different options are available. Which option fits best for this application will need to be evaluated.
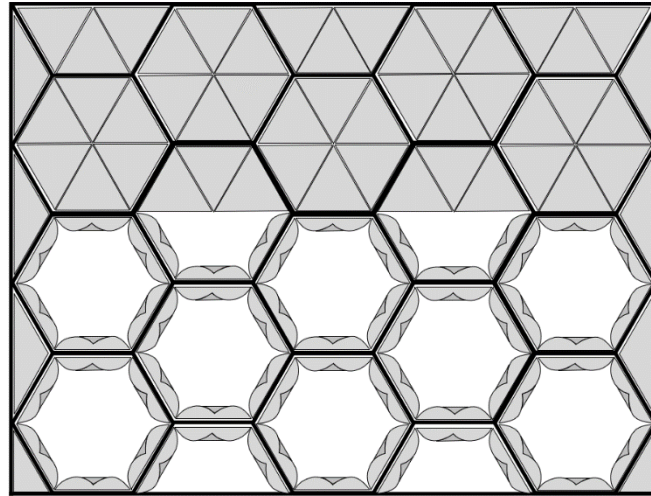
Figure 13 Concept shape memory actuator in a sandwich panel with a hexagonal pattern

1.3 Problem statement

The main properties that determine the overall performance of a façade panel are its structural performance, thermal insulation, sound insulation, moisture resistance, optical performance, and fire safety. Finding the optimal combination of all these properties can be challenging since they can work contradictory. For the thin glass panels, previous research has mostly focused on the structural performance and for example on the thermal performance of the thin glass sandwich panel. However, little research has been done on the optical influence of the non-transparent parts of the core. This partly blocks the view outside, has the potential to control glare and daylight transmittance of the panel. Adding dynamic aspects to this core in combination with the thin glass is yet to be researched.

1.4 Objectives

The main objective of this thesis is to design a façade element which is optimised not only for its structural performance but also its daylight performance. The concepts for the panel will be evaluated on structural performance and visual comfort. The design should respond dynamically to generate a panel with the desired transparency, amount of direct light, control glare and solar heat gain. Different concepts will be evaluated using digital models, then one concept will be further developed in a fully functional system. For this system, a design strategy will be generated, which is then applied to a case study to show its effectiveness.

1.5 Research questions

The purpose of this research is to broaden the knowledge of thin glass and its structural behaviour and to propose a dynamic solution in the core of the 3D-printed sandwich panel. Therefore, the main research question can be formulated as follows:

How can an optimal design be achieved for a thin glass façade sandwich panel that both meets the structural requirements and daylight requirements, finding the right balance between glare control and daylight performance?

To be able to answer this main question, it can be divided into sub-questions. The first few questions try to define the properties of the sandwich panel, together with the evaluation process of daylight performance of a panel and the possible dynamic solutions that can be integrated within the panel. These are to be answered in chapter 2 Literature review:

What are the physical properties of thin glass?

What are the characteristics of the different structural sandwiches currently available?

What methods of 3D-printing are available and how do these work?

Which adhesives are appropriate to use in the thin glass façade panel?

How is the daylight performance of a panel determined and evaluated?

What options are available to dynamically control the daylight performance of a panel?

What other dynamic solutions are available that can act within the core of a panel?

After the literature review has given insight into the properties of a panel and existing solutions, a new dynamic solution to be integrated in the thin glass sandwich panel can be designed. This design process is represented with the two questions below, to be answered in chapter 3 Design façade panel:

What are the structural and visual comfort requirements of a typical façade panel?

What is an effective design for a façade panel which is able to dynamically control the visual comfort?

Lastly, the designed system needs a design strategy to be able to apply it in façade design. Here the strategy to find the optimal solution for both structural requirements and visual comfort is defined. This is represented in the following sub-question, to be answered in chapter 4 Design strategy:

What is the design strategy for a panel optimised for both structural and daylight performance?

1.6 Methodology

This research can be classified as a design thesis, where the main deliverable is developing a functional design concept with a design strategy. The design and design strategy is then applied in a case study to prove its effectiveness. The methodology is structured into four main phases: literature review, design façade system, development design strategy and case study. This approach aims to systematically go through the initial concept to the realisation of a full design strategy, supported by a case study.

Phase 1: Literature Review

In the first part of the thesis, a literature review will be performed to determine the properties of thin glass. The available techniques and materials to realise the core of the panel will be researched, together with the structural behaviour of sandwich panels. Then, the available optimisation processes will be addressed.

Then, the available methods to evaluate the daylight performance of the panel will be discussed. Following this, the possible dynamic systems that could be applied in the core of the panel are explained and evaluated. The structural requirements and requirements

for building physics can then be laid out based on the Dutch national regulations. Lastly, the conclusion shows which parts of the research are relevant to the final design of the concept.

Phase 2: Design façade system

Starting from the conclusions of the literature review, the possible design choices will be explored and evaluated. A parametric model will be developed with a Rhino model defined in Grasshopper. Here different dimensions of the glass panes, the core and the dynamic system will be explored. These geometries can then be evaluated on its structural performance using Karamba3D in Grasshopper and in Diana, a finite element modelling program. The daylight performance will be evaluated using the analyses of the Honeybee plugin.

Phase 3: Development design strategy

The resulting properties of the façade system are then matched with the structural and daylight requirements of such a panel. Emphasis will be put onto how an optimal design can be accomplished for both structural and daylight performance. This process will show the design strategy of a single façade panel and the full façade system.

Phase 4: Case study

Then, the developed façade system is applied to an existing building to show its effectiveness. The design strategy will be followed through for this case study, showing each of the steps and how this applies to a larger scale. The resulting design is then evaluated by comparing it to the existing façade system. Lastly, a conclusion of this research is written and recommendations for future possible research are made.

1.7 Goals

The main goal of this thesis is to develop a design for a thin glass façade panel with dynamic daylight control with a suitable design strategy. This design strategy will be supported with a worked-out case study to show the effectiveness of the system. The goal is to develop a functional system that can effectively control glare while still performing well in meeting daylight requirements.

1.8 Relevance

The use of thin glass in façade elements is an innovative idea with economic and environmental benefits. It is lightweight, flexible, durable, has high strength properties and results in a reduction of raw material usage in comparison with regular glass. It can also potentially reduce the total deadweight of a façade structure, which can further decrease material usage in the supporting structure. The lack of stiffness and instability of the ultra-thin glass can be compensated by including a stiffer core, which can make this panel meet the safety requirements.

Adding a dynamic core results in a panel that can respond to incoming daylight, instead of having to install an extra external element to the façade. Making this dynamic response inside the panel results in a compact system.

2 LITERATURE REVIEW

In this chapter, existing literature is reviewed to get a better understanding of the topics discussed in this thesis. It first evaluates the thin glass sandwich panel and explains how this works. Then, the visual comfort is defined and existing façade solutions are evaluated. Lastly, possible dynamic solutions to be integrated in the sandwich panel are discussed. The sub-research questions answered in this section are listed below:

What are the physical properties of thin glass?

What are the characteristics of the different structural sandwiches currently available?

What methods of 3D-printing are available and how do these work?

Which adhesives are appropriate to use in the thin glass façade panel?

How is the daylight performance of a panel determined and evaluated?

What options are available to dynamically control the daylight performance of a panel?

What other dynamic solutions are available that can act within the core of a panel?

2.1 (Thin) glass

2.1.1 Chemical composition

Glass, as defined by Schittich et al. (2007), is a uniform material which exhibits amorphous isotropy, meaning the properties of glass are independent of direction. The molecules are randomly ordered and do not form a crystal lattice, which is why glass is transparent. Glass is a solidified liquid at room temperature, when heat is applied it gradually changes from solid to a plastic-viscous state, to a liquid state, it does not have a singular melting point.

Glass consists of an irregular three-dimensional network of the elements silicon (Si) and oxygen (O), which are connected with cations in the interstices. The type of glass that is most used in the building industry is soda-lime-silica glass. Figure 14 shows a schematic representation of the chemical structure of this glass. There are different kinds of glasses that include silicon dioxide (SiO_2), most commonly soda-lime glass, lead glass, borosilicate glass and aluminosilicate glass. In these glasses the silicon dioxide forms the network and helps shape the chemical structure of glass.
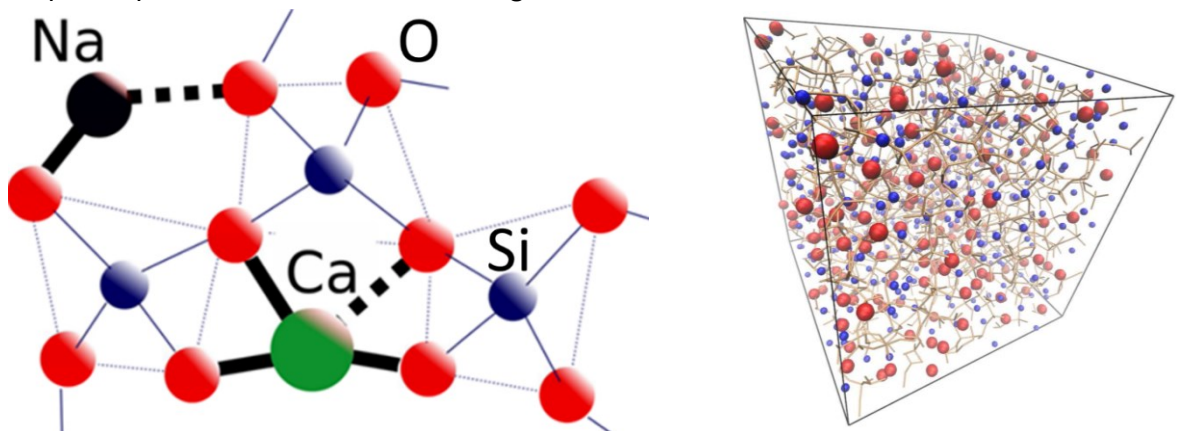

Figure 14 Chemical structure and topology of soda-lime-silica glass (Laurent et al., 2014)

The chemical composition can be used to classify the different types of glass, as shown in Table 1 for soda-lime-silica glass, borosilicate glass and aluminosilicate glass. The soda-

lime-silica glass can be recognised by the presence of the silicon, calcium and sodium in the composition. Whereas borosilicate glass can be similar but tends to have a higher percentage of boron- (calcium) oxide. Aluminosilicate glass has a significant percentage of aluminium trioxide in its composition.

Table 1 General composition of glass (Schittich et al., 2007)

		Soda Lime Silica Glass	Borosilicate Glass	Aluminosilicate Glass
Silicon dioxide	SiO_2	69 – 74 %	70 – 87 %	50 – 80 %
Calcium (Boron) oxide	CaO	5 – 12 %	7 – 15 %	0 – 8 %
Sodium oxide	Na_2O	12 – 16 %	1 – 8 %	0 – 2 %
Magnesium oxide	MgO	0 – 6 %	1 – 8 %	0 – 8 %
Aluminium trioxide	Al_2O_3	0 – 3 %	1 – 8 %	16 – 27 %

Soda-lime-silica glass is often used in the building industry due to its relative low costs of production. Borosilicate glass is applied when particular characteristics are required. The higher percentage of born oxide results in a lower coefficient of thermal expansion, resulting in a considerable higher thermal fatigue resistance. Furthermore, this type of glass also has a higher resistance to alkaline solutions and acids (Schittich et al., 2007). Aluminosilicate glass has comparable properties to borosilicate glass, only it has a higher chemical resistance. However, it is comparatively difficult to fabricate.

2.1.2 Physical properties

Table 2 gives an overview of the main physical and mechanical properties of the three main types of glass. Notable differences are the lower thermal expansion coefficient for borosilicate glass and the higher Young's modulus for aluminosilicate glass.

Table 2 Physical and mechanical properties of different glasses, valid in temperature range 20 – 300 °C (Belis et al., 2019)

Property		Soda Lime Silica Glass	Borosilicate Glass	Aluminosilicate Glass
Density ρ	kg/m^3	2500	2200 – 2300	2480
Young's modulus E	N/mm^2	*Annealed:* 73000 *Tempered:* 70000	63000	74000
Poisson's ratio v	-	0.23	0.20	0.22
Specific heat capacity C_P	$J/(kg\ K)$	800	830	840
Thermal expansion coefficient α_T*	K^{-1}	9×10^{-6}	3.3×10^{-6}	8.8×10^{-6}
Thermal conductivity κ	$W/(m\ K)$	1.05	1.2	0.96
Refractive index n	-	1.52	1.47	1.51
Knoop's hardness	-	6	4.5 – 6	5.3

All glasses exhibit linear elastic behaviour at ambient temperatures with a brittle failure mode. Glass can be modelled as a linear elastic, homogenous and isotropic material, which can be expressed by its Young's modulus and its Poisson's ratio (Belis et al., 2019). Figure 15 shows how the stress-strain behaviour of glass compares to steel. Both materials start with a linear elastic behaviour, where the glass immediately has a brittle failure, while the steel first shows a plastic deformation with a ductile failure mechanism. Glass therefore is inherently not a safe building material as it has an immediate failure mechanism that does not warn.
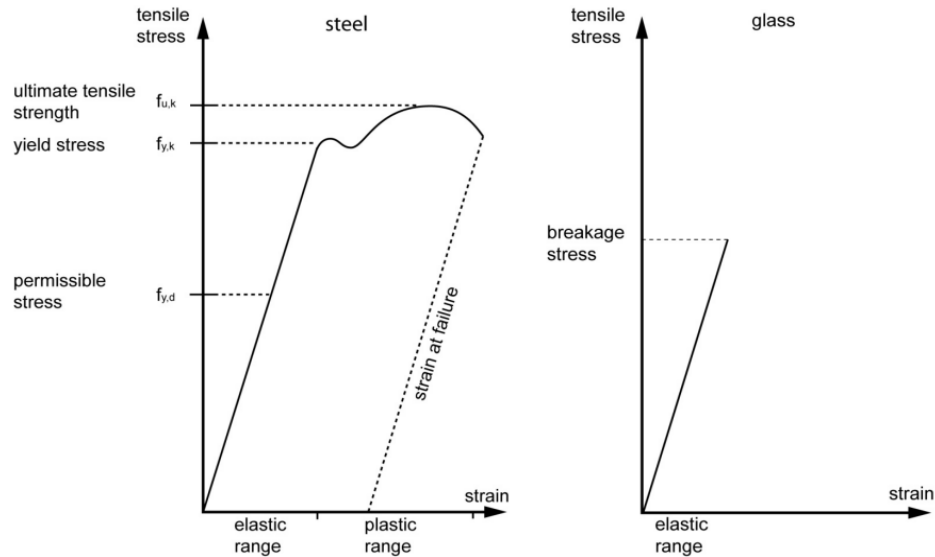
Figure 15 Stress-strain curve of steel and glass (Louter, 2022)

The glass strength is mostly dependant on flaws present in the glass. These flaws can be small surface defects, caused by production, transport, handling and cleaning of the glass pane. These defects are usually not noticeable by the naked eye but do cause stress singularities when a load is applied to the pane of glass. The governing failure mode of glass is a splitting mode where the two sides of the crack are pulled apart, see Figure 16a. Thus, the failure force is a tensile stress acting perpendicular to the crack. Based on this relation, a relation between this macroscopic failure and the crack depth of these surface flaws can be drawn, see Figure 16b (Belis et al., 2019).
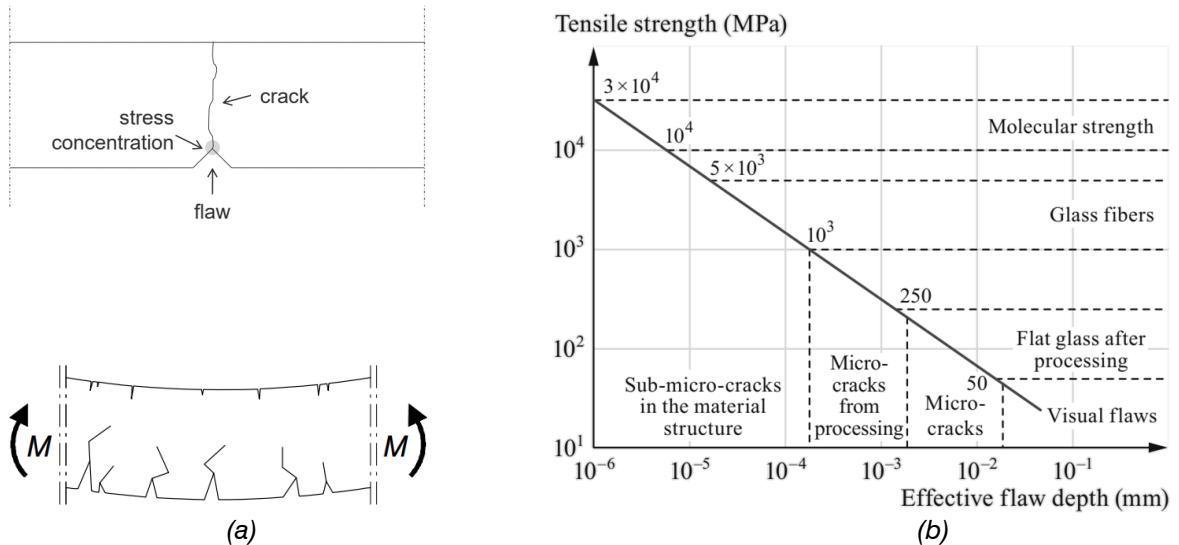
Figure 16 (a)Schematisation of flaws on the surface resulting in cracks in the glass pane (Louter, 2022); (b) simplified relation between failure stress and crack depth (Belis et al., 2019)

Over time, a glass pane accumulates more and more surface flaws, therefore reducing the usable strength of the pane. During the design process with glass, glass strength reduction factors depending on the stress duration are applied to accommodate this effect.

As the micro flaws in glass cannot efficiently be detected non-destructively, the glass strength is typically evaluated using statistical methods like a two-parameter Weibull distribution and calculating a 5% quantile, see Table 3 for the characteristic bending strength (Belis et al., 2019). Based on the Weibull concept, the size of the stressed area

15

can be related to the probability of failure. Larger surfaces will statistically have a lower failure stress than smaller areas, due to the increased probability of the presence of surface defects.

Table 3 Typical values for the characteristic bending strength of soda-lime-silica glass from European standards (5% quantile for a 95% confidence level) (Belis et al., 2019)

Glass type	Standard	Characteristic bending strength [N/mm^2]
Annealed float glass	EN 572-1 (2016)	45
Heat strengthened glass	EN 1863-1 (2012)	70
Enamelled heat strengthened glass	EN 1863-1 (2012)	45
Tempered glass	EN 12150-1 (2015)	120
Enamelled tempered glass	EN 12150-1 (2015)	75

2.1.3 Production floating process

The industry standard for producing glass for the building industry is the float glass process. With this process large quantities of high-quality flat glass can be made in thicknesses ranging from 2 to 19 *mm* (Schittich et al., 2007). The float process is a continuous process able to produce long glass panes, where the sizing is limited by transportation, handling and mounting of the panes. A standard size of 6 *m* length and 3.21 *m* width is used, but custom sizes can be made upon request, with lengths up to 20 *m* possible. Standard float glass thickness nominal values are 2, 3, 4, 5, 6, 8, 10, 12, 15, and 19 *mm*; some factories also produce 25 *mm* (Belis et al., 2019). Due to the tolerances of specific products, the actual glass thickness is typically slightly smaller than the nominal glass thickness.

Figure 17 shows the whole float process, starting at the raw materials. For soda-lime-silica glass these include silica sand, lime, soda and additives are mixed and heated in a furnace to completely melt. Then, the hot glass melt is moved into a float bath where it can float on top of molten tin, which has a higher density than glass. This part of the process creates an almost completely flat surface at the contact area. The surface in contact with the tin is referred to as the tin side, with the other side being the air side.

Next, the glass is moved through the annealing lehr, where it rests on top of rollers. The speed of these rollers determines the final thickness of the glass. Here the glass must cool down to room temperature. When the cooling process happens too quickly, it can create stresses within the glass, which can result in spontaneous breakage. To prevent this from happening, the glass is slowly cooled down in a controlled annealing process. Carefully controlling the cooling process allows the atoms to relax and prevents any residual stresses to act within the glass. Finally, the glass is cut into the desired sizes and visibly inspected for any flaws.
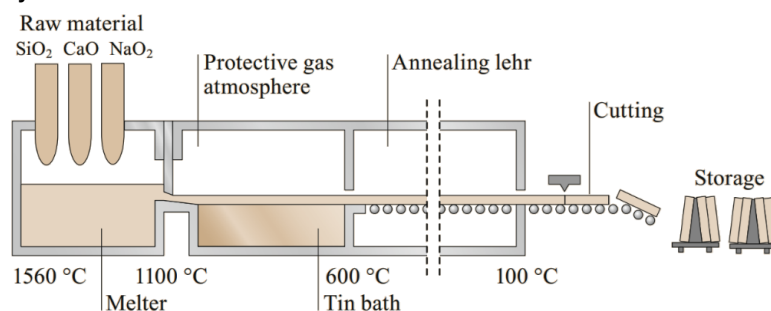
Figure 17 Schematic representation of the float process (Belis et al., 2019)

This process can also be used as the starting point of more advanced glass products, like pre-stressed glass and laminated glass.

2.1.4 Production process thin glass

Float glass start at a thickness of 2 *mm*. To make thin glass, two other methods can be used, the overflow fusion downdraw process and the downdraw process. To make this thin glass, (boro-)aluminosilicate glass is used. The thickness of the glass can range from 100 *μm* to 1 *mm* and has comparatively less flaws at the glass surface than float glass.

The full process is shown in Figure 18, starting with the melting furnace where the components are mixed. This composition is then poured onto a bath called an 'isopipe', which then overflows evenly on both edges. The two sides then rejoin at the bottom, where the two streams of glass fuse together. The glass is then drawn down to form a continuous sheet of flat glass, where the speed at which the sheet is drawn away from the root determines the thickness of the sheet. After the glass has fully annealed, it can be cut into the wanted sizing and inspected to ensure quality.
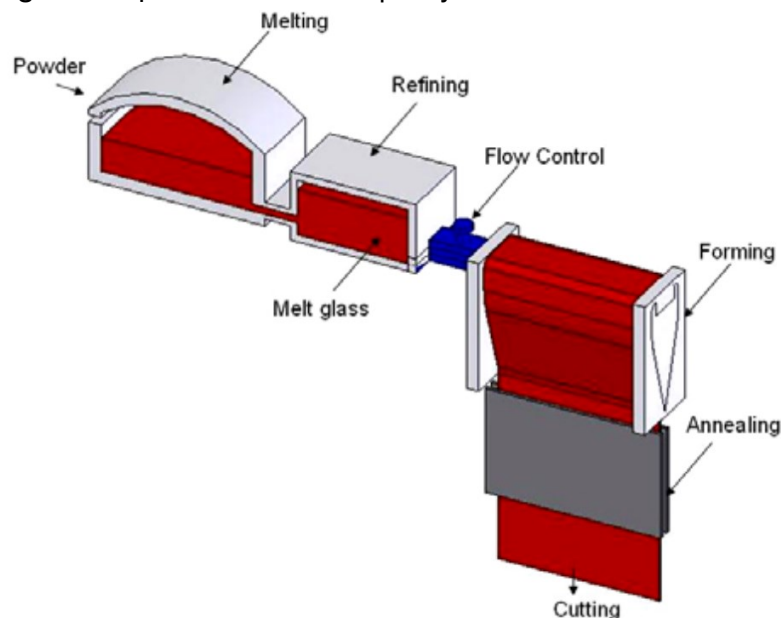
Figure 18 Schematic diagram of overflow fusion downdraw process (Lin & Chang, 2007)

The drawing equipment is located far away enough from the root, so that the glass has cooled down and become solid before coming into contact with any object. This ensures the quality of both surfaces of the glass sheet. Strict monitoring of the process is necessary to ensure a uniform thickness of the panel and good surface quality of the glass.

The other method for creating thin glass is the downdraw process, which creates a thickness typically ranging from 25 *μm* to 1.1 *mm*. This is also a vertical process, only now the glass pane is drawn down using rollers. The full process is shown in Figure 19.
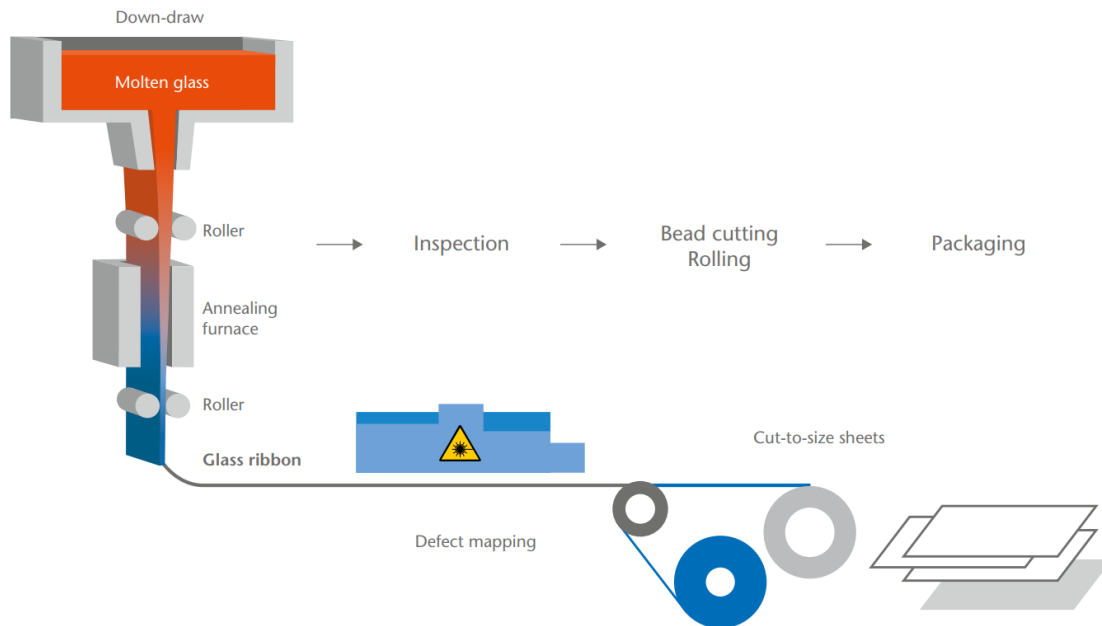
Figure 19 Schematic diagram of the down-draw process (SCHOTT, 2020)

2.1.5 Mechanical processing

After the glass pane is made, it needs to be cut into the right dimensions. Cutting the glass is usually done with automated mechanical cutting tables, but waterjet cutting and laser cutting are also available options. The edge of the cut can get several types of finishings that reduce the sharpness, see Figure 20. These finishings do reduce the mechanical resistance of the edge and the resistance to thermal breakage.

(a) *(b)*

(c) *(d)*
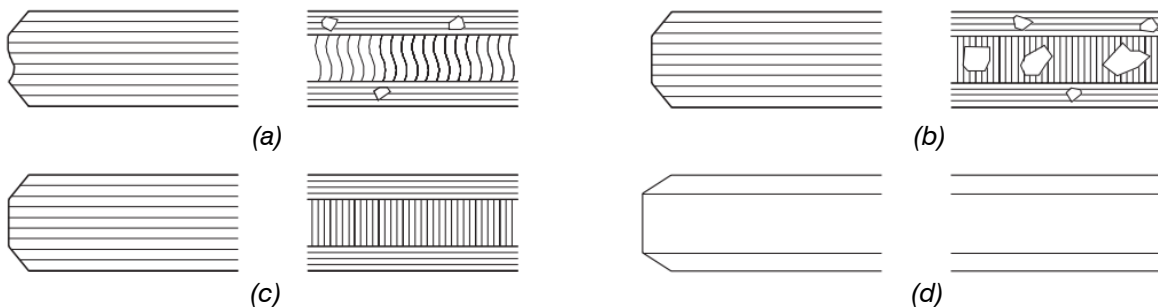
Figure 20 Types of edge working for glass: (a) edge with arrissed corners; (b) ground edge with blank spots; (c) ground edge with no blank spots; (d) polished edge (Schittich et al., 2007)

When other details need to be added to the glass like holes for connections, different drilling methods can be used. Figure 21 shows three common methods used for drilling in glass. These holes do cause a local weak point in the glass, since potential damage can occur at the bore hole, reducing the local strength of the glass. To reduce this vulnerability, it is recommended to chamfer the hole's edges (Belis et al., 2019).

(a) *(b)* *(c)*
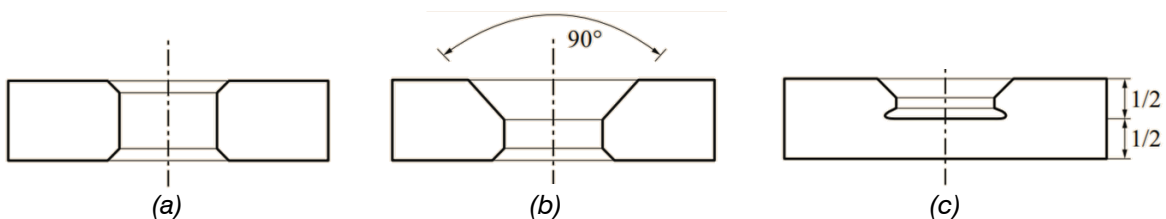
Figure 21 Common drilling/coring typologies: (a) cylindrical; (b) conical; (c) undercut holes (Belis et al., 2019)

18

2.1.6 Post processing

As mentioned before, the strength of glass is governed by small flaws located at the surface. To enhance the strength of glass, a surface compressive pre-stress can be applied, which put the flaws located on the surface in a permanent state of compression (Belis et al., 2019). Pre-stressing the glass can be done thermally and chemically. This greatly improves the resistance against fractures, thereby increasing the characteristic strength from 45 N/mm^2 for normal annealed glass to 70 and 120 N/mm^2 for heat strengthened and thermally toughened glass, respectively. This strength will also be time independent opposed to annealed glass.

The most common method is thermal pre-stressing, shown in Figure 22. This method can result in tempered (heat-strengthened) or thermally toughened glass. This method starts after the production process, so after cutting, edge treatment and potentials drilling. First, the glass is cleaned and then heated up until it reaches its visco-elastic state. Then, the glass is quenched, where the surfaces of the glass are cooled down faster than the core. This difference in temperature allows the surface layers to solidify and contract without creating significant stresses due to still soft hot core.
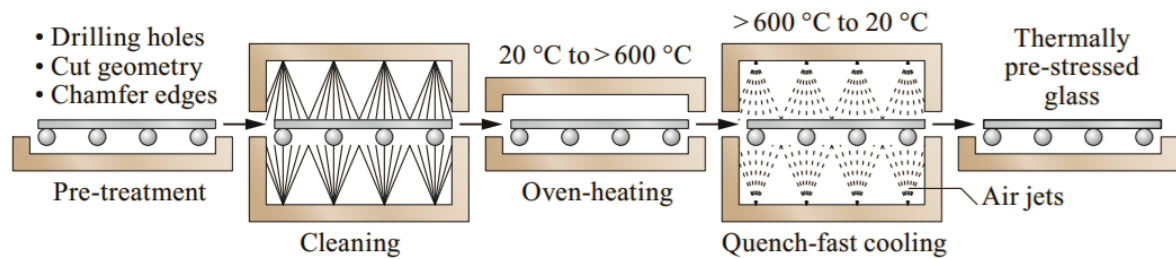
Figure 22 Schematic representation of the thermal pre-stressing process (Belis et al., 2019)

As the cooling progresses, the core solidifies and contracts as well, exposing the outer surfaces of the pane to significant residual compressive stresses, whereas the core stays in tension. The cooling rate during the quenching phase determines the residual stress values in the glass pane. Highly pre-stressed glass is known as thermally toughened glass or (fully) tempered glass and is highly pre-stressed, while heat strengthened glass is more moderately pre-stressed.

Thermal pre-stressing significantly alters the fracture pattern of a glass pane, see Figure 23. The smaller fragments have relatively blunt edges, reduce the risk of injury and increasing the safety of the glass. A disadvantage of these smaller fragments is the reduced residual bending stiffness after fracture in laminated applications.
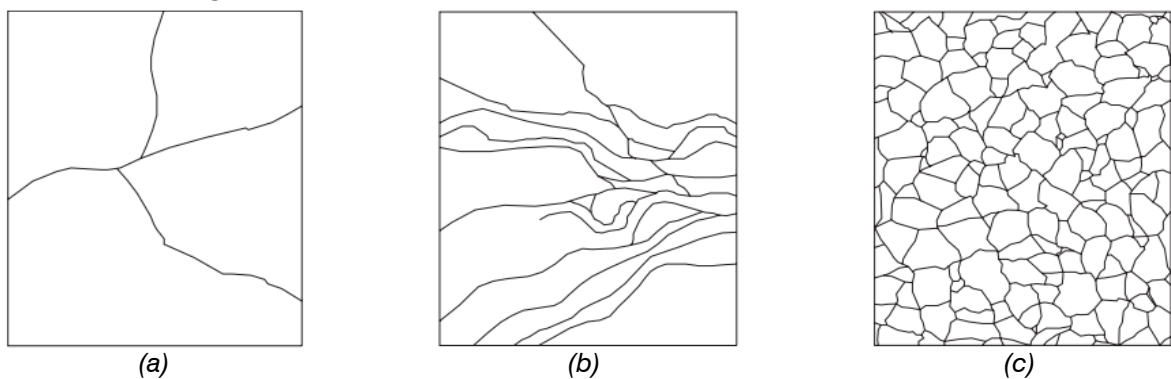
Figure 23 Fracture patterns (not to scale) of: (a) normal (annealed) glass; (b) heat-strengthened glass; (c) thermally toughened glass (Schittich et al., 2007)

Another downside is that thermally toughened glass may show visual distortions, like an edge lift or roller waves. Furthermore, mainly thermally toughened glass but also to a lesser extent heat strengthened glass may show spontaneous failure due to nickel sulfide inclusions or other inclusions that are barely visible to the naked eye (Belis et al., 2019). This risk can be reduced by applying a heatsoak procedure prior to the transport of glass. This heatsoak accelerates the phase change of the nickel sulfide inclusion by reheating the glass to provoke failure. Most thermally toughened glass is heat-soaked, though this might affect the pre-tension of the pane.

The glass can also be chemically pre-tensioned. In this process, an ion exchange process takes place over a set time, resulting in compressive stresses at the surface, see Figure 24. These surface compressive stresses are usually significantly higher compared to thermally induced stresses. However, they appear on a much thinner zone of the cross-section.
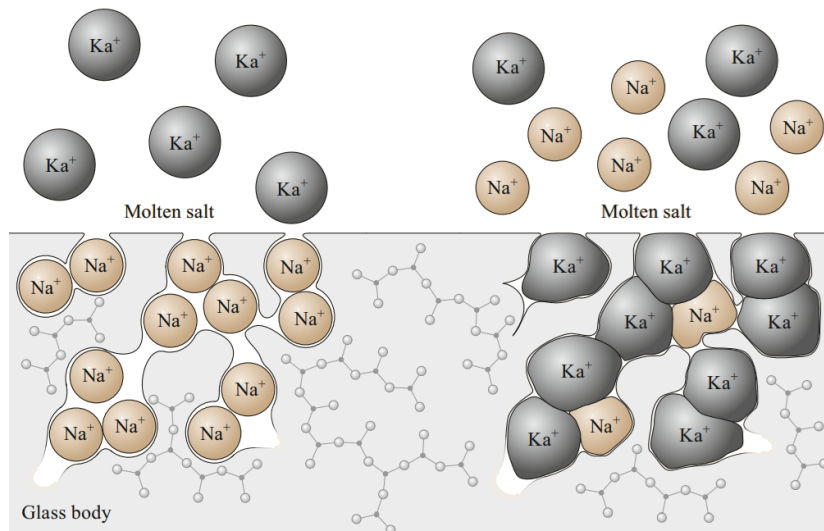
Figure 24 Schematic representation of the chemical tempering process (Belis et al., 2019)

For chemical pre-stressed glass, the stress distribution is much more sudden, compared to the parabolic shape of thermally pre-stressed glass, see Figure 25. Near the edges, holes and other irregularities near the stress progression becomes more complex and finite element analysis is necessary to predict the stress behaviour. Chemically induced prestressing is primarily used for thin panes of glass, because of its thin compressive zone. These thin glass panes will have a fracture pattern similar to that of (normal) annealed glass, due to the relatively low tensile stresses in the core of the glass.

| (a) | (b) | (c) |
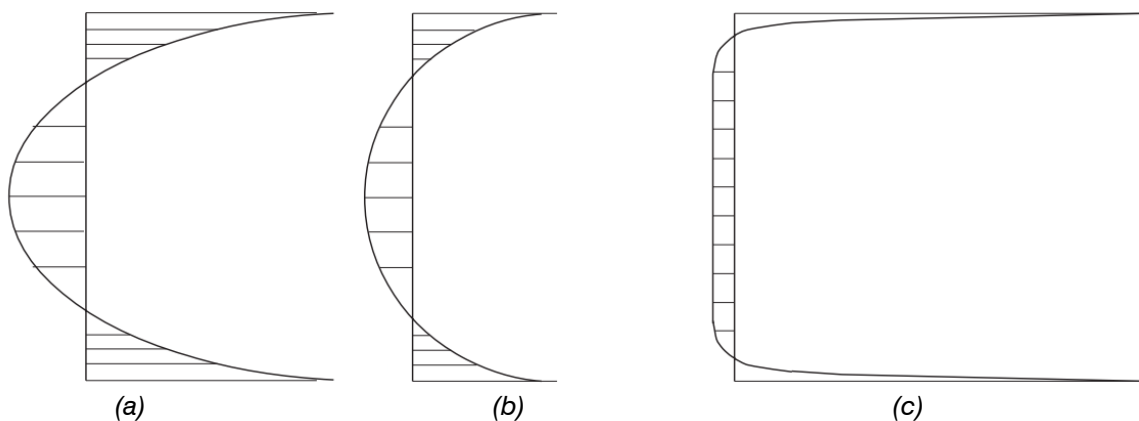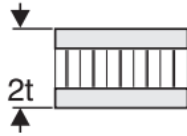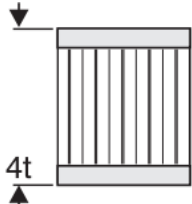
Figure 25 Stress distribution in pre-stressed glass: (a) thermally toughened glass; (b) heat strengthened glass; (c) chemically strengthened glass (Schittich et al., 2007)

2.2 Core

2.2.1 Sandwich theory

A sandwich panel is a composite structure consisting of two thin and stiff sheet elements connected to a low weight core. The result is a panel that is both lightweight and with a high stiffness. The sandwich theory rest on the same principle as an I-profiled beam, where the flanges resist the compressive, tensile and bending stresses while the web resists shear and buckling. Placing the solid material further away from the centre, increases the stiffness and flexural strength, without significantly increasing the weight, see Table 4. It is important to connect the core and sheets well together, to ensure it can resist the shear and tensile stresses acting here and keep the sandwich panel intact.

Table 4 Relative stiffness and weight of sandwich panels compared to solid panels (Hexcel Composites, 2000)

	Solid material	Core thickens t	Core thickness 3t
Stiffness	1.0	7.0	37.0
Flexural strength	1.0	3.5	9.2
Weight	1.0	1.03	1.06

A sandwich element allows for an efficient design that can use each material component to its ultimate limit. The most obvious advantage is a very high stiffness-to-weight ratio and also a high bending strength-to-weight ratio (Zenkert, 1997). Furthermore, using cellular core materials with a low thermal conductivity result in no need for additional thermal insulation. A sandwich panel can be susceptible to damage, reducing the strength of the panel. Manufacture induced flaws like different types of disbonding, voids in the core and delamination can occur, or damage while the product is in use, like over-loading, fatigue and impact.

A sandwich panel has seven main failure modes, see Figure 26. All these failure modes need to be assessed in the calculations. First, the two sheets and the core should be able to withstand the tensile, compressive and shear stresses. The adhesive should be able to transfer the shear stresses between the core and sheets. Second, the panel should have sufficient bending and shear stiffness, to limit the deflection.

Third, the core thickness and shear modulus must prevent the panel buckling under end compression loads. The core should also be able to prevent the core from prematurely failing in shear under end compression loads, known as shear crimping. Next, the core compressive strength must be able to resist localised compression. Following, the compressive modulus of the facing shin and the core compression strength must prevent skin wrinkling failure. Lastly, the core cell size must be small enough to prevent intra cell buckling.
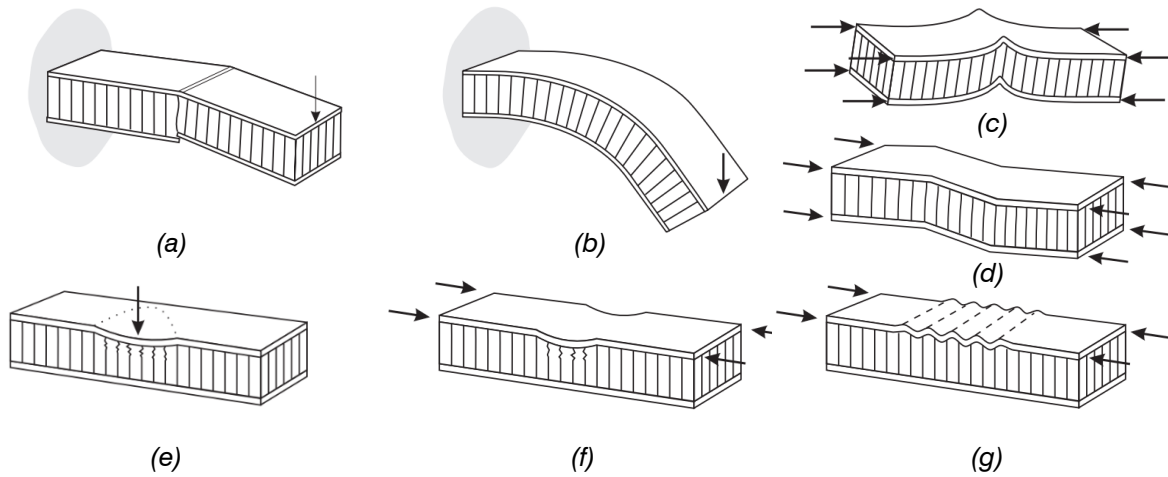
Figure 26 Failure modes sandwich panel; (a) strength (skin compression failure); (b) stiffness (excessive deflection); (c) panel buckling; (d) shear crimping; (e) local compression; (f) skin wrinkling; (g) intra cell buckling (Hexcel Composites, 2000)

2.2.2 Topologies

For the core of the sandwich panel, its topology can be used to maximise the stiffness, while keeping the self-weight low. Different types of cellular core structures have been developed and evaluated, with the main structures shown in Figure 27. Here there are patterns which can be produced in 2D and 3D, where for example a 3D-printer can be used.
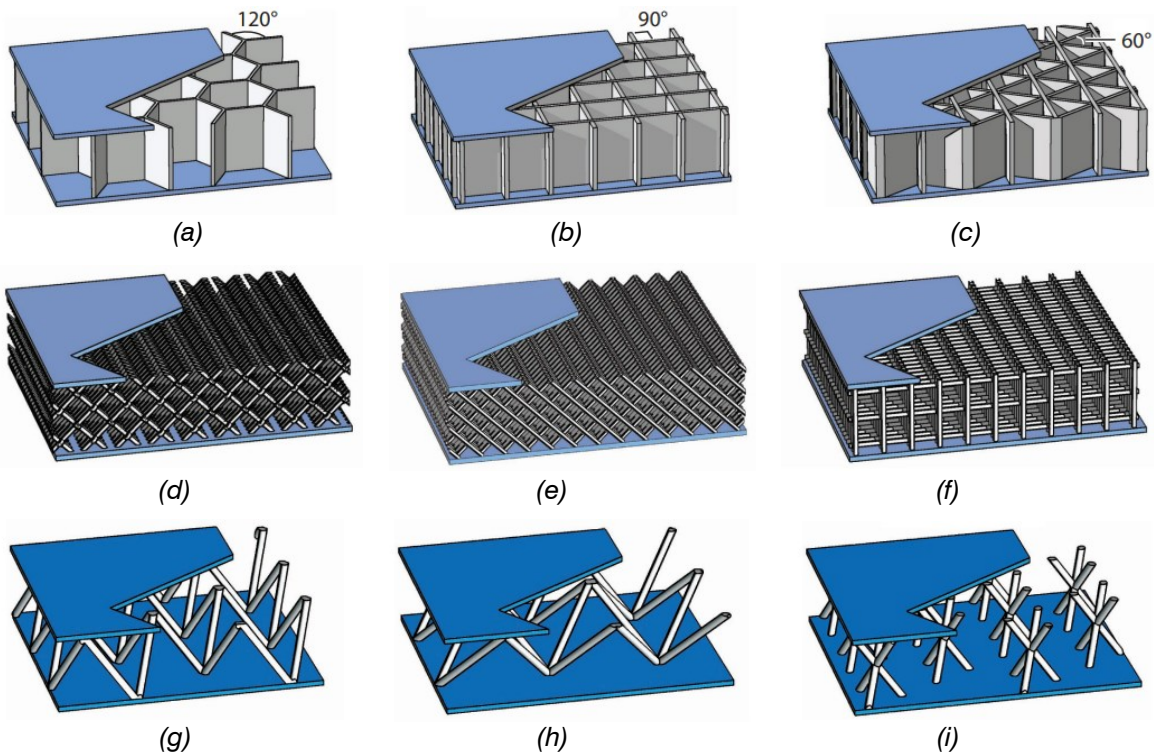
Figure 27 Cellular structures for sandwich panels; (a) hexagonal honeycomb; (b) square honeycomb; (c) triangular honeycomb; (d) diamond textile; (e) diamond colinear; (f) square colinear; (g) tetrahedral; (h) pyramidal; (i) 3D kagomé (Schaedler & Carter, 2016)

First, there are the honeycomb cores, which are a 2D pattern stretched over the third axis. The pattern consists of closed cells where the angle between the walls determines the shape of the pattern (see *a*, *b* and *c* of Figure 27). Honeycomb cores currently offer the

22

greatest shear strength and stiffness to weight ratios but require care in ensuring adequate bonding to the faces (Zenkert, 1997).

Next are three-dimensional periodic patterns (*d*, *e*, and *f* of Figure 27) which are based on the same geometrical concept as the 2D patterns. The difference is that the cavities are no longer just stretched over the third axis, but they can be completely closed. This can result in a better performance to solve the cross-flow air and humidity retention problems that may occur in the 2D pattern (Ma et al., 2021).

Lastly, truss structures with open cells can be applied in the core (*g*, *h* and *i* of Figure 27). These lattice truss topologies have a high stiffness and allow for cross flow heat exchange. The connection to the sheets of the sandwich structure is punctual, so it has a relatively small area of contact.

The performance of the different types of core structures can be summarised in the graph of Figure 28. Here the yield strength is plotted against the density of the material, showing how effective each method is. Remarkable is the location of the honeycomb pattern, which shows a relatively high yield strength compared to its density, showing the effectiveness of the pattern.
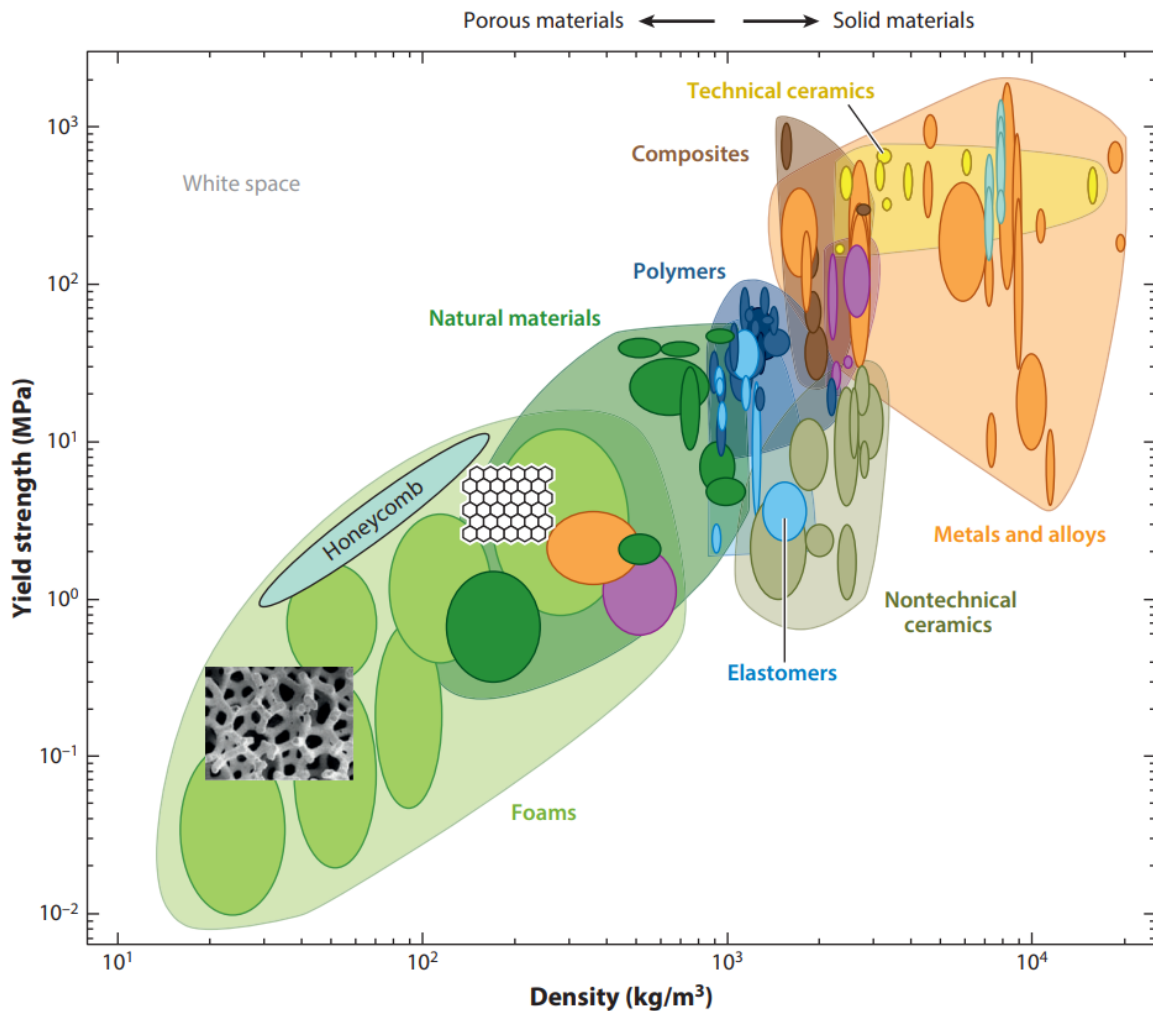
Figure 28 Material property space obtained by plotting yield strength versus density of all commercially available materials with the CES Selector database (Schaedler & Carter, 2016)

2.2.3 Manufacturing methods

In the past, there were two main ways to produce honeycomb cores, namely the corrugating and expansion process. The corrugating process uses thin sheets of the core material that are pressed in the desired shape. Then, they are stacked and bonded together to form the core. The expansion process begins with stacking the thin sheets of the core material on which adhesive node lines have been printed (Zenkert, 1997). Once the adhesive has cured, the layers are pulled apart until they reach the desired cell shape. Cores made from metal start at the desired thickness and then yield plastically, thereby remaining the desired thickness. Non-metallic materials are heat treated after the expansion step to retain their shape. Then, the core is dipped in resin and cured in an oven.
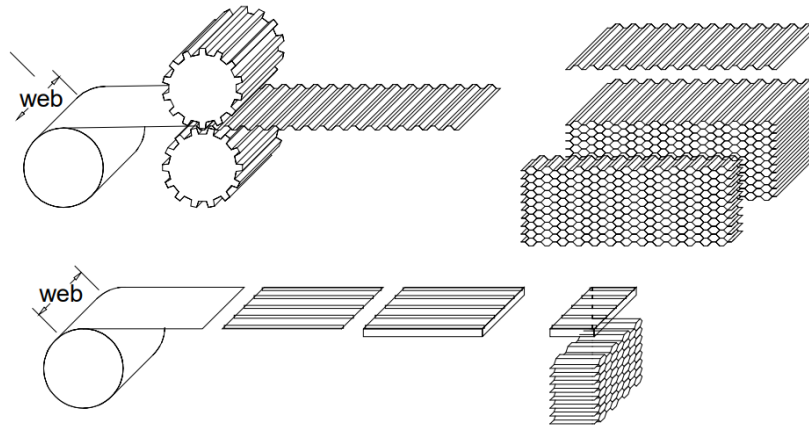
Figure 29 Manufacture of honeycomb cores - corrugating and expansion process (Zenkert, 1997)

Nowadays, the method of additive manufacturing, otherwise known as 3D-printing, has opened a lot of possibilities and making more complex pattern possible. Additive manufacturing is based on a process that produces an object with an additive approach, building the product layer for layer. The object can be designed using a Computer Aided Design (CAD) model, which can then be translated into instructions for the printing machine.

Developing the CAD model can be done using form finding methods, focussing on the following four design categories: structural design, functional design, aesthetic design and manufacturing design. Each of these categories may have different objectives, which may result in different topologies (Pfarr & Louter, 2023). Therefore, defining the parameters, boundaries and minimal requirements is important in finding the optimal design.

There are many different techniques currently available for additive manufacturing, there are different types of printers; namely fusion and deposition technologies (extrusion), technologies based on liquid polymers, laminated solid technologies and powder-based technologies (Cunico, 2019).

Fused Deposition Modelling

Fused Deposition Modelling (FDM), a type of Fused Filament Fabrication (FFF), is a 3D printing technology where it begins with a rolled string, the filament, which is then guided through a heated nozzle. After the filament has become fluid, it can be used to build the product. The nozzle can move along the *x* and *y* axes for each layer, where the next layer must be connected to the previous layer, or an additional support material is required. This support material results in a significant increase in manufacturing time, costs and material waste.
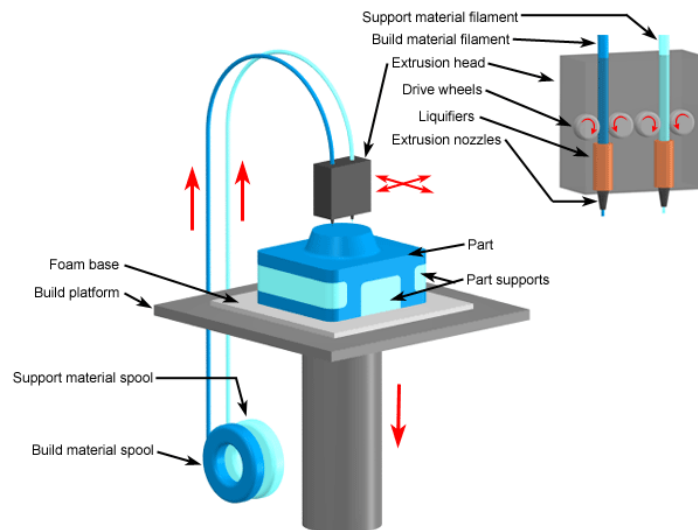
Figure 30 Schematic representation of Fused Deposition Modelling (CustomPartNet, 2008)

Stereolithography

Stereolithography Apparatus (SLA) is a rapid prototyping technology. The process cures localised photosensitive resin by use of a UV laser beam, which can move along the *x* and *y* axes. This laser beam focuses on a resin-immersed container to construct the layer silhouette (Cunico, 2019). This bottom-up trajectory can use a sweep, contour, weave or 3D meshing strategy. Compared to FDM, this method is much more precise, but it has a low thermal resistance since the softening temperature is at $40-80\ °C.$
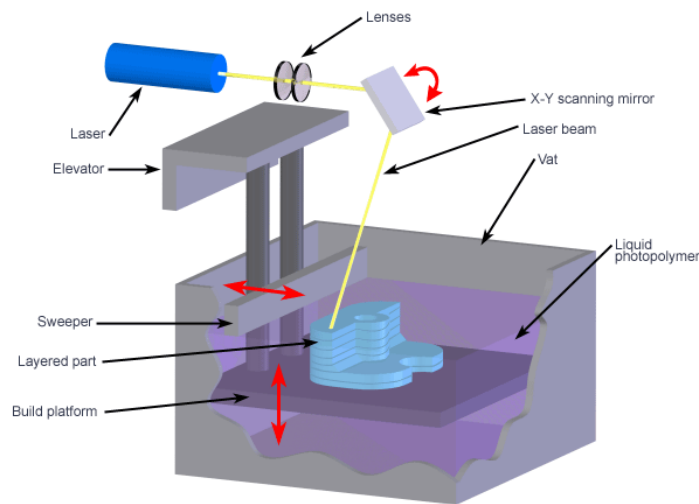
Figure 31 Schematic representation of Stereolithography (CustomPartNet, 2008)

Selective Laser Sintering

Selective Laser Sintering (SLS) is similar to SLA, as it is a rapid prototyping process that uses a moving laser beam to trace and sinter powdered polymer or metal composite materials. The platform adjusts its height for each new layer when new powder is applied again so that the new layer can be sintered. In comparison to SLA, additional support material is not required. SLS allows for a wide range of materials, including nylon, glass-filled nylon, SOMOS (rubber-like), Truform (investment casting) and metal composite (CustomPartNet, 2008).

25
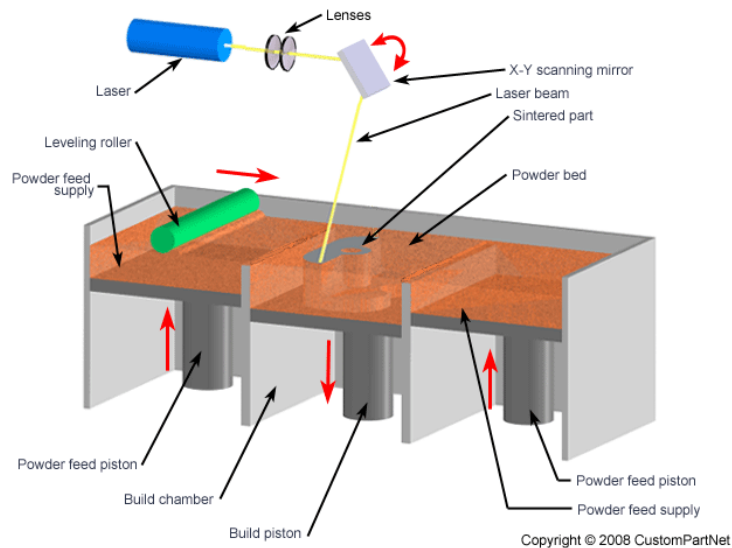
Figure 32 Schematic representation of Selective Laser Sintering (CustomPartNet, 2008)

3D Printing

The process of three-dimensional printing (3DP) is similar to SLS, but instead of a laser the ink-jet printing head deposits a liquid adhesive binding the material together. The 3D-printed parts are usually infiltrated with a sealant to improve strength and surface finish. Materials that can be used are ceramic powders or metals. It has a fast building speed, but is not as good on accuracy, surface finish and strength compared to other methods. Therefore, it is typically used for rapid prototyping of conceptual models.
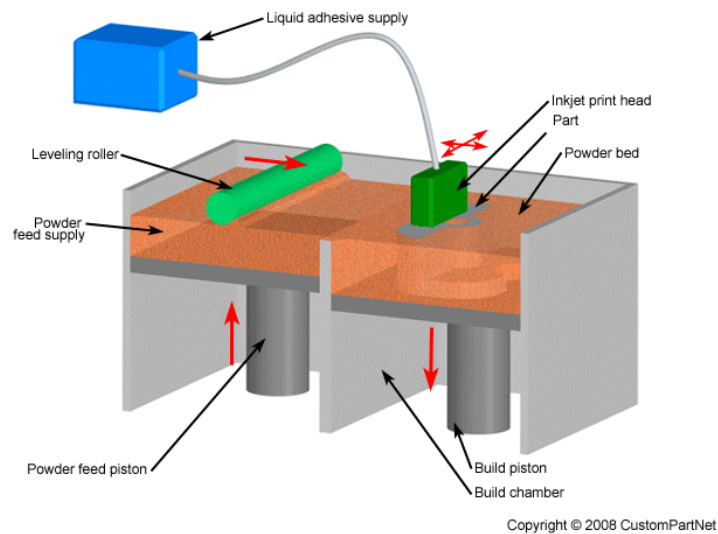
Figure 33 Schematic representation of three dimensional printing (CustomPartNet, 2008)

Inkjet printing

Inkjet print (IJP) is a rapid prototyping technology that creates layers by depositing droplets of material through an inkjet head. The construction platform moves along the *z*-axis, while the liquid photo curable material is deposited moving along the *x* and *y* axes. Advantages are the accuracy and smooth surface finishes. Limitation are slow build speeds, few material options and fragile parts. Therefore, it is mostly used for prototypes for form and fit testing.
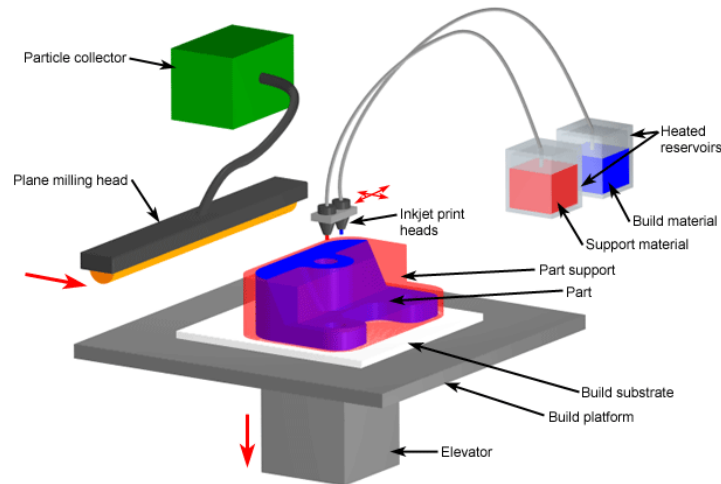
Figure 34 Schematic representation of Inkjet printing (CustomPartNet, 2008)

A comparison of the main characteristics of these techniques can be found in Table 5 (Guidi, 2019).

Table 5 Comparison between additive manufacturing techniques (Guidi, 2019)

	Accuracy	End surface	Building speed	Support material	Max part size [*mm*]
FDM	+	+	-	Needed	915 x 610 x 915
SLA	+ +	+ +	+	Needed	1500 x 750 x 500
SLS	+ +	+	+	Not Needed	550 x 550 x 760
3D Printing	+	+	+ +	Not Needed	1500 x 750 x 700
Inkjet Printing	+ +	+ +	-	Needed	304 x 152 x 152

2.2.4 Materials

For the core, a large number of materials are available and have been used in sandwich panels. Finding the right material can be a challenge due to the many options available, where the combination of the geometry of the material can change the properties of the material. Materials are often chosen not only for its mechanical properties, but rather for reasons such as, environmental resistance, surface finish, the use of a specific manufacturing method, cost, wear resistance etc. (Zenkert, 1997). The main properties determined by the core of the panel are:

- Density
- Shear modulus
- Shear strength
- Stiffness perpendicular to the sheet material
- Thermal insulation
- Acoustic insulation
- Transparency (open-close ratio)

The last point is especially relevant for this thesis, since the main focus is to be able to dynamically influence the daylight transmittance of a panel. To allow the panel to have a changeable transparency, a structure with open cells is required. Therefore, the materials applicable for honeycomb structures will be focused on. Furthermore, it is expected that additional details will need to be added to the core's main structure to allow the dynamic

aspect to work properly. Therefore, the core will be produced using additive manufacturing. This limits the materials that can be used for the core of the sandwich panel, since not all materials are printable.

Additive manufacturing uses thermoplastics as a material, which offers a wide selection of different polymers. Initial preliminary investigations of small-format materials have already reduced the number of polymers that are considered suitable for use in a façade (Pfarr & Louter, 2023).

Polycarbonate (PC) is a material with high strength, high stiffness and provides heat and UV stability. The main downside is that a high temperature is required for the bed of the printing chamber, making it a difficult process. Therefore, there are few manufacturers available that can print with this material. On the other hand, glycol modified polyethylene terephthalate (PETG) can be produced at relatively low temperatures and bears a lower risk of introducing thermal stresses and distortion in the component (Pfarr & Louter, 2023). Previous experiments using PETG as a core material for façade panels have been successful, with the material performing well. The material does show to age under UV light, which can result in yellowing of the material. The material properties of PETG are shown in Table 6.

Table 6 Material properties of polyethylene terephthalate (PETG) (Ashby, 2013)

Mechanical properties		
Density	1290 – 1400	kg/m^3
Young's modulus	2.76 – 4.14	GPa
Yield strength (elastic limit)	56.5 – 62.3	MPa
Tensile strength	48.3 – 72.4	MPa
Compressive strength	62.2 – 68.5	MPa
Elongation	30 – 300	%
Hardness (Vickers)	17 – 18.7	HV
Fatigue strength (10^7 cycles)	19.3 – 29	MPa
Fracture toughness	4.5 – 5.5	$MPa*m^{1/2}$

2.3 Adhesive

The last part of the sandwich panel is the two adhesive layers connecting the core to the glass. To decide on the type of adhesive suitable, it needs to bond well to both glass and the core material, so polymers. A study by Kothe et al. (2021) investigated possible adhesive bonds glass and 3D-printed polymers, with a focus on the resistance to temperature and UV aging. Four adhesives were selected that showed adequate aging resistance and a rapid curing at room temperature, see Table 7.

Table 7 Selected adhesives for research of Kothe et al. (2021)

Adhesive	Type	Viscosity [$mPa \cdot s$]	Curing conditions
LOCTITE EA 3430	2C epoxy resin	18000	*RT > 3d* (fixture time: 15 min.)
LOCTITE 3345	Urethane methacrylate	2000	UV 60 *mW*/*cm*^{2}, 60 *sec*.
Technicoll 9430-1	2 K polyurethane	3000	*RT > 3d* (fixture time: 20 min.)
Photowell 1270	Acrylate	15000	UV 60 *mW*/*cm*^{2}, 60 *sec*.

The results of this research showed that polyurethane Technicoll 9430-1 resulted in accurate, bubble-free and highly transparent bonds which were not affected by aging. A downside of this material is the short open time of the adhesive, meaning that it is necessary to apply fully automatic adhesive application and adequate joining technology.

Another recommended adhesive is the acrylate Loctite 3345, which shows well bonded joints, though it did show yellowing and a loss of strength after the aging process. The big advantage of this material compared to Technicoll 9430-1 is the easier handing by curing with UV radiation, as well as the remaining stiffness at high temperatures. The use of specific surface preparation on the 3D-printed polymer surface should be envisaged, as it was primarily on this surface that the adhesive failures occurred (Kothe et al., 2021).

It is important to note that these testing results were not based on a connection with thin glass. Thin glass is produced with a chemically strengthened surface, which may respond differently than the surface of normal glass.

2.4 Visual comfort

A façade element is highly influential on the overall experience of a room. Natural light is often associated with a better quality, feeling healthier and improving the well-being of the people inside. The use of daylight openings in a building highly depends on the function of the indoor spaces. Different types of buildings have different requirements in terms of privacy, view, glare protection, solar heat gain etc., resulting in different types of façade systems.

2.4.1 Illuminance

Illuminance is the level of light on a surface, expressed as the luminous flux Φ over the area A. Illuminance can therefore be expressed as follows:

$$E = \frac{\Phi}{A} \left[\frac{lumen}{m^2} = lux\right]$$

$$(\ 1\ )$$

The luminous flux can be described as the luminous intensity [I] multiplied with the solid angle [ω]:

$$\Phi = I * \omega \ [lm * sr = lumen]$$

$$(\ 2\ )$$

The solid angle ω is defined as the part cut from a spherical surface [A] divided by the squared distance [R^2]:

$$\omega = \frac{A}{R^2} \ [sr]$$

$$(\ 3\ )$$

The illuminance will generally decrease with the square root of the distance (van der Linden, 2015). The angle at which the light source enters the room is also trivial in determining the illuminance. Light that enters the room from an angle, will be divided over a larger area. Therefore, the illuminance can also be defined as follows:

$$E = I * \frac{\cos(\theta)}{R^2} \ [lux]$$

$$(\ 4\ )$$

Here I is the luminous flux related to the solid angle, ϑ the angle at which the light falls on the object and R the distance to the light source.

The maintained illuminance value of a room needs to meet the requirements as stated in NEN-EN 17037+A1 (2022), which are dependent on the function of the room. Below the factors used to determine the visual comfort range of illuminance values are listed.

- Visual comfort and well-being
- Requirements for visual tasks
- Visual ergonomics
- Practical experience
- Contribution to functional safety
- Economy

2.4.2 Luminance

Luminance is used to express the brightness of a certain area. Brightness is a subjective term, but it correlates to the luminance of the area. The definition of luminance is the amount of light emitted by (or reflected by) a surface at a given rate within a three-dimensional angle over an area. Here $I(\vartheta)$ is the luminous intensity as it is radiated from the are in the direction of ϑ, $A*cos(\vartheta)$ is the apparent surface area.

$$L(\theta) = \frac{I(\theta)}{A * \cos(\theta)} \left[\frac{cd}{m^2}\right]$$

$$(\ 5\ )$$

2.4.3 Contrast

Visual comfort can be influenced by the level of contrast in the room. The contrast of an object is the difference in luminance of the object itself and the surrounding area. When something is obstructing the façade opening, it can cast shadows on objects, thereby resulting in contrast. This perceived contrast can be reduced by maintaining ambient light levels inside.

The level of horizontal contrast can be expressed in a contrast ratio (*CR*), where the luminance of one part of the room is related to the luminance of another:

$$CR = \frac{L_{area\ 1}}{L_{area\ 2}}\ [-] \qquad\qquad (6)$$

The recommended minimum contrast according to ISO 9241-3 should be 3:1, so the ratio between two connecting surfaces should be less than 3.

2.4.4 Glare

Glare can be described as the negative experience when the luminance from bright sources is much higher than what eyes are adapted to. This results in discomfort, loss of visual performance and visibility and should be prevented when possible. Glare can occur from looking into direct sunlight or due to vertical contrast, which is the luminance difference between areas within a person's view.

Glare perception increases with an increase of the size or luminance of the light source. Larger angular distance of the glare source to the line of sight of the occupant decreases glare perception. Perceived glare increases when the contrast ratio between foveal and central or peripheral vision increases. Usually the foveal vision is directed towards the visual task (NEN-EN 17037+A1, 2022).

The glare can be measured using Daylight Glare Probability (*DGP*), which shows how well a room performs in protection against glare. It is recommended to do this when activities like reading are likely to take place in the room. The *DGP* is an empirical formula relating measurable physical elements to the experienced glare (NEN-EN 17037+A1, 2022):

$$DGP = 5.87 * 10^{-5} * E_v + 9.18 * 10^{-2} * \log\left(1 + \sum_i \left(\frac{L_{s,i}^2 * \omega_{s,i}}{E_v^{1.87} * P_i^2}\right)\right) + 0.16 \qquad (7)$$

Here E_v is the illuminance at eye level, *I* is the number of glare sources, $L_{s,i}$ is the luminance of a glare source, $\omega_{s,I}$ is the solid angle subtended by the glare source and P_i [-] is the position index, which describes the reduction of the glare perception by the angular displacement of the source from a person's line of sight.

The resulting *DGP* value shows whether glare is likely to be perceived, see Table 8 for the categories of factors. The minimum recommendation for glare protection is that the *DGP* does not exceed 0.45 for more than 5 % of the occupation time of the relevant space (NEN-EN 17037+A1, 2022).

Table 8 DGP values categorised in the following ranges (NEN-EN 17037+A1, 2022)

Criterion	Level of recommendation	*DGP*
Glare is mostly not perceived	High	$DGP \leq 0.35$
Glare is perceived but mostly not disturbing	Medium	$0.35 < DGP \leq 0.40$
Glare is perceived and often disturbing	Minimum	$0.40 < DGP \leq 0.45$
Glare is perceived and mostly intolerable		$DGP \geq 0.45$

The visual comfort can be further quantified by looking at the luminance values in the views inside the rooms. Research has defined visual comfort by giving luminance threshold values as shown in Table 9. Suk (2019) investigated the visual comfort for an office setting, where the threshold is located at a luminance of 2420 cd/m^2 and the contrast ratio at 11.7.

Table 9 Visual comfort luminance thresholds resulting from varying research groups (Suk, 2019)

Research Group	View direction parallel to windows	View direction facing to windows
Wienold and Christofferson	< 2000 cd/m^2 – perceptible > 6000 cd/m^2 – uncomfortable	< 1500 cd/m^2 – perceptible* > 4500 cd/m^2 – uncomfortable*
Sutter et al.	< 2800 cd/m^2 – visual comfort > 3200 cd/m^2 – visual discomfort	-
Linney	> 2740 cd/m^2 – visual discomfort	> 2160 cd/m^2 – visual discomfort
Osterhaus	-	> 2570 cd/m^2 – visual discomfort*
Wymelenberg et al.	< 2000 cd/m^2 – visual comfort	-
Shin et al.	-	< 1800 cd/m^2 – noticeable > 5600 cd/m^2 – uncomfortable
Wymelenberg and Inanici	< 2500 cd/m^2 – visual comfort > 4000 cd/m^2 – visual discomfort	-
Suk et al.	-	< 1920 cd/m^2 – visual comfort > 5014 cd/m^2 – visual discomfort

* view direction 45° diagonal to windows

2.4.5 Daylight

Daylight can be defined as the resulting effect of both sunlight and skylight. Daylight can vary highly during the year and during a day. Time of the year, weather conditions and the location on earth all influence the level of daylight in a room. Artificial lighting can be used instead when there is not enough light from outside, but this uses electricity and decreases the visual quality in terms of colour rendering. Therefore, the available daylight should be used as much as possible.

To be able to design a building with appropriate levels of daylight, the NEN-EN 17037+A1 (2022) specifies the recommended values of daylight provisions by daylight openings, see Table 10. The levels minimum, medium and high represent the different requirements per space. This includes a target illuminance E_T that should be achieved across 50 % of the reference plane within a space. The minimum target illuminance E_{TM} should be achieved across 95 % of the reference plane. This reference plane should be located at 0.85 m above the floor.

Table 10 Recommendations of daylight provision by daylight openings in vertical and inclined surface (NEN-EN 17037+A1, 2022)

Level of recommendation for vertical and inclined daylight opening	Target illuminance E_T [lux]	Fraction of space for target level $F_{plane,\%}$	Minimum target illuminance E_{TM} [lux]	Fraction of space for minimum target level $F_{plane,\%}$	Fraction of daylight hours $F_{time,\%}$
Minimum	300	50 %	100	95 %	50 %
Medium	500	50 %	300	95 %	50 %
High	750	50 %	500	95 %	50 %

Note: Table 11 gives target daylight factor (D_T) and minimum target daylight factor (D_{TM}) corresponding to target illuminance level and minimum target illuminance, respectively, for the CEN capital cities

The minimal target illuminance determines when the room is sufficiently lit opposed to underlit. However, the room can also be over-lit, causing visual discomfort. The visual discomfort can be set at the threshold of 2000 *lux*, in accordance with the research of Nabil and Mardaljevic (2006).

Daytime lighting

During the day, the intensity and colour composition are influenced by the solar position and the clear or cloudy sky conditions. The luminance of a clear sky ranges between 2000 and 12000 cd/m^2, depending on atmospheric scattering effects. A cloudy sky ranges between 1000 and 6000 cd/m^2, depending on the altitude of the sun and the density of the cloud cover (Müeller, 2013).

NEN-EN 17037+A1 (2022) recommends that a space should receive a minimum of 1.5 hour of sunlight exposure. For medium level this is 3 hours and for the high level 4 hours. This should occur on a selected date between 1st February and 21st March.

Maximum horizontal illuminances can be found on clear sky days, depending on the solar altitude, see Figure 35a. Here you can see that the illuminance caused by sunlight is much higher than that of skylight. Looking at Figure 35b, this can be seen again. On cloudy days, so when there is very little sunlight, the total illuminance is much lower. This shows that depending on the climate, the design of a façade panel can have vastly different daylighting conditions, depending on the amount of illuminance due to sunlight during the year.
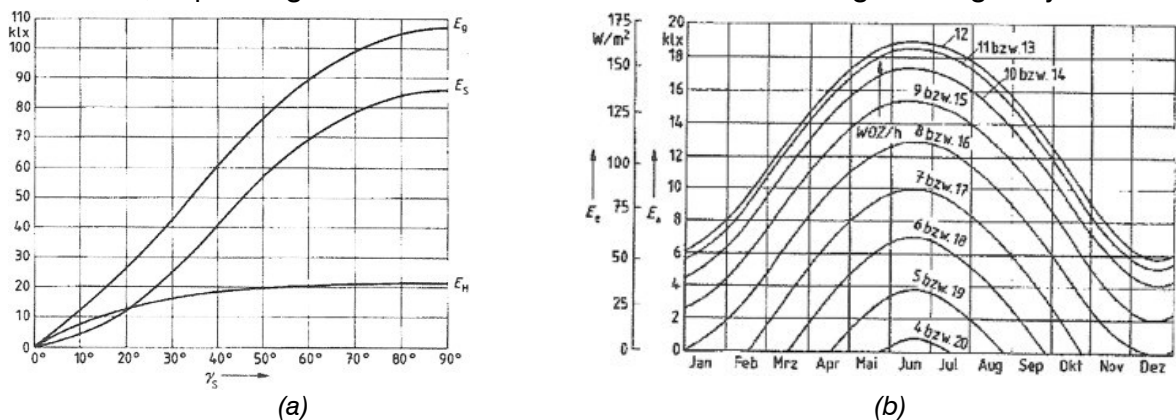

(a) *(b)*

Figure 35 (a) Horizontal illuminance for clear sky conditions vs. solar altitude, E_S by the sun, E_H by the sky and E_G as the total illuminance; (b) horizontal illuminance and solar radiation for overcast sky conditions at 51° norther latitude vs. time (Müeller, 2013)

Since the level of daytime lighting is dependent on the latitude and climate of the location, standardised climate files are used to determine the hours of daylight per location. The hours of daylight are determined by ordering the 8760 values for diffuse horizontal illuminance from high to low and then extracting the highest 4380 hourly values (NEN-EN 17037+A1, 2022). The median diffuse horizontal illuminance value $E_{v,d,med}$ during daylight hours is determined for each capital of CEN member countries, with the values for Amsterdam, the Netherlands given in Table 11:

Table 11 Daylight Factor [DF] for daylight openings to exceed an illuminance level of 100, 300, 500 or 750 lux for a fraction of daylight hours $F_{time,\%}$ = 50 % for Amsterdam, the Netherlands (NEN-EN 17037+A1, 2022)

Geographical latitude φ	Median external diffuse illuminance $E_{v,d,med}$	DF > 100 lux	DF > 300 lux	DF > 500 lux	DF > 750 lux
52.30 °	14400 lux	0.7 %	2.1 %	3.5 %	5.2 %

This table uses the daylight factor to define the daytime lighting. However, solar path studies can also be used to determine the daylight performance. Therefore, two methods are defined. First, a calculation method based on daylight factors and cumulative daylight availability data. The second method is based on simulations of illuminance levels using hourly climate data. With both these calculation methods there are always approximations and uncertainties, for example the reduction of transparency of glass due to dirt build up.

2.4.6 Daylight factor

The first calculation method uses a daylight factor, which represents the ratio between the illuminance inside E_i and illuminance outside E_o, in the open field, at the same time. Expressed as a percentage, it gives the following formula:

$$DF = \frac{E_i}{E_o} * 100\%$$
(8)

To relate the daylight factor to the wanted illuminance during a percentage of the time, the graph in Figure 36 can be used. The lines here represent the timeslot where a certain illuminance is wanted. For example, if during 08:00-16:00 hour an illuminance of 300 *lux* is desired for 90 % of the time, an illuminance of 6000 *lux* can be read from the graph. This results in a daylight factor of 300/6000 = 5 %.
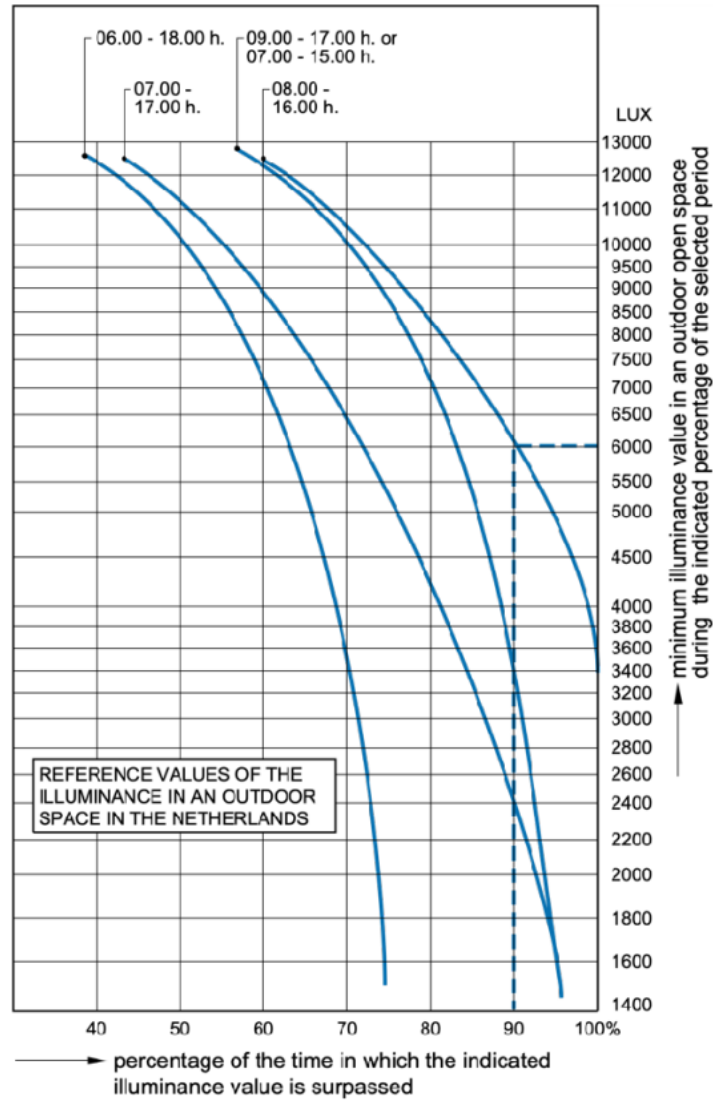
Figure 36 Illuminance in the free field (van der Linden, 2015)

This daylight factor is not only dependent on the sunlight and skylight but has many influencing parameters. Window sizing, surrounding buildings blocking light, transparency of the glass, reflections of the light by inside walls etc. can all contribute to changes to the daylight factor. Therefore, the daylight factor can be split into different aspects (van der Linden, 2015):

$$DF = (DF_h^* + DF_e^*) * c + DF_i^* * \frac{LTA}{0.9}$$

(9)

- DF_h^* = Daylight Factor of sky component
- DF_e^* = Daylight Factor of external reflection component
- DF_i^* = Daylight Factor of internal reflection component
- LTA = light transmittance absolute

c stands for the total losses in the light opening, consisting of possible window frames inside the panel or other obstructions c_k and the effect of dirt c_v:

$$c = c_k * c_v * LTA$$

(10)

In this thesis, these components will be influenced by the design choices made. A denser core pattern will result in a higher reduction for c_k and the thickness of the glass will influence the *LTA* value.

35

Determining the daylight factor with these formulas has the advantage that it is relatively simple to understand and calculate with a single numerical value at each point. Furthermore, it is a well-established and widely agreed standard for measuring daylight performance. Disadvantages are that it does not consider sunlight and the building's orientation and location.

Aside from using the daylight factor formula, software can be used to calculate the daylight performance. This method requires a detailed daylight calculation where (sub-)hourly internal daylight illuminance values for a typical year are computed using (sub-)hourly sky and sun conditions derived from climate data appropriate to the site (NEN-EN 17037+A1, 2022). This method uses climate-based daylight modelling, including the built environment to recreate realistic sky luminance distributions, by means of physically accurate lighting simulation tools. This method produces results directly from the simulated illuminance values, including dynamic shading devices when these are applied.

2.4.7 Photometry

Photometry is the science of measuring the visible light performance. There are many different methods available, all with different advantages and disadvantages. Part of the light performance is a subjective experience, for example with glare, so it is important to properly define the required properties of a façade opening.

Most daylight measuring metrics asses a horizontal plane at typical table heights. This ignores the fact that most people now use digital screens to work or as entertainment. Therefore, using a vertical plane at these heights can be very useful. Measuring light using computer-based simulation can broadly be done in two different categories, each expressing unique photometric qualities. The first is grid-based and typically based on illuminance. The second category is image-based and typically based on luminance. (special) daylight autonomy or useful daylight illuminance (*UDI*) rely on illuminance levels of the horizontal plane, while daylight glare probability (*DGP*) or unified glare index (*UGI*) rely on luminance or vertical eye illuminance (Sawyer et al., 2022).

Simulation software

Two different techniques can be used for the simulation: ray tracing and radiosity. Ray tracing follows the light rays from the eye or camera, which is the opposite of what light does in reality. This approach is efficient, since the majority or light rays from the source do not directly make it into the viewer's eye. Radiance is a program based on ray tracing, which is applied in many different models, like Relux or Daysim (Müeller, 2013). The models use radiance images of the view at a certain time. After doing this for many different optional daylight hours, each image can be analysed to obtain the luminance values. This immediately illustrates one of the difficulties since it takes much computational power.

Radiosity is a process that takes light paths which start at the light source and can make multiple diffuse bounces before it reaches the viewer's eye (Müeller, 2013). This way, it links the luminance of the sky to the illuminance of a surface in the room. This method is used in many daylight factor calculations. To properly simulate the sun path and the consequential daylight, many types of software are available. Examples are the previously mentioned Radiance, or similar programs like ClimateStudio, Ladybug and Honeybee.

More advanced daylighting systems, referred to as Complex Fenestration System (*CFS*), can be much more difficult to property simulate or assess its performance. These systems are often dynamic and can have multiple goals which may contradict themselves. The main

goals are usually redirecting daylight to optimise the illuminance of the room, adjust the daylight flux at working level and prevent the risk of glare. When measuring these qualities in a simulation, it is important to properly model how the *CFS* responds.

A method of simulating this is using the bi-directional scattering distribution function (*BSDF*), which models light transmission through complex materials dependent on the angle of the light. This method concerns only the microscale of a material and does not give information at the buildings scale. Therefore, it should be further incorporated into the full building simulation of a façade analysis.

A full façade photometry is a bi-directional technique which uses sensors modelled on the concave face of an imaginary hemispherical surface, see Figure 37 (Sawyer et al., 2022). The sensors each have their opening angle restrained and follow the direction normal to the surface of the hemisphere. Different sensor locations and fields of view can be used for the sensors, depending on the goal of the test. For recognizing over-lit areas, the hemisphere should be placed closest and centred on the façade opening.

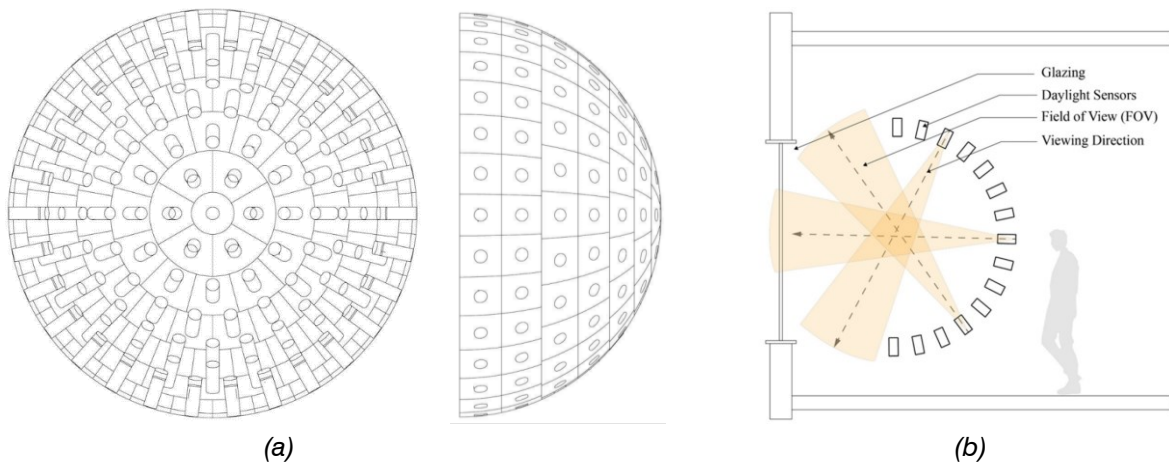|	
(a)	*(b)*

Figure 37 (a) front and side view of imaginary hemispherical surface and the 145-sensor arrangement; (b) concept diagram of the sensors, viewing directions and FOV (Sawyer et al., 2022)

Measuring tools

The daylight performance can also be measured of existing windows. Multiple tools are available, where each tool can measure a certain light assessment value. For measuring the illuminance of a room, a luxmeter [*lx*] can be used. This tool consists of a photoreceptor and a reader. The luxmeter measures the illuminance at a certain location, moving the luxmeter will give different results. Measuring the illuminance at different points along a grid can give similar results as the simulations used. For outside measurements of the illuminance, a daylight sensor [*klx*] can be used.

To measure the luminance of an item, a luminance meter [cd/m^2] can be used. This is a tool that can measure both the luminance of a light source or of reflected light of a surface. A *HDR* Camera [cd/m^2] can also be used, which gives an image of which the luminance can be read. For measuring the absorption or transmission of a material, a spectrophotometer can be used. This tool measures the number of photons absorbed after it passes through a sample of the material. Lastly, glare can be measured using a 180° fisheye camera. Here the angle and location of the camera itself influence the result, but also that of the light source. It is important to plan the experiment well to limit variations in experimental design.

2.5 Adaptive façades

In spaces where activities comparable to reading, writing or using screens are conducted, shading devices should be provided to reduce visual discomfort. In colder months, solar gains can positively contribute to heating up a room, but in warmer months this works counteractive. Therefore, sunlight should then be restricted by applying solar shading devices or construction other shading elements to a structure. Furthermore, for glare protection, moveable solar protection devices should be applied to be able to adjust a façade element to these personal needs.

The ideal sun shading device is effective, adjustable, low in costs, low in maintenance and aesthetically pleasing. There are many different types developed, each having their own advantages and disadvantages. These devices can be applied outside, inside or integrated in the panel, each position influencing the effectiveness of the shading system.

2.5.1 Assessment sun shading

Glass selectively lets through radiation of different wavelengths. There is high transmission in the visible range, resulting in the transparent quality of glass. The near infrared range up to 2800 nm has a reduced transmission and the long-wave infrared range is impermeable (Schittich et al., 2007). The transmission in the visible range can be referred to as daylight, which has wavelengths ranging from 380 to 780 *nm*. The level of daylight entering the windows determines the illuminance of a room, together with the reflectivity of the interior of the room. It is important to keep in mind that this daylight transmission is a form of energy that converts into heat radiation when absorbed.

Light transmittance, or optical transparency, is a measure of the proportion of visible radiation directly penetrating the glass in the range of visible light (380–780 nm) and is related to the brightness sensitivity of the human eye (Schittich et al., 2007). Light transmittance is expressed as a percentage and is influenced by the thickness of the glass and other factors. The light transmittance should be chosen according to the building's function and the desired internal environment.

For a glass pane, an energy balance can be made for the visible light and solar radiation, see Figure 38. The equilibrium of the energy balance shows that all energy either passes through (transmittance), is turned back (reflectance) or is absorbed by the material and converted into heat (absorptance), which can then be released onto the surroundings.
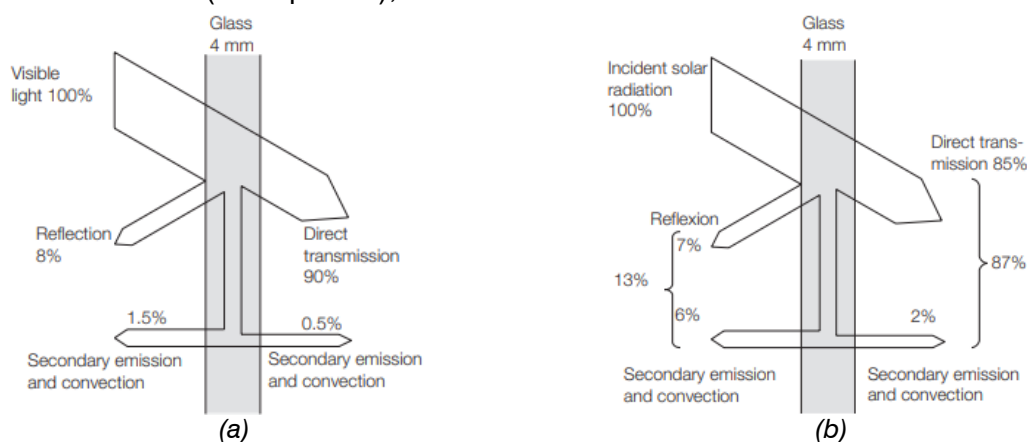

Figure 38 Energy and daylight balance for a 4 mm glass pane: (a) visible light; (b) solar radiation (Schittich et al., 2007)

The *g-value* is the total solar energy transmitted in the range of wavelengths from 300 to 2500 *nm*, expressed as a percentage. It consists of the radiation transmittance and the heat emission from radiation absorbed by the glass in the form of heat radiation plus convection towards the inside, i.e. the secondary heat emission index q_i. When calculating the *g-value* for an insulating unit, the multiple reflections at the various panes of multiple glazing plus the influence of coatings and any gas filling must be taken into account (Schittich et al., 2007).

$$g = \sigma_e + q_i \qquad (11)$$

The total energy transmittance of the glazing is the product of this *g-value* and the reduction factor F_c of the corresponding sun shading arrangement.

$$q_{total} = F_c * g \qquad (12)$$

The above formulae only consider the glass, while in buildings a window system is applied with glass, sun shading etc. The combined solar energy transmittance *g-value* and the convection factor *CF* can therefore be defined as follows (van der Linden, 2015):

$$g - value = \frac{heat\ transmitted\ through\ the\ window\ system}{total\ solar\ irradiation} = \frac{q_d + q_{ci} + q_{si}}{q_{ze}} \qquad (13)$$

$$CF = \frac{q_{ci}}{q_d + q_{ci} + q_{si}} \qquad (14)$$

Here q_d is the direct transmission, q_{ci} is the convection of each element, q_{si} is the radiation of each element and q_{ze} is the total incident solar radiation.

2.5.2 Façade typologies

First, the different properties of façade systems are explained, so that each system can be properly defined using similar terminology. It is important to define the requirements, limitations and potential uses of the systems, to later be able to find the best option for the thin glass sandwich panel. For each system, aspects such as the control mechanism, response time, adaptability, performance, maintenance and costs should be considered when designing a façade system. The effect on the transparency of the panel should also be considered since blocking (part of) the view has an influence on the overall experience of the room and the view out.

Adaptive façades can be distinguished through its ability of actively responding to feedback, defined as *extrinsic control*. This extrinsic control typically consists of sensors, processors and actuators, integrated by a logical control system (Tabadkani et al., 2021). This system can be centralised at a supervisory control system, which groups actuators together and controls them. When the system is decentralised, it has embedded local processors which control the local actuators directly. The system can be designed to allow direct user control or be fully automated.

Adaptive façades can also have *intrinsic control*, often these have smart materials which do not allow feedback. It is a self-adjusting system which is automatically triggered by environmental conditions. The adaptation happens immediately without consuming extra energy, but as a disadvantage this system does not respond to user input.

Active façades can be defined as a system with an integrated active technological system without sophisticated electronics that enable envelopes to self-adjust using internal and external parameters to improve energy savings without user interactions. A *passive façade* is a passive design solution that responds to climate variations as a weather protecting layer of a building to improve the overall interior comfort condition (Tabadkani et al., 2021). Active façades therefore have intrinsic control, while passive façades have extrinsic control.

Biomimetic or bio-inspired façades use plants or the human skin as inspiration. The system can be problem-based, responding to light in phototropism or sun in heliotropism. It can also respond solution-based, which follows the biological principle in combination with a translation system within the façade, for example to generate energy. Biomimetic systems are mostly applicable by using intrinsic material specifications as the actuator to control the adaptation, in which they are limited to respond to ambient conditions within certain thresholds instead of responding to the indoor environment (Tabadkani et al., 2021).

Kinetic façades entail a complex mechanical system in which a certain kind of motion result in the wanted adaptivity. The type of movement can be for example dynamic, retractable, transformable, foldable, expansive or displacive. They can be reactive to the outside environment, for example blocking the sun to protect against glare.

Smart façades have technological functions embedded in the system that involve certain responses to the environmental conditions. It operates by either changing its internal physical properties or external exchanges (Tabadkani et al., 2021). This response can be immediate, transient, intrinsically controlling, selective or local, without requiring external power. Examples are using phase changing materials, photovoltaics or thermochromic polymers.

Intelligent façades can respond to internal and external environments and have the ability to learn and respond in time. It combines an automatic control with the users control and then tries to optimise its performance, taking into account how the user controls the façade. This controlling strategy tries to minimise users' intervention by using predictive models.

2.5.3 External shading devices

External shading devices are placed at the outside of the window, a few examples are shown in Figure 39. Here both static and dynamic solutions are shown. An advantage of a dynamic solution is that during winter, it can be moved away to allow maximum benefit of the heat of the sunlight. It can also help protect the shading device from damage due to weather influences, since an external shading device is exposed to the environment.
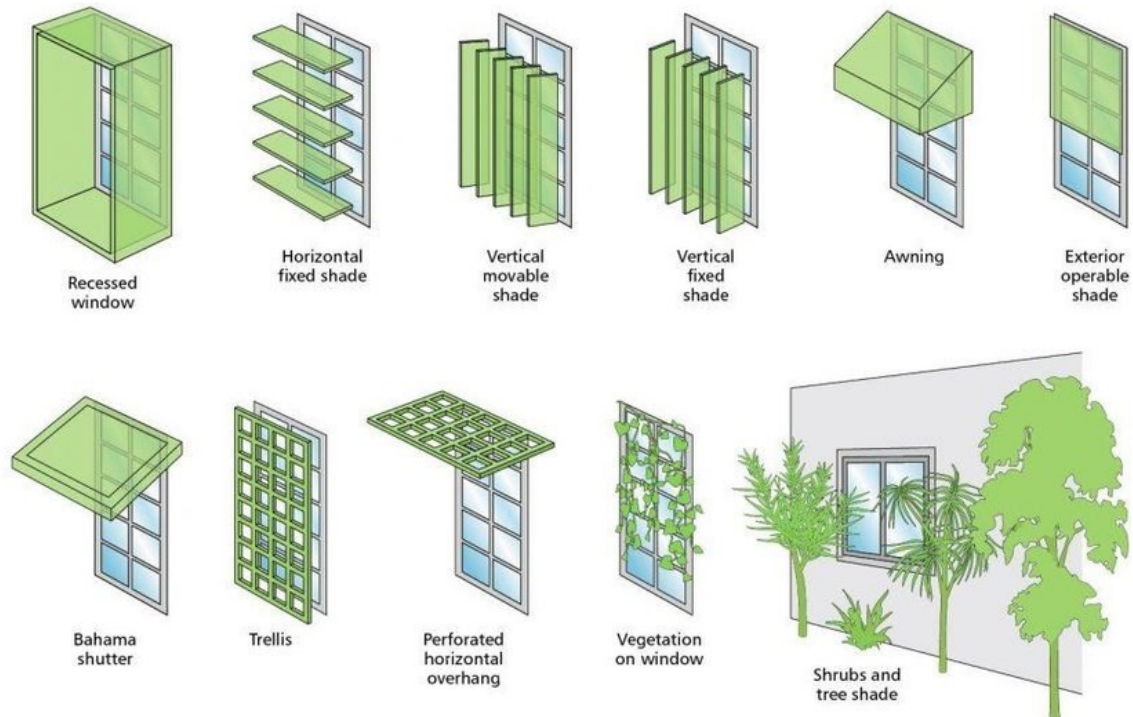
Figure 39 Types of external shading devices (Al-Yasiri & Szabo, 2021)

External shading devices prevent a large part of the sun's rays from reaching the glass and instead reflects them. Another large part gets absorbed by the shades and then released to the outside air through to convection. Any heat from the sun entering the window is due to transmitted radiation. In numbers, a good working external shading device can reach a *g-value* of 0.15 and a *CF* smaller than 0.1 (van der Linden, 2015). The total solar heat entering the room therefore is only 0.15*0.1=1.5 %.

Disadvantages of external shading can be that they limit the amount of ventilation possible on a window, for example it can block the window from opening. Since the shading is placed outside, it is exposed to the weather and can experience wear and fatigue. If the shading is permanent, it will also influence the daylight performance when this is not necessarily wanted. Lastly, the blinds contribute to the overall aesthetics of a building since they are very visible.

For dynamic external shading devices, there have been many different options developed, some designed specifically for its building. Below are a few examples where the architect used the shading devices to create unique façade designs. These can be used as inspiration and show how varied feasible solutions can be.

ThyssenKrupp Quarter Essen, Germany

This active façade system has panels which can rotate 180 degrees, with the two panels combined can move along a full circle, see Figure 40. The lamellas in this system are made from stainless steel and rotate in response to the location of the sun. Because of the shape they can be rotated such that the entire façade is covered, but they can also be 'hidden' in vertical shade elements. This way people inside the building can still look outside without the view being obstructed, see Figure 41.
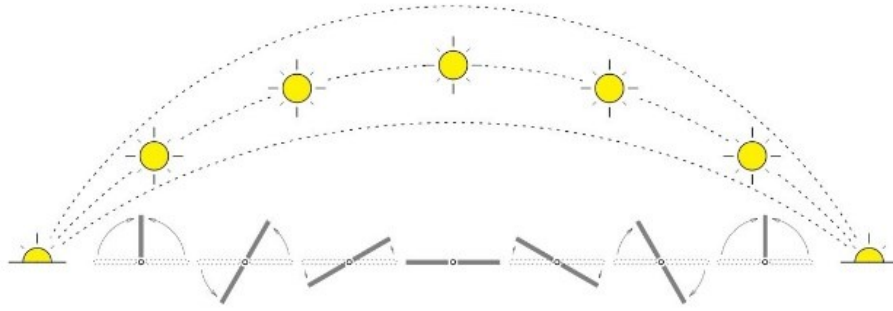
Figure 40 Sunshade diagram (ArchDaily, 2013)
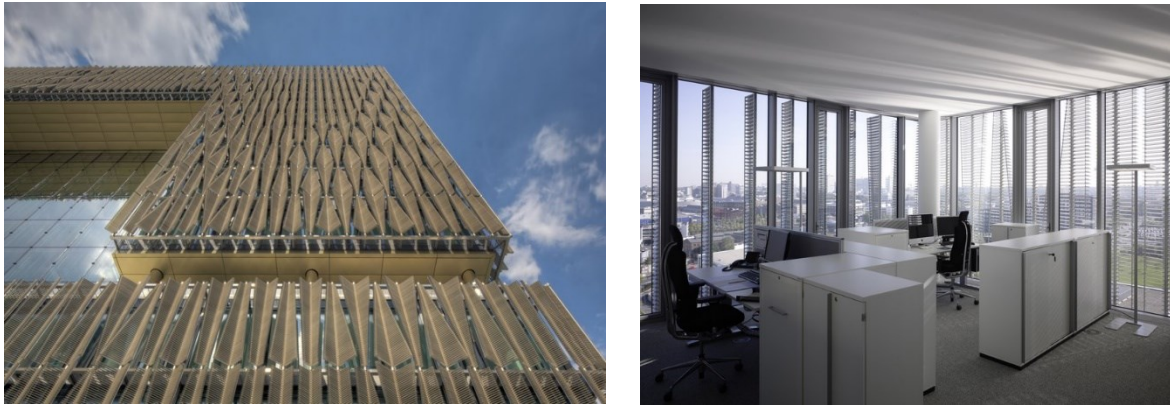
Figure 41 Shading system of ThyssenKrupp Quarter, Essen, Germany (ArchDaily, 2013)

Al Bahr Towers, Abu Dhabi

The façade of the Al Bahr Towers is based on a traditional Islamic "mashrabiya", an architectural element used for achieving privacy while reducing glare and solar gain (Livin Spaces, 2017). The geometry is based on simple triangular origami which can fold in response to the position of the sun, thereby reducing solar gain up to 50 %. The computerised dynamic façade was designed using performance-based technology, where simulations were used to model the sun's path. It is a dynamic system that gives the building a uniquely looking façade.

Figure 42 Shading system of Al Bahr Towers, Abu Dhabi (Livin Spaces, 2017)

42

Institut du Monde Arabe, Paris, France

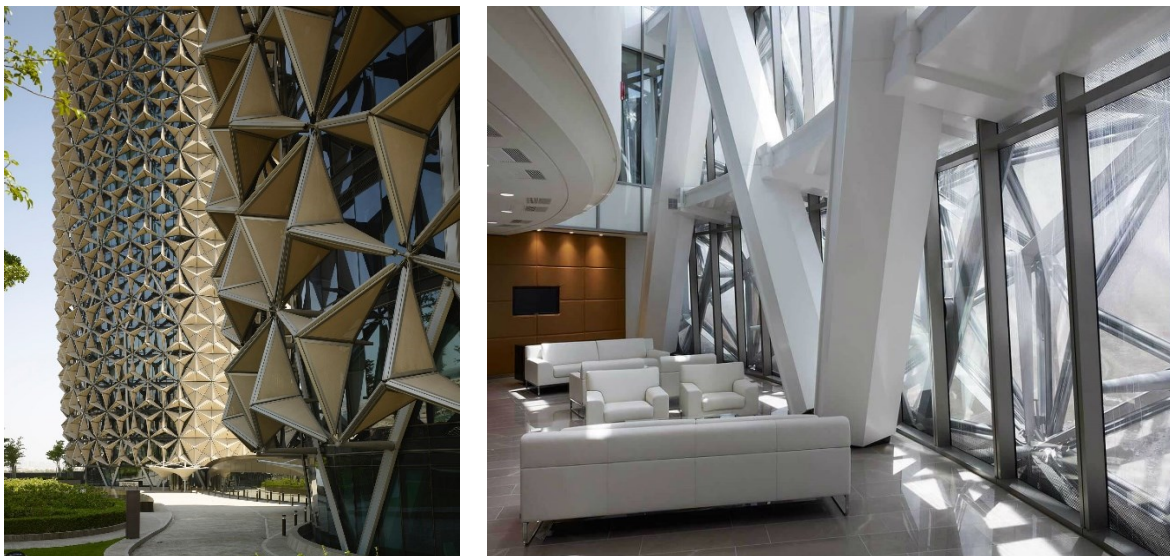The Arab World Institute has a kinetic façade system consisting of 240 mashrabiyas. These have photoelectric cells and mobile apertures which can dynamically control the daylight performance. The mechanism of the cells closes and opens responding to the amount of direct sunlight, thereby controlling daylight and glare. Compared to the other examples, this is a relatively flat design. Many different configurations are possible, Figure 43 shows what one of the panels looks like, with a few possible circular shapes.
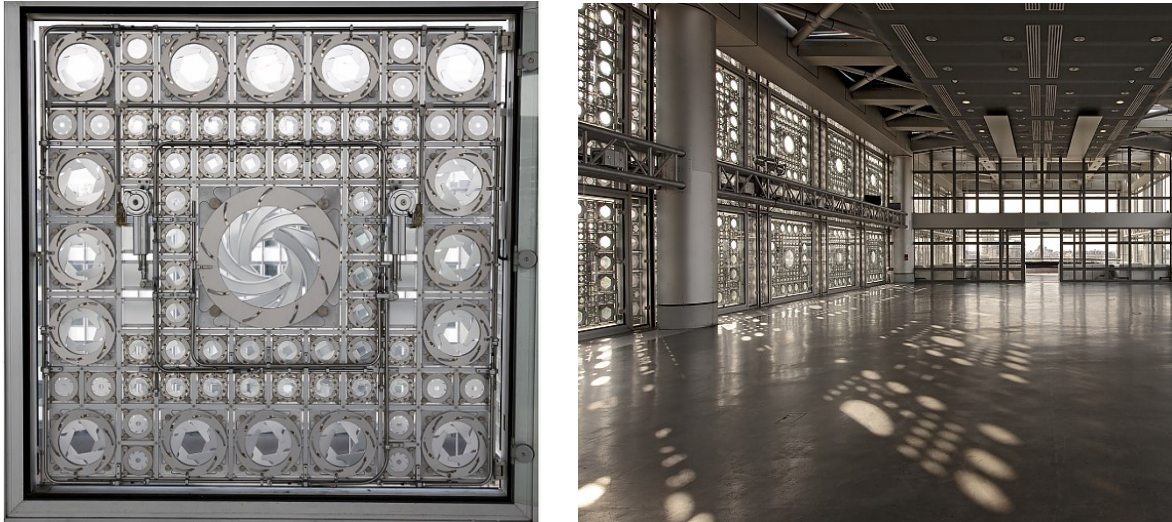
Figure 43 Shading system of Institut du Monde Arabe, Paris, France (Institut du Monde Arabe, 2016)

Simons Center, New York, United States

The façade system used here consists of stainless-steel panels with the same pattern printed on them. When aligned, this creates a pattern with open cells allowing light to come through. When the panels are shifted, they can create an increasingly denser pattern, see Figure 44. Each of the motorised panels revolve around one another on an engineered track defined by the designed components, thereby making it an adaptive fritting pattern.

Figure 44 Shading system of Simons Center, New York, United States (Zahner, 2016)

2.5.4 Internal shading devices

Internal shading devices are located at the inside of a building. Therefore, the glass of the façade is not protected from this shading element and will be exposed to solar gains from the sun. Furthermore, the shading device itself will absorb solar heat and then give of heat through convection to the inside air and heat radiation. The shading 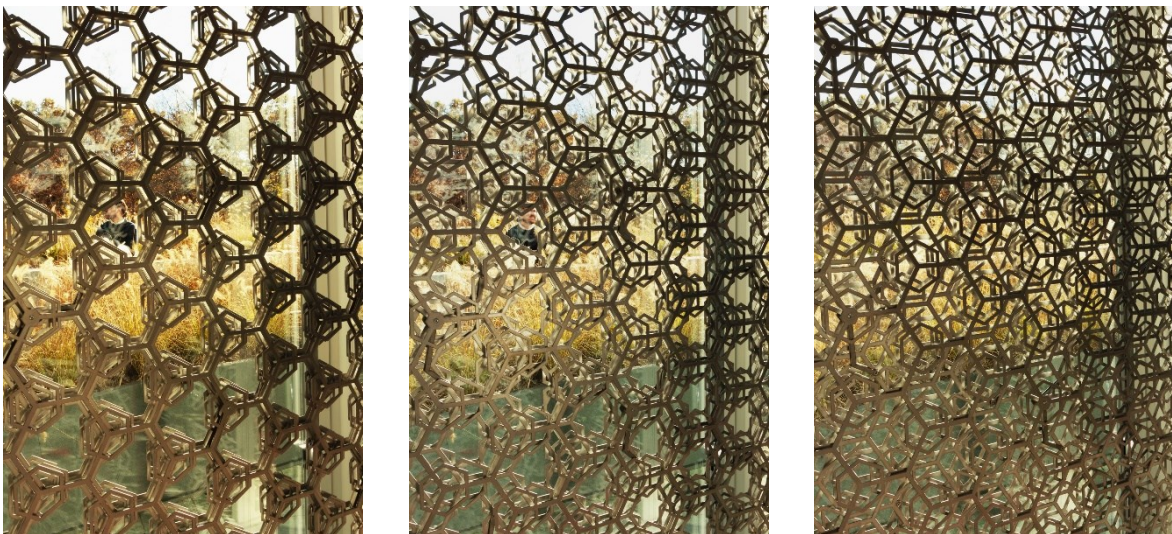device only works for blocking glare and limiting daylight. The resulting *g-value* will therefore not be more than 0.4, while also having relatively high *CF* values (van der Linden, 2015).

Internal shading devices can be used when external shading is not possible, for example in renovated buildings. A main advantage is that the device is protected from weather influences and can therefore be much cheaper. Common examples are lamellas or curtains (possibly with a reflective layer).

2.5.5 Integrated shading devices

The shading device can also be integrated in the façade panel itself, where it is placed in between the two outer glass panes. First, a solar control coating can be used to largely reflect the UV and (short wave) infrared parts of the solar spectrum while letting the visible light pass through. These surface coatings with thicknesses of 0.01−1 μm reduce the emission level of the glass to ε = 0.01-0.05, whereas uncoated glass has a high emissivity of ε = 0.84. The position of the coating creates various refractive effects, or it can release the absorption gains inside the room or to the outside, depending on the direction of the radiation.

For applying coatings there are two processes, on online and offline process. The online process is for the hard, pyrolytic coatings and uses Chemical Vapour Deposition (CVD). It is typical for thermal control coatings, as it is designed to maximise solar heat gain into a building, thereby creating the effect of passive heating (Louter, 2022). The offline process is for soft coatings, using the Magnetron Sputter Vacuum Deposition (MSVD), where the coating is applied in a vacuum chamber at room temperature.

Apart from coatings, a full device can be integrated inside the panel. These devices can have shape changing, colour changing or moving elements to allow a change in the open-close ratio. Furthermore, the angle at which the light is reflected can be influenced, by for example curving the reflective material. Below a few examples are shown of integrated shading devices.

Smart façade systems

There have been many smart façade systems designed which focus on optimizing its performance. There are many different types with different main focusses, for example some panels can generate energy or focus on optimizing the effect of the heat generated by the sun.

The first example is a prototype system developed by TNO called SunSmart technology, see Figure 45. Here the panel can block the heat from the sun when outside temperatures are high. But when the temperature of the window falls below a certain value, the heat can be admitted through the panel. This is done by blocking the infrared part of the light spectrum, but still allowing the visible light through the window, thereby staying transparent. The switch happens automatically and is part of the laminated glass. This allows for no extra installation requirements of the panel.
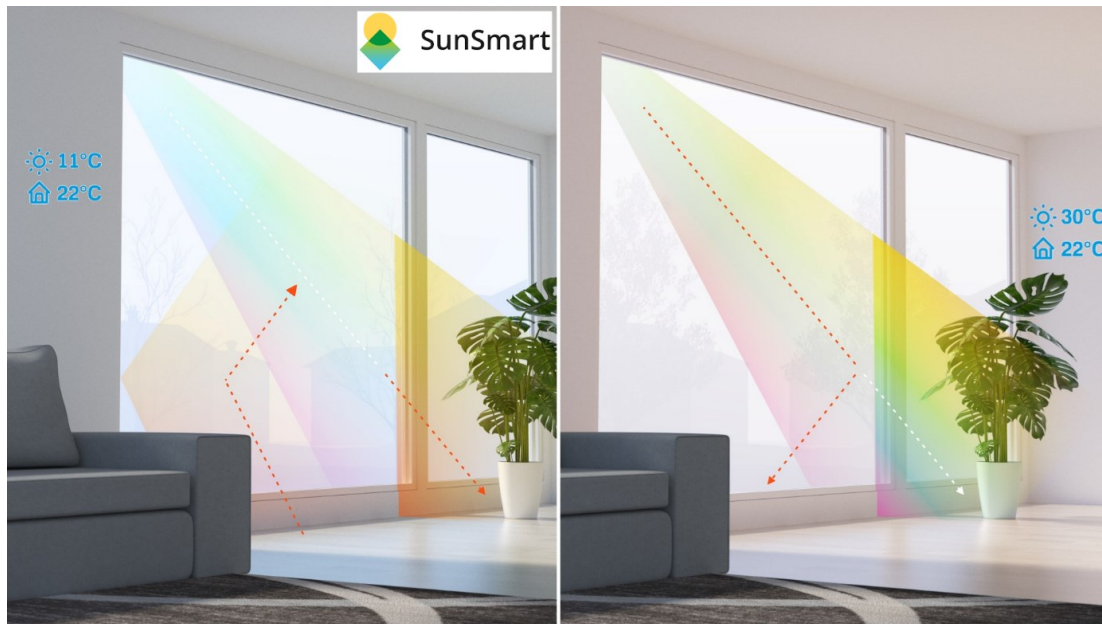
Figure 45 Window developed by TNO using SunSmart technology (TNO, 2022)

Adaptive foil façade system

This system uses ethylene-tetrafluoroethylene (ETFE) foil instead of glass as a double-skin façade. By making it switchable, it can moderate daylight and the internal light distribution by actively responding to weather conditions and solar light intensity. A study by Flor et al. (2022) showed that employing this switchable system resulted in an increase in useful daylight illuminance and an increased resistance against glare.
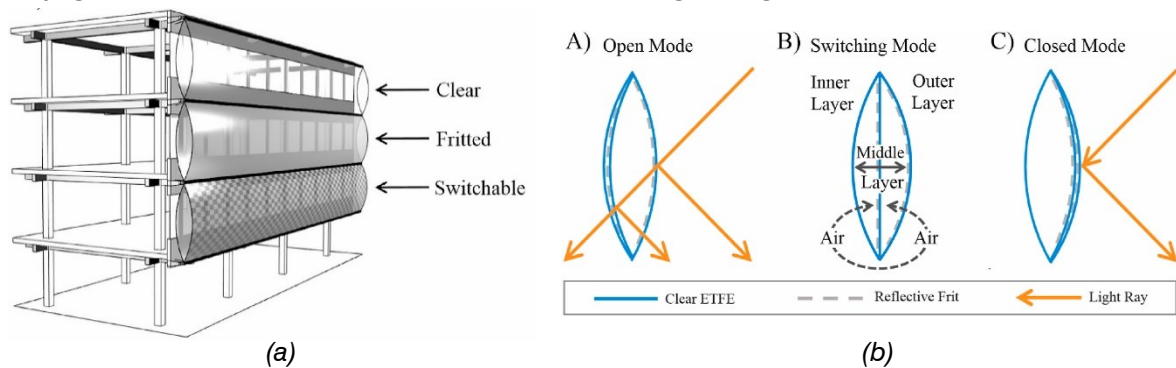
Figure 46 (a) Visualization of a building structure with a double-skin façade with different ETFE foil types; (b) light transmittance and reflectance of a switchable ETFE cushion (Flor et al., 2022)

Homeostatic façade system

This system consists of a line maze with a material that can bend similarly to a muscle. This way it can change its own shape in response to solar influences. This system directly responds to the environmental conditions with no computer programming necessary. Therefore, it has a clear advantage over computer-controlled systems since it requires less electrical power and can respond locally to incoming sunrays.

This shape changing material is an elastomer wrapped over a flexible polymer core. The elastomer is covered in a silver coating and can distribute and electrical charge across its surface, causing it to deform, see Figure 47. The silver layer also reflects light, further contributing to the solar control.

45
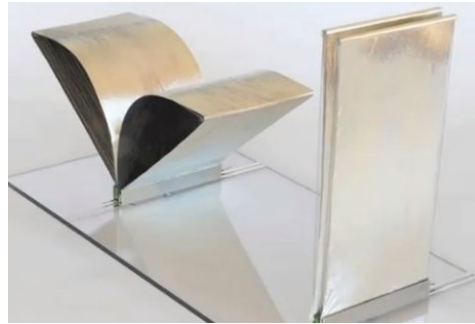
Figure 47 Homeostatic façade prototype (Minner, 2011)

Breathing skins

This prototype developed by Tobias Becker is based on the concept of breathable skin. Inspired by the pores in our skin, he designed a façade that can adjust its permeability by increasing or decreasing the size of the cells placed inside the glass panel. The channels can be compared to pneumatic muscles that can collectively inflate to control the light and visibility properties of the panel.

For the core of this panel, only a light under pressure is needed to open each muscle. Therefore only a small amount of energy is needed to operate this system, while not needing any visible technical components (Doroteo, 2016). This sophisticated yet simple innovation allows the façade to be free of any visible technical components, providing a sleek and seamless finish.

Figure 48 Breathing skins façade prototype (Doroteo, 2016)

2.6 Dynamic systems

As seen in chapter 2.5 Adaptive façades, there are many different types of façades, with a few systems highlighted there. Many of these take inspiration out of the adaptability of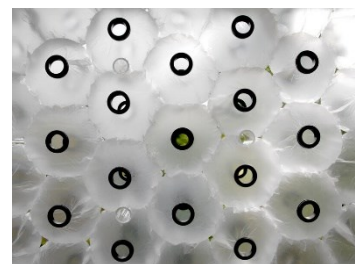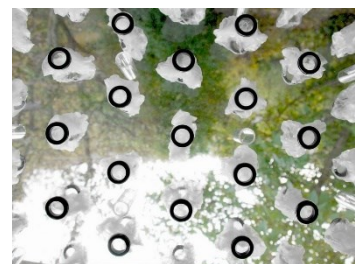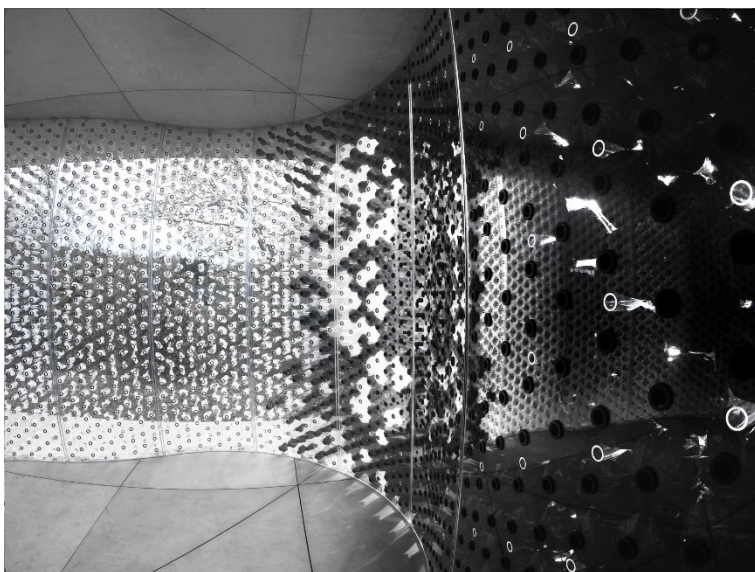 nature, trying to design a system including adaptive elements that can change function and configuration responding to the physical requirements. The aim of this chapter is to dive deeper into different possible technologies for the dynamic aspect of the façade.

2.6.1 Curved-line folding

Curved-line folding is the act of folding a material along a curved creased pattern to change the three-dimensional shape. This folding mechanism consist of a bending element (elastic deformation) and folding element (plastic deformation). The stored elastic energy can then be used to reverse the deformation and return the material to its initial state. Curved-line folding has the potential to transform a one dimensional actuation into a three dimensional deformation, see Figure 49 (Tabadkani et al., 2021). This does require a material that has the required flexibility to ensure an elastic deformation, while still providing enough stiffness to manage external forces.

Figure 49 Curved-line folding with three and two curves (Tabadkani et al., 2021)

The major design challenge of using curved-line folding, is deciding on the number of bending lines, the location and the wanted resulting shapes. Table 12 shows various types possible with changing the crease patterns. These are all symmetrical systems, allowing for an easier control and design of the system. When using an asymmetrical system, the adjacent surface areas, actuation forces and/or moments also become asymmetrical, significantly increasing the complexity of the whole system.

Table 12 Various types of crease patterns which generate a bending-active kinetic system (Vergauwen et al., 2014)

Number of creases:		2	3	4
Reflection	Concave			
	Mixed			
	Convex			
	Inflection point			
Translation	Inflection point			
	No inflection point			

It is also important to take the length of the crease and the thickness of the material into account, referred to as the length-thickness ratio. According to experiments done with small scale polypropylene models by Vergauwen et al. (2014), the higher the stiffness of the material, the higher the actuation force necessary to make the bend. When the length-thickness ratio exceeds 400, the system loses its reversibility, because the elastic energy stored is not enough to return to its initial state. A length-thickness ratio below 300 however has a low stiffness. Therefore, this research recommends a ratio between 300 and 400 for creating a good balance between stiffness and needed actuation forces, while allowing the structure to be reversible.

2.6.2 Smart materials

The dynamics within a panel can be a movement of elements or a material deformation. The movement can be a translation and/or a rotation, which can be in or out of plane direction. The curved-line folding technique is an example of such a movement of elements. A material deformation can be self-changing, due to temperature or humidity, or it can be from an external input, like electricity or a fluid. Therefore, it is referred to as a smart material since it can activate itself.

Many smart materials are inspired by nature, where the way they move or react is similar to for example how a flower responds to sunlight. Plants show a vast variety of movements, which is responsive to the environment and typically shows only elastic deformation. This results in them being less vulnerable to fatigue since there are less stress concentrations.

A technique inspired by passively actuated plant structures, uses a multi-layered structure to control the timescale of its change in shape. The functional bilayers that influence this timescale are 3D-printed using a hygroscopic bio-composite filament that shrinks and swells depending on its moisture content, and a hydrophobic thermoplastic polymer that restricts movement and blocks the surface area from being exposed to water (Tahouni et al., 2021). The layers of the full material consist of a blocking layer, restrictive layer and active layers, see Figure 50a. The active layers are oriented perpendicular to the bending direction since the major expansion and shrinkage occurs perpendicular to the printed path. The restrictive layer is oriented along the bending direction, while the blocking is again perpendicular to the bending direction. This limits this layer from affecting the overall stiffness of the material.

The timescale of the bending process can be influenced by changing the number of layers, see Figure 50b. Here the additional layers slow down the movement process, where these sections bend later, see Figure 50c.

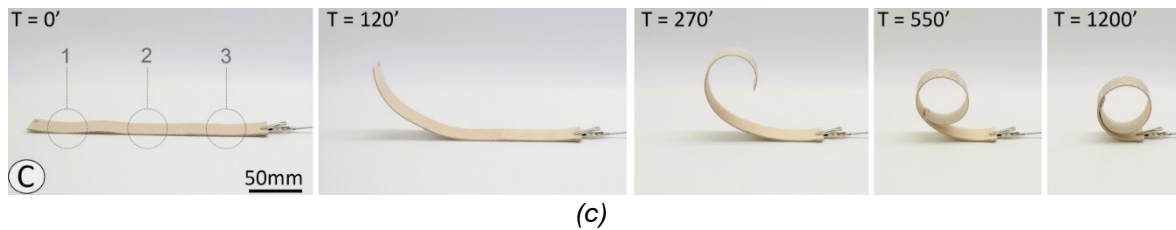*(a)*   *(b)*

(c)
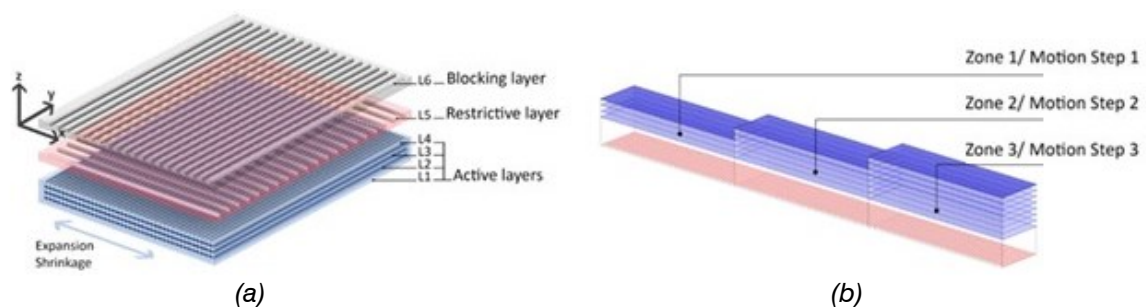
Figure 50 (a) Schematic of the multilayered structure with layers for actuation, mechanical restriction and permeability regulation; (b) schematic of zones creating different timing of movement; (c) time-lapse images showing the multi-stage self-shaping process in minutes. (Tahouni et al., 2021)

The bending mechanism can also be applied to different initial shapes, thereby also changing the resulting shape. Figure 51 shows how this technique can be applied in a shape that resembles a flower. Here each leaf is programmed to bend at its own time, therefore resulting in the movement sequence shown.
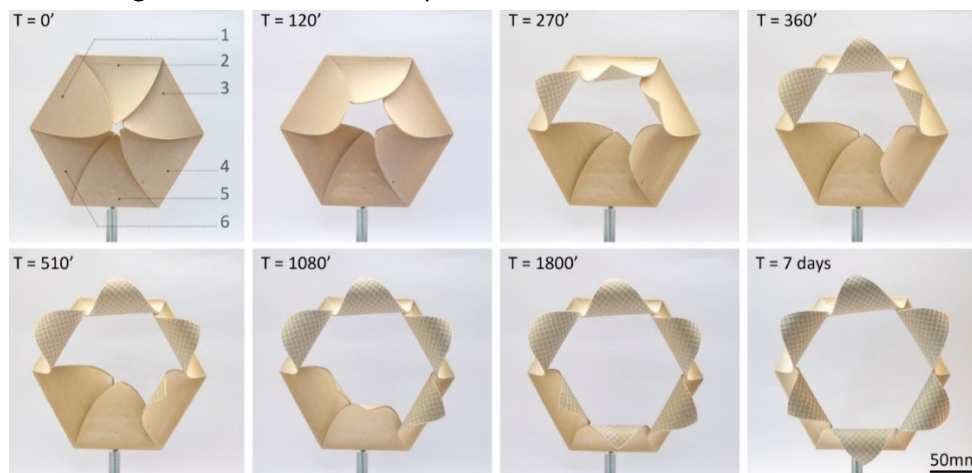

Figure 51 Timelapse of prototype printed with sequential motion programmed per element (Tahouni et al., 2021)

The example above showed a shape memory material actuated by time. Shape memory materials include all materials able to hold the deformed shape until a stimulus is applied to return to the initial shape. This stimulus can be a property of the material itself, or an externally generated stimulus, for example an electric current. Shape change materials work similarly, but these can also accept a feedback loop to respond properly.

The stimulus of a material can be an electric current, but it can also be an intrinsic property of the material itself. These can be divided into four main areas, light, temperature, humidity and chemical adaptive materials.

Light adaptive materials

The first response mechanism to discuss is the light adaptive materials. These can be light responsive polymers that can deform temporary under certain light conditions. This works similarly to a flower that opens during the day and closes at nighttime. For a façade system this can be used to control glare or limit daylight, by designing the material to respond to a certain level of light. The main advantage is that this system functions wireless and without an external control system.

A Photochromic dye can also be added to a façade to reversibly change its colour when exposed to a specific range of ultraviolet light (Tabadkani et al., 2021). This could also be designed to turn colourless when ultraviolet light is absent. An example whit a light adaptive material was done in the research of Zhang et al. (2014), where a polymer was attached to

a single-walled carbon nanotube (SWNT) resulting in a large and fast (0.5 s) deformation, see Figure 52. By turning the light on and off, a quick deformation can be achieved, where the shape and placement of the actuated material can determine the resulting shapes.
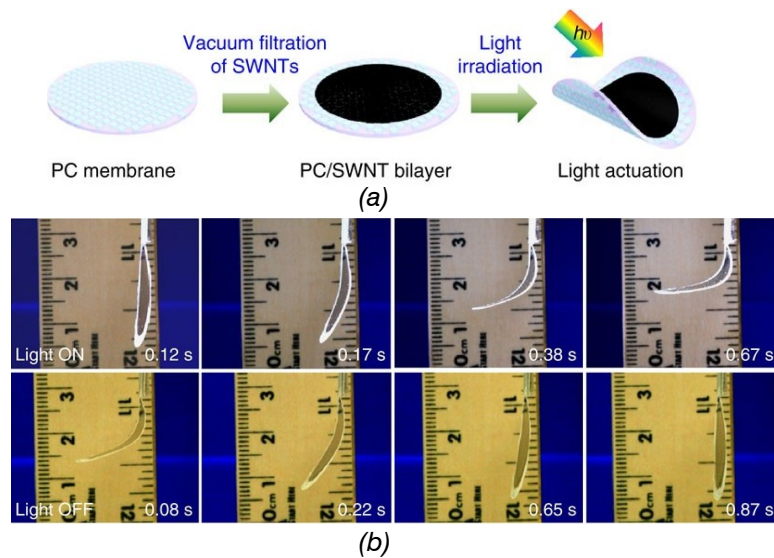

(a)

(b)

Figure 52 (a) Schematic illustration of polymer with single-walled carbon nanotube (SWNT) layer attached; (b) series of optical images showing the light-actuation process (Zhang et al., 2014)

Temperature adaptive materials

Temperature adaptive materials can be thermo-bimetal materials which deform and curve or thermo-expansive polymers that can expand in response to temperature changes, this process is shown in Figure 53a. Thermochromism materials don't change their shape but their colour in response to temperature changes. An example of a thermally induced shape-memory effect is shown in Figure 53b, where the material is heated to 50° C. Within 10 seconds it returns to its initial shape, without showing plastic deformations.

(a)

(b)
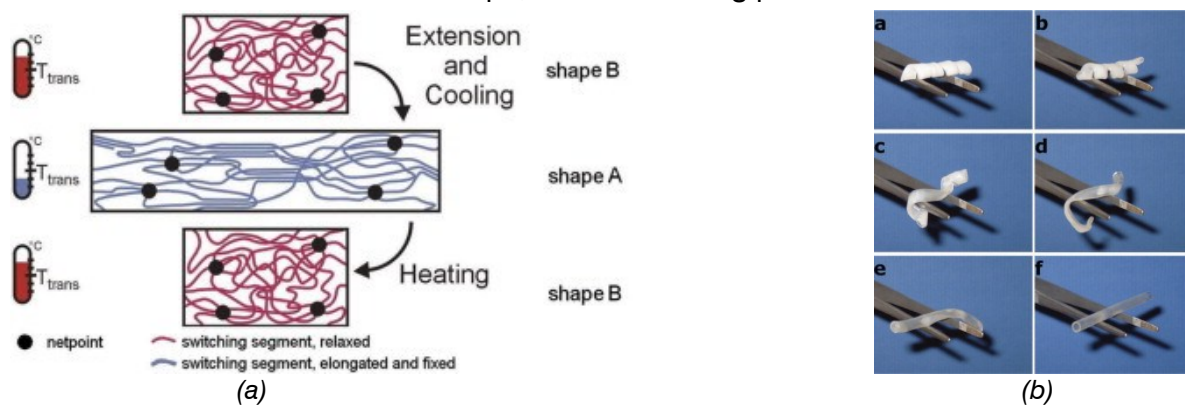
Figure 53 (a) Molecular mechanism of thermally induced shape-memory effect, where T_{trans} is the transitional temperature (b) time series of 10 seconds at 50° C to return to its initial shape (Behl & Lendlein, 2007)

Humidity adaptive materials

Humidity adaptive materials are based on biobased materials since the cellular structure seeks to keep the right moisture balance by continuously changing its dimensions. An example in nature is the pinecone, which can close itself in response to moisture and

humidity in the air. The example shown in Figure 51 works based on humidity. Here the moisture content of the material gradually changes over time, resulting in the movement. This example spans a long duration, but much quicker responses can be made as well.

Chemical adaptive materials

Chemical actuations convert chemical gradients into movement. In nature, this adaptation is largely in response to changes in the environmental conditions. However, it can also be in response to osmotic pressure of an insect landing on a flesh-eating plant, as seen in the Venus flytrap. For synthetic materials like polymers, the chemical adaptive actuation acts in the form of anisotropic swelling. Designing the molecular orientation can influence the direction of this actuation.

Electric activated materials

Using an electric current as the activator of a shape memory material allows for mechanical control of the system, it can be changed on demand. Opposed to the intrinsic activators, this system allows for manual control. This allows the occupant of a room to adjust the façade when wanted, which enriches the experience of the space significantly.

There are several types of electrical activation, like the field-driven actuation. This requires a high voltage of up to 1000 V. Another type is using electrochemical ionic actuators, which are capable of using a much lower voltage, staying below 10 V under a wet electrolyte environment (Li et al., 2015). Current-driven electrothermal actuators (CNTs) require a low voltage but can also be used in a dry environment without an electrolyte. This makes them an interesting actuator to use in generating movement in a material.

An example using these CNTs together with a heat resistant polydimethylsiloxane (PDMS) layer is shown in Figure 54. The CNTs provide anisotropy in both the electrical conductivity and the movement, where the cutting angle determines the resulting bending, see Figure 54b-e.
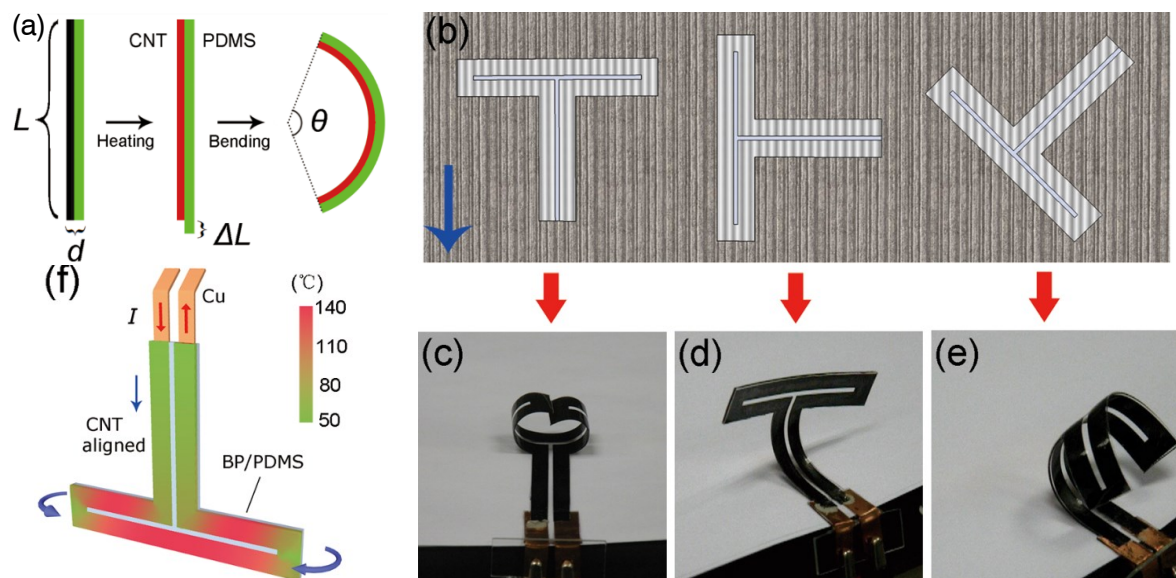

Figure 54 (a) Schematic illustration of electrothermal actuation mechanism for CNT-PDMS double-layer ETA; (b-e) three ways of processing T-shaped BP electrodes and how these deform; (f) schematic of temperature distribution under current heating of (c) (Li et al., 2015)

2.6.3 Soft material robotics

The examples shown for the smart materials have mostly been two-dimensional, thin materials. Soft material robotics allows for many different configurations of materials and making many different three-dimensional shapes. Soft materials further increase the possibilities of movement opposed to rigid materials, since these can also greatly expand in size. The soft materials used can be smart materials, where they have an intrinsic actuating property. External actuators are also often applied, which allows for manual control.

The soft material robotics often take inspiration from biomimetic systems. It requires an integration of sensing, passive mechanics, active movement and control. Soft robotics are composed of easily deformable materials with similar elastic and viscoelastic properties to soft materials that occur in nature. These materials typically are silicone elastomers, urethanes, hydrogels, braided fabrics, hydraulic fluids and gasses (Coyle et al., 2018). The low stiffness of these materials results in elastic deformation when a force is applied and no plastic deformations.

Silicone elastomers are often used in applications that involve a high cycle loading, since they provide a high elastic resilience. When a more viscous material is required, soft polyacrylates can be used in dielectric elastomer films, which is able to achieve large strains and a high electrical field in stretched position (Coyle et al., 2018). Figure 55 shows the relation between the time-dependent viscosity (Loss Modulus G) and the elasticity (Storage Modulus G) for various soft materials.
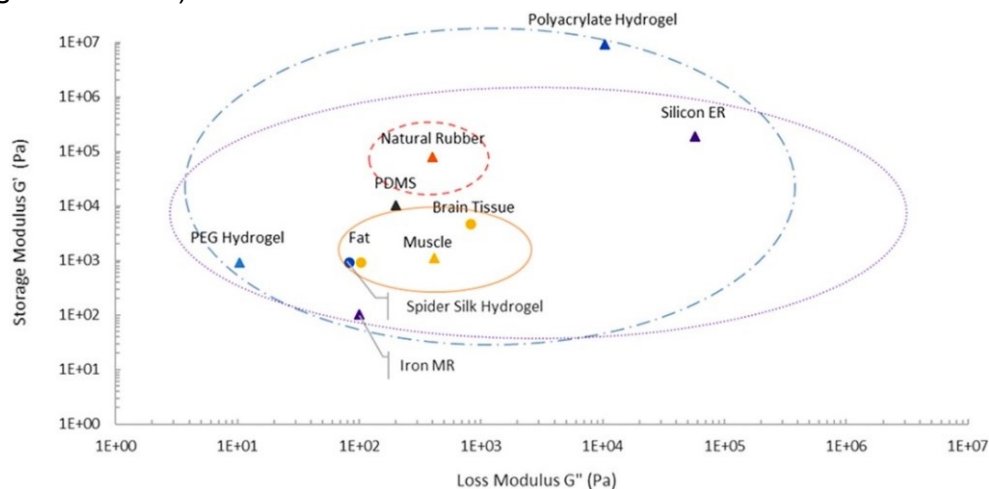
Figure 55 Approximation of Storage Modulus vs. Loss Modulus of various organic and inorganic materials (Coyle et al., 2018)

The fracture toughness is an important property of soft materials, since the elastic strain limit is susceptible to inhomogeneous deformations, like cracks or other stress concentrations. Hydrogels can be used to increase the fracture toughness of a material, by integrating it into the material. This can be done by ionically and covalently crosslinking the network.

Lastly, the work energy density relates the compliance of materials with its energy density. This value estimates the volume of material required to perform its task, where a higher density results in less volume needed. This value is also related to how the soft robotic is shaped, where there are many different actuating systems available. Figure 56 shows four common approaches of how soft robotics can be applied.

Figure 56 Common approaches to actuation of soft robotics in resting (left) and actuated (right) states (Rus & Tolley, 2015)

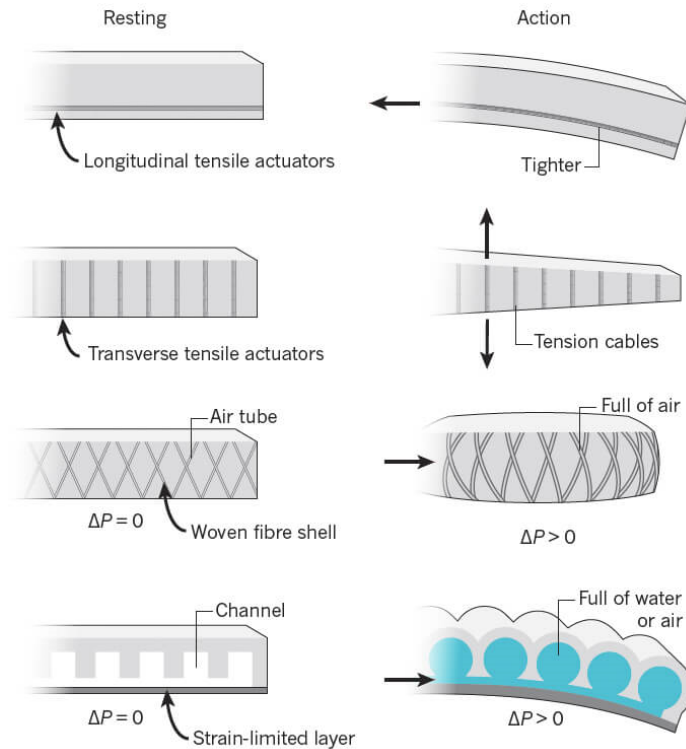A soft material robot usually consists of the soft material and an actuator to control the movement. The longitudinal, tensile and woven actuators shown in Figure 56 help guide the movement, constricting the movement into the wanted directions. The movement can also be guided by varying the stiffness of the material. Then, the actuation can be generated by tensioning the actuators, or by inflating the channels with a fluid. It is important to think about the systems possible vulnerabilities, like damage to the fluid coverings, a low structural rigidity or degradation of elastic resilience due to material fatigue (Kim et al., 2023).

Modelling the kinematics and dynamics behaviour of soft robotics can be challenging because of its non-rigid nature. Theoretically speaking, the activated shape of the robot can be described using continuous functions. However, these continuous functions can be difficult and complex to model properly. Often a simplified assumption is used to model the kinematics, leading to the piecewise constant curvature (PCC) model (Rus & Tolley, 2015). This method models the movement, but the actuation space, especially with inflatable actuators, needs additional methods. These are robot specific and developed to model the morphology of the specific robot. Examples include the use of Bernoulli-Euler beam mechanics, or by defining a relation between the joints and curvature arc parameters (Rus & Tolley, 2015).

Inflatable soft robotics

The shape of the soft robot can be specifically designed for the required movement or change of shape. The location of restricting layers, the thickness of each element and the stiffness of the materials used all contribute to the possible shapes. Wang (2023) investigated different configurations of an inflatable module, see Figure 57. By changing how the sample is connected, the resulting shape after inflation can be controlled.

Figure 57 Sample swelling testing and morphology detection of inflatable module, the patterns used respectively none, central, average, average central, periphery and one-sided (Wang, 2023)

The actuated shape can further be controlled by designing folds into the material, as was done in the research of Digumarti et al. (2017). Here a soft robot was designed inspired on the euglenoid shape, see Figure 58. By placing the folds under a certain angle, four states of actuation can be created, namely vacuum, neutral, axially stretched and ballooned out.

The research looked at the influence of the folding angle on the pressure needed to inflate. In varying the half angle from 15° to 45°, it showed that less pressure is needed when the angle is reduced. The prototype of Figure 58b also shows the possibility of creating different segments, which can be inflated separately.

(a)   *(b)*
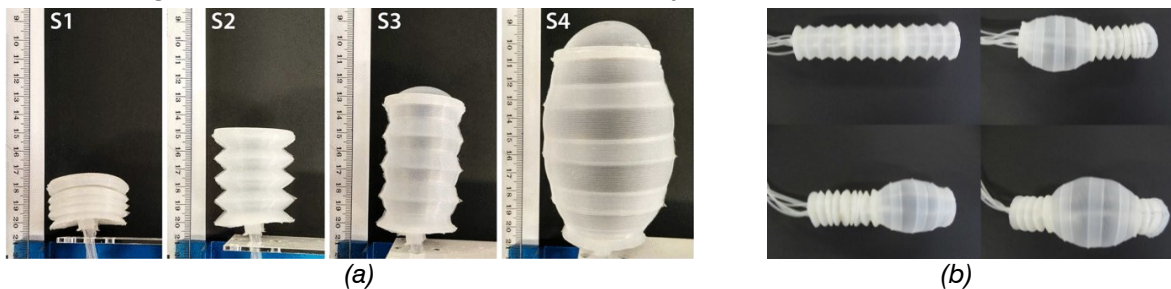
Figure 58 Euglenoid-inspired soft robot; (a) four states of actuation, S1 is vacuum, S2 is neutral state, S3 stretched axially, S4 ballooned out; (b) three segment robot that resembles euglenoids (Digumarti et al., 2017)

The technique of using inflatable soft robotics has also been applied in the topic of adaptive façades. Below, two prototypes developed with soft robotics are shown, resulting in a pneumatic façade system. The first system uses a thermochromic silicon actuator, which can control sunlight, ventilation and regulate temperature within its double skin building façade, see Figure 59. The thermochromic dye on the actuators responds to the ambient temperature and can change its level of transparency, thereby controlling the daylight performance of the panel. The magnetised silicon seals the soft actuator within the curtain wall system and helps control the ventilation of the system (Zarzycki, 2018).
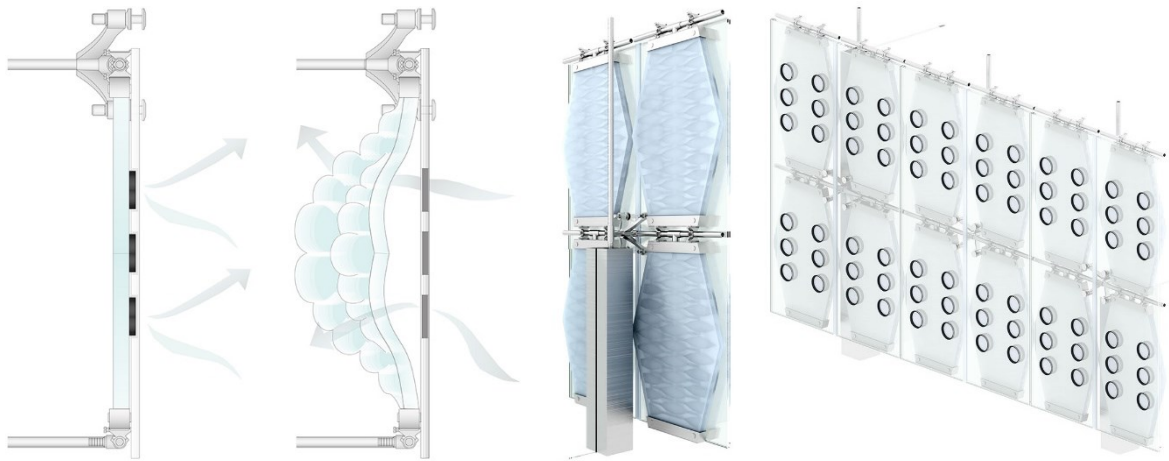
Figure 59 Pneumatic double-skinned façade system by Zarzycki (2018) that controls sunlight, ventilation and temperature.

The next façade system uses a hybrid soft robot actuator in combination with a fabric membrane. The prototype developed by Kim et al. (2023) uses a gripper-shaped pneumatic elastomer actuator in combination with a shape memory alloy (SMA) spring to curve a fabric membrane. The SMA allows the membrane to snap back into the initial position after the system is activated.

Figure 60 Parts assembly and system operation scheme of hybrid soft robot actuator with fabric membrane (Kim et al., 2023)

2.6.4 Textiles in robotics

Another method that is yet to be discussed is the use of fabrics to create adaptive materials. Machine knitting can rapidly produce textiles which are breathable, flexible and lightweight. The fibres used in the textiles can vary greatly, each with their own strength, stretchiness, thermal resistivity, electrical conductivity, tendency to felt, solubility, and colour and surface characteristics (Albaugh et al., 2019).
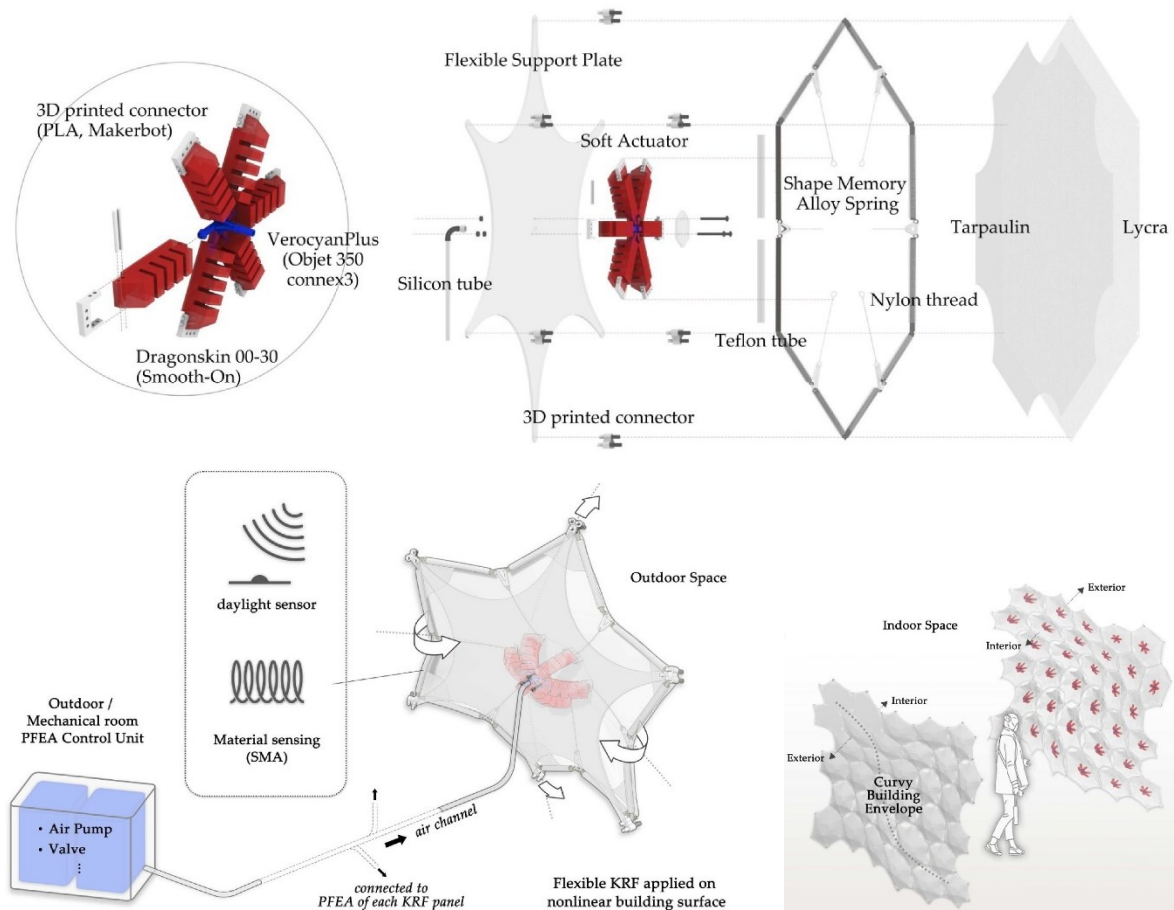
Textiles have the potential to be applied in many different functions, see Figure 61 for the main classifications of textiles in soft robots. The geometry of the textile can be categorised starting with one-dimensional fibres to full three-dimensional braids. The method of connecting the fibres determines the strength of the material, which can provide a high tensile strength. Active textiles can sense, react and adapt based on given input, similarly to actuators in soft material robotics.
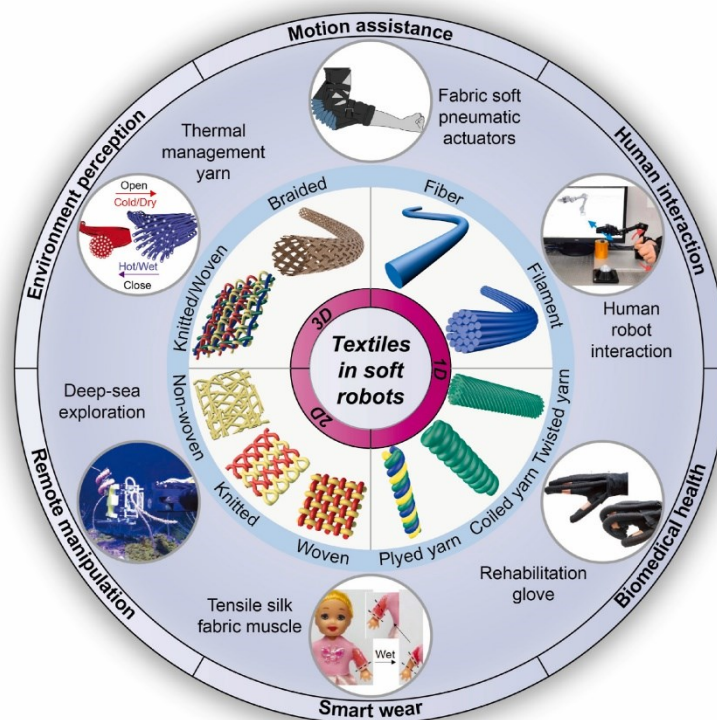
Figure 61 Classification of textiles from the perspective of structural dimensions and application demonstration of textile-based soft robots (Fu et al., 2022)

For knitted actuation design, there are three different methods to apply in machine knitting, see Figure 62a. The first method is by placing actuatable tendons in the fabric, this can be placed horizontally, vertically or diagonally. The different placements result in different actuated movements of the fabric, a combination can be used as well to create more complex three-dimensional shapes. Secondly, basic shapes can be used to shape the robot. By using additional techniques like introducing short rows or increasing/decreasing stitches, the final shape can be further modified. Lastly, an anisotropic texture can be created by alternating knit stitches. The main stitches available in machine knitting are the knit stitch, purl stitch or garter stitch. These can be combined in a pattern to create the wanted texture, or to better control potential curling of the fabric (Albaugh et al., 2019).

Figure 62 Knitting machine strategies (Albaugh et al., 2019)

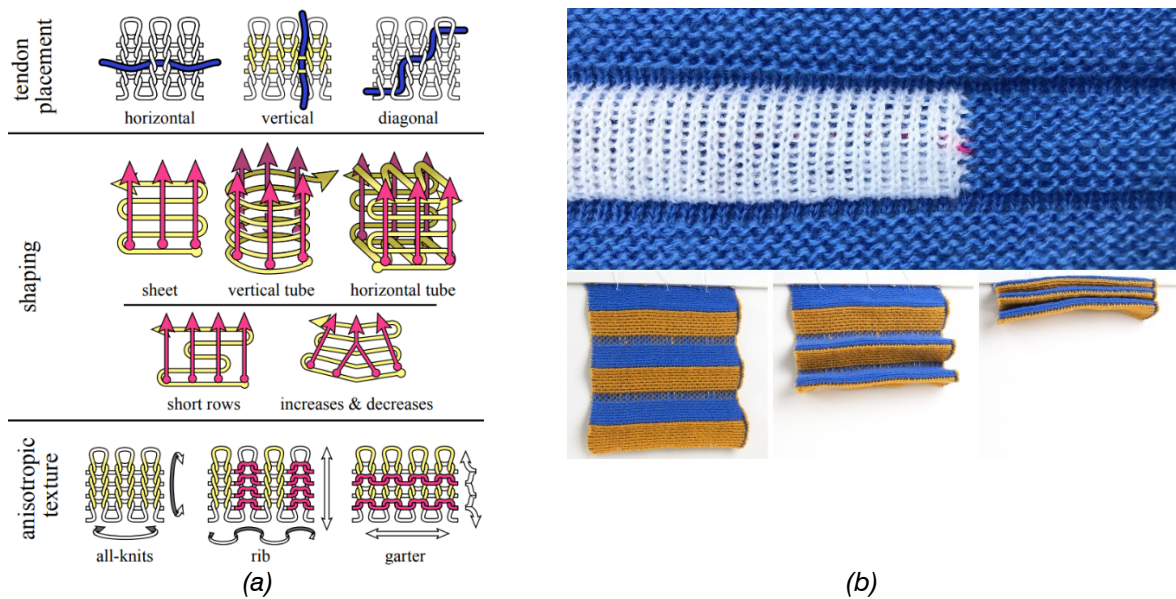An example where the anisotropic texture was used can be seen in Figure 62b, where an alternating knit/purl pattern was applied to create hinges in the material. By adding vertical tendons in the fabric, the actuated folded state can be created. These different methods can also be applied in façades. Below a few examples of adaptive façades using fabrics are shown.

Bimetallic Eye (Fabric + Bimetal)

This façade from Auer et al. (2019) uses a textile to stretch over a window opening, thereby controlling the transparency. Thermo-sensitive bimetallic strips are woven into the textile surfaces, responding to the ambient temperature. The strips are made of an active Iron-Nickel-Manganese alloy and a passive Invar layer, which bend the metal strips due to a difference in the thermal expansion coefficient of these two metals. An increase in temperature expands these strips, thereby also expanding the fabric. The fabrics are placed in a double concave and double convex curved frame, together being able to fully cover a rectangular surface in activated state. These are then hanged up at three points, see Figure 63.
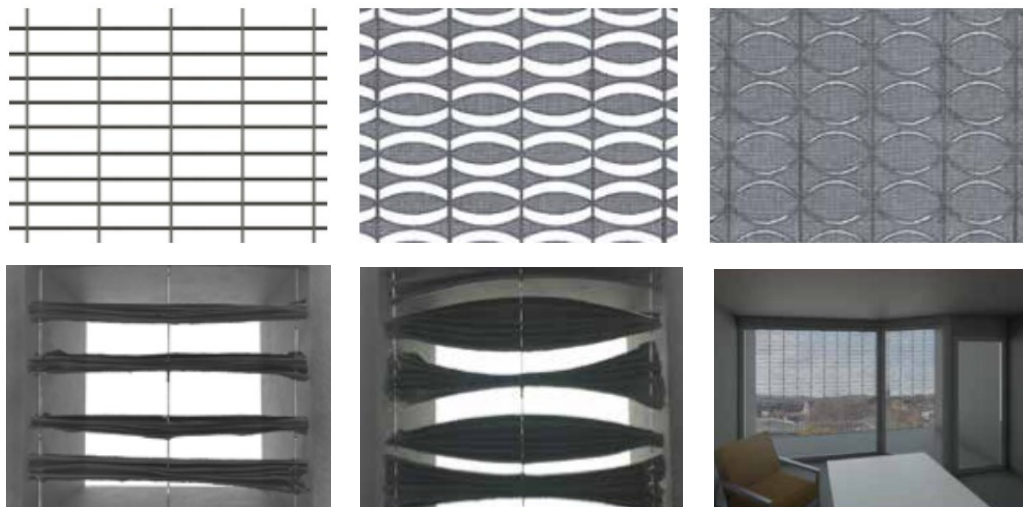

Figure 63 Bimetallic Eye façade, combining a fabric with bimetallic strips (Auer et al., 2019)

Hexagonal Façade (Fabric + SMP)

This façade developed by Auer et al. (2019) uses hexagonal openings to let in light. The surrounding area is made from elastic textile, which can be stretched over the whole surface. The hexagonal openings are made with shape memory polymers (SMP) hinges that can deform to create a closed rectangle, see Figure 64. The polymer is thermoplastic, closing once the temperature exceeds 60 °C.
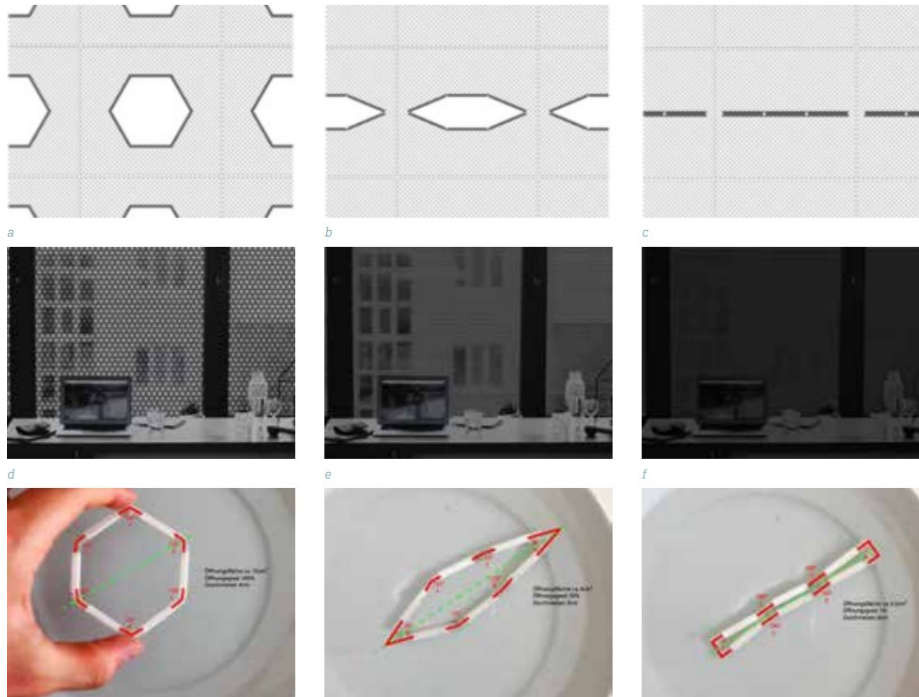
Figure 64 Hexagonal façade with fabric and shape memory polymers (Auer et al., 2019)

Pneumatically Actuated Origami Sun Shading

This prototype developed by Eisenbarth et al. (2021) uses a textile in combination with origami, see Figure 65. The folding geometry is inspired by the "Starshade" geometry developed by NASA, which is characterised by a high difference between its open and closed state. After optimizing its shape, it is connected to a pneumatically actuator creating an adaptive façade. The system can be activated locally, therefore better controlling daylight and glare.
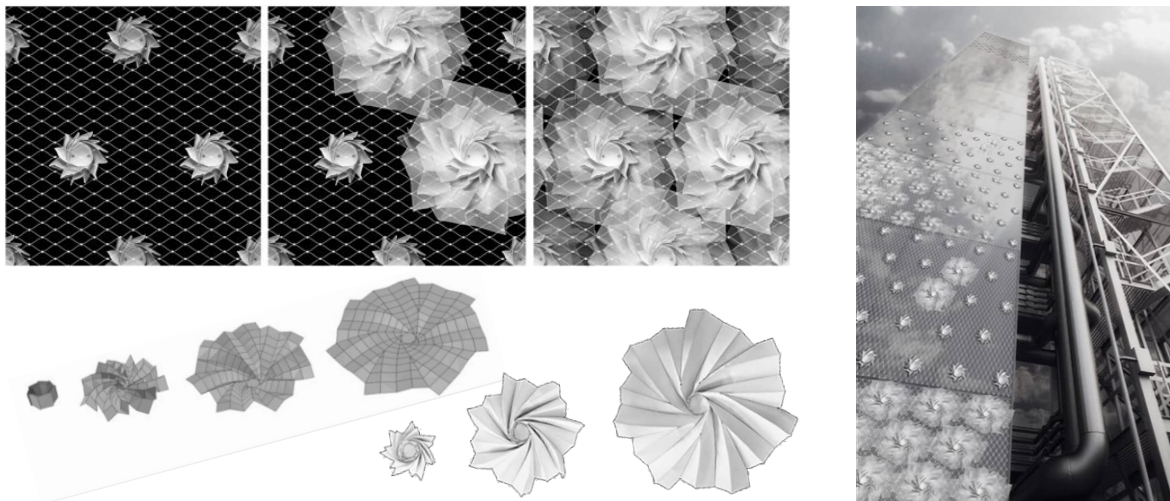
Figure 65 Pneumatically Actuated Origami Sun Shading (Eisenbarth et al., 2021)

58

2.7 Conclusion

The main goal of this literature review is to broaden the knowledge on thin glass sandwich panels and its structural behaviour, together with gaining knowledge on how to evaluate the daylight performance of a panel. Then, different possible dynamic façade solutions where evaluated, including shape memory materials, soft material robotics and fabrics. This literature review aimed to answer the following sub questions of the main research question:

What are the physical properties of thin glass?

The properties of glass are dependent on the type of glass, which most commonly are soda-lime-silica glass, borosilicate glass and aluminosilicate glass. The characteristic strength can be increased by heat strengthening or tempering the glass. Glass behaves linear elastic with brittle failure. Thin glass, produced from aluminosilicate glass with the downdraw process, is chemically strengthened and therefore has high strength properties. The thickness can range 25 μm to 1 mm and has comparatively fewer surface flaws than float glass.

What are the characteristics of the different structural sandwiches currently available?

Structural sandwiches are based on the sandwich theory, where the strong material is placed in thin layers on the outside, filling the core material with an open pattern. Increasing the thickness of the core can greatly increase the strength of the full sandwich panel. The topology of the core mainly determines the stiffness of the panel. Here the honeycomb pattern is noteworthy because of its relative high stiffness for a low density.

What methods of 3D-printing are available and how do these work?

3D-printing starts from a Computer Aided Design (CAD) model, where, depending on the printing method used, additional supports for printing can be added. The main methods available are Fused Deposition Modelling, Stereolithography, Selective Laser Sintering, 3-Dimensional Printing and Inkjet Printing. Thermoplastics can be used as printing material, where a wide selection of polymers is available, like polycarbonate and glycol modified polyethylene terephthalate (PETG).

Which adhesives are appropriate to use in the thin glass façade panel?

A study by Kothe et al. (2021) investigated possible adhesive bonds between glass and 3D-printed polymers, with a focus on the resistance to temperature and UV aging. Technicoll 9430-1 and acrylate Loctite 3345 were the recommended adhesives following this research.

How is the daylight performance of a panel determined and evaluated?

The daylight performance is determined by quantifying the visual comfort inside a building. For a shading system, the illuminance in a room, contrast and glare control are the main properties determining the overall visual comfort. Illuminance is the level of light on a surface, which can be used to evaluate the quantity of daylight in a room. This can be measured for a moment in time, but also on annual basis expressed as the daylight factor, which is the ratio between illuminance inside and illuminance outside of the room.

Contrast is the difference in luminance of the object itself and the surrounding area. It can be measured using the contrast ratio, which compares the luminance of one surface of the room with a connecting surface. Glare is the negative experience when the luminance from bright surfaces exceeds the comfort level of the human eye. It can be measured using the

daylight glare probability, which is an empirical formula relating the measurable physical elements to the experienced glare.

The daylight performance can be evaluated using simulation models. Radiance is a program based on ray tracing, which can be used to simulate the solar path and how it effects the light experience of a room. Analyses can be done annually, for example the daylight factor, or for a moment in time, which for example can be used for evaluating glare using a generated fisheye image.

What options are available to dynamically control the daylight performance of a panel?

Dynamically controlling daylight can be done by applying shading systems to the façade. The shading system can be evaluated by defining the energy balance, which consists of reflectance, transmittance and absorptance. The shading devices can be placed externally, internally or integrated within the façade element.

External shading devices are most effective since they prevent the light and heat of the sun from entering the building. The main disadvantage is the exposure to the weather and it can become defective, especially for dynamic façade systems. Internal shading devices are protected from the outside environment but are much less effective since the shading device itself will absorb solar heat and thereby warm up the room.

Integrated systems can be applied in the form of a solar control coating, which can largely reflect UV and infrared parts of the solar spectrum, while letting visible light pass through. Other prototypes of integrated systems are an adaptive foil system, a homeostatic system and a system inspired by breathable skins. These systems are permanently in place, but the area of façade they cover can be changed, thereby being able to control glare.

What other dynamic solutions are available that can act within the core of a panel?

The main constricting element of an integrated dynamic system is the limited space available and limited access possibilities for maintenance. The three dynamic systems evaluated are folding mechanisms (shape memory materials), (inflatable) soft material robotics and fabric-based mechanisms.

For folding mechanisms, the resulting shape can be designed by introducing (curved) folding lines and by (gradually) changing the material properties along the fold. Smart materials can also be used, where the actuator responds to the environment. This response can be to changes in daylight, temperature, humidity, chemical or electrical current.

Soft material robotics offer more possible response shapes and movements than the previously mentioned smart materials due to its flexible nature. Materials often used are silicone elastomers, which provide a high elastic resilience. The actuation often is a tensioning element, woven shell or by inflating it with a fluid.

Textiles can also be used in façades, where for example the actuation can be integrated into the knitting of the fabric itself. The textile can also be connected to moveable elements like wires or shape memory polymers, thereby utilizing the elasticity of the fabric. Lastly, origami inspired systems can used, where the fabric can be bend into a different shape onto actuation.

3 DESIGN FAÇADE PANEL

In this chapter, multiple design concepts are explored to arrive at the best design for the façade panel. Various design options are explored using models and simulations. First, the possible core patterns are evaluated on their structural performance using finite element analyses. Then, the feasibility and overall performance of the two design concepts as described in the research plan are explored, concluding with a selection of the winning concept. Then, the façade system is designed and evaluated on its daylight performance. The sub-questions answered in this chapter are listed below:

What are the structural and visual comfort requirements of a typical façade panel?

What is an effective design for a façade panel which is able to dynamically control the visual comfort?

3.1 Computational design core pattern

3.1.1 Standard room

To be able to design and optimise the façade system, a standard room is defined. This room can be used for determining the boundary conditions, requirements and functions of the room, which determine the requirements of the panel. The function of the room is chosen to be an office, which will have a height of 3 m, with an area of 4x6 m^2. The window opening will have a 2x2 m^2 area, placed 0.5 m from floor level. Adding a typical desk with a height of 0.85 m from floor level gives us the full simulation office, see Figure 66a.
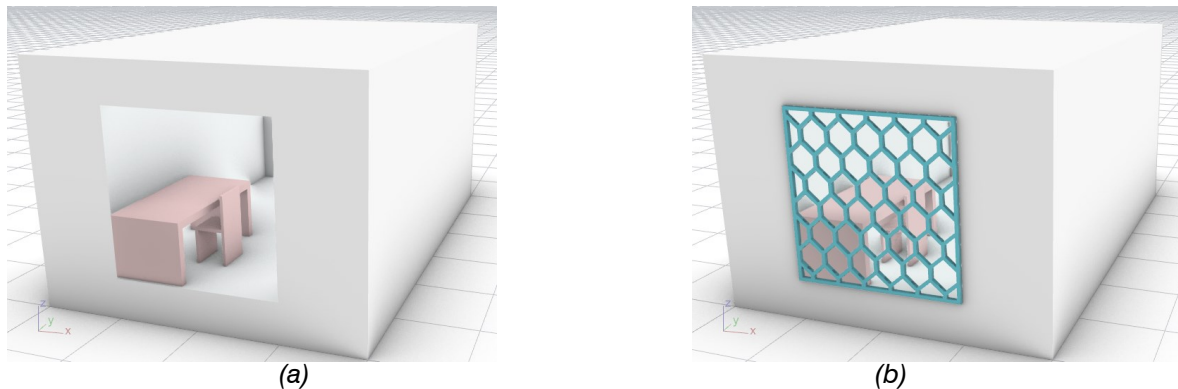

| (a) | (b) |

Figure 66 (a) Standard room used for testing; (b) example model with façade sandwich panel

The façade panel consists of two thin glass panes with the 3D-printed core in the middle. The first parameters here are the thickness of each of these layers. Next is to decide on the pattern of the core, which can be parametrised in a horizontal (*x*) and vertical (*z*) component. This core can then be changed further, changing it along its third axis (*y*), adding openings, etc.

In the literature review, many different adaptive façade systems were explored, using a variety of moving elements. To choose which methods would be suitable in a thin glass façade panel, the boundary conditions of the panel should be defined. The first limiting factor is the thickness of the total panel. It needs to realistically fit inside a typical wall opening of a building, therefore not being significantly thicker than an ordinary window element. For now, the maximum thickness of the core is set at 50 mm, and the maximum thickness of the thin glass at 2 mm.

3.1.2 Exploring patterns

The stiffness of the panel is determined by the thickness of the glass panes and the design of the core, where the pattern used influences the amount of material used and the resulting stiffness. A few possible patterns are explored in Figure 67. These are two-dimensional patterns extruded over the normal axis, allowing people to look through the panel. Three-dimensional patterns are excluded since they block the view through the panel and severely limit the possibilities of integrating a solar control system within this core pattern.

For the core pattern, its material contributes to the stiffness of the panel, while the open cell space contributes to the transparency of the panel. Increasing the number of cells in *x* and *z* direction decreases the transparency, while increasing the stiffness.

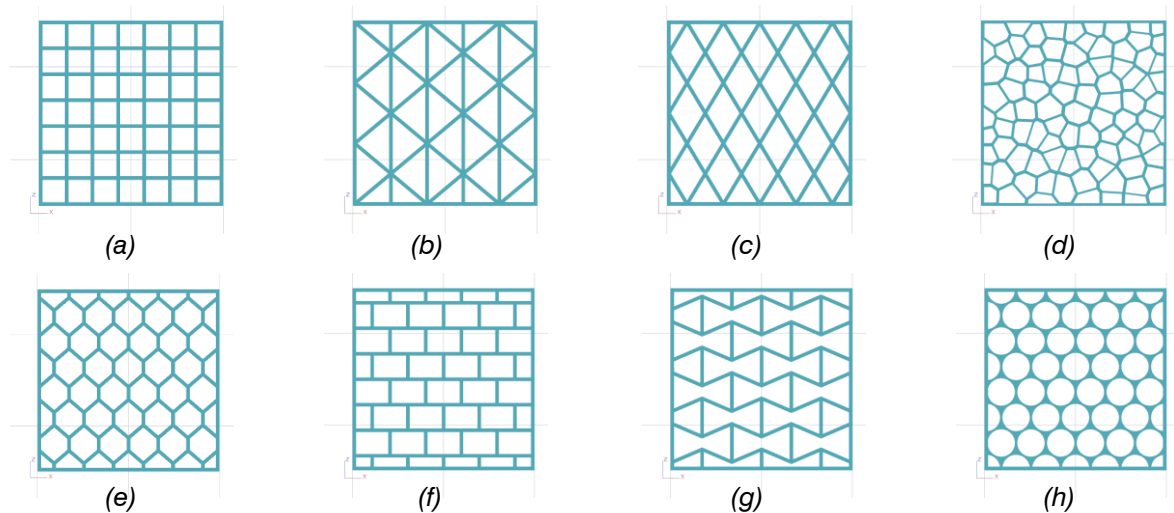| (a) | (b) | (c) | (d) |
| (e) | (f) | (g) | (h) |

Figure 67 2D-patterns with equal volume. (a) quadrangular panels; (b) triangular panels; (c) diamond panels; (d) random Voronoi panels; (e) hexagonal panels, 0.25 angle (honeycomb); (f) hexagonal panels, 0.50 angle; (g) hexagonal panels, 0.75 angle; (h) hexagonal panels, circular cell shape

Having open cells allows the geometry to be relatively simple. Furthermore, having uniform cells simplifies the design process significantly. In Table 13 the complexity of these patterns is evaluated. First, the uniformity of the cells together with the shape of the cells along the edge is taken into consideration. Following, the complexity of the geometry is rated, where a simpler geometry receives a higher score. Lastly, the suitability for an inflatable design is rated, where more sharp corners in the pattern result in a lower rating.

Table 13 Comparing cell shape patterns

Panels	Uniform shape centre cells	Shape edge cells	Complexity geometry	Suitable for inflatable design
Quadrangular	✓	Equal to centre	★★★★★	★★★
Triangular	✗ (mirrored)	Equal to centre, half of centre	★★★★	★★
Diamond	✓	Half of centre	★★★★	★★
Random Voronoi	✗	Unique	★	★
Hexagonal 0.25	✓	Half of centre	★★	★★★★
Hexagonal 0.5	✓	Half of centre	★★★★	★★★
Hexagonal 0.75	✓	Half of centre	★	★★★
Circular	✓	Half of centre	★	★★★★★

The pattern for the designs in this thesis will be combined with a system mainly focused on preventing glare. To prevent unnecessary complexity in this system, a uniform cell shape is preferred. Therefore, the (random) Voronoi pattern is not further explored. The cell shape should also be relatively simple, small angles and corners can result in more complex design solutions within the cell. Therefore, the hexagonal pattern with 0.75 angle is not further explored.

Aside from preventing glare, the façade system will also influence the daylight performance in the room. The dynamic part of the façade will function to control glare, but when there is no glare, the façade will still be in place. For this situation, the transparency of the façade should be maximised to allow the most amount of natural light inside the room. Furthermore, the two-dimensional patterns can be varied in the third dimension as well. This can influence the angle at which light is reflected, thereby improving the daylight performance further.

Concluding, a pattern should be selected with uniform cell size, be material efficient, structurally sufficient and not introduce unnecessary complexity. As previous research has shown, hexagonal patterns perform most efficient structurally in terms of material use. Together with the high uniformity and general cell shape, this pattern is chosen to be the main focus of this thesis. In the next section, this pattern, together with the variation with circular openings is explored further by analysing its structural performance.

3.1.3 Structural analyses
3.1.3.1 Structural requirements
First, the structural requirements of the panel are determined based on NEN 2608 (2014). Here, the consequence class of the building determines the factors to be added to the loads. For an office/public building, the consequence class is *CC2*. The factor K_{FI} for *CC2* is 1.0, so this will not influence the calculations. The partial factors are dependent on this consequence class, as shown in Table 14.

Table 14 Partial load factors depending on consequence class

	Permanent Unfavourable	Permanent favourable	Variable unfavourable
CC1 ULS1	1.2	0.9	1.35
CC1 ULS2	1.1	0.9	1.35
CC2 ULS1	1.35	0.9	1.5
CC2 ULS2	1.2	0.9	1.5
CC3 ULS1	1.5	0.9	1.65
CC3 ULS2	1.3	0.9	1.65

For the Ultimate Limit State (*ULS*), the maximum stresses acting in the glass and core need to be checked. Here the normative load combinations are defined as below (NEN-EN 1990+A1+A1/C2, 2019):

$$E_{d,ULS1} = \sum \gamma_{G,j} * G_{k,j} + \gamma_{Q,1} * \psi_{0,1} * Q_{k,1} + \sum \psi_{Q,i} * \psi_{0,i} * Q_{k,i} \qquad (15)$$

$$E_{d,ULS2} = \sum \xi_j * \gamma_{G,j} * G_{k,j} + \gamma_{Q,1} * Q_{k,1} + \sum \psi_{Q,i} * \psi_{0,i} * Q_{k,i} \qquad (16)$$

- $\gamma_{G,j}$ is the partial factor for the characteristic value of permanent load $G_{k,j}$.
- $\gamma_{0,1}$ is the partial factor for the dominant variable load $Q_{k,1}$
- $\psi_{0,1}$ is the combination factor for the dominant variable load
- $\gamma_{Q,i}$ is the partial factor for the variable load $Q_{k,i}$

- $\psi_{0,i}$ is the combination factor for the variable load
- ξ_j is a reduction factor for unfavourable, permanent loads (already included in ULS2 of Table 14.

The permanent load is the self-weight of the façade, which is neglected in the following calculations. For a wind load, the combination factors are defined as ψ_0 = 0.6, ψ_1 = 0.2 and ψ_2 = 0. The wind load is heavily dependent on the location of the building and the façade. The wind load can be determined with the following formula (NEN-EN 1991-1-4+A1+C2, 2011):

$$F_w = c_s c_d * c_f * q_p(z_e) * A_{ref}$$ (17)

Here $c_s c_d$ is the structural factor, depending on the height of the building. For the office, a low rise is assumed, resulting in a $c_s c_d$ of 1.0. The c_f is the force coefficient dependent on the size and shape of the full building. $q_p(z_e)$ is the peak velocity pressure at height z_e, which is dependent on the height of the building and the location (near a coast, etc.). For the calculations in this section, a wind load F_w/A_{ref} of 1 kN/m^2 is assumed. This results in the following design combinations:

$$E_{d,ULS1} = \sum 1.35 * 0 + 1.5 * 0.6 * Q_{k,1} \left[\frac{kN}{m^2}\right]$$ (18)

$$E_{d,ULS2} = \sum 1.2 * 0 + 1.5 * Q_{k,1} \left[\frac{kN}{m^2}\right]$$ (19)

Since the self-weight is neglected, the ULS2 option is always normative.

The design strength of the glass can be estimated using the characteristic bending strength of chemically strengthened glass as defined in table 6 of NEN-EN 16612 (2019), with $f_{b,k}$ = 150 N/mm^2. This is a conservative value since the process conditions and duration of chemically strengthening can vary greatly. The material partial factor can be set at $\gamma_{M;v}$ = 1.2, in accordance with table A.2 of (NEN-EN 16612, 2019). The design value of the strength of glass can be determined using the definition of NVN-CEN/TS 19100-1 (2021):

$$f_{g,d} = k_e \cdot k_{sp} \cdot \lambda_A \cdot \lambda_1 \cdot k_{mod} \cdot \frac{f_{g,k}}{\gamma_M} + k_p \cdot k_{e,p} \cdot \frac{f_{b,k} - f_{g,k}}{\gamma_p}$$ (20)

- $f_{g.d}$ = total design bending strength [N/mm^2]
- $f_{g.k}$ = characteristic bending strength of annealed glass [N/mm^2], 45 N/mm^2 for drawn sheet glass
- $f_{b,k}$ = characteristic bending strength [N/mm^2]
- k_e = edge finishing factor [-], 1.0 for polished edges float glass
- k_{sp} = surface profile factor [-], 1.0 for drawn sheet glass, as produced
- λ_A and λ_1 = size effect factors [-], 1.0 if area of the pane < 18 m^2 and length of a side < 6 m
- k_{mod} = modification factor [-], 1.0 for non-annealed glass
- k_p = pre-stressing process factor [-], see table A.4 in NVN-CEN/TS 19100-1 (2021)
- $k_{e,p}$ = edge/hole pre-stressing factor [-], see table A.5 in NVN-CEN/TS 19100-1 (2021)

The value for k_p can vary from 1.0 for heat treatment with a horizontal process, while being 0.6 for heat treatment with a vertical process. The actual value used should be assessed for the specific type of chemically strengthened glass used. The same applies to the $k_{e,p}$ value. Taking this into account, the formula for the design strength of chemically strengthened glass is defined as below:

$$f_{g,d} = \frac{45}{1.2} + k_p \cdot k_{e,p} \cdot \frac{f_{b,k} - 45}{1.2} \left[\frac{N}{mm^2} \right]$$ (21)

To make an estimate of the strength, which can be used in this thesis, the factors are based on heat-strengthened glass:

$$f_{g,d} = \frac{45}{1.2} + 0.6 \cdot 1.0 \cdot \frac{150 - 45}{1.2} = 90 \ \frac{N}{mm^2}$$

For the serviceability limit state (*SLS*), the normative design combination for deflection is as defined below NEN-EN 1990+A1+A1/C2 (2019).

$$E_{d,SLS} = \sum 1{,}0 * G_{k,j} + 1{,}0 * Q_{k,1} + \sum \psi_{2,i} * Q_{k,i}$$ (22)

As the self-weight is neglected, the design SLS load is equal to the wind load.

The maximum allowed deflections are defined in NEN 2608 (2014). Here the maximum deflection located at the sides u_{max} [*mm*] for isolating glass is defined with the following formula, where l_z [*mm*] is the length of the side of the window:

$$u_{max} \leq \frac{l_z}{200}$$ (23)

The maximum deflection in the middle of the glass pane $u_{dia;max}$ [*mm*] can be calculated with the following formula, where l_{dia} [*mm*] is the diagonal length of the window:

$$u_{dia;max} \leq \frac{l_{dia}}{65} \leq 50$$ (24)

For the window dimensions of 2x2 m^2, the diagonal is $\sqrt{2000^2 + 2000^2} = 2828.43 \ mm$. This results in a maximum deflection of the sides at $\frac{2000}{200} = 10 \ mm$ and a maximum deflection of the middle of $\frac{2828.43}{65} = 43.51 \ mm$.

3.1.3.2 Analytical analysis

The resulting stiffness of the panel can be first determined using analytical formulas. This will simplify the panel since the three-dimensional effect of the core is left out of these calculations. However, this does give an indication of the order of magnitude of the resulting stiffness and deflection.

The façade element is supported along all four edges in the direction of the wind load; therefore, it can be analysed as a two-way slab with line supports. The line supports do allow for rotation; therefore, they are rigid supports with no rotational fixity. The maximum moment acting in the slab and the resulting deflection can be determined using the theory of elasticity. Here NEN 6720 table 18 is used to determine the maximum moment in each direction of the slab, depending on the ratio of l_x (longer edge) and l_y (shorter edge), see Table 15.

Table 15 Bending moments and maximum deflection in a two-way simply supported slab, according to the theory of elasticity (NEN 6720 table 18)

l_y/l_x		1.0	1.2	1.4	1.6	1.8	2.0	2.5	3.0
$m_{vx} =$	0.001*q*l_x^2	41	54	67	79	87	97	110	117
$m_{vy} =$	0.001*q*l_x^2	41	35	31	28	26	25	24	23
$w_{max} =$	0.001*q*l_x^4/(EI)	4.1	5.6	7.0	8.2	9.2	10	11.4	12.2

If one side is significantly larger than the other ($l_y > 2*l_x$), the middle strip of the two-way supported slab will behave similarly to a one-way supported slab. This can be calculated analytically by assuming it behaves like a Euler-Bernoulli beam, which is based on bending

only. For an equally distributed load q [N/mm] the maximum deflection w_{mid} [mm] of a beam with stiffness EI [Nmm^2] and length l [mm] is defined as follows:

$$w_{mid} = \frac{5}{384} \frac{ql^4}{EI}$$ (25)

The factor 5/384 would be equal to a factor of 13.02 in Table 15. This shows that the Euler-Bernoulli beam is a more conservative estimate of deflection for two-way supported slabs.

To determine the stiffness of the sandwich panel, the representative Young's modulus E and moment of inertia I needs to be determined. Since most of the bending stiffness comes from the two glass plates, the Young's modulus of glass is used, which is 70000 N/mm^2. The moment of inertia is based on a shape with most of the material located near the edges, with minimal material in the middle (the core). Neglecting the influence of the core on the moment of inertia, it leaves to rectangular shapes at a given distance from the core of the profile. This can be determined using the rule of Steiner:

$$I_z = I_c + a^2 * A$$ (26)

- I_z is the moment of inertia around axis z [mm^4]
- I_c is the moment of inertia at centre of element [mm^4]
- a is the distance of centre element to axis z [mm]
- A is the total area of element [mm^2]

Therefore, the moment of inertia of the 2x2 m^2 sandwich panel with two times a 1.0 mm glass pane and a 12 mm core is:

$$I_{sandwich} = \frac{1}{12} * b * h_1{}^3 + a^2 * b * h_1 + \frac{1}{12} * b * h_2{}^3 + a^2 * b * h_2$$ (27)

$$I_{sandwich} = \left(\frac{1}{12} * 1000 * 1.0^3 + \left(\frac{12}{2} + \frac{1.0}{2} \right)^2 * 1000 * 1.0 \right) * 2 = 8.47 * 10^4 \ mm^4$$

Therefore, the resulting deflection can be analytically determined using the factor of the two-way supported slab from Table 15:

$$w_{mid} = 0.001 * 4.1 * \frac{1 * 2000^4}{70000 * 8.47 * 10^4} = 11.07 \ mm$$

Compared to the one-way supported slab using the Euler-Bernoulli beam formula (25):

$$w_{mid} = \frac{5}{384} \frac{1 * 1000^4}{70000 * 1.81 * 10^5} = 35.15 \ mm$$

3.1.3.3 Karamba3D analysis

The main design process will be performed in a Rhino model with Grasshopper. For structural analysis, the plugin Karamba3D is used. This tool allows line elements and shell elements to be added to the model, but it does not include solid elements. Therefore, this analysis can only be used to analyse a two-dimensional core pattern with a certain thickness. Variation along the thickness of the pattern will need to be further analysed using a finite element analysis program, such as Diana FEA. This will be described in the next section.

The geometry of the façade panel is simplified into three interconnected shells. Each of these shells is made by meshing the defined surface. To ensure an accurate connection between the glass and core meshes, the points of the core mesh are included in the glass meshes. The properties of the mesh are dependent on the input mesh resolution, which determines the target mesh size. Decreasing this value will increase the accuracy of this model but it will also increase the calculation time.

When generating the mesh, it is important to also define the limit distance for coincide points. When the mesh resolution is reduced, this limit distance needs to be reduced as well. Otherwise, non-duplicate points will be recognised as duplicates and therefore be culled from the meshes, potentially resulting in issues with generating support points.

The connection between the three layers of the sandwich panel is modelled to be completely rigid. This is done by creating line segments in between the mesh points of the core and the two glass meshes, see Figure 68.
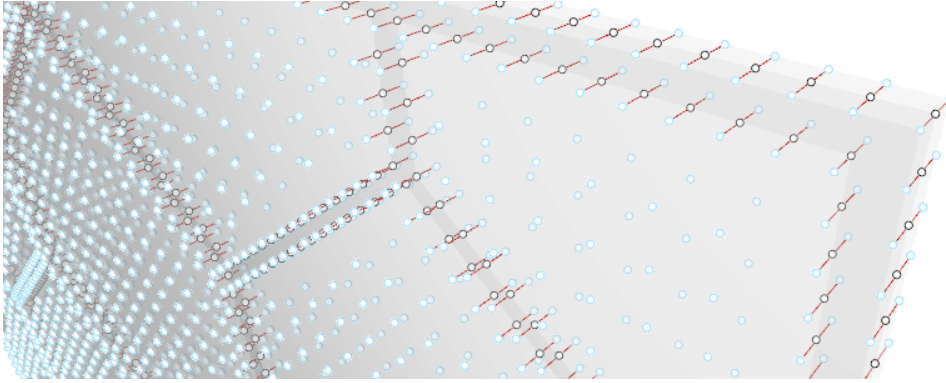
Figure 68 Modelling shell elements in Karamba3D using connecting elements. Mesh refinement of 20 mm, where the points of the meshes are connected via the red lines.

The support conditions are added to the model by isolation the edge points of the mesh of the inside glass pane. The bottom points are supported in *y* and *z* direction. The two vertical sides and top side are supported in y direction. The load is applied to the mesh of the outside glass pane, where the surface load is an equally distributed load of 1 *kN/m²*. For this analysis, the same value is used for both deflection and stresses, for now excluding the effect of additional factors in *ULS* vs *SLS*.

The material properties as used in the Karamba3D model are shown in Table 16. For the properties of the adhesive, a rigid connection is assumed to simplify the calculation. Therefore, the strength properties are chosen to be exceedingly high and the self-weight is set at 0 *kg/m³*, to ensure that the connection behaves rigid and does not influence the results.
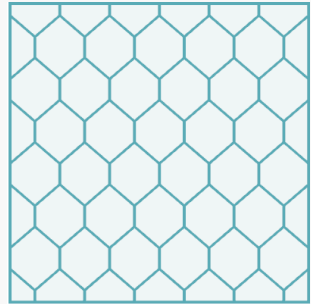
Table 16 Material properties used in Karamba3D model

Material	Thin glass (chemically tempered)
Young's modulus *E*	74 *GPa*
In-plane shear modulus *G12*	30 *GPa*
Transverse shear modulus *G3*	30 *GPa*
Mass density *ρ*	2480 *kg/m³*
Specific weight *gamma*	24.33 *kN/m³*
Tensile strength *ft*	90 *MPa*
Compressive strength *fc*	90 *MPa*

Material	PETG
Young's modulus *E*	2.02 *GPa*
In-plane shear modulus *G12*	0.90 *GPa*
Transverse shear modulus *G3*	0.90 *GPa*
Mass density *ρ*	1270 *kg/m³*
Specific weight *gamma*	12.46 *kN/m³*
Tensile strength *ft*	50 *MPa*
Compressive strength *fc*	50 *MPa*

Material	Adhesive: rigid connection
Young's modulus *E*	50000 *GPa*
In-plane shear modulus *G12*	20000 *GPa*
Transverse shear modulus *G3*	20000 *GPa*
Mass density *ρ*	0 *kg/m³*
Specific weight *gamma*	0 *kN/m³*
Tensile strength *ft*	1000 *MPa*
Compressive strength *fc*	1000 *MPa*

The elements of the assembled model are generated using the mesh to shell component, which resembles the TRIC element. This is a triangular element with three nodes, which neglects the transverse shear deformation. Here the shell is assumed to have bending stiffness. The cross section of the elements is defined using the materials as described in Table 16, with a prescribed height.

Once the full model has been assembled, it can be analysed using the first order theory for small deflections. The analysis is executed for the panel as defined in Table 17. The larger the window, the higher the number of elements the meshes consists of, which increases the calculation time and processing power necessary for running the analyses. It is therefore important to analyse which mesh element size gives accurate results.

Table 17 Parameter settings for panel

	2x2 m^2 panel	
Width window	2 m	
Height window	2 m	
Height glass panes	1.0 mm	
Height 3D core	12 mm	
U divisions	12	
V divisions	7	
Thickness sides	10 mm	
Thickness pattern x	10 mm	
Thickness pattern z	10 mm	
Factor x	1.0 mm	
Factor z	1.0 mm	

The results for both the maximum deflection and equivalent stress (utilisation) of the panels for varying mesh element sizes are shown in Figure 69. For the deflection, the difference in results between mesh size steps is relatively low, ranging from 0-1.6 %. The convergence shows declining behaviour as the mesh size is reduced. The resulting deflection also decreases with smaller mesh size, so a larger mesh size overestimates the deflection.
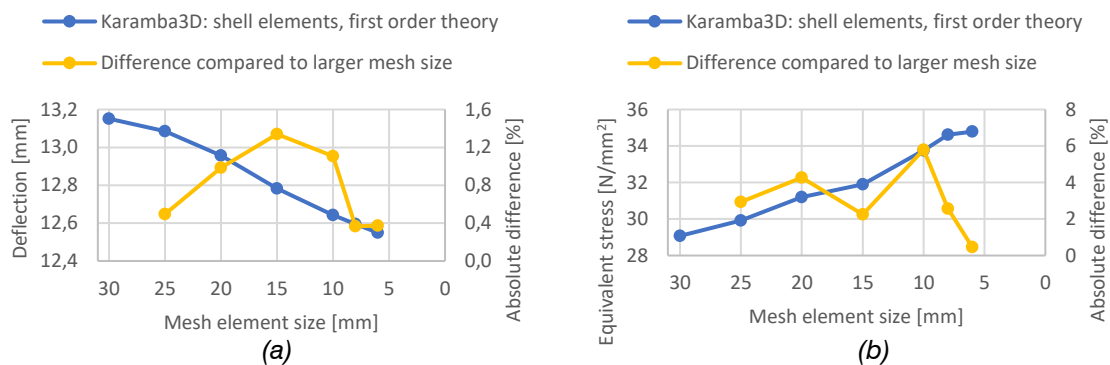
Figure 69 Convergence per mesh element size in Karamba3D with shell elements; (a) deflection; (b) equivalent stress (utilisation)

The maximum equivalent stress acting in the panel shows an increase when the mesh size is reduced. The absolute difference between mesh sizes is also larger compared to the deflection. However, the behaviour does show to level once the mesh element size is reduced to 8 mm, showing the results converge.

3.1.3.4 Diana FEA analysis

The sandwich panel as calculated in Karamba3D, is modelled as three connected shells. However, it is more accurate to model it as solid elements. This better shows the effect of how the two glass panes and the core structure work together to provide stiffness. It also makes it possible to evaluate the effect of adding variations along the thickness of the core, since these occur in 3D.

The results of the analysis using solid elements can also be used to make a comparison with the results of the shell analysis of Karamba3D, to verify the accuracy of these results. If a considerable difference is to be found, potentially an additional factor can be added to make the results more accurate.

For this structural analysis, a finite element analysis is executed using Diana FEA (version 10.8). This program can import models from Rhino/Grasshopper, making this a compatible

program to use. For analysing a three-dimensional element, Diana FEA offers shell elements and solid elements. In the following analyses, the solid element method is used to evaluate the sandwich panel. First, the panel as described in Table 17 is modelled in Rhino, where they can be directly imported into Diana using a STEP file export.

The meshes of the solid elements are generated using the properties as defined in Table 18. The mesh size is defined using the seeding method of the element size of the shapes.

Table 18 Diana mesh properties

Shape dimension	3D
Topological dimension	3D
Element class	Structural solids
Mesher type	Tetra/Triangle
Interpolation	Linear
Element type	Tetrahedron (TE12L)
Degree of freedom's	u_x, u_y, u_z
Shear deformation	Included

The support conditions are added as edge supports to the inside glass pane. The bottom edge is supported in y and z direction. The two vertical sides and the top side are supported in y direction. Lastly one corner vertex is supported in x direction. The load is applied as a distributed force on the outside pane in the normal direction. The adhesive connection is modelled as a rigid connection between the two glass panes and the core. The translations in all three directions are connected. An overview of the Diana model is shown in Figure 70. The material properties as used in the Diana model are shown in Table 19.
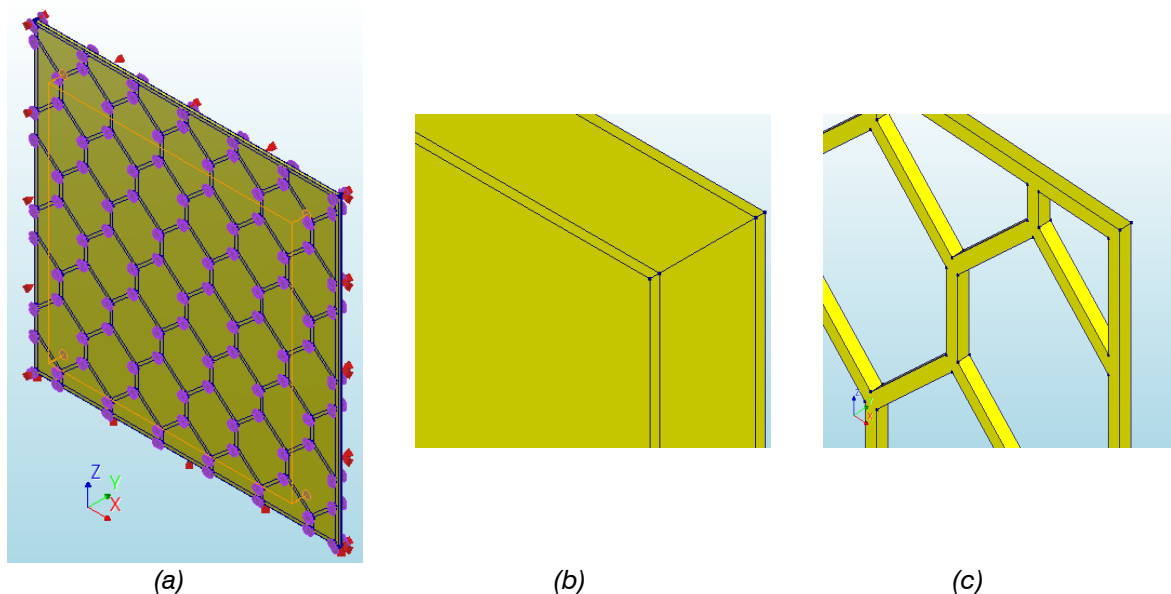

| (a) | (b) | (c) |

Figure 70 Diana model; (a) full model with supports, loads and connection visualised of 2x2 m² panel; (b) zoomed in visual of the three layers; (c) the core isolated

Table 19 Material properties used in Diana models

Material	Glass
Class	Concrete and masonry
Material model	Linear elastic isotropic
Young's modulus	74000 N/mm^2
Poisson's ratio	0.23
Mass density	2480 kg/m^3

Material	PETG
Class	Concrete and masonry
Material model	Linear elastic isotropic
Young's modulus	2020 N/mm^2
Poisson's ratio	0.4
Mass density	1270 kg/m^3

The analyses can be linear static or nonlinear. The adhesive connection between the glass and core is assumed rigid. Furthermore, glass has a linear stress-strain behaviour, see Figure 15 in the literature review. Therefore, the chosen analysis is the linear static analysis with solid elements. The results of the maximum deflection and equivalent stress is shown in Figure 71, together with the convergence over decreasing mesh size.
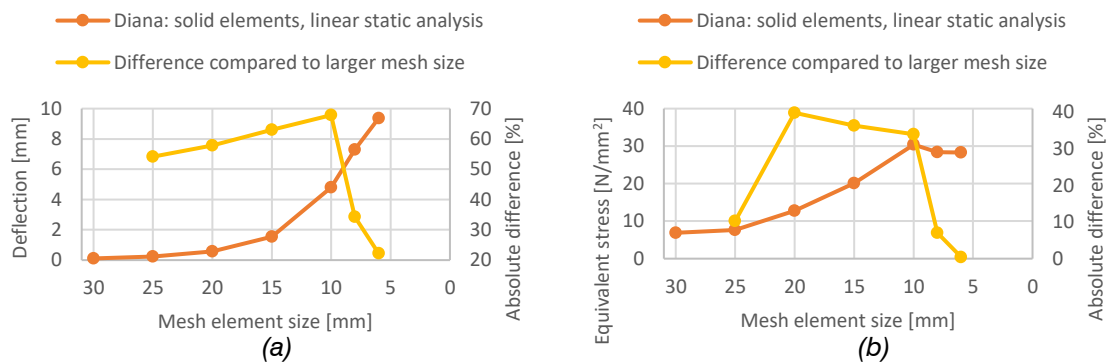
Figure 71 Convergence per mesh element size in Diana FEA with solid elements; (a) deflection; (b) equivalent stress (utilisation)

Where the Karamba3D shell analysis showed better convergence for the results of deflection, it is the opposite for the Diana FEA analysis. Both the results of the deflection and equivalent stress increase with decreasing mesh size, though the unity check does show convergence from a mesh size of 8 *mm*. The mesh size of 6 *mm* meets the limits of the capabilities of the computer used in the calculation, but the convergence does show a significant decrease once the mesh size reduces.

To illustrate how the forces act within the panel, the resulting contour plots of the deflection and equivalent stresses are shown in Figure 72 and Figure 73, respectively. The results of the 6 *mm* mesh element size are used to show the most accurate results. Further information on the principal stresses acting in the panel can be found in Appendix E.1.
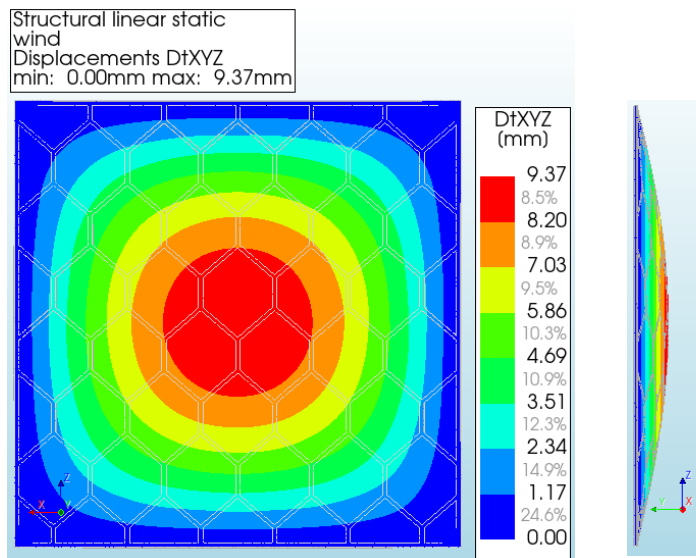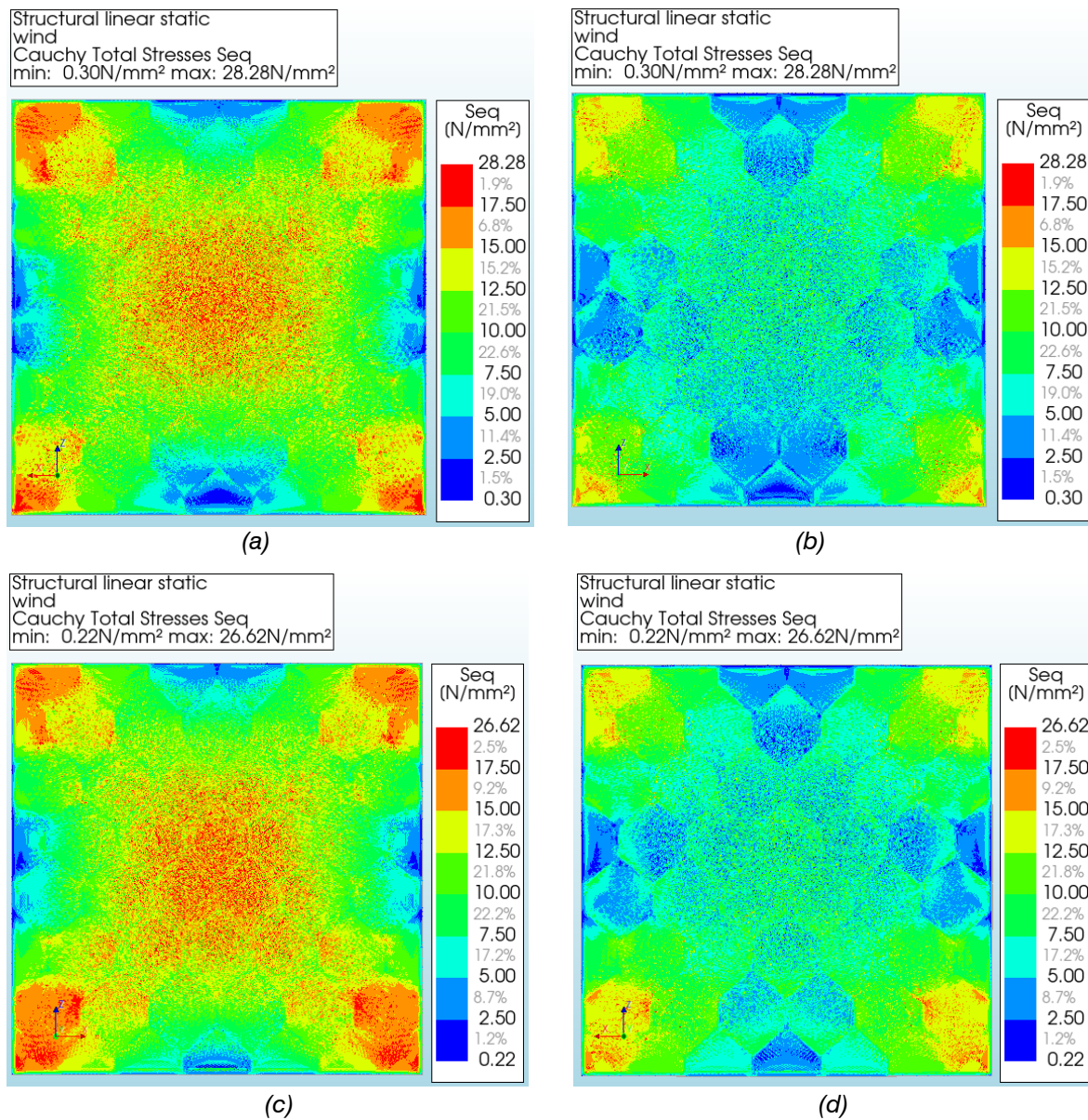
Structural linear static
wind
Displacements DtXYZ
min: 0.00mm max: 9.37mm

DtXYZ
(mm)

9.37
8.5%
8.20
8.9%
7.03
9.5%
5.86
10.3%
4.69
10.9%
3.51
12.3%
2.34
14.9%
1.17
24.6%
0.00

Figure 72 Results Diana deflection in DtXYZ direction

Structural linear static
wind
Cauchy Total Stresses Seq
min: 0.30N/mm² max: 28.28N/mm²

Seq
(N/mm²)

28.28
1.9%
17.50
6.8%
15.00
15.2%
12.50
21.5%
10.00
22.6%
7.50
19.0%
5.00
11.4%
2.50
1.5%
0.30

(a)

Structural linear static
wind
Cauchy Total Stresses Seq
min: 0.30N/mm² max: 28.28N/mm²

Seq
(N/mm²)

28.28
1.9%
17.50
6.8%
15.00
15.2%
12.50
21.5%
10.00
22.6%
7.50
19.0%
5.00
11.4%
2.50
1.5%
0.30

(b)

Structural linear static
wind
Cauchy Total Stresses Seq
min: 0.22N/mm² max: 26.62N/mm²

Seq
(N/mm²)

26.62
2.5%
17.50
9.2%
15.00
17.3%
12.50
21.8%
10.00
22.2%
7.50
17.2%
5.00
8.7%
2.50
1.2%
0.22

(c)

Structural linear static
wind
Cauchy Total Stresses Seq
min: 0.22N/mm² max: 26.62N/mm²

Seq
(N/mm²)

26.62
2.5%
17.50
9.2%
15.00
17.3%
12.50
21.8%
10.00
22.2%
7.50
17.2%
5.00
8.7%
2.50
1.2%
0.22

(d)

(e)   *(f)*

Figure 73 Results Diana equivalent stresses acting in each part of the sandwich panel: (a) inside glass pane, side facing inside; (b) inside glass pane, side facing core; (c) outside glass pane, side facing outside (d) outside glass pane, side facing core; (f) core side facing

3.1.3.5 Comparison results

To be able to evaluate the resulting deflections and unity checks of the varying types of calculations, they are first compared in Figure 74. The minimal mesh element size shown in this graph are limited by the abilities of the computer used. It is important to take into consideration that smaller mesh element sizes take considerably longer computational time and require more memory.

(a)   *(b)*
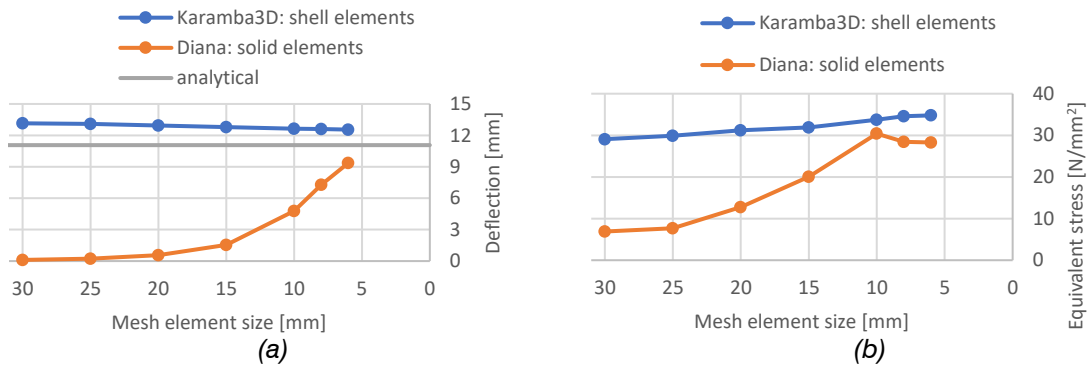
Figure 74 Comparison shell element calculation in Karamba3D, solid element calculation in Diana FEA and analytical calculation per mesh element size; (a) deflection; (b) equivalent stress (utilisation)

This shows that the Karamba3D analysis consistently has higher resulting values compared to the results of Diana and analytical. The resulting values do start approaching each other once the mesh element size is reduced.

The results generated in Karamba3D overestimate the deflection and stresses, but that does generate a safe design. Concluding, the resulting values from the Karamba3D analysis can be used to safely assume if the structure meets the structural requirements. For the 2x2 *m²* panel, the mesh element size can be set at 8 *mm*, or a larger size while using a correcting factor.

The analytical solution only takes into account the contribution of stiffness of the two glass panes and assumes that the core works perfectly in transferring the forces towards the

glass. When the contribution of the core becomes more trivial to the overall stiffness of the sandwich panel, this assumption no longer holds. The variation in results can therefore be explained by the actual contribution of the core to the stiffness of the full panel.

The solid element results are most likely to generate realistic values since it approaches the actual geometry more accurately. They can be used to see the effect of more complex geometry, since this is not possible in Karamba3D. The deflection of Diana increases when the mesh element size is reduced, but it stays below the calculated Karamba3D results. The resulting maximum stress decreases after a mesh element size of 10 *mm*, showing that this is the maximum mesh size that can be used to estimate the stresses acting within the panel.

3.1.4 Varying parameters and patterns core in the 2D plane

In this section, the effect of changing different parameters of the core on its structural performance is evaluated. Here the focus is only on varying the parameters in the two-dimensional plane of the pattern. Therefore, the panel can be evaluated using Karamba3D with shell elements.

First, the effect of changing a single parameter is evaluated, keeping the other parameters the same. This gives insight in how the parameter influences the results. It is important to remember it is a multi-parameter problem, different sets of parameters may show different behaviours. To be able to find an optimum design, an optimisation algorithm can be used. However, for such an algorithm all the relevant requirements of the façade system should be determined first, which extend to both practical and daylight-performance related requirements.

Starting, the variables represented in the analytical calculation are evaluated. The distance of the glass to the centre of the sandwich panel and the thickness of the glass panes themselves contribute to the analytical stiffness. The first parameter is the thickness of the core t_y. Both the analytical solution and the calculated solution in Karamba3D of the 2x2 m^2 panel as defined in Table 17 are shown in Figure 75.
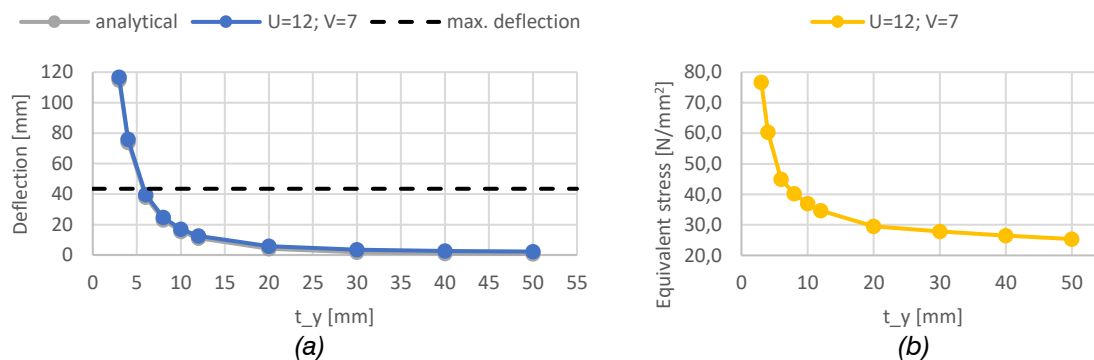

Figure 75 Varying thickness core t_y for a 2x2 m^2 panel: (a) deflection; (b) equivalent stress (utilisation)

The behaviour of the calculated value closely matches that of the analytic solution. Both show that the deflection barely reduces after a thickness of 20 *mm*. The stresses acting within the panel do not appear to surpass the tensile bending strength of 90 N/mm^2, unless the thickness is unpractically thin. This shows the deflection is normative, where the thickness should exceed 5 *mm*. Since the thickness of the core mainly determines the overall size of the full panel, the boundary conditions of the façade should be determined first, to ensure a structurally sound panel is possible.

The other parameter determining the analytical stiffness is the thickness of the glass t_{glass}. The results of varying this parameter are shown in Figure 76. The behaviour of this parameter is similar to that of the thickness of the core, showing that the deflection is normative. This can be explained by the maximum stresses acting in the glass pane, resulting in lower stresses when the thickness of the glass increases.
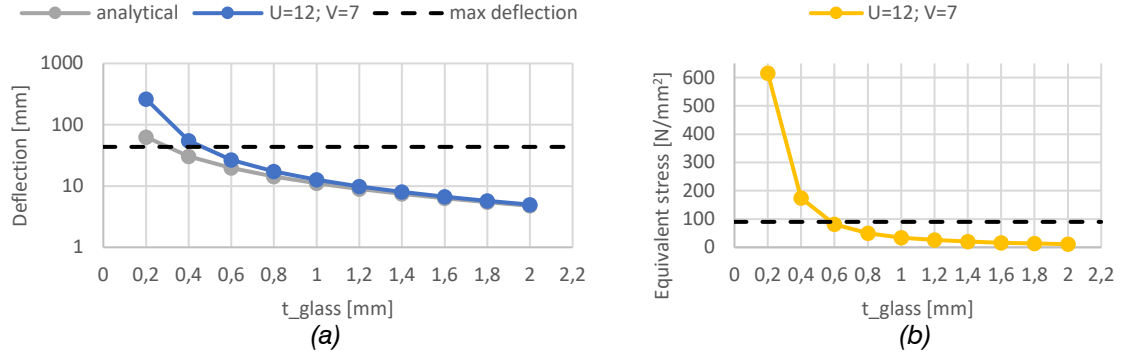

Figure 76 Varying thickness glass pane t_{glass} for a 2x2 m² panel: (a) deflection (logarithmic y-axis); (b) unity check (logarithmic y-axis)

The analytical calculation ignores the effect of the core and assumes it is successful in directing the stresses from one glass pane to the other. However, the actual design of the core pattern determines whether the sandwich panel is effective. Here the amount of material used in the two-dimensional plane and the distribution of this material determine the overall stiffness of the sandwich panel.

The main parameters of the core are the choice of pattern and its thickness. Starting with the honeycomb pattern, four different division are selected to be evaluated, see Figure 77. The cells are kept mostly equal in width and height since it is a square panel. For different width to length ratios, it may be more beneficial to have a different ratio between the U- and V-division.
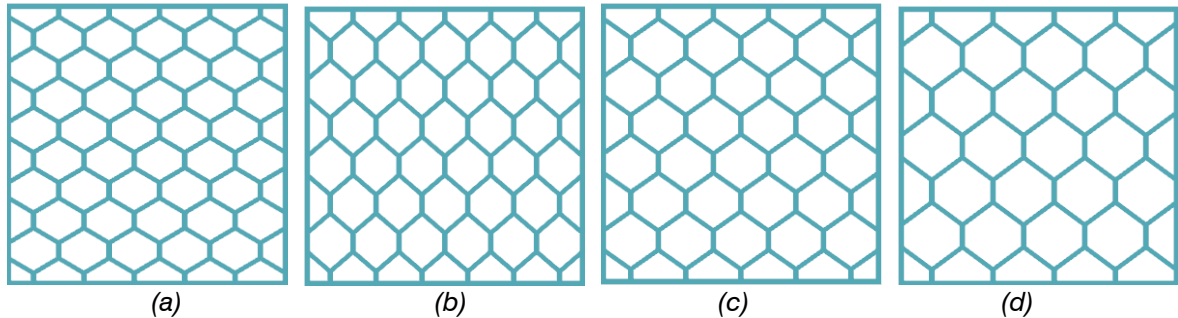
Figure 77 2x2 m² panel with: (a) U-division=11, V-division=9; (b) U-division=12, V-division=7; (c) U-division=10, V-division=7; (d) U-division=9, V-division=6

For these four panels, the thickness in x and z direction is varied as shown in Figure 78. The results show a steady reduction in both deflection and equivalent stress value once the thickness is increased. However, the effect of changing the U- and V-division is much larger. This can be explained by the change of cell size in the pattern. When this reduces, the stresses are more equally distributed throughout the glass pane, reducing the overall deflection and maximum stresses.
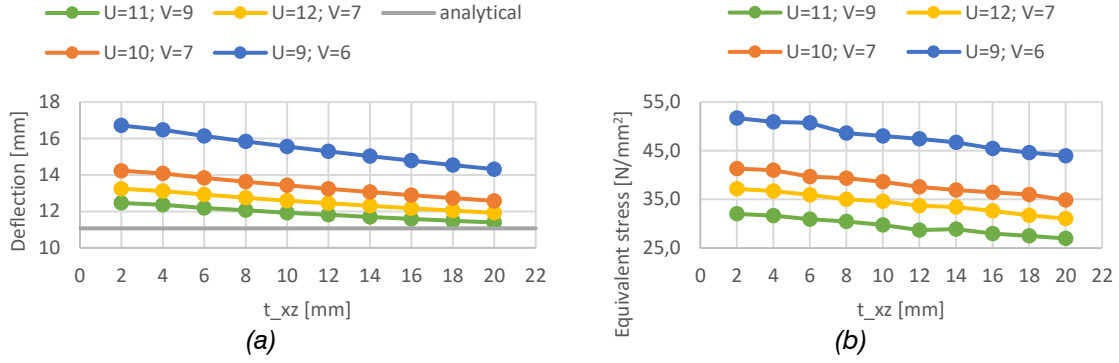
Figure 78 Results varying thickness of pattern for a 2x2 m² panel: (a) deflection; (b) equivalent stress (utilisation)

The thickness of the pattern in Figure 78 is changed uniformly in both *x* and *z* direction. This can also be varied by applying a changing factor over the width (*x*) and height (*z*) of the panel. This is applied to the pattern by multiplying the thickness with a factor, increasing or decreasing the thickness over the height of width of the panel. In Figure 79 the effect of the factors is shown for a few cases.
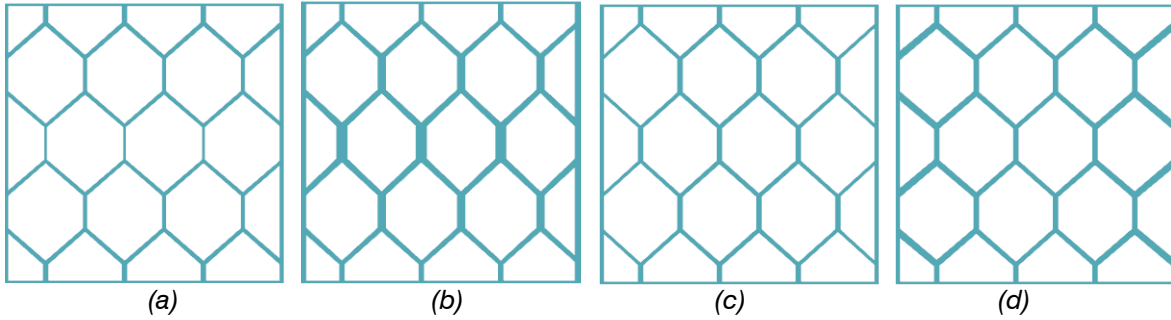
Figure 79 (a) t_x = 0.5, t_z = 1: inside verticals decrease thickness; (b) t_x = 2, t_z = 1: inside verticals increase thickness; (c) t_x = 1, t_z = 0.5: outside diagonals decrease thickness; (d) t_x = 1, t_z = 2: outside diagonals increase thickness

Further combinations can be made, where the resulting deflection and unity check is calculated, see Figure 80 for the results. For the deflection, the effect of increasing the factor along the *x*-axis is significantly less than over the *z*-axis. For the maximum equivalent stress, the opposite effect can be seen. It can be concluded that changing the factors will influence the relation between deflection and equivalent stress and it can be used to improve on only one of these. However, it is important to realise this is heavily dependent on the pattern used, so this should be evaluated per case.
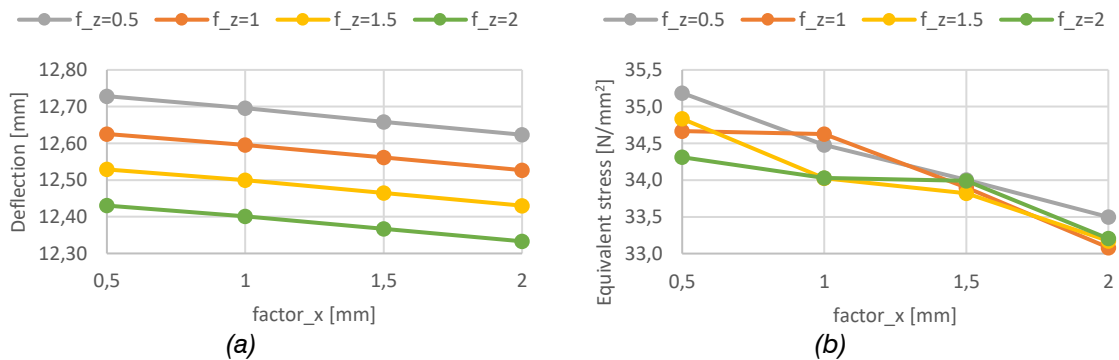
Figure 80 Varying thickness along the pattern in x and z direction for a 2x2 m² panel: (a) deflection; (b) equivalent stress (utilisation)

In this evaluation of the core so far, only the honeycomb pattern has been used. Other patterns are available as well, where the pattern with circular openings is especially interesting. For the inflatable concept, this may be a suitable pattern for inserting round inflatables. An additional option where the inside of the hexagon is followed using a second degree nurbs curve is also explored here, see for the visualisation of both.
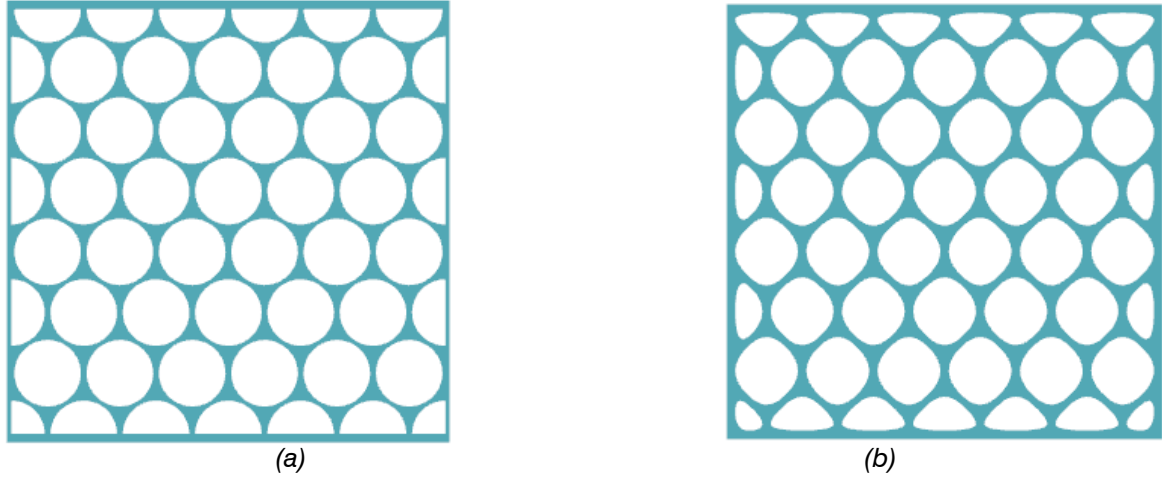

(a)   *(b)*

Figure 81 Based on U=12, V=7 hexagonal pattern: (a) pattern with circular openings (r=150 mm shown); (b) pattern with second degree nurbs curves (10 mm thickness shown)

First, the circular pattern is analysed for varying inside radius in Figure 82. To be able to compare these results to the hexagonal pattern, the results of the pattern with 10, 20 and 30 *mm* thickness are added. For example, the hexagonal pattern with $t_{xz}=10$ *mm* performs equally in terms of deflection compared to a circular panel with $r = 160$ *mm* open cell. The total surface area of this circular and hexagonal pattern is 0.622 m^2 and 0.555 m^2, respectively. This comparison shows that for the circular pattern, much more core material is needed to achieve the same level of stiffness as the hexagonal pattern.

(a)   *(b)*
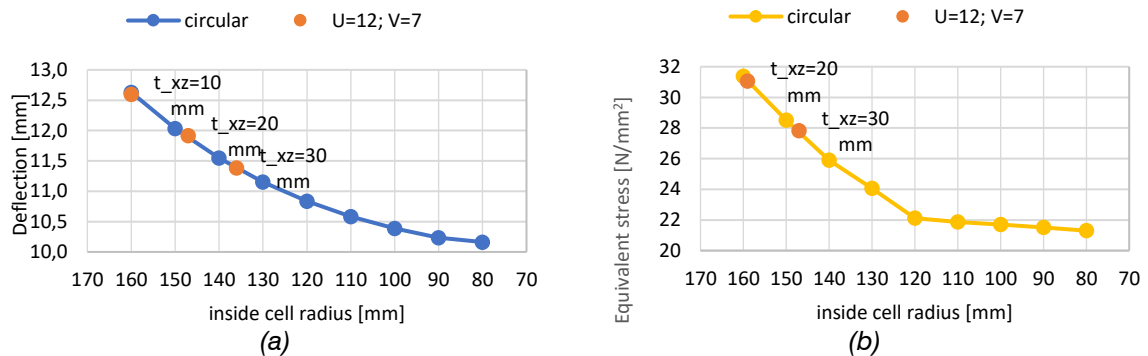
Figure 82 Results panel with circular cells, U=12, V=7. Additional comparison points with hexagonal U=12, V=7 panel: (a) deflection; (b) equivalent stress (utilisation)

The results of the analysis of the nurbs curves are shown in Figure 83, compared to the results of the normal hexagonal pattern with varying thickness. This shows a decrease in both deflection and equivalent stress, showing that softening up the edges of the hexagonal cells is both an effective way to reduce the sharpness of the corners of the cells, but also in increasing its structural stiffness.
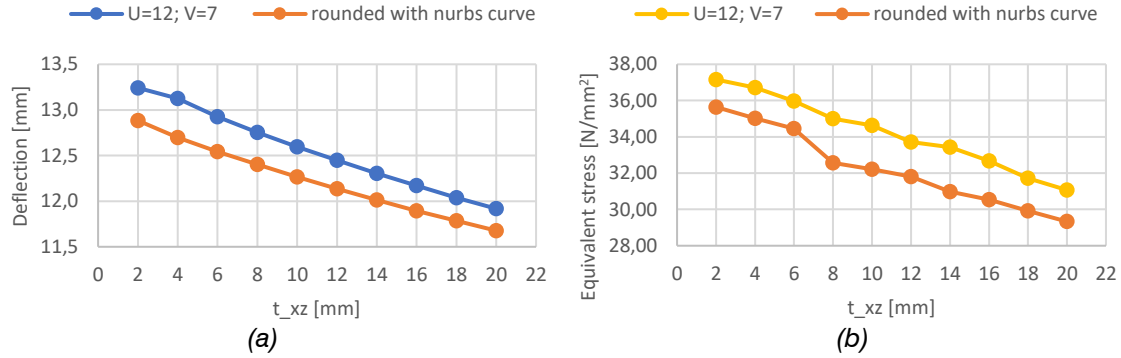
Figure 83 Results panel with nurbs curves, U=12, V=7. (a) deflection; (b) equivalent stress (utilisation)

3.1.5 Varying parameters core in the 3D plane

In this section, the effect on structural performance of the panel due to variation along the third axis, in the *y* direction, is studied. Since the core material is made with a three-dimensional printer, variations along the thickness of the core are possible as well. This allows the core to be modified to the requirements of the integrated dynamic system. This can result in openings to the core pattern, splitting the core in separate parts, or changing the thickness of the pattern along its *y*-axis. The effect of these adjustments on the structural stiffness of the panel is evaluated here.

First, the effect of adding holes or openings to the core is studied. The openings are added over the width of the panel, where tubes or other elements could be inserted. First, a round hole with radius of 4 *mm* is modelled, so that for a 12 *mm* core depth there is still 2.5 *mm* at both edges of the hole. This allows the core to stay a singular piece. The other two options explored here have a rectangular opening of 20 and 40 *mm*, which separates the core into five sections, see Figure 84.
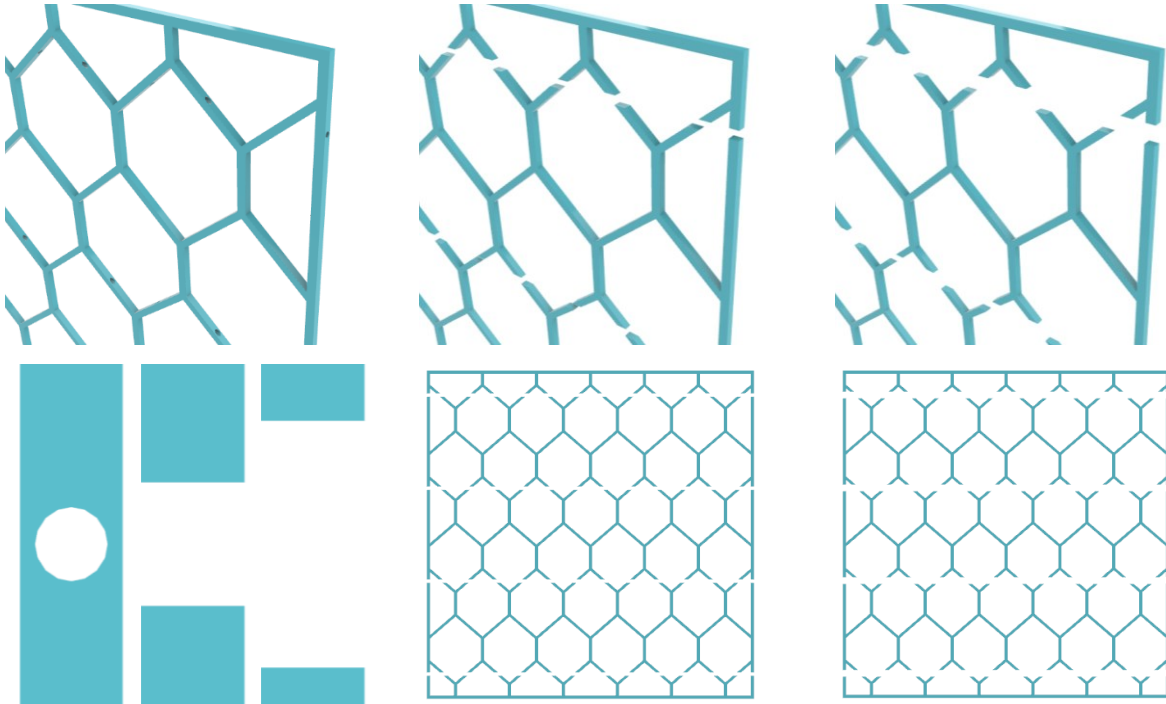
Figure 84 Hexagonal core with openings: round r=6 mm, rectangular t = 20 mm and rectangular t = 40 mm; Total volumes are 0.009285 m³, 0.008971 m³ and 0.008501 m³, respectively.

Next, the thickness of the core pattern is changed along the *y*-axis of the core. The first option lets the two sides connected to the glass at the same thickness but reduces the middle of the core to 10 *mm*, see Figure 85a. Here the surface is curved to create a smooth transition. The other option evaluated has a 20 *mm* thickness on one side of the panel and a 5 *mm* thickness on the other, see Figure 85b. Here the transition is kept straight.
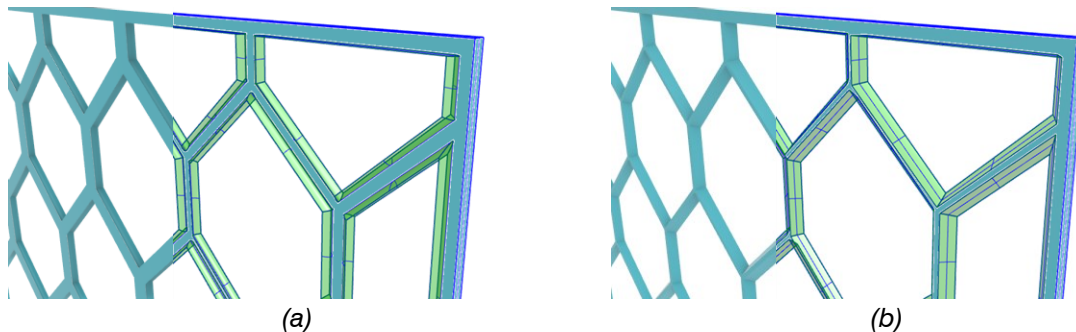

| (a) | (b) |

Figure 85 Changing pattern along y-axis; (a) 20 mm on the outsides, 10 mm in the inside, curved; (b) one side 20 mm, the other 5 mm, straight. Total volumes are 0.011794 m³ and 0.010947 m³ respectively

To be able to determine the structural strength of the panel with full three-dimensional detailing, the solid elements analysis in Diana FEA is needed. First, the 2x2 *m²* as defined in Table 17 is evaluated for different thicknesses of the pattern. This will function as the basic stiffness at which the panels with adjustments can be compared to. The results in this section first use the deflection to evaluate the stiffness. The calculated maximum stress acting withing the panel is dependent on the mesh division, which differs slightly because of the additions. Therefore, the stresses are evaluated by looking at the stress distribution images.

The deflection of the extruded two-dimensional pattern with no adjustments made over the *y*-axis is plotted against the thickness of the pattern. In this graph, the resulting deflections of the patterns with adjustments are added, to be able to compare their performance, see Figure 86.
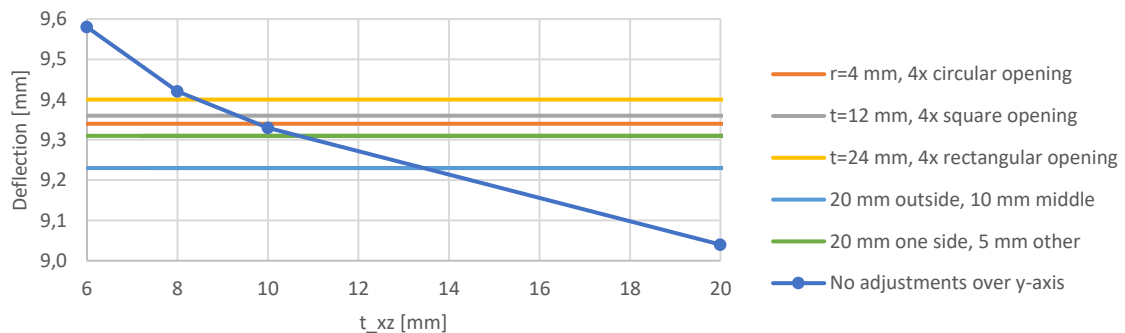

Figure 86 Results deflection of different adjustments in the y-axis of the core pattern, compared to a pattern with no adjustments

The results show that adding small openings barely influences the deflection of the panel, as can be seen in the circular 4 *mm* opening and the 12 *mm* square opening. The larger rectangular opening of 24 *mm* does show an increased deflection, but this is still relatively limited. The two adjustments along the *y*-axis show a significant increase in deflection compared to the 20 *mm* pattern thickness panel. The amount of core material used in these adjustments is reduced, so an increase in deflection is to be expected.

To be able to compare the stresses acting in the panel, the equivalent stresses are shown with a standardised scale, see Figure 87. These scales still include the maximum stress value and show the percentage of each range of stresses. This shows the decline in stresses in the panel when the thickness increases.
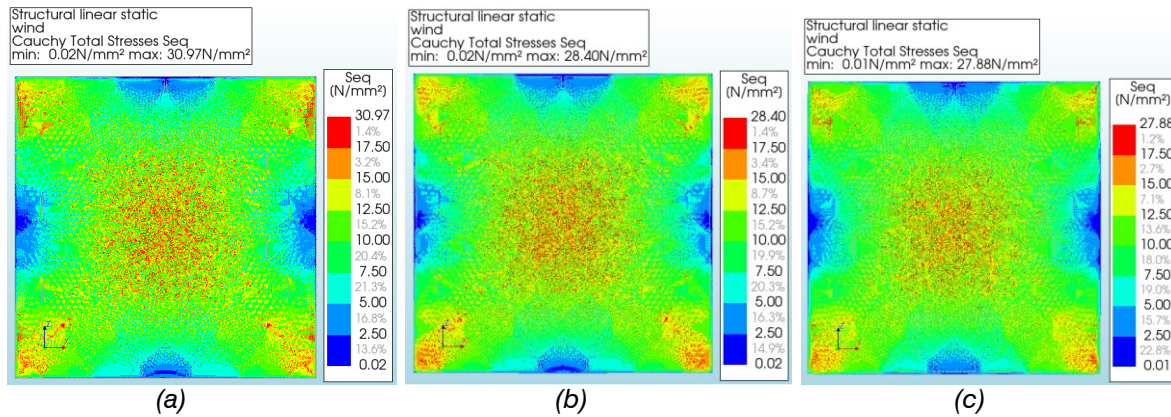

Figure 87 U=12, V=7 pattern with no adjustments (a) t_{xz} = 8 mm; (b) t_{xz} = 10 mm; (c) t_{xz} = 20 mm. Total volumes are 0.007995 m³, 0.009442 m³ and 0.016408 m³ respectively

The resulting stresses of the panels with the adjustments are shown in Figure 88. The three options with openings (Figure 88a, b and c) show an increase in the stress division in the panel compared to the panels with no adjustments (Figure 87b), however the maximum stress does not significantly increase. The two options with varying thickness along the y-axis (Figure 88d and e) appear to both be most similar to the stress divisions of 20 *mm* (Figure 87b and c). This shows that it is safe to assume the strength of the minimal thickness along the y-axis, where the actual strength will be higher.
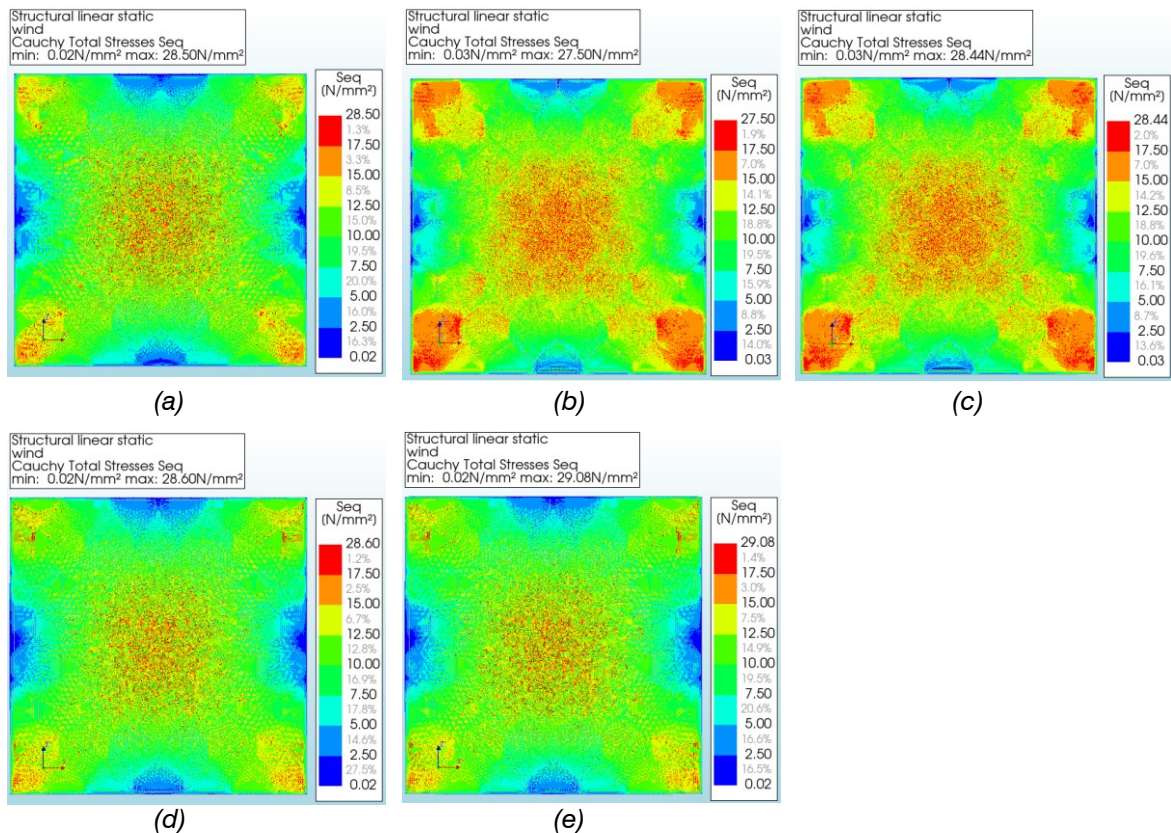

Figure 88 (a) r=4 mm, 4x circular opening; (b) t=120 mm, 4x square opening; (c) t=24 mm, 4x rectangular opening; (d) 20 mm outside, 10 mm middle; (e) 20 mm one side, 5 mm other side

3.2 Developing Concepts

In this section, the two design concepts are further explored and developed. Possible issues will be discussed and based on the feasibility of the designs; one will be selected to develop further. Both the designs will be modelled using the Grasshopper model in Rhino, see Appendix A.2 and A.3.

3.2.1 Inflatable design

The first design concept uses inflatable elements placed inside the open cells of a pattern. As a starting point, the octagonal pattern is used, with spherical inflatable elements. The inflatable elements are connected via tubes, which means the inflatables can be inflated separately per row. For the location of these rows, multiple options are considered, see Figure 89. The first option can control each row individually, allowing a more precise control. However, these tubes will still be visible once the façade is deflated, thereby obstructing the view. The second option therefore is closer to the pattern of the core material, allowing the cells to be more open.
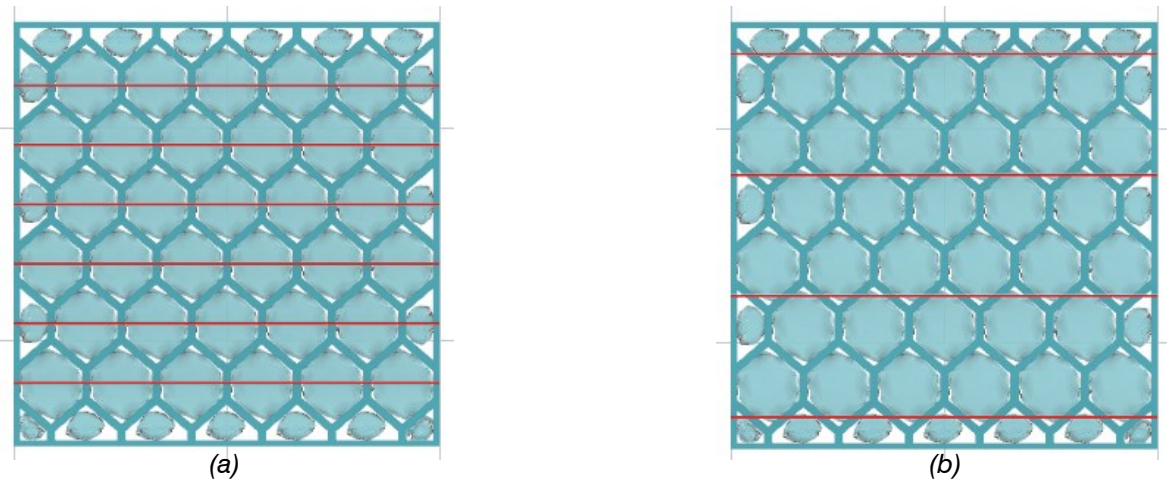

(a)	(b)

Figure 89 Possible locations of tubing for inflatables: (a) located in centre of each cell horizontally; (b) located to connect two rows

The design of the inflatables themselves is done using the Kangaroo plugin within Grasshopper. Here the spherical inflatables are modelled using a triangular mesh pattern. The model then applies the pressure to each triangle and allows the edges of each triangle to lengthen as defined. The actual material properties can then be derived from this elasticity. Figure 90 shows the resulting inflatables. Here you can clearly see the triangular mesh used instead of a smooth surface of an actual spherical shape.
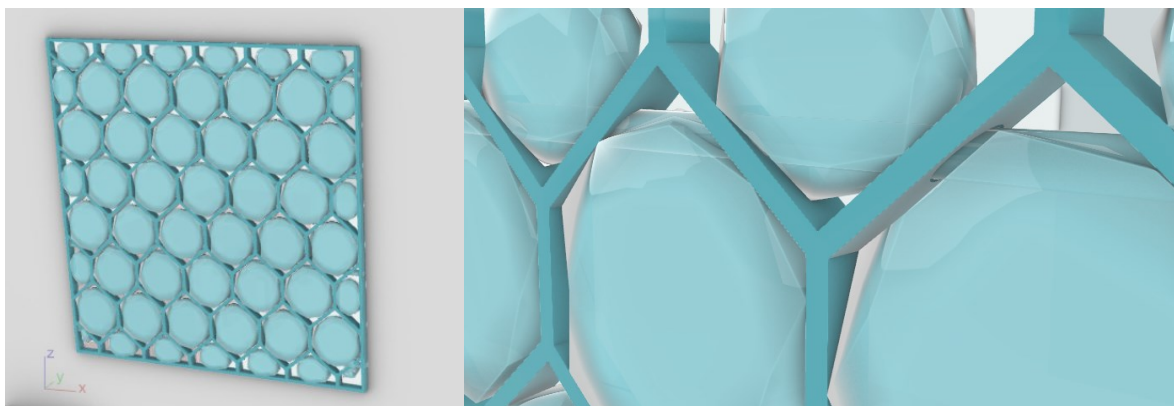

Figure 90 Inflatables in hexagonal core

When using the hexagonal core, the spherical shapes used as the inflatables do not fully align near the edges. This can be solved by increasing the air pressure or by increasing the flexibility of the material. However, this does increase the risk of modelling unrealistic designs. An inflatable will try to divide the air pressure equally, resulting in rounded shapes. This does not fit closely in sharp corners of the core, potentially leaves open gaps.

An initial solution is to make the core match the shape of the spherical inflatables by having circular cells. In Figure 91 this is shown, where you see the inflatables aligning much more closely to the core pattern. The edges, where the pattern is half a circle, does still show a large difference in shape.

Figure 91 Inflatables in core pattern with circular cells

Another solution would be to design the inflatables such that they match the inside shape of the cells. Figure 92 shows the result of these inflatables, where the inflatables very closely align with the pattern. The openings still visible are due to the triangular modelling of the inflatables. This solution increases the complexity of designing the inflatables, but it keeps the core pattern in an efficient hexagonal pattern.

Figure 92 Inflatables in hexagonal core, where the inflatables have the same shape as each cell

Another method of preventing gaps from forming, is to hollow out the sides of the pattern along the y-axis, see Figure 93. This allows the inflatable to connect better to the core material, reducing the chance of creating gaps. For the structural stiffness, it lies in between the widest and smallest thickness, see section 3.5.1. To be safe, the smallest thickness can be assumed for structural analyses. For daylight analyses the thickness at the edges should be taken.
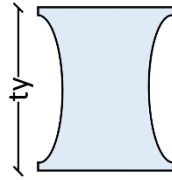
Figure 93 Rounding the sides of the pattern

The main goal of these inflatables is to control glare, while still allowing daylight to enter through the panel. Like common external shade systems, often only the top part of a window is covered. This blocks solar rays at eye level, while still having open windows. The system with inflatables can also be used like this, by only inflating certain rows, see Figure 94. The placement of the connecting tubes and the placement of these tubes in connection to the air compressor should be designed further.
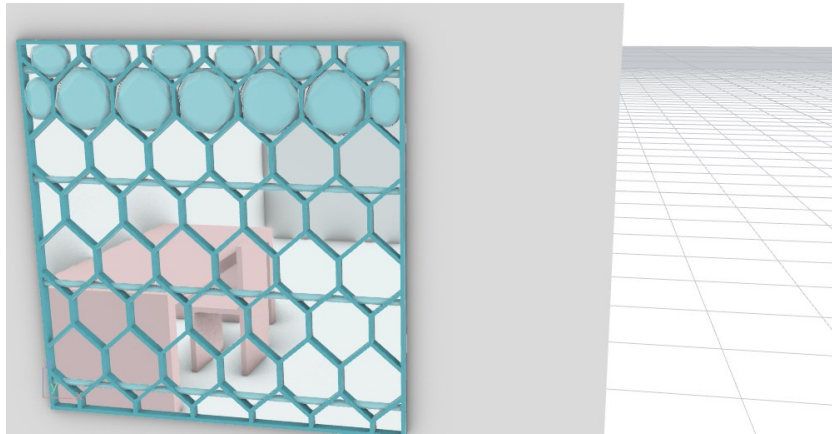
Figure 94 Option with only the top two rows inflated

3.2.2 Folding design

The second design alternative uses a folding mechanism to cover and uncover the open cell space. For exploring this option, the hexagonal pattern is used here, but this could also be applied to the other patterns. Each hexagon is divided into triangles, so that the cell can open from the middle. First, this design is made by bending the triangle around the axis where it is connected to the core, see Figure 95. The triangles themselves do not bend here, which is why they take up a lot of space in the y-direction. Since this mechanism will be placed integrated into the panel, the height should be limited to allow the full panel to stay compact and practical to use.
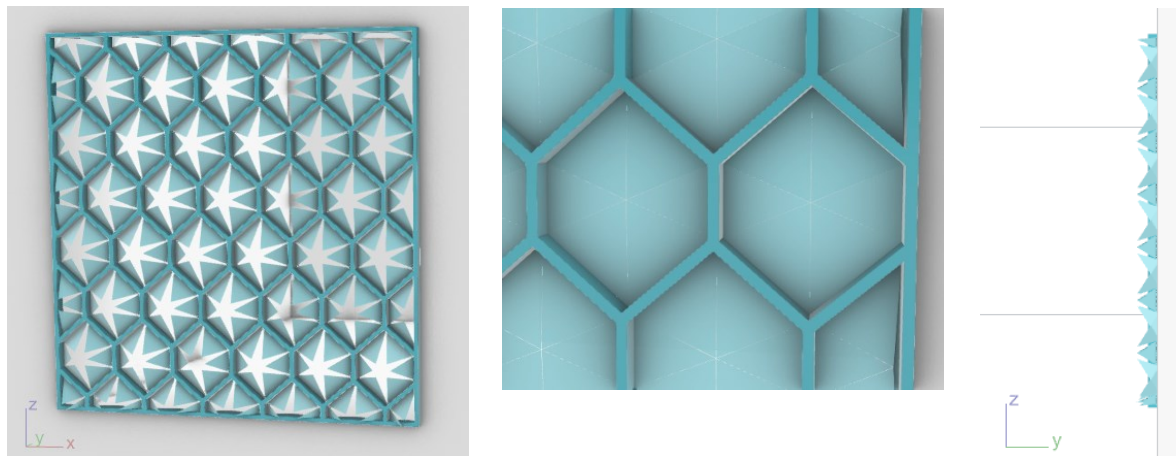

Figure 95 Folding design without curve

To limit the space needed over the y-axis, the triangles can also curl up instead of only bending at the connection to the core. Inspired by the bending mechanisms explored in the literature review, the resulting curve to open the cells is shown in Figure 96. Depending on the size of the cell, the size of the triangles and the space available over the y-axis, the final curve can be adjusted.
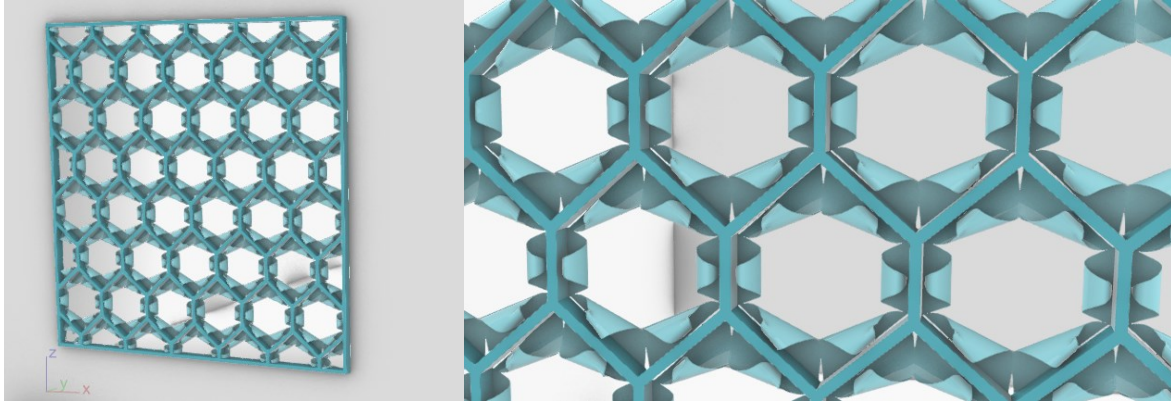

Figure 96 Folding design in opened state with predefined curve

This curling motion is modelled using a predefined curve. To be able to achieve this curvature, the material needs to be carefully designed to match this shape once activated. The constricting space between the two glass panes can also be a source of issues. The material could catch itself against the glass and thereby not being able to fully curl up.

Lastly, this system introduces a lot of separate parts. For preventing glare, the cells need to be able to fully close with no gaps. For this design concept, the material needs to fully straighten again to fully close the panel. Since these are dynamic parts, they can be vulnerable to fatigue, or are at risk of failure. Fixing a cell would require the entire panel to be replaced, which makes this a panel very vulnerable to become dysfunctional.

3.2.3 Comparison concepts

The two concepts described both offer a way to fully close a façade on demand. The method and materials used are different. In this section, the two concepts are compared on both the complexity of the system and the long-term functionality. Based on their performance one concept is selected for the remainder of this thesis.

Complexity

Complexity in the design should be minimised where possible, since this can increase calculation times, increase its risk of failure and make the product more costly. Furthermore, it is preferable if the design has more repetition. This allows for standardisation of the product and ease in designing.

The inflatable system consists of three main parts, the inflatables, the tubing connected to these inflatables and the air compressor which controls the system. The inflatable completely fills each cell, reducing the number of separate parts. Furthermore, since each cell has the same shape, each inflatable also has the same dimensions. The cells near the edges are half the size, so these do need different dimensions. The inflatables need to be connected to tubing, which needs to be integrated within the core. This increases the complexity of the core pattern since openings need to be added for the placement of these tubes.

The folding system also consists of four main parts, the foldable triangles, the actuator added to these triangles, the connecting electric wiring and a source of current which can control the system. Each cell results in the same triangle shapes, including the cells near the edges. However, depending on the uniformity of the cell size, the triangles do have a slightly different shape within each cell. This can potentially result in six different types of triangular elements within the design. The electrical wiring can be very thin, allowing for minimal holes in the core material and allowing for more discrete placement.

In conclusion, the properties for the inflatable system are more uniform, allowing for a faster and less complex design process compared to the folding system. The downside of need for bigger tubing does not weigh as heavy, since the required stiffness of the core pattern is easily achievable, even with added openings for this tubing.

Long term functionality

The design of a façade system should always take its longevity into account. A façade element should remain functional during its service life since it is an element of the buildings' envelope. If the risk of failure is very high, it becomes an unfeasible design. Therefore, the design should be judged on the level of fatigue, possibilities in maintenance and overall vulnerabilities in the design.

The inflatable system consists of inflatables connected to tubing that is placed in rows in the panel. When the openings in the core material are designed large enough, it could allow both the tubing and inflatables to pass through. This will allow the inflatables and the tubing to be replaced if necessary. This increases the service life of the panel and reduces the risk of the panel becoming defective.

For the elements themselves, it is important that the inflatables, the tubing and the connecting elements remain airtight. For the inflatables it is important that the deformations of the material remain elastic. Once plastic deformations occur, the quality of the material will reduce over time, increasing the risk of air leakage. For the tubing and the connecting elements leakage is the main concern in terms of the system becoming defective. Lastly, once the inflatables are inflated, they will apply a force onto the core material and the thin glass. This may contribute to fatigue in the adhesive between the glass and the core material.

The folding system consists of moving elements, controlled by an electric actuator that is attached to electric wiring. The main concern in this design in the connectivity of the many different elements and the vulnerability of the electrical actuator and wiring. Each triangle is connected to the core, where loss of this connection will result in this part becoming defective. The actuator is also attached to the triangle, determining how the triangle will curl. If this is placed wrong, it will perform differently and may result in the triangle getting stuck in an unwanted position. Since the space between the two glass panes is very small, there is a risk of the folding triangles catching onto the glass as well.

Since this is an electric system, there is a risk of the electric wiring getting damaged or losing connection to an element somewhere in the system. Because the cells are inaccessible once the façade has been made, a potential failure cannot be fixed. The full panel will need to be reconstructed or replaced, which is not efficient and very costly.

Based on the main properties of the two conceptual designs, the inflatable design appears more feasible and realistic. The risk of failure is very high in the folding design, whereas the inflatable design allows for replacement and in general consists of less parts, reducing the overall complexity. Therefore, the remainder of this thesis will focus on the inflatable design.

3.2.4 Design considerations

With the design concept selected, the main design considerations are discussed here, in particular the system wide level of design choices. The design concept determines the functionality of each individual cell, but also guides the possibilities of a full façade system for a building.

It is important to come to a design which has benefits over existing solutions. Using thin glass significantly reduces the environmental footprint of this façade system compared to conventional systems. The reduction of glass material needed contributes to a much lower energy consumption of the production of the panel.

When designing the core of the system, the thickness will determine how much core material is needed, but also how compact the system is. Keeping this distance small, allows for easy handling of the façade panel, reduces the overall space and material used for this panel.

The system designed here for the office will have an active response system, meaning it can be activated on demand. This allows for manual control of the system, thereby being able to respond directly to glare, increasing the users comfort. Having an active system can also prevent unnecessary frequent opening and closing of the system, which might be perceived as distracting.

The main risk of this design option is to create a too complex system, where the benefits do not weigh up to the functionality of the system. This can be avoided by keeping the design as simple as possible, for example by introducing as much repetition and uniformity as possible, allowing for a more standardised solution. The complexity can also be reduced by increasing the cell size, overall reducing the number of individual parts.

The optimisation process of the panel is mostly based on the daylight performance. The systems' main function is to control glare. However, blocking the solar glare will also influence the amount of daylight entering the room. The main design goal should therefore be to create a system that is able to sufficiently control glare, while still allowing enough daylight into the room and limiting contrast.

This can be achieved on both a macro level and a per cell level. On macro level, the whole solar control system should be considered. Depending on the location of the windows placed in the façade, an overarching system can be designed to optimise the daylight performance for the rooms specifically. This system should be designed keeping the buildings design and location in mind, so it can respond to the present solar path appropriately.

The influence on daylight can also be controlled by looking at the properties at cell level. Here the colour, opaqueness and transparency of the inflatable will determine how much daylight can pass through each cell. Depending on the required glare control of these cells, the properties of these inflatables can be determined.

3.3 Daylight analysis: methodology

3.3.1 Requirements visual comfort

A façade system needs to be able to provide the required visual comfort, visual performance and safety. This entails that the people inside the building can perform their tasks well and are not negatively impacted by the façade system. The actual requirements highly depend on the function of the building, so these will have to be determined first. For the design it is important to create an adaptable product which can be designed to match these specific requirements.

The criteria which determine the luminous environment with respect to daylight are the luminance distribution, illuminance, glare, direction of light and colour appearance of light in the room. The focus will be on glare, contrast and illuminance, which are mostly influenced by the façade system.

A point in time simulation can evaluate the façade at a given moment. The daylight distribution in the room can be measured in its illuminance [*lux*], while glare can be expressed in the *DGP* (Daylight Glare Probability) value. The contrast in the room can be defined by looking at the differences in luminance across the room, expressing it as a ratio between the average luminance in different areas.

The requirement for glare is set at imperceptible glare, which is a *DGP*-value of less than 0.35, see Table 8. The minimum contrast ratio should be set at 3:1, see section 2.4.3 Contrast. The minimum illuminance for 95 % of the office room should be 100 *lux*, where the target average illuminance should be 300 *lux* for 50 % of the total area, see Table 10. These values are based on the annual performance, so the appropriate points in time should be selected to evaluate the performance.

The daylight analyses are executed using the parametric model in Rhino with Grasshopper. For the daylight analysis, the Ladybug plugin with Honeybee is used, which simulates daylight using its radiance functionalities. The goal is to determine how the different parameters effect the resulting daylight, glare and contrast properties of the façade panel and to generate a functional design for the standard office room.

3.3.2 Simulation model

First, a Honeybee model is generated that represents the office room as defined in 3.1.1 Standard room. The model consists of a room with window opening, where the core material and inflatables are modelled as shades, see Appendix C.1. Here, the material properties of the walls, ceiling, floor, ground and glass are defined.

The simulated daylight is dependent on the location of the building and the buildings orientation related to the north. The direct surroundings of the building also need to be included, since they can block the sun from certain directions and influence the results. Therefore, designing a system suitable for a specific building should take the local climate into account, but also the orientation of each individual façade element. A north facing window will get different angles from the sun compared to a south facing window. Furthermore, different functions of rooms may result in different requirements for different sections of the façade. Therefore, the façade should be seen as part of a full system for the whole building. Finding a suitable solution may result in different types of inflatables at different locations within the building.

For the office in this example, the location is set in Amsterdam, where its weather data is used for generating the sky model. North is set in the y-direction of the model. The sky conditions can be used for annual simulations, where it can be used to calculate the daylight factor, spatial daylight autonomy, direct sun hours and the annual radiation.

For the point in time simulations, a specific day and time need to be selected, where the location is used for the location of the sun. The point in time simulations can be used for analysing glare and contrast, but also the illuminance at that time. Throughout the year, the sun has a different altitude. For evaluating the façade system, the two extreme situations are used, which are 21st December (lowest sun) and 21st June (highest sun). For visualisation purposes, three timeslots in a normal workday are selected throughout these days, see Figure 97.

city: AMSTERDAM
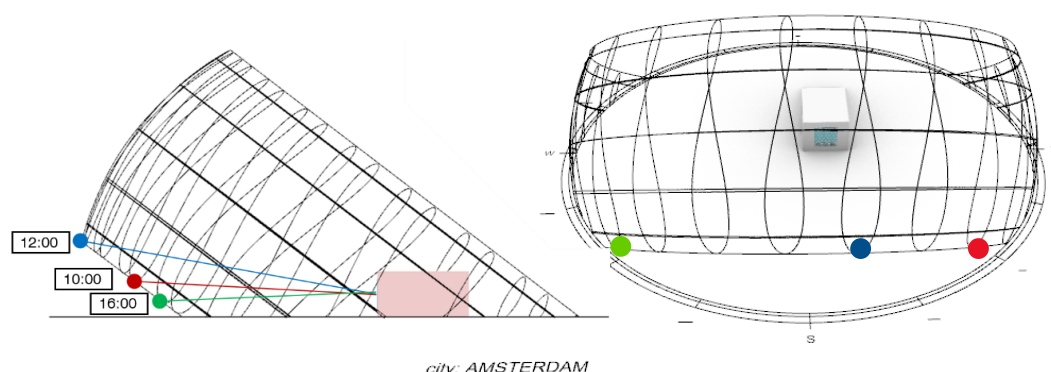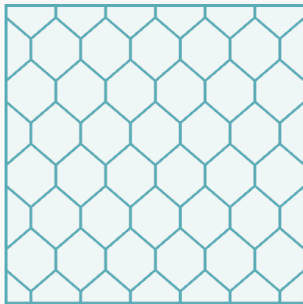
Figure 97 Solar path on 21st December 10:00, altitude = 6.82°; 12:00, altitude = 13.85°; 16:00, altitude = 2.80°

The sky conditions can be selected based on the wanted situation, which can range from sunny to cloudy. For generating the maximum possible glare, the sky conditions are set at sunny with sun. The standard sky component of Honeybee is used to generate this sky, see Appendix C.1.

For the initial daylight analyses, the façade panel for the office is a 2x2 m^2 panel with the dimensions as specified in Table 20. A parameter may divert from this, which will be noted for the particular section. The remaining parameters will still be in accordance with the parameters below.

Table 20 Parameters used for panel

2x2 m^2 panel		
Width window	2 *m*	
Height window	2 *m*	
Height glass panes	1.0 *mm*	
Height 3D core	12 *mm*	
U divisions	12	
V divisions	7	
Thickness sides	10 *mm*	
Thickness pattern x	20 *mm*	
Thickness pattern z	20 *mm*	
Factor x	1.0 *mm*	
Factor z	1.0 *mm*	
Properties inflatables		
Diff_reflectance	0.30	
Diff_transparency	0.15	
Spec_transparency	0	

3.3.3 Grid

To reduce the complexity of the full model, normative rooms can be selected to show the performance of the façade. Depending on the complexity and dimensions of the room, further simplifications may be necessary to be able to quickly generate results. First, the grid size for the calculations is determined in accordance with the requirements defined in NEN-EN 12464-1 (2021), which gives the maximum grid cell size p [m] in relation to the longer dimension of the calculation area d [m]:

$$p = 0.2 * 5^{\log_{10}(d)} \qquad\qquad (28)$$
$$p = 0.2 * 5^{\log_{10}(6)} = 0.70 \ m$$

Using the standard room as defined in 3.1.1 Standard room, the maximum grid size is 0.70 m. Therefore, a grid of 0.5 m by 0.5 m is used at desk height of 0.85 m. The resulting geometry of the room and location of the sensor grids is shown in Figure 98.
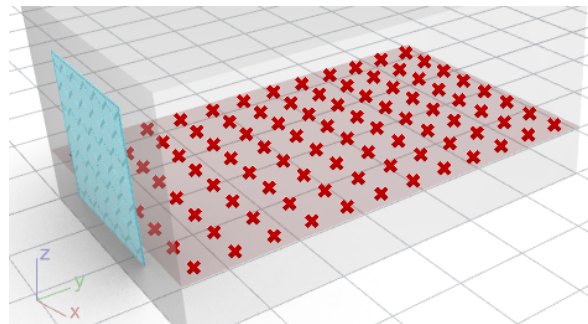
Figure 98 Location of sensor grid in standard office room

On these grid points, several daylight analyses can be executed. These results can then be shown using a heatmap, where each grid point determines the shown colour at that location. The calculation can be a point in time calculation, or an annual based calculation.

3.4 Daylight analysis: results

3.4.1 Annual analyses

The annual simulations can be executed for the façade system without the dynamic inflatables. The honeycomb core is permanently placed in the façade and will influence the daylight performance throughout the year. To study the effect of the core pattern in the façade, a comparison study is done for different thicknesses of the core.

Starting, the thickness of the pattern in y-direction t_y is set at 20 mm and 50 mm and compared to the performance of the façade without the core. For these three settings, the daylight factor is calculated, see Figure 99. This shows that increasing the thickness of the core pattern decreases the daylight factor across the room.
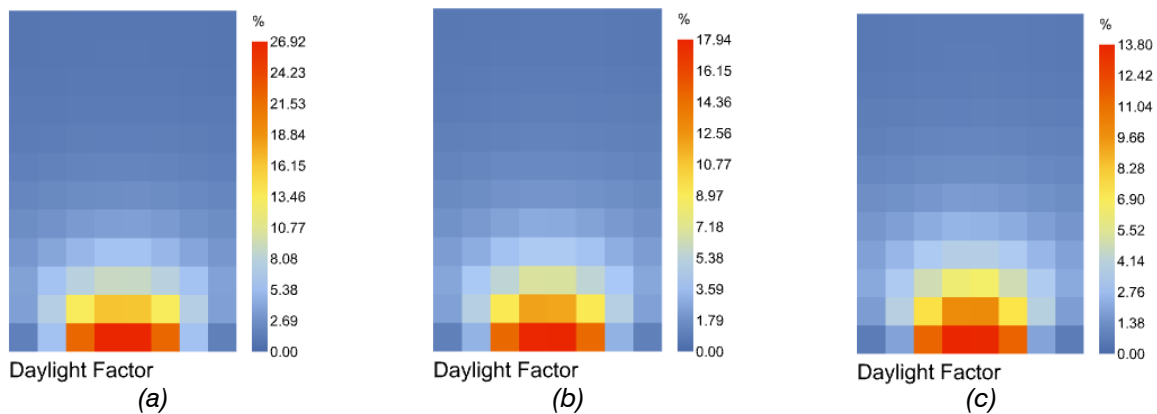
Figure 99 Daylight factor for façade (a) without core, (b) with t_y = 20 mm honeycomb core; (c) with t_y = 50 mm honeycomb core

For the same three settings, the Daylight Autonomy (*DA*) is calculated, which is the percentage of occupied hours that each sensor receives more than the illuminance threshold. The occupied hours timeslot is set from 8 AM to 5 PM and the minimal illuminance at 300 *lux*. The results are shown in Figure 100, where the influence of the core pattern is most notable in the back of the room.
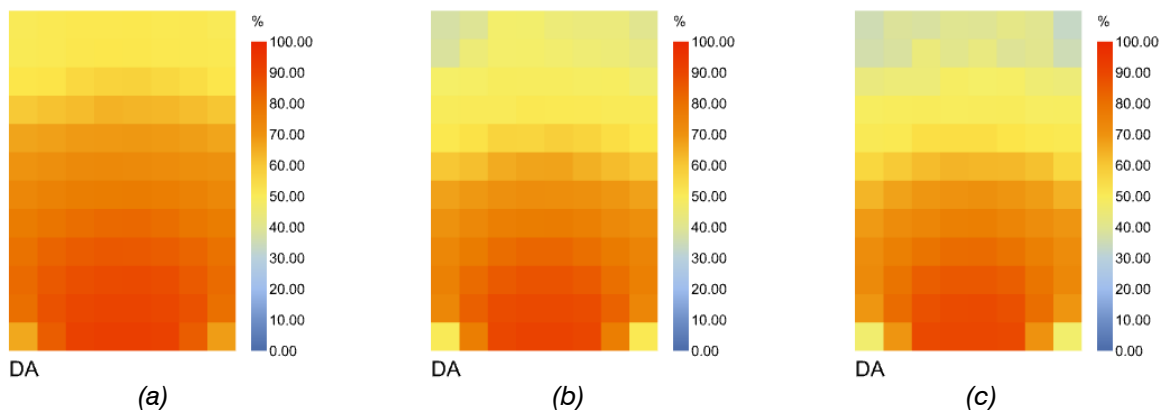
Figure 100 Spatial daylight autonomy for façade (a) without core; (b) with t_y = 20 mm honeycomb core; (c) with t_y = 50 mm honeycomb core

Both the daylight factor and the daylight autonomy show that adding a honeycomb core to the façade reduces the annual illuminance. For the design it can therefore be beneficial to reduce the thickness in y-direction, to allow for a better annual daylight performance.

3.4.2 Glare

The level of glare is dependent on the location of the perceiver. Therefore, three locations are selected in the office to evaluate when and where glare occurs and how this can be managed. These views are located at 0.75, 2.75 and 4.75 *m* away from the façade, at a height of 1.2 *m* representing eyelevel when seated. Two situations are considered, one where the viewer looks directly outside and one where the viewer looks parallel to the façade, see Figure 101.
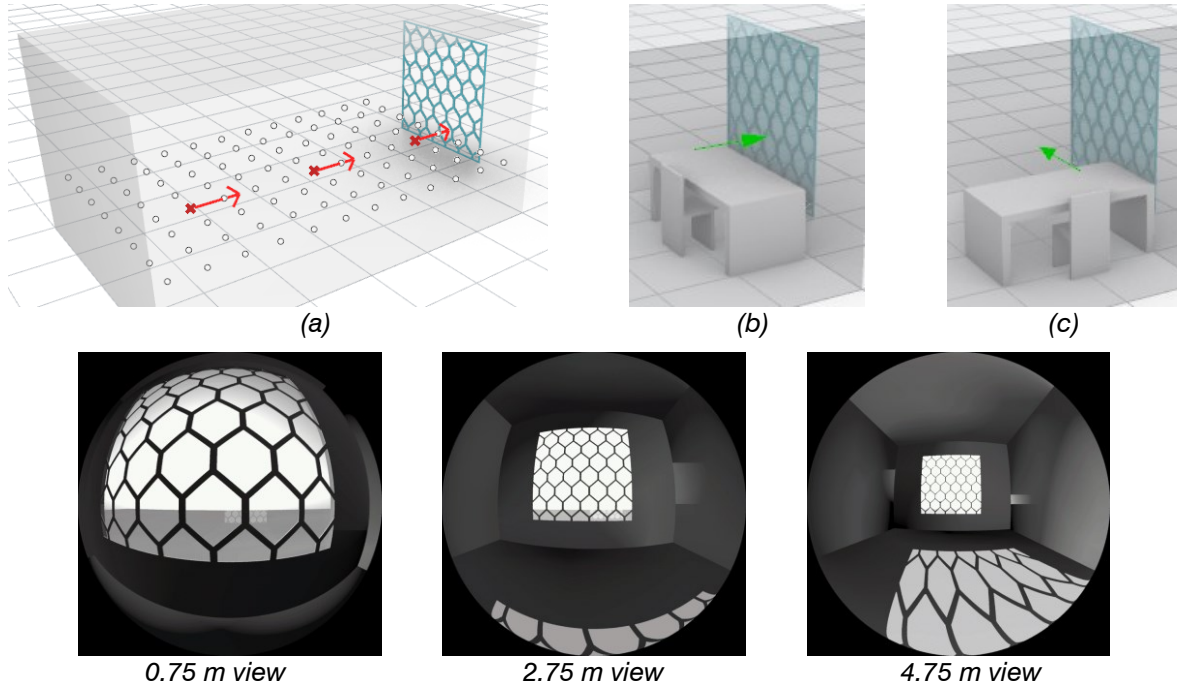

(a)	*(b)*	*(c)*

0.75 m view	2.75 m view	4.75 m view

Figure 101 (a) Locations viewer at 0.75, 2.75 and 4.75 m from the façade; (b) view directly outside; (c) view parallel to outside

The glare can be visualised by generating a HDR image using the point-in-time view analysis. The resulting image can be shown as a GIF image and as a false colour version. The detail level of the radiance parameter can be set at low, medium and high, where the calculation time increases significantly once the detail level increases. The more complex the façade is or the deeper the room geometry, the higher the detail level should be to generate accurate results.

For this office room, the parameters were determined by executing a convergence test, see Table C.1. In this test, the accuracy of the ambient is iteratively increased, where the values with a stable result (+-10 %) are chosen. These resulting values for the *DGP* calculation are -ab 1, -aa 0.4, -ar 8, -ad 32, -as 16.

To assess the effectiveness of the dynamic façade, the day with the lowest solar path is chosen, see Figure 97. To get an idea of the luminance within the room, first the false colour images of three timeslots are shown in Figure 102, when the viewer is close to the façade (0.75 m) facing outside. The shadow cast by the core pattern is clearly visible on the walls and floor of the room. This shadow may result in contrast on both vertical and horizontal surfaces in the room, which can be experienced as disturbing.
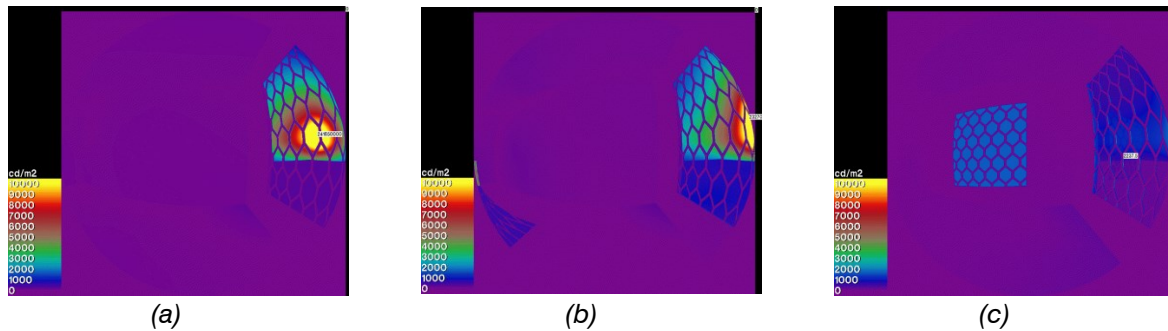
| (a) | (b) | (c) |

Figure 102 Glare on 21st December (a) 10:00, (b) 12:00 and (c) 16:00, not inflated. Point in time fisheye view of view parallel to outside with viewer close to the façade (0.75 m)

The design requirement for disturbing vertical contrast is represented with a *DGP*-value below 0.35, so that glare is imperceptible. The translucency of the inflatables can be designed to just meet this requirement, thereby still maximising the natural light inside the room, reducing the need for additional lighting inside the room.

First, the façade is analysed when only the core pattern is in place, the façade system is not inflated. This is followed by the system fully inflated, with the properties of the inflatables designed to prevent disturbing glare. The measured *DGP*-values as shown in Table 21 are shown to be intolerable in most cases when the inflatable system is not activated (*DGP* > 0.35). However, this value reduces significantly once the system is fully inflated, showing that the inflatables are fully effective in preventing disturbing glare.

Table 21 Glare on 21st December 10:00, 12:00 and 16:00 hour. Resulting DGP-values of system deflated with only the core pattern and the system fully inflated. The results are from the fisheye view located near the façade (0.75 m), directed outside and parallel tot the façade

21st December, 0.75 *m*	10:00	12:00	16:00
Only pattern:			
View directly outside *DGP*	1.000	1.000	0.564
View parallel to outside *DGP*	0.904	0.722	0.195
Fully inflated:			
View directly outside *DGP*	0.217	0.344	0.207
View parallel to outside *DGP*	0.179	0.228	0.174

When looking at the *DGP*-values, only the 12:00 view directly outside is nearing perceptible glare, the other views have much lower *DGP*-values. The system is fully inflated here, but they can also be opened partly. This allows more daylight to enter the room, thereby increasing the illuminance. This option is further analysed when the bottom row is left deflated, see Figure 103 and where the top row is also deflated, see Figure 104. The resulting glare is still imperceptible (*DGP*<0.35) at the depicted timeslot, while increasing the illuminance in the room.
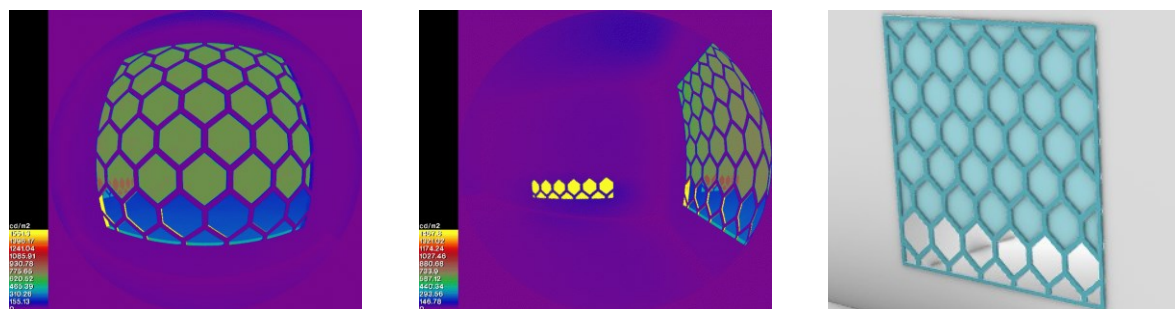

Figure 103 Glare on 21st December 16:00, bottom row not inflated. Point in time fisheye view directly outside (DGP = 0.203), fisheye view parallel to outside (DGP = 0.182)
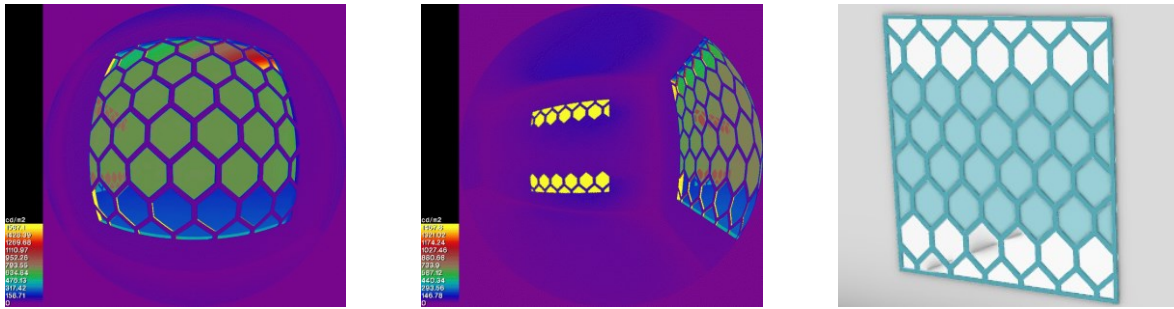
Figure 104 Glare on 21st December 16:00, bottom and top rows not inflated. Point in time fisheye view directly outside (DGP = 0.205) and fisheye view parallel to outside (DGP = 0.188)

The situation with only the core pattern, the fully inflated system and the partly inflated system (both top and bottom row) are further analysed in their performance, see Figure 105. Here the three locations, 0.75 *m*, 2.75 *m* and 4.75 *m* away from the façade are used to show the effect of glare throughout the room. By analysing each view at the different times throughout the day, its vulnerability to glare can be further investigated.
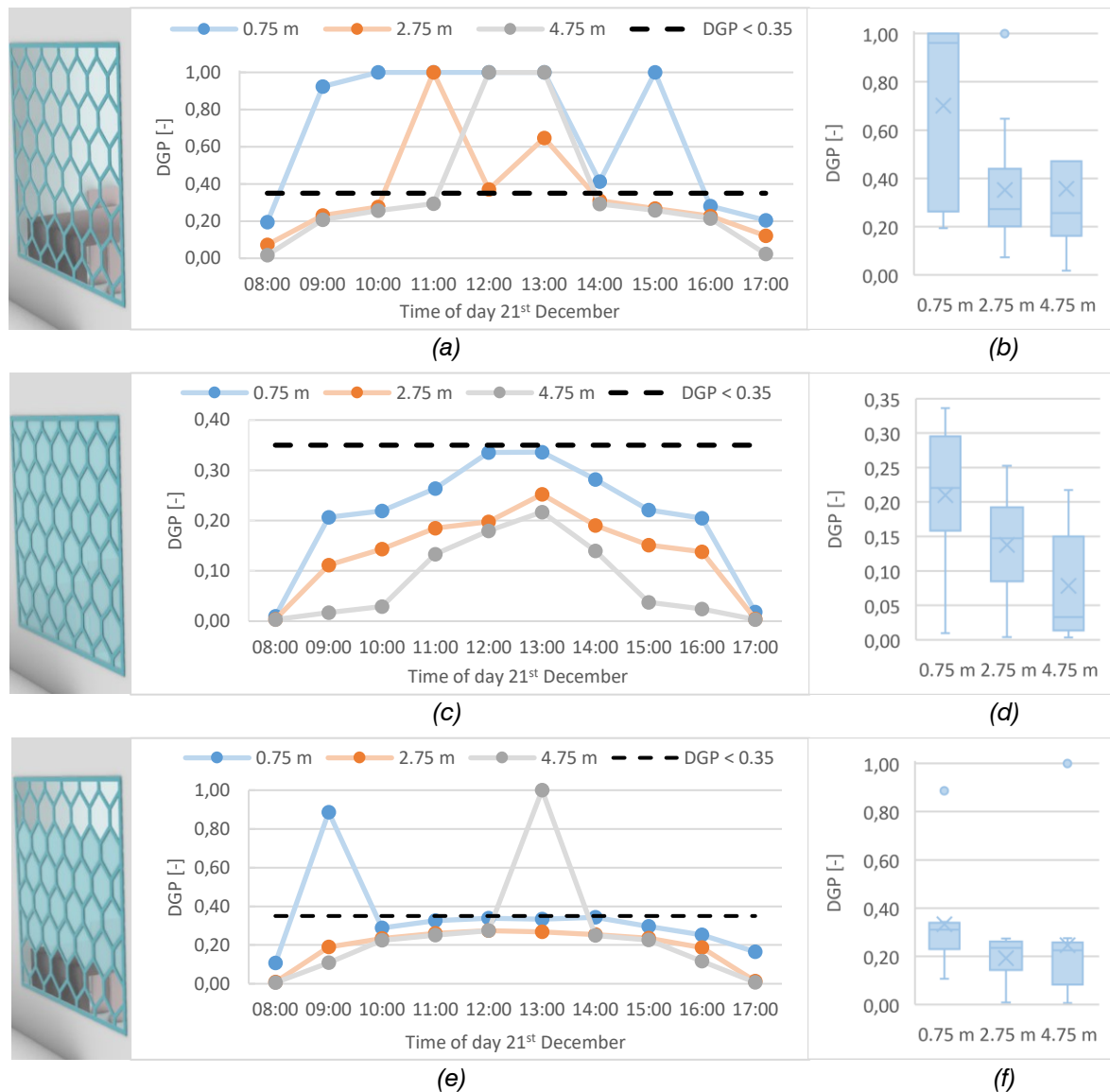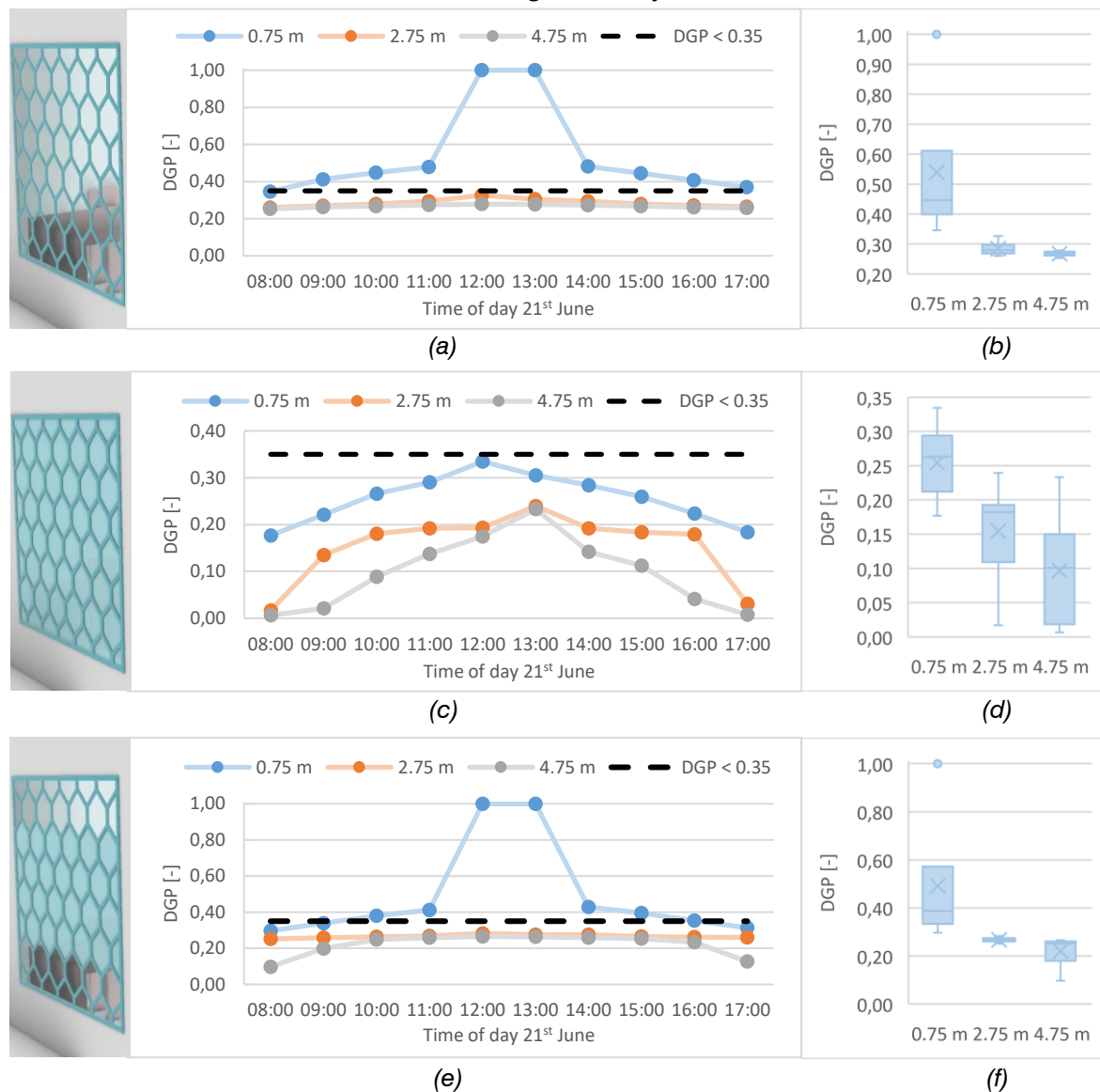

Figure 105 DGP-values at location 0.75 m, 2.75 m and 4.75 m from façade facing directly outside on 21st December. Results depicted throughout the day and with a boxplot. (a, b) Deflated system; (c, d) Fully inflated system; (e, f) Partly inflated system

These results show that once the system is fully inflated, all the views are protected from perceptible glare. The viewer at 0.75 *m* away from the façade is most susceptible to glare, which therefore is the normative position for designing the translucency of the inflatables.

The partly opened system also appears to work most of the time. However, it does show peaks in glare, depending on the location of the viewer. This can be explained by the different altitudes and direction of the solar rays throughout the day. Since part of the façade is not blocked by the inflatables, it can still let the solar rays through. During these timeslots, the system can be inflated completely to prevent the disturbing glare.

Another solution is to further investigate which parts of the façade need to be inflated at which timeslot. Designing the division of rows should be part of the full design process, taking glare control and illuminance into account. Here, the full year should be considered, not only the day with the lowest sun, 21st December. Therefore, the day with the highest sun, 21st June, is also analysed, see Figure 106. Analysing the two extremes gives an indication of the influence of the sun throughout the year.

(a)   *(b)*

(c)   *(d)*

(e)   *(f)*

Figure 106 DGP-values at location 0.75 m, 2.75 m and 4.75 m from façade facing directly outside on 21st June. Results depicted throughout the day and with a boxplot. (a, b) Deflated system; (c, d) fully inflated system; (e, f) partly inflated system

The higher position of the sun on 21st June can be seen in the *DGP*-value throughout the room. The view at 0.75 *m* from the façade clearly experiences glare, while the other views deeper into the room do not experience perceptible glare while the system is not yet inflated. Like 21st December, the fully inflated system is effective in preventing perceptible glare. However, the partly inflated system is no longer effective for the view close to the façade, where especially in the middle of the day the *DGP*-value is high.

The level of glare can be further evaluated by looking at the vertical illuminance at eye level. This shows the contrast in luminance values in the façade and of the shadow cast onto the room. This can be visualised using the false-colour image of the view, where the level of luminance is shown with different colours.

For the office, the resulting false-colour images are shown in Figure 107 with only the core, with the dynamic system deflated. These images show that the casted shadow outline has a luminance in the range of 1500-2000 *cd/m²*. This appears to stay below the threshold of disturbing the viewer, as specified in Table 9.

(a)   *(b)*   *(c)*

(d)   *(e)*   *(f)*
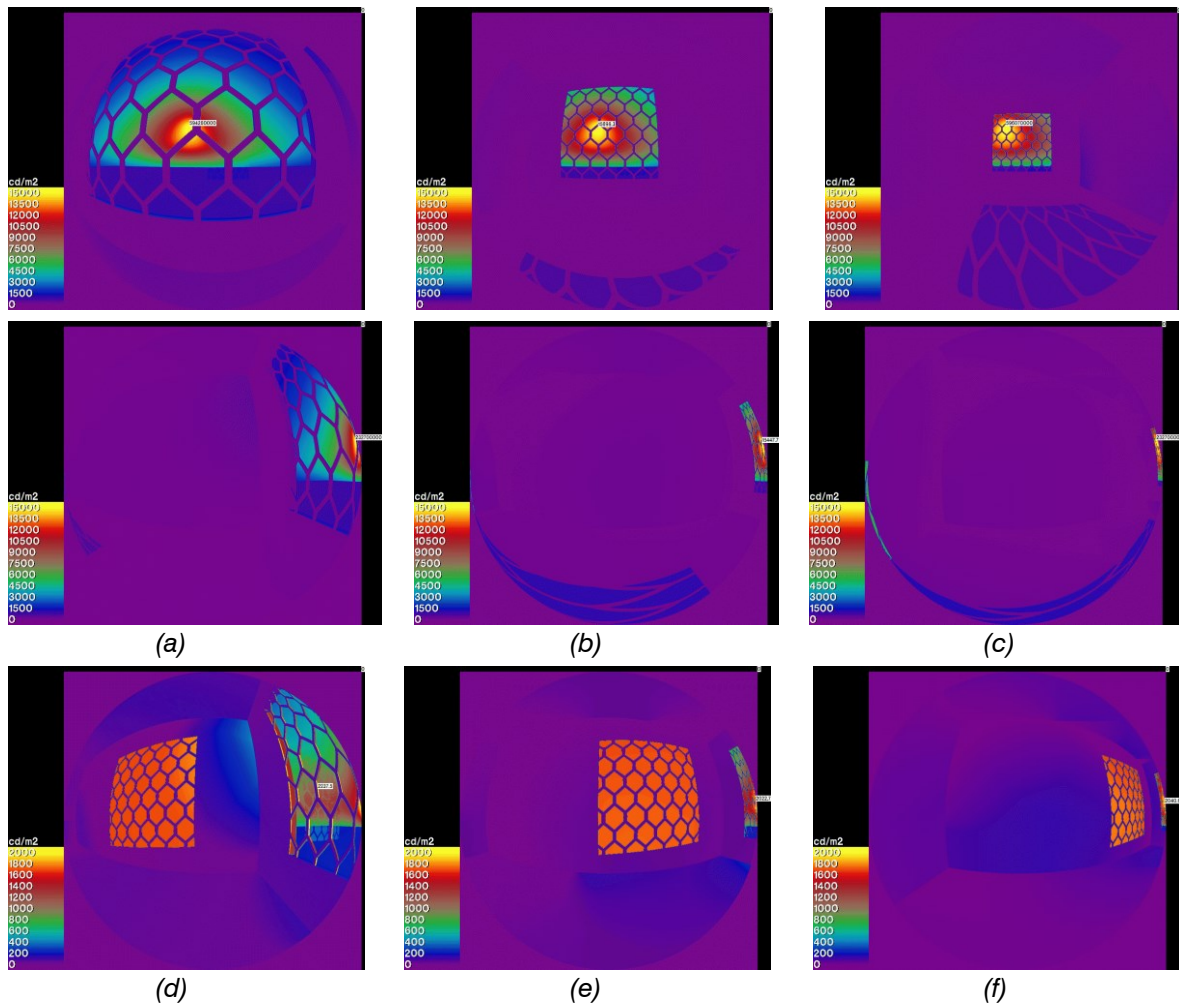
Figure 107 False-colour images of view facing the façade and parallel to façade at 12:00 for viewer located (a) 0.75 m, (b) 2.75 m and (c) 4.75 m from façade. False colour images of view parallel to façade at 16:00 for viewer (d) 0.75 m, (e) 2.75 m and (f) 4.75 m from façade

3.4.3 Illuminance

The illuminance is measured using the Honeybee Point-in-time Grid-based study. Here the input values are the model of the room, the sky and the radiance parameters. After executing the convergence test, see Table C.2, the selected radiance parameters are -ab 4, -aa 0.4, -ar 32, -ad 512, -as 256. The façade system can be fully deflated, fully inflated or partly inflated. The resulting illuminances are shown for 21st December at 10:00, 12:00 and 16:00. First, the system while not inflated is analysed, with the results shown in Figure 108. Here the path of the sun is clearly visible, where much higher illuminance values are present.
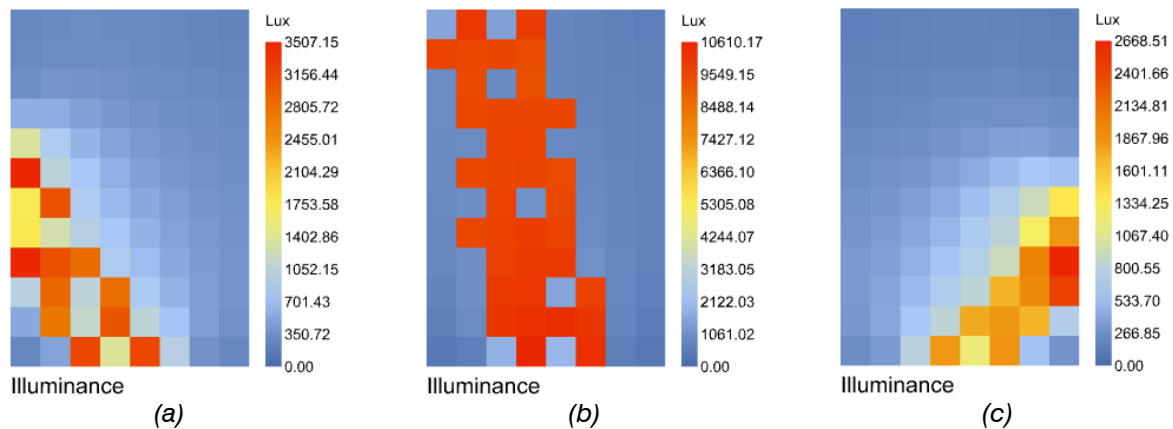
Figure 108 Point in time grid calculation of illuminance [lux] in the office room on 21st December, not inflated; at (a) 10:00, (b) 12:00 and (c) 16:00

In Figure 109 the illuminance is shown when the system is fully inflated, for the same material properties as used in Table 20. The full path of the sun is no longer clearly visible, instead only an increase of illuminance can be seen near the façade. The overall illuminance in the room reduces significantly, especially in the back of the room. Here the requirement of minimal 100 *lux* is no longer met.
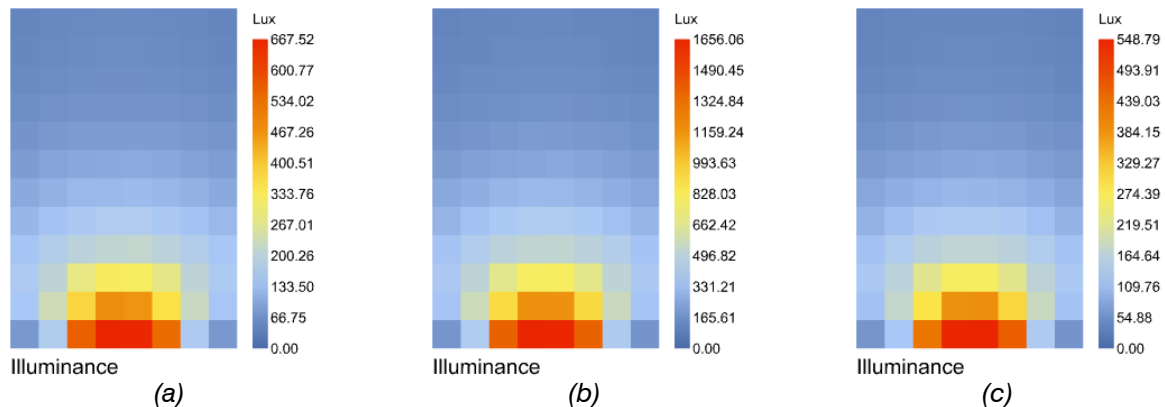
Figure 109 Point in time grid calculation of illuminance [lux] in the office room on 21st December, fully inflated; at (a) 10:00, (b) 12:00 and (c) 16:00

In order to improve the illuminance in the office, certain rows of the inflatables could stay deflated, as shown in Figure 103 and Figure 104. The inflatables in the middle of the façade stay inflated, to protect against glare. To show the effect of the partly inflated system, it is compared to the façade with only glass and only the core pattern, see Figure 110.
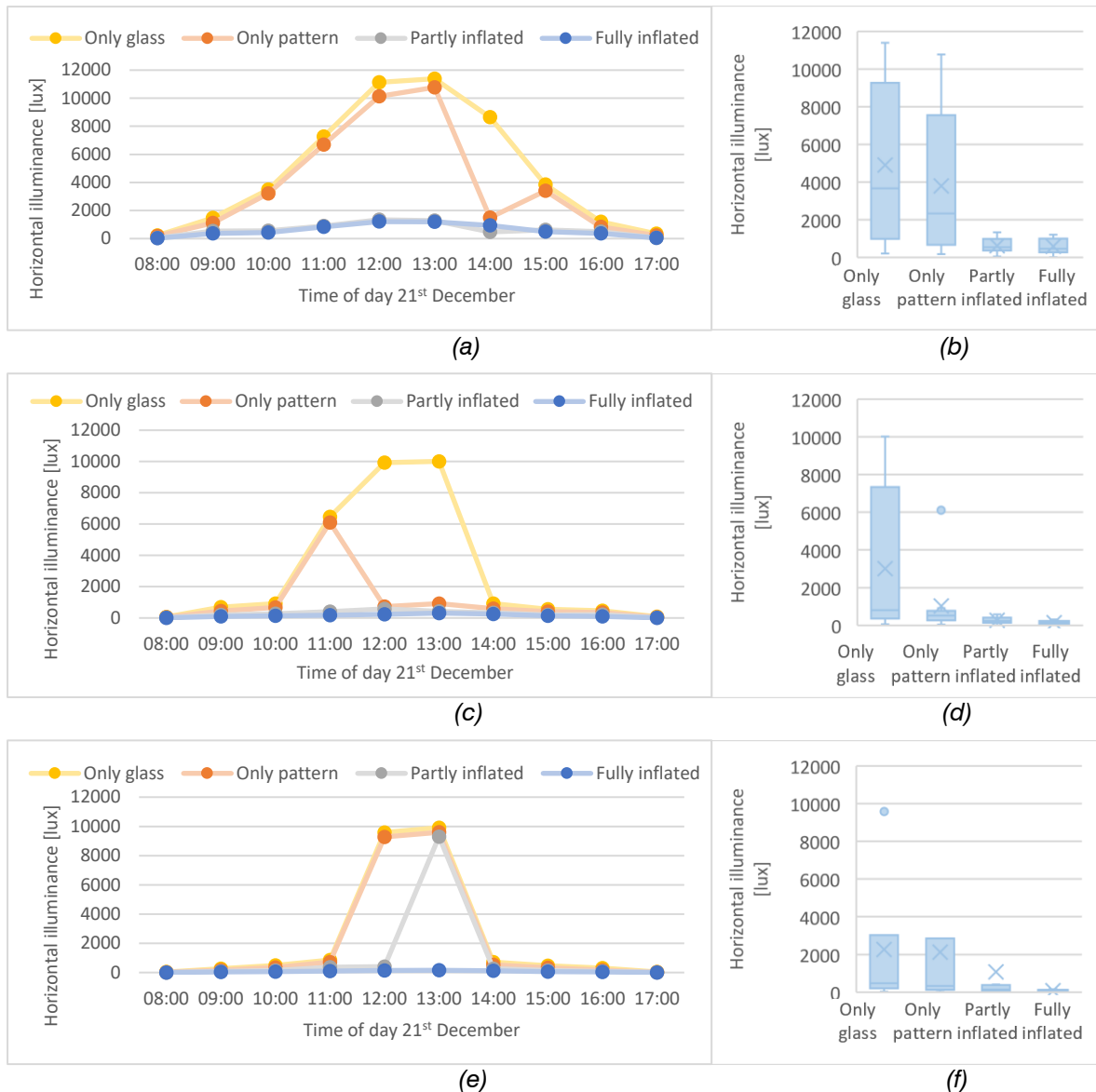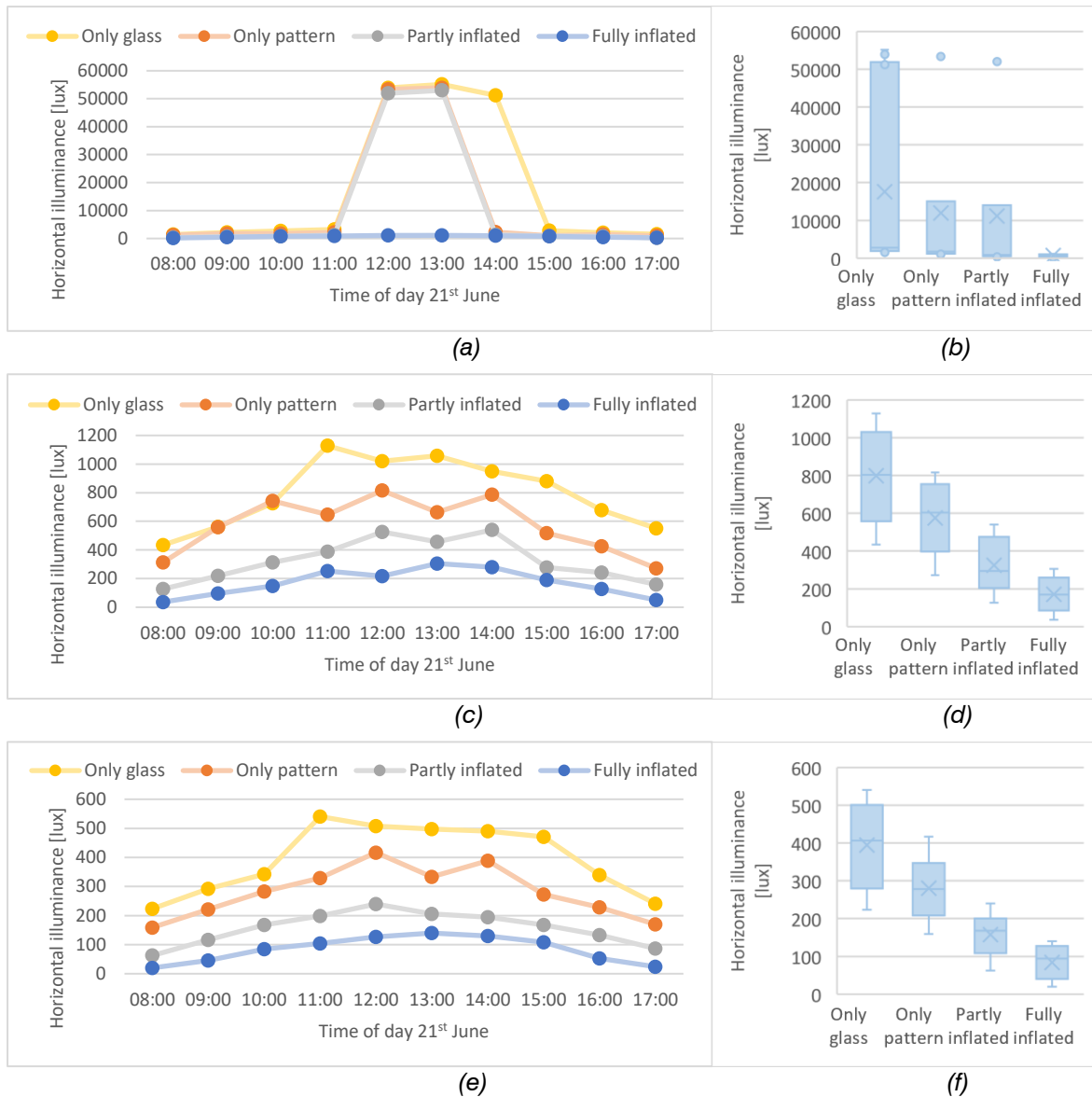
Figure 110 Horizontal illuminance on 21st December located at (a, b) 0.75 m, (c, d) 2.75 m and (e, f) 4.75 m from façade. Results for only glass, only core pattern (deflated system), fully inflated system and partly inflated system (top and bottom row open). Results depicted throughout the day and with a boxplot.

At 2.75 *m* from the façade, the deflated system with only the core pattern is already showing a significant reduction in illuminance. This can be explained by the shadow of the core pattern falling onto the horizontal surface that is measured. The inflated systems reduces the illuminance significantly more, especially during the middle of the day. The horizontal illuminance is also analysed on 21st June, where the sun has the highest position, see Figure 111.

Figure 111 Horizontal illuminance on 21ˢᵗ June located at (a, b) 0.75 m, (c, d) 2.75 m and (e, f) 4.75 m from façade. Results for only glass, only core pattern (deflated system), fully inflated system and partly inflated system (top and bottom row open). Results depicted throughout the day and with a boxplot.

Here the effect of the partly and fully inflated façade compared to the deflated system is more clearly visible, especially further into the room. To study the effect of the inflatable system more accurately, the illuminance values can be compared to the requirements for an office. As defined above, this room should provide a minimum illuminance of $E_{TM} = 100$ *lux* for 95 % of the room, during 50 % of the workday. The target illuminance should be $E_T = 300$ *lux* for 50 % of the room, during 50 % of the workday. The maximum illuminance should not exceed 2000 *lux*, to provide a comfortable experience in the room.

Using the horizontal illuminances calculated for the grid, the percentage of the room which meet these three thresholds can be calculated. For both the winter and summer, the results are shown in Figure 112 and Figure 113, respectively.
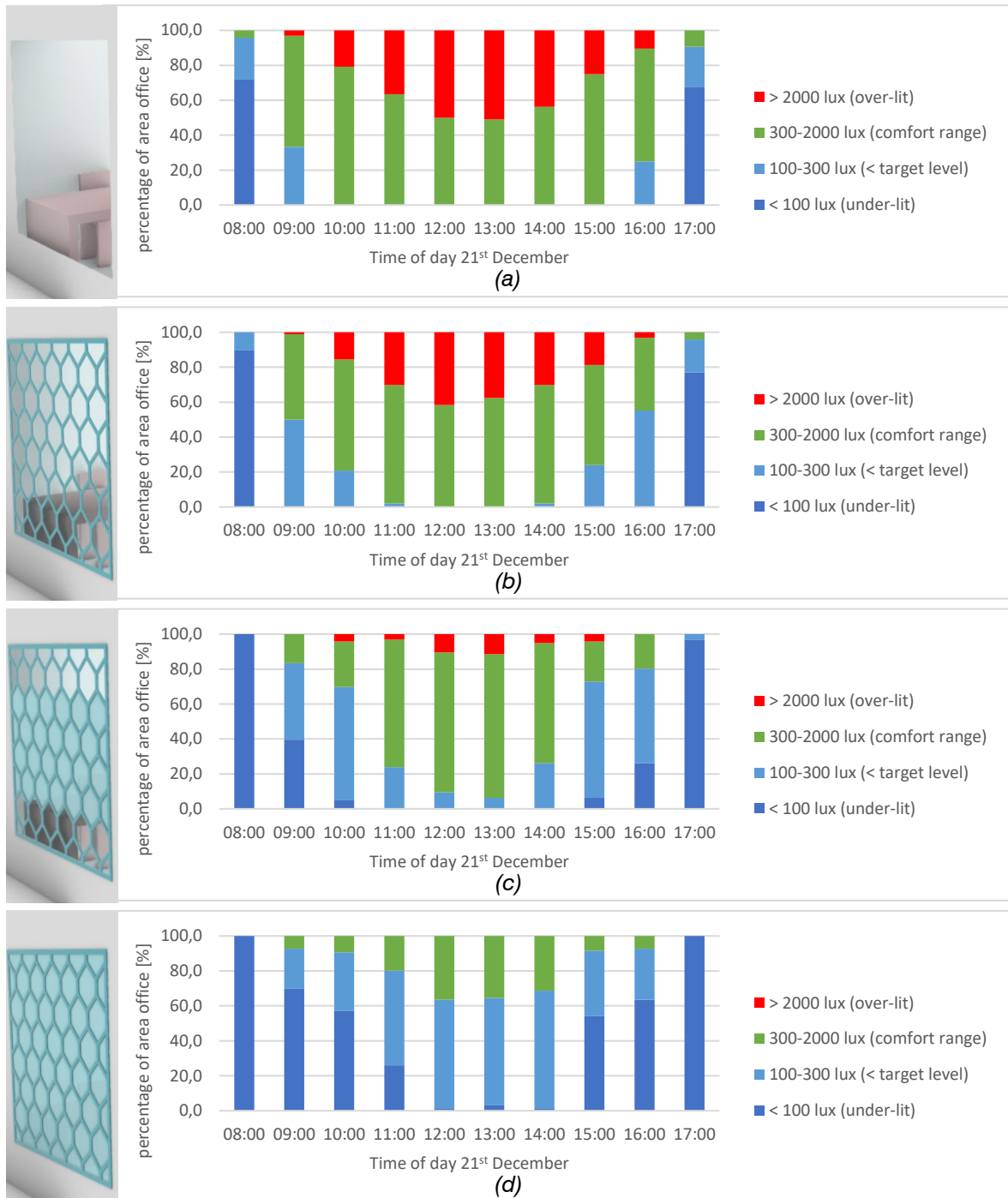
Figure 112 Percentage of area office which meets the target minimal illuminance E_{TM} (100 lux), target illuminance E_T (300 lux) and maximum illuminance E_{max} (2000 lux) on 21st December; Results for (a) only glass, (b) only core pattern, (c) partly inflated and (d) fully inflated
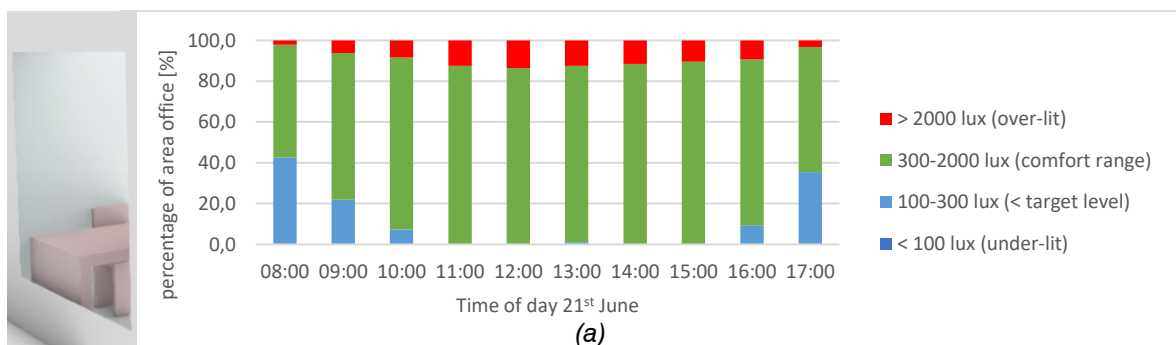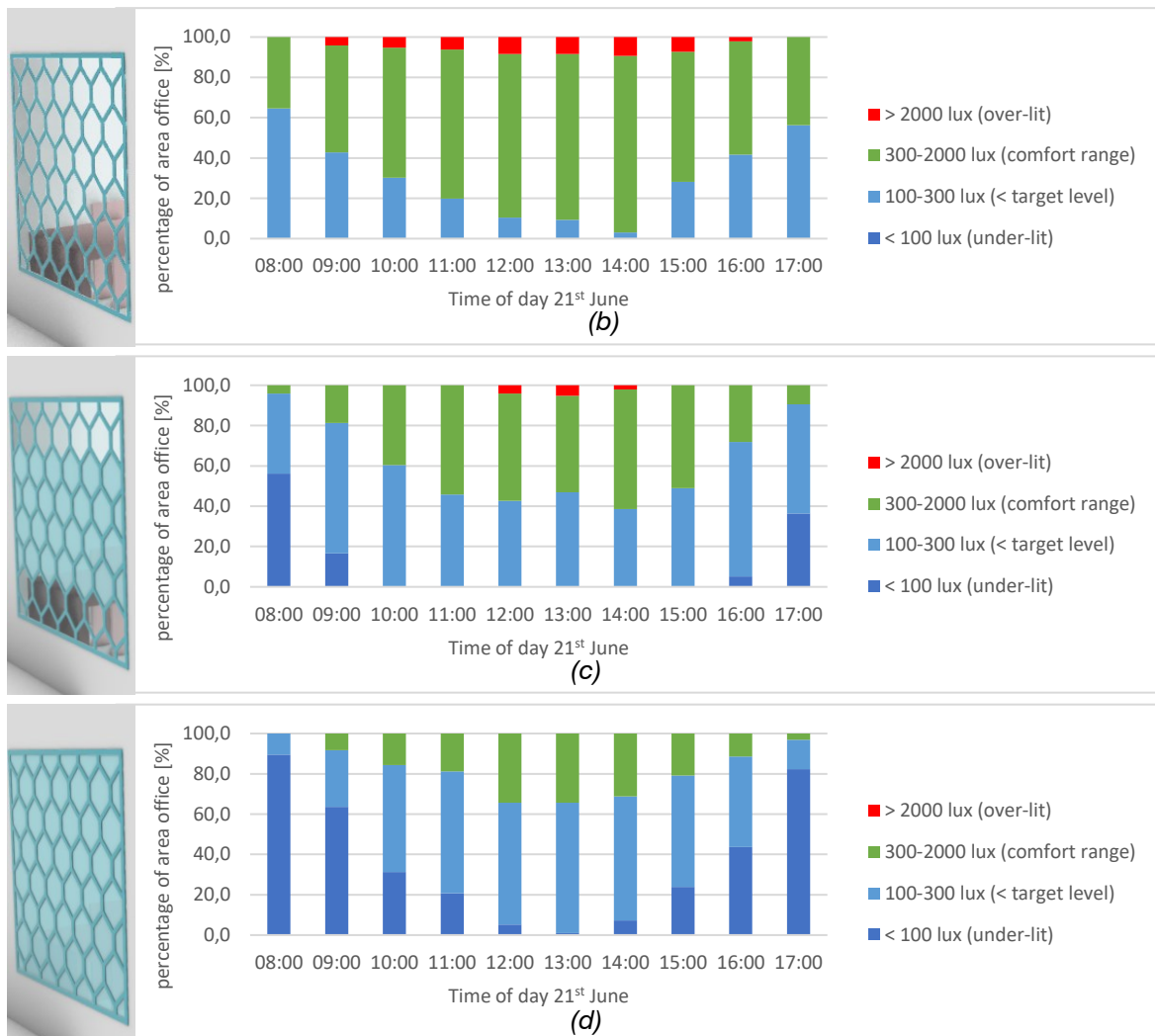
Figure 113 Percentage of area office which meets the target minimal illuminance E_{TM} (100 lux), target illuminance E_T (300 lux) and maximum illuminance E_{max} (2000 lux) on 21st June; Results for (a) only glass, (b) only core pattern, (c) partly inflated and (d) fully inflated

The system meets the requirements when the criteria is met 50% of the workday, so the lines in the graph need to stay above the line more than 50% of the time. When the system is deflated, the minimal requirements are easily met in both summer and winter. When the system is full inflated, it only meets the minimum requirement in the middle of the day and it does not meet the target illuminance requirement.

However, the partly inflated system does show the needed improvement in illuminance to meet these requirements. It is therefore important to not only design the properties of the inflatables to be able to manage glare, but to also design the distribution of separate sections which can be inflated. Allowing part of the façade to stay open, allows the illuminance inside the room to meet the required levels.

Another consideration can be to variate the level of transparency of the inflatables along a façade. This will be highly dependent on the function of the room, for example the locations of working desks, to decide which parts of the façade can have an increased level of transparency even when inflated. Since the office has only one window, the division is kept in the shown rows, to keep this design simple.

3.4.4 Contrast

Aside from glare, a large difference in luminance within a room can also introduce visual discomfort. To determine the level of discomfort due to contrast, first the room is divided into three sections, see Figure 114. Each section represents one of the views as used in the glare calculations.
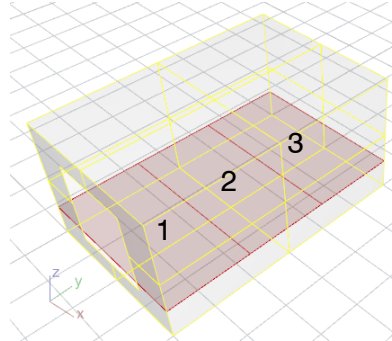

Figure 114 Division of the room for contrast ratio calculation

The contrast is measured in the Contrast Ratio (*CR*), where it takes the average luminance of each area and divides it by the average luminance of the connected area. *CR 1* is between section 1 and 2, whereas *CR 2* is between section 2 and 3. The luminance is determined using the point-in-time grid-based calculation. The radiance parameters used in this calculation are determined using the convergence test, see Table C.3. The parameters used are -ab 4, -aa 0.4, -ar 32, -ad 512, -as 256. The results of the façade panel not inflated, fully inflated and partly inflated are shown in Figure 115.

(a)   (b)
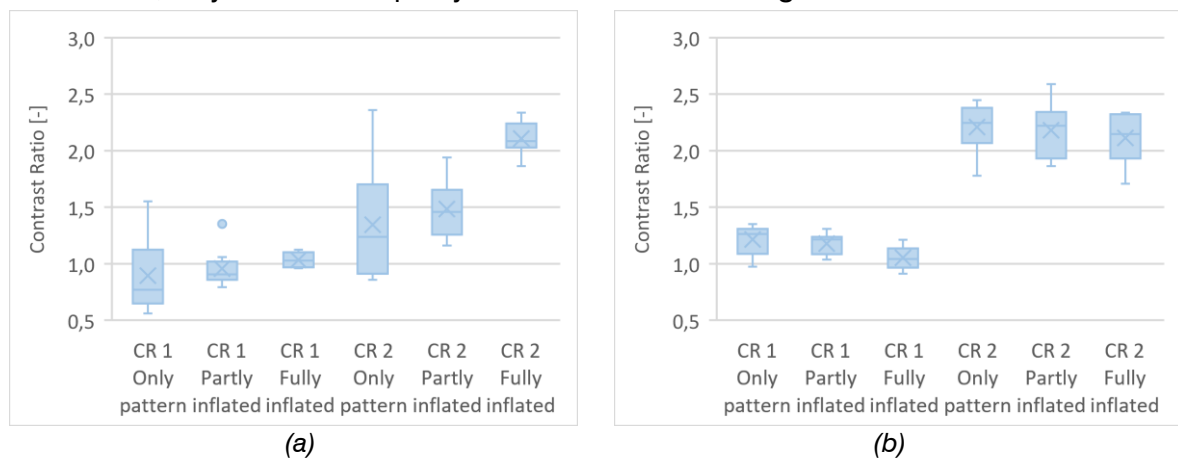
Figure 115 Horizontal contrast ratio of office at (a) 21st December; (b) 21st June. Results for only core pattern (deflated system), fully inflated system and partly inflated system (top and bottom row open)

The requirement is that the *CR* should not exceed 3:1, so the value needs to stay between 1/3 and 3. This is true for all the situations assessed. During the lowest sun, 21st December, *CR 2* significantly increases during the middle of the workday once the system is inflated. However, the partly inflated system is much more similar to the deflated option. Therefore, opening the panel partly can be a good solution to reduce contrast in this zone.

For the day with the highest sun, 21st June, the difference between *CR 1* and *CR 2* is much more evident. However, the influence of the inflatables is much less visible, showing a slight reduction in contrast during the middle of the day. Concluding from this graph, contrast is less likely to be influenced by the inflatables during the summer compared to the winter.

3.4.5 The effect of gaps

In the analyses above, the inflatables are assumed to completely fill the cells of the pattern. However, it may be possible that the inflatable does not properly fit in the hexagonal cells, leaving gaps in between the core pattern and the inflatables that can let through light. The effect of this is studied by using round inflatables that do not properly fit inside their cells, see Figure 116. The properties of the inflatables are otherwise kept the same, so with the same level of transparency and reflectance.
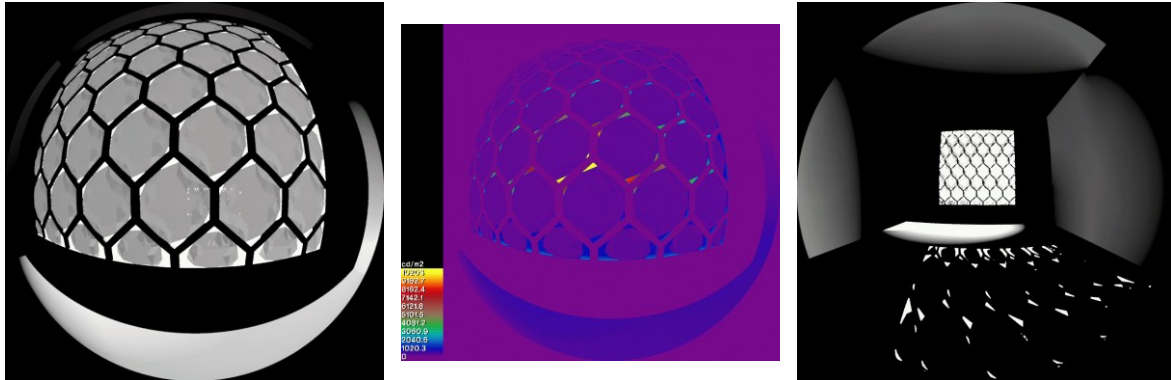
Figure 116 HDR images of design with gaps in between core pattern and inflatables

The resulting effect on glare for 21st December is shown in Figure 117. The results with gaps show multiple timeslots where a *DGP* value of 1.0 is reached at all three view locations. This is in contrast to the results without gaps, which stays below the noticeable glare threshold of DGP>0.35. This shows that small gaps in the system can make is ineffective in preventing disturbing glare. Therefore, creating a design which preventing gaps from forming is essential and should be prioritised in the design of the core pattern and inflatables.
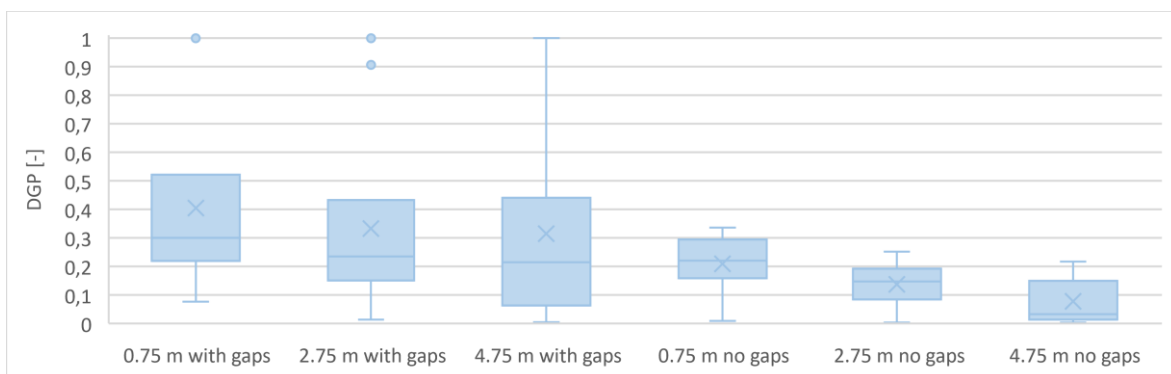

Figure 117 Comparison DGP-values of inflatables with and without gaps between core pattern, selected views located at 0.75, 2.75 and 4.75 m from façade, facing directly outside

3.4.6 Influence parameters core pattern

When the system is fully deflated, only the core pattern is influencing the illumination within the room. In this section, the effect of changing the main parameters of the core is studied, to see which are effective in either reducing or increasing the illuminance within the room.

First, the effect of the colour of the core material is studied. To evaluate the effect of the reflectance, this parameter varied from 0 to 1.0 and the horizontal illuminance in the office and the glare probability of the three viewpoints is calculated. These results however, showed no relation towards these results. Even when increasing the thickness of the core pattern to 50 *mm*, covering a significantly section of the façade, the reflectance level did not show a relation in the results.

Therefore, it is concluded that the level of reflectance can be chosen based on aesthetic reasons alone, since it does not significantly influence the daylight performance in the room. It can be left out of the optimisation process of the core pattern.

The influence of the core pattern is dependent on the type of pattern, the thickness and changing the angle at which the light is reflected. First, the influence of the thickness of the core is studied. This parameter determines the total area of the façade which is blocked by the core, not letting through light. The effect on both the horizontal illuminance and glare is evaluated in Figure 118 and Figure 119, respectively.
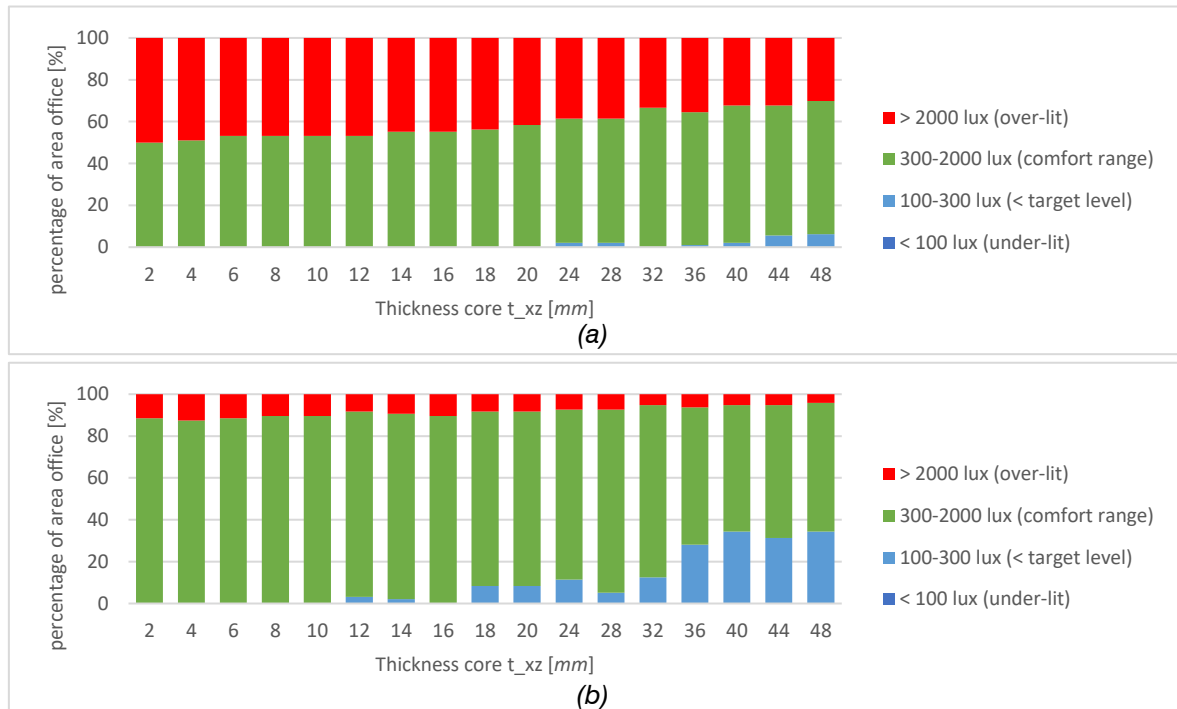
Figure 118 Effect varying thickness core pattern t_{xz} on percentage of area room which meets the target minimal illuminance E_{TM} (100 lux), target illuminance E_T (300 lux) and maximum illuminance E_{max} (2000 lux). (a) 21st December 12:00; (b) 21st June 12:00

These results show a clear decline in horizontal illuminance across the room, with the percentage of the room which is over-lit reducing when the thickness is increased. It also shows that the percentage of area which is in the visual comfort range decreases as the core thickness is increased, especially in summer. It can be concluded that increasing the thickness of the pattern is an effective way to reduce the illuminance levels inside the room. Whether this is wanted, should be investigated based on the specific design conditions.
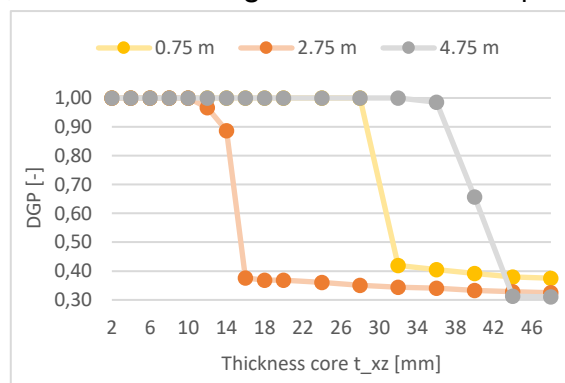

Figure 119 Effect varying thickness core pattern t_{xz} on DGP-value on 21st December 12:00

Figure 119 shows that increasing the thickness can also influence the level of perceptible glare for certain timeslots, for example 21st December 12:00. It is important however, to consider that the values may reduce for a very specific section inside the room, but it may still be intolerable when the location of the viewer is slightly moved. The core pattern only blocks glare at the specific location of its shadow path, but it does not fully prevent glare.

3.5 Conclusion

The structural requirements are expressed in a maximum allowed deflection and by a maximum stress level acting inside the elements of the panel. The maximum allowed deflection is directly related to the dimensions of the panel and the maximum allowed stresses are related to the tensile and compressive strengths of the materials used. The deflection should be checked with the Service Limit State load combination and the maximum stresses with the normative Ultimate Limit State load combination.

Visual comfort is quantified in requirements for glare, illuminance and contrast. Glare is measured in the Daylight Glare Probability value, which is generated using an HDR-image for different possible views. The requirement is set at imperceptible glare, which is represented by the threshold of $DGP < 0.35$.

The horizontal illuminance within the room is measured for a grid of points, where the requirements define the domain between which these values should fall. For an office, the minimum illuminance of $E_{TM} = 100$ *lux* should be met for 95 % of the room, during 50 % of the workday. The target illuminance of $E_T = 300$ *lux* should be met for 50 % of the room, during 50 % of the workday. The maximum illuminance should not exceed 2000 *lux*, to prevent over-lit sections and provide a comfortable experience in the room.

The level of contrast in a room can be measured with the luminance values of different sections in the room. The horizontal contrast is measured by measuring the average luminance of different sections in the room, where the ratio between these different sections should stay below 1:3.

What is an effective design for a façade panel which is able to dynamically control the visual comfort?

The design selected in this thesis is a thin glass sandwich panel with a honeycomb core pattern, where the cells of this pattern are filled with an inflatable which can be dynamically controlled. This design has an integrated solar control system, eliminating the need for an external or internal additional system to the façade. Furthermore, the thin glass has a much lower material quantity compared to an ordinary façade panel, reducing the environmental footprint of the panel.

The design of the core pattern allows for a high level of customisation, able to generate a structurally efficient system that can also be optimised for visual comfort. The design does introduce complexity in both the inflatables themselves and the connecting tubes that can control the system. This complexity can be reduced by keeping the cell shape uniform and relatively large, reducing the total number of cells.

Furthermore, the design should avoid gaps in between the core pattern in the façade and the inflatables. This allows light to pass through these gaps, potentially being able to create disturbing glare or unintentionally increasing illumination within the room.

4 DESIGN STRATEGY

To be able to design a functional façade system which suits the building and its location, an appropriate design strategy should be executed. This is done by first identifying which parameters influence which results, so that the design process can be divided into separate compartments. The process of each of these compartments is then described and executed for the standard office. The sub-question answered in this chapter is as follows:

What is the design strategy for a panel optimised for both structural and daylight performance?

4.1 Design parameters

To be able to determine the design strategy, first the available parameters need to be identified and grouped together based on which results they have a big impact on. For finding an optimal solution, every additional parameter will increase the computational time of the optimisation algorithm. Therefore, this should be reduced when possible, together with clearly defining the realistic ranges of these parameters.

First, the parameters of the building itself are mostly dependent on the location. The latitude and annual weather conditions are defined by this location, together with the orientation of the façade in relation to the solar path. The design problem can be seen at the scale of the full building, where the location and divisions of the façade are included into the optimisation process. However, when reducing complexity of the design process is important, normative rooms can be selected to perform the design process. The results of these rooms can then be used to apply to the full building.

The rooms themselves have a certain orientation related towards north, have their dimensions and the size of the façade opening(s). The functionality of the rooms should be determined as well, to come to the structural and daylight requirements. On the scale of the façade panel itself, the dimensions of the glass and core pattern, together with the properties of the inflatables can be optimised.

The parameters as defined above can be divided into three scales, at building level, at room level and at façade element level. The choices made at each of these levels influence each other, but they can be approached separately first to decrease the complexity of the full design problem. In the following sections, the design is separated into these compartments and an optimised solution is found.

4.2 Design inflatables

4.2.1 Parameters

Since the main goal of the inflatables is to prevent glare, the selected timeslot of the calculation, the season, time of day and sky conditions should be chosen to generate the highest possible *DGP*-value. This timeslot can then be used to optimise the properties of the inflatables. After the optimal design has been found, it should still be evaluated at the other timeslots, to ensure it functions as expected.

The façade will consist of the core material and the inflatable material, which together function to prevent glare. It is assumed that the core material is fully opaque. Therefore, the transparency of the inflatables will fully determine the resulting *DGP*-value of the views inside the room. The dimensions of the core pattern do influence the ratio of area of façade covered by the inflatables versus the core material. However, this effect is assumed to be negligible in favour of being able to find the optimal properties of the inflatables fast.

The optical properties of the elements in the core are defined by the surface properties of the material used. The surface colour will determine how much light is reflected, where bright colours have higher reflectance compared to dark materials. The level of roughness also increases the reflectance once it is more polished. The relation between colour, specularity, roughness and reflectance can be evaluated using the colour picker tool for Radiance, see Figure 120 (JALOXA, 2021).

Figure 120 Radiance Colour Picker tool(JALOXA, 2021)

These properties of the core material are modelled in Honeybee as an opaque material, see Figure 121. For a plastic material, the specularity typically ranges between 0 - 0.1 and the roughness between 0 - 0.2. For the 3D-printed core, a matte material with a polished surface is assumed, setting both values at the default (0). The reflectance can be fully controlled by changing the colour of the core, so this ranges between $0 - 1$.

The properties of the inflatables in the panel are modelled by defining its transmittance and reflectance. In Honeybee this is defined using the translucent modifier applied to the inflatable shade geometry. This translucent modifier consists of a diffuse reflectance

component, a transmitted diffuse component, a transmitted specular component, the fraction of specularity and the roughness of the material, see Figure 121.
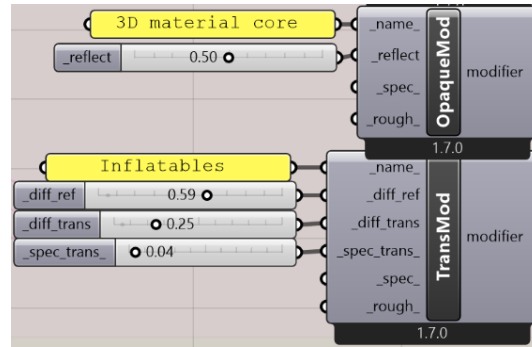

Figure 121 Opaque modifier for core pattern and translucency modifier of inflatables

The inflatable material is assumed to be fully matte and polished, where similarly to the 3D-printed core the colour can be changed based on the required level of reflectance. The translucency of the material is defined by the haze of the material used. Here, haze [%] is the diffused transmittance divided by the total transmittance, which is both diffused and specular:

$$Haze = 100 * \frac{diff_{trans}}{diff_{trans} + spec_{trans}} \ [\%] \qquad (29)$$

The lower the haze, the more transparent the material becomes, whereas a frosted material has a much higher level of haze. Therefore, for the inflatables the controllable parameters are reflectance, diffused transmittance and specular transmittance.

The inflatable can be made from a flexible polymer or rubber, where the choice of material and thickness will determine its reflectance and translucency. The thickness of the material will decrease once inflated, since the material is stretched. The materials ability to scatter light decreases once stretched, so it becomes a more translucent material. Colourless polymeric materials can range from highly transparent to fully opaque, since the loss of transparency arises from light scattering processes within the material.

Concluding, the three optimisable parameters in the inflatable design are the reflectance of the inflatables, the diffused transmittance and the specular transmittance.

4.2.2 Objectives

The design requirements can be expressed in three values. First, the *DGP*-value should stay below 0.35, which can be determined with the point-in-time view based simulation. Here the normative design timeslot and view should be used, which is 21st December, 12:00 near the façade. Furthermore, the contrast should stay below 3:1, which is determined using the point-in-time grid-based luminance calculation. Lastly, the illuminance of the room should meet the target illuminance of 300 *lux* for 50% of the room and 100 *lux* for 95% of the room. This is determined using the point-in-time grid-based illuminance calculation.

The above defined objectives use three distinct types of simulation, each adding significantly to the overall calculation time. To reduce this time during the optimisation process, as soon as one of the requirements of glare and contrast are not met, a low fitness level is returned and the next option can be assessed. Options which exceed the energy balance are also not calculated, since these parameter combinations are not possible.

The target illuminances are used to find the optimum solution. The values are penalised based on how well they meet the requirements. If the targets are met, the penalty is set at 0. Otherwise, the penalty is defined as the difference between the actual and target value, multiplied with 10. This way, the algorithm tries to find solutions that meet all the requirements, even if the winning combination does not fully meet the target illuminances. The full process is shown in Appendix Optimisation script inflatable design.

4.2.3 Optimisation

With the design parameters and design goals defined, an optimisation algorithm can be used to find the optimum. For the office, the Opossum algorithm is used. The selected optimisation algorithm is RBFOpt, which gives a fast and good result. After running the algorithm for 200 iterations, the convergence is as depicted in Figure 122. The jumps are due to the algorithm finding solutions that no longer receive a penalty for not meeting one of the requirements.
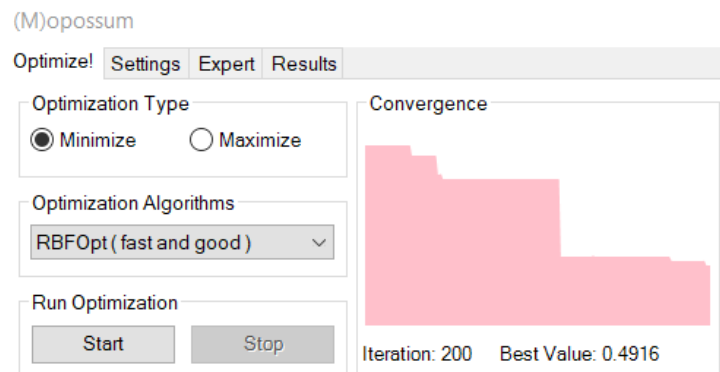
Figure 122 Convergence of (M)opossum optimisation algorithm for inflatables

The results of the winning solution are shown in Table 22. The transmitted diffuse component is mostly responsible for the change in results since this defines the level of transparency of the inflatables. This solution is found with a core pattern with a thickness of 40 *mm*. When this significantly changes, this solution should be checked again. If more computational power is available, this optimisation process can be included in the determination of the core pattern, but for now they are kept separate.

Table 22 Optimised solution of inflatables for U=12, V=7 honeycomb pattern with t_{xz} = 40 mm

Properties inflatable	Optimised solution
Diffused reflectance	0.5
Transmitted diffuse component	0.2
Transmitted specular component	0.0
Results	
DGP (<0.35) [-]	0.331
CR 1 (<3) [-]	1.040068
CR 2 (<3) [-]	1.763157
Percentage area E_{TM} = 100 lux reached (>95 %) [%]	96.875
Percentage area E_T = 300 lux reached (>50 %) [%]	32.291667
Percentage area E_{max} = 2000 lux exceeded [%]	0

4.3 Design core pattern

The main function of the core pattern is to provide stiffness to the panel. It also provides the boundaries of the cells in which the inflatables are placed. The core must also provide space for tubing connecting the cells and provide an edge around each panel. Aside from the structural requirements, the core also contributes to the distribution of daylight when the dynamic system is deflated. Therefore, the reflectance and overall design of the core also contributes to the daylight performance of the panel.

4.3.1 Parameters

For this design process, it is important to clearly define the boundaries of each parameter. The resulting set of parameters should be realistic and practical. Since the pattern has many different parameters, it can also be beneficial to predefine some of the parameters, to reduce the number of combinations and speed up the optimisation process.

The main parameters of the core are the thickness, the type of pattern and the number of cells in a panel. The limiting factors are determined by the printability of the pattern and the window frame in which the panel should fit. The influence of these parameters on structural strength have been studied in 3.1.3 Structural analyses. The effect on the daylight performances is explored in 3.4.6 Influence parameters core pattern.

4.3.2 Objectives

To find the optimal design for the core pattern, the structural requirements, daylight requirements and practical requirements need to be considered. It is important to distinguish between requirements and wishes, representing this in the appropriate penalties for the results. For the structural strength, the minimal thickness across the core can be used, whereas for the daylight calculations, the full 3D geometry should be used.

The structural performance of the panel is represented by the resulting deflection and the resulting equivalent stresses within the panel. In the objectives, this is represented by adding a penalty when the requirements are exceeded (*u.c.* > 1). To speed up the calculation, a larger mesh element size is selected, namely 20 *mm*. To account for the error this larger mesh element size introduces, in combination with openings to be added to the pattern, the actual aimed value for the unity check is set at 0.9.

Aside from the structural requirements, the practical requirements are also added to the objectives. The thickness of the glass is dependent on what sizes are available to use. The thickness of the core is dependent on the size of the frame. The core pattern itself will determine the geometry for the inflatables, but also the connecting tubes and other required elements. Both the number of cells per panel and the cell shape should be considered when finding the optimal solution.

The range for the number of cells is determined by the minimal required control of the façade, allowing the option to leave parts of the façade open. The maximum number of cells can also be limited to keep the number of inflatables low, reducing unnecessary complexity in the design.

The shape of the cell is also important to ensure the connection between the inflatables and core pattern is fully connecting, not showing gaps. This is represented in the objectives by evaluating the sharpness of the corners of the cells. The distance between the corner and a second degree nurbs curve inside the cell is used to quantify this sharpness.

110

Reducing this number favours cell shapes which more closely resemble a round shape, so this returns options suitable for the inflatables.

Additionally, the total volume of materials used can be minimised, reducing the weight and environmental footprint of the panel. At the same time, the thickness of the pattern can be used to influence the daylight performance, potentially reducing the illuminance within the room. For the office, the target illuminances should be met and over-lit sections in the room should be prevented.

4.3.3 Optimisation

Since the structural strength is dependent on the minimal thickness of the core pattern, whereas the daylight performance is dependent on the full geometry of the panel, this design objective can be isolated. First, the optimal solution for practical and structural objectives is found, which can then be adjusted to find the optimal solution for the daylight objectives.

The optimised solutions for the core pattern are found using the Galapagos plugin in Grasshopper. Using the simulated annealing solver, multiple optimal combinations of the parameters can be found. Therefore, first the core pattern design is selected, for which then an optimal combination of thickness in *x, y* and *z* direction for the pattern can be found using the optimisation algorithm.

For the design of the office, a thickness of the glass of 0.7-0.8 *m* is used. For a few different combinations of the thickness of the core, an optimal solution is found and presented in Table 23. This shows that for a certain pattern division, multiple optimal structural solutions can be found. To check the validity of the results using the 20 *mm* mesh element size, the results of an 8 *mm* mesh element size are calculated as well, showing the expected increase in maximum stresses.

Table 23 Structural optimised solution of core pattern

Parameters			
Thickness glass [*mm*]	0.7	0.8	0.7
Thickness core [*mm*]	8	7	7
U-division	12	12	12
V-division	7	7	7
Thickness pattern *x* [*mm*]	25	10	40
Thickness pattern *z* [*mm*]	25	10	40
Factor *x* [-]	1.0	1.0	1.3
Factor *z* [-]	1.0	1.0	1.3
Results			
Total area pattern [*m²*]	0.447722	0.555398	2.158168
Number of cells	52	52	52
Sharpness of corners [*mm*]	0.060055	0.05845	0.02967
Mesh 20 *mm*:			
Max equivalent stress [*N*/*mm²*]	81.70371	80.09509	73.45447
Deflection [*mm*]	34.74749	39.80327	41.150657
Mesh 8 mm:			
Max equivalent stress [*N*/*mm²*]	89.58344	87.80223	75.73886
Deflection [*mm*]	34.06552	38.327875	40.35974

To decide on the thickness of the pattern, the daylight performance is considered. Considering the results of varying the thickness of the core pattern for the office, as shown in Figure 118, a high thickness is beneficial for the overall daylight performance. Therefore, the options with a thickness of 40 *mm* is selected, see the last column of Table 23.

Using this thickness as the minimal thickness over the *y*-axis, the thickness can be further varied along this axis. Here, it is important to consider the printability of the core design. Most 3D-printers have a limited angle of 45-60 degrees. If the middle section of the pattern is kept at 40 *mm*, the outside edge can be 44.5 *mm* at most. If one outside edge is set at 40 *mm*, the other side can be 49 *mm* at most. Three variations are evaluated with the parameters as described in Table 24.

Table 24 Design options core pattern for optimal daylight performance

Parameters				
Thickness glass [*mm*]	0.7	0.7	0.7	0.7
Thickness core [*mm*]	7	7	7	7
***U*-division**	12	12	12	12
***V*-division**	7	7	7	7
Side core facing inside				
Thickness pattern *x* [*mm*]	40	44	40	48
Thickness pattern *z* [*mm*]	40	44	40	48
Factor *x* [-]	1.3	1.3	1.3	1.3
Factor *z* [-]	1.3	1.3	1.3	1.3
Middle section core				
Thickness pattern *x* [*mm*]	40	40	44	44
Thickness pattern *z* [*mm*]	40	40	44	44
Factor *x* [-]	1.3	1.3	1.3	1.3
Factor *z* [-]	1.3	1.3	1.3	1.3
Side core facing outside				
Thickness pattern *x* [*mm*]	40	44	48	40
Thickness pattern *z* [*mm*]	40	44	48	40
Factor *x* [-]	1.3	1.3	1.3	1.3
Factor *z* [-]	1.3	1.3	1.3	1.3

The horizontal illuminance in the office is calculated for 21st June and 21st December. The resulting percentage of area which meets the target illuminance E_T and maximum illuminance to prevent over-lit E_{max} are shown in Figure 123. The target minimum illuminance E_{TM} is met for all cases, so this is left out of the evaluation.

(a)

(b)

(c)

(d)
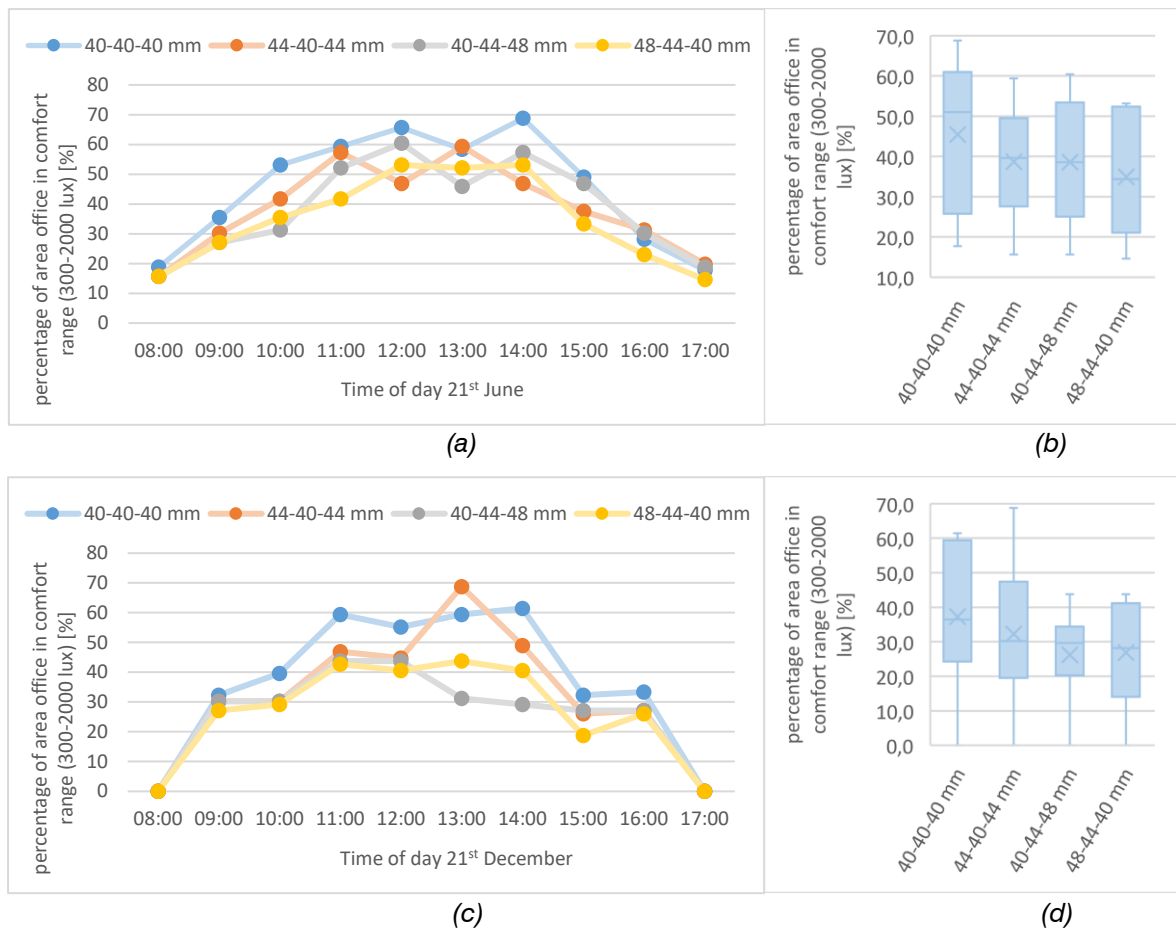
Figure 123 Percentage of area office in which the horizontal illuminance lies in between the comfort range (300-2000 lux). Results calculated throughout the day of (a, b) 21st June and (c, d) 21st December, together with a boxplot representation of the results

These graphs show that for the increase in thickness helps further reduce the illuminance in the room. It also shows that the requirement that the target illuminance E_T = 300 *lux* be reached > 50 % of the time is normative in deciding the maximum used thickness. Especially the 48-44-40 *mm* combination does not meet this requirement, with the 40-44-48 *mm* not meeting the requirement in winter. These two patterns are most effective in reducing over-lit sections in the room, but this reduction weighs less compared to the lost light creating under-lit sections.

Since the thickness of the core is only 9 *mm*, the effect of adding changes along this *y*-axis is minimal, the results mostly just showing the effect of the added thickness. For other designs with higher thicknesses, this change may be more effective. For the standard office panel, the option with 44-40-44 *mm* thicknesses appear to be the optimal design choice for practical, structural and daylight related requirements.

4.4 Design façade system

So far, the focus has been on the façade panel itself. However, the full system of panels can also be included in the design process. A building can have an entire section of a façade made with the inflatable system, where the properties of these panels can vary over the surface. The parameter to be determined here is the division of these different sections.

4.4.1 Detailing frame

It is important to keep the practical constrictions in mind. Since the inflatables are connected via tubing, there needs to be sufficient space available for these tubes to get to the air compressor. The frame in which the façade is placed has limited space, so the maximum number of tubes and dimensions of these are dependent on this. The design of the frame can also be included in the design to provide space for these tubes, which can increase the possibilities.

In conclusion, the actual design of the full building should be taken into consideration when designing with this type of panel. In the design for the standard office, the inflatables were divided into four rows which can be controlled separately. This means that four separate tubing needs to be integrated into the window frame. The average window frame however, does not provide much space.

As an example, a normal double-glass window frame is shown in Figure 124a. The cavity space around the edge of the window panel can be used to place tubing. In Figure 124b a few possible locations of 6 *mm* tubes are drawn into this cavity space. It is important to keep in mind it needs to connect to the core material, it cannot pass through the glass. If the space next to the glass is to be used, the glass pane should leave an opening on this side, to allow this connection to happen. This can potentially create problems with water tightness of the connection, so this should be avoided.
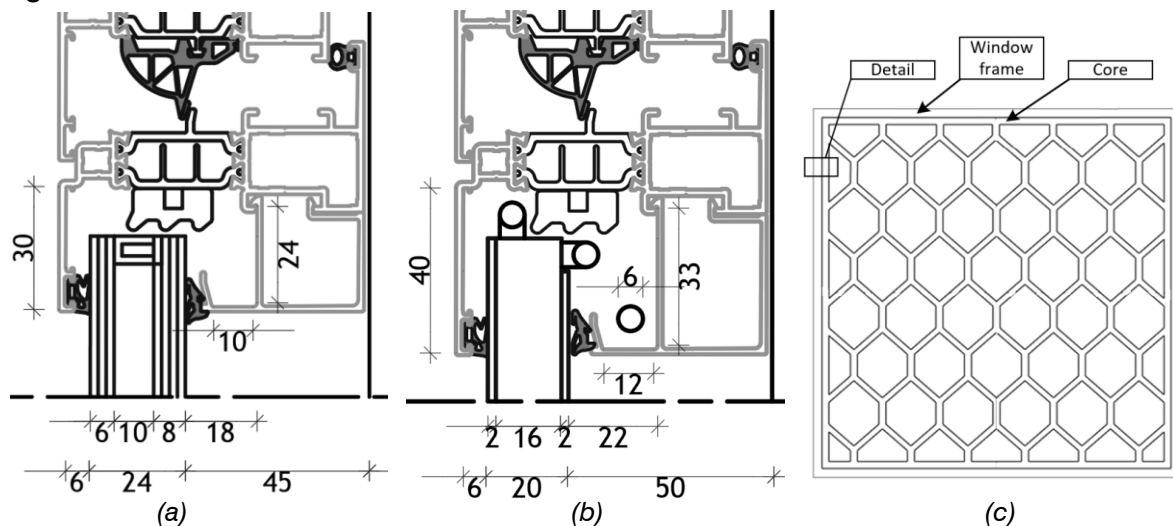
Figure 124 Horizontal window detail of (a) double-glass window panel; (b) thin glass panel with possible locations for 6 mm tubing; (c) location detail

The tubing to be used can be made from a rigid or flexible material. There are many different sizes available on the market, for example the PEN flexible tubing, size ranging in 4-16 *mm* outside diameter or the PUN-H rigid tubing, size ranging 2-16 *mm* (FESTO). Both can manage an air pressure of up to 10 *bar*, which is well within the margins used in this design (< 5 *bar*).

The tubing needs to be connected to each other and to the air compressor. Especially for rigid tubing, designing enough space for these connections is important to create a realistic design. As shown in Figure 124, the frame only has so much space, so the sizes of the connecting elements may be normative for the choice of size of tube radius. To further give an idea of what these elements can look like, an example of a PEN flexible tubing with a corner connecting element (push-in fitting QS(M) is shown in Figure 125.

Type	
[1]	Housing
[2]	Screwed trunnion
[3]	Releasing ring
[4]	Tubing seal
[5]	Tube clamping segment
[6]	Plastic tubing, standard O.D.
[–]	Nut (QSS/QSSF)
[–]	Hollow bolt (QSLV/QSTF/QSYLV)
Note on materials	
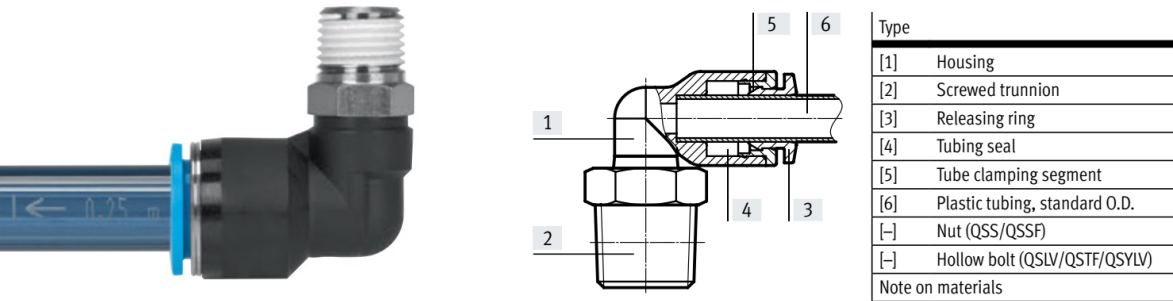
Figure 125 Corner push-in fitting QS(M), suitable for flexible and rigid tubes (FESTO)

4.4.2 Division of control groups

Looking at the design from the scale of the whole building, not only the design of single panel is important, but also how these can work together. Based on the position on the façade, different properties can be given to the inflatables, core pattern or even sizes of the panel. These choices heavily correlate to the function inside the rooms and its exposure to the sun throughout the year.

When analysing the full façade, the part which responds dynamically can be limited to certain parts of the façade, where for example the top section is permanently kept close. The opposite, where certain sections are always kept open, is also possible. Furthermore, the transparency of the inflatables can also be varied along the façade, for example with the goal to improve illuminance performance.

The main constricting parameter is the space available in the frame (or other housing of the window panels). If this only allows for a certain number of tubes to be placed next to each other, this number will determine the maximum controllable sections. For the standard office design, the four rows provide sufficient control of both daylight and glare, while limiting the number of different sections to 4. These can be further split into 2 on each side, meaning these tubes can easily fit into existing frames.

4.5 Conclusion

What is the design strategy for a panel optimised for both structural and daylight performance?

The design strategy starts with determining the necessary material properties of the inflatables. The main goal of these inflatables is to prevent disturbing glare, so these should be designed that for the given façade, the maximum perceived *DGP*-value stays below a value of 0.35.

Next, the thickness of the glass and the parameters of the core pattern can be determined, based on the structural and daylight requirements. Increasing the thickness of the core pattern increases the structural strength of the panel, while reducing the transparency of the façade panel, reducing the horizontal illuminance inside the room. Based on the wanted results, an optimisation algorithm can be used to find the optimal combination of parameters which most efficiently meets both requirements.

Lastly, the detailing of the façade system can be designed based on the dimensions of the frame of the panel, the support conditions and the needed tubes and connectors for the inflatables. Furthermore, the division of control groups will also determine the number of tubes needed in the frame, which is limited by the space available in the frame.

5 CASE STUDY

In the previous sections on both the design of the façade element and the design strategy of the full system, a design is made for a single panel used in a standard office. This design only consists of one façade element for a single small room. However, most buildings have much more complex façades, where multiple panels work together to form the whole building envelope. To show the full design process for an actual building, this case study is executed.

5.1 Introduction

To show the effectiveness of the developed façade system, a modern building is selected with varying functions inside and with a large open façade system currently in place. This allows the inflatable design system to show how it can fit into different types of façades, different functions inside the building and how it can function overall.

The building selected for this case study is the educational Echo building, located on the campus of the technical university of Delft. Most of the building envelope consists of glass panels, spanning from floor to ceiling. The design focused on maximising the use of daylight, giving the building a transparent and open feeling (UNStudio, 2022). Solar control is established by the horizontal aluminium awnings located between each floor, combined with climbing plants placed along cables spanned between them. Furthermore, additional sun protection is provided by using glass with a low solar penetration factor.

Figure 126 Echo, TU Delft (UNStudio, 2022)

The design of Echo has a large focus on sustainability and climate control. It uses multiple tools to maximise the natural benefits of the environment, like daylight and temperature control. The glass façade of this building was nominated for the Glass Award 2023, showing the progressive sustainable ambition of this this design (Octotube, 2023).

In comparison to other buildings, the façade excels in its design. For the inflatable façade system, it is important to generate a system that can perform comparatively to modern façade systems. Therefore, choosing this building as a case study shows the full potential of the façade system.

5.2 Building characteristics

5.2.1 Functionality

The Echo building is an educational building, functioning to support other faculties. The functions inside the building range from lecture halls, study workspaces, a restaurant and circulation rooms. The full overview of the functions is shown in Figure 127. Most of these spaces have a flexible layout, to allow for future changes in function.
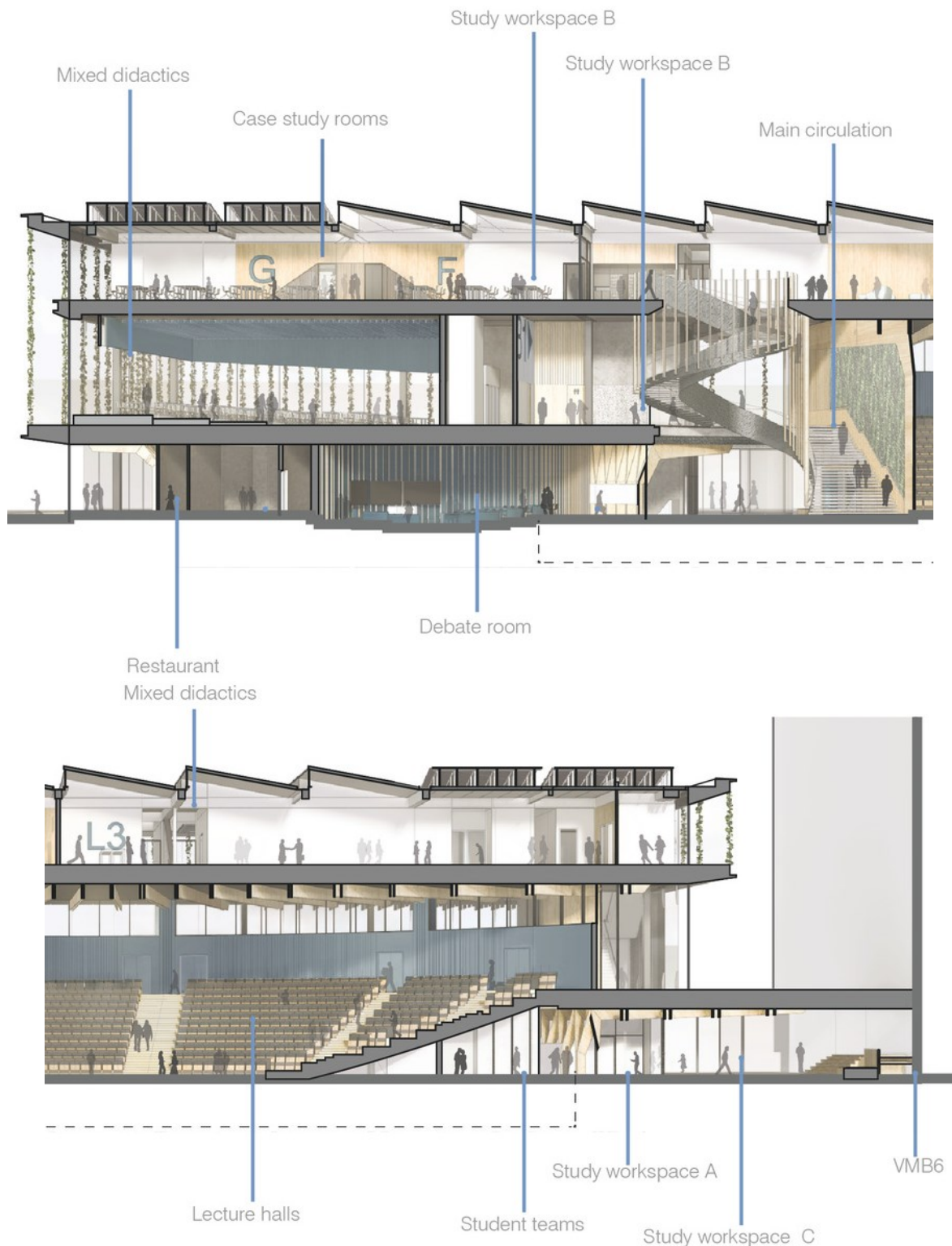
Figure 127 Overview functions inside Echo building (UNStudio, 2022)

The functions can be categorised as congregation areas, ranging from category C1: areas with tables (restaurant, study workspaces) and C2: areas with fixed seats (lecture halls). Together with the consequence class, which is CC2 for educational buildings, the resulting load and action factors can be determined, as shown in Table 25:

Table 25 Echo building load factors for Service Limit State and Ultimate Limit State

Consequence Class	2
K_{FI}	1.0
Load factors: γ	
ULS1 permanent unfavourable	1.35
ULS2 permanent unfavourable	1.2
Permanent favourable	0.9
Variable	1.5
Action category	C: congregation areas
Factor combination value variable load ψ_0	0.25
Factor frequent value variable load ψ_1	0.7
Factor quasi-permanent value variable load ψ_2	0.6

5.2.2 Location

The building is located on the campus of the technical university of Delft, surrounded by multiple other faculty buildings. For daylight analyses, it is important to take these surroundings into account since they can cast shadows and heavily influence the daylight results throughout the year. The surrounding geometry, including the Echo building is added to the model as shown in Figure 128, together with the solar path.
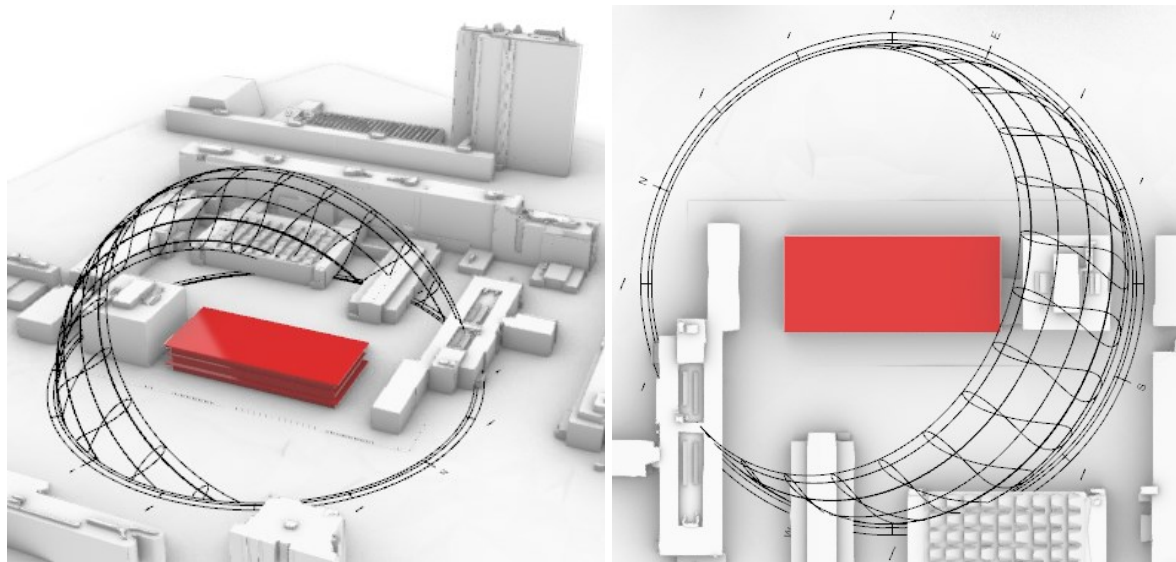
Figure 128 Rhino model of Echo building and surroundings

For the weather data to be used in the daylight calculation, the location of Amsterdam is used, considering this is the closest city with the weather data available. The location is also important in determining the wind load acting on the façade of the building. Delft is located in wind region II of the Netherlands, with the building located in an urban setting.

The building is estimated to have a total height of 16 m, with the three floors located at 0, 5 and 10 m. The floorplan is set at 35x85 m^2, which means the building should be considered as one part for the wind load calculation, see Appendix F.1. Therefore, $q_P(z) =$

$q_p(z_e)$, which results in the value $q_p(z) = 0.80 \, kN/m^2$ (Appendix F.2). The $c_s c_d$ factor is assumed to be 1.0.

Since the wind load only needs to be determined for the façades, the c_f factor can be determined using the external pressure coefficients for vertical walls of rectangular plan buildings (Appendix F.3). The resulting factor can be determined for both wind directions. assuming a building with flat roof. For the longer width ($b = 85 \, m$, $d = 35 \, m$), the value for e is set at 36 m since $b > 2*h$ ($18*2 = 36 \, m$). This means $e > d$, so the factors of A and B are to be used, with $h/d = 0.51$. For the shorter width ($b = 35 \, m$, $d = 85 \, m$), the value for e is set at 35 m, since $b < 2*h$. This means $e < d$, so the factors of A, B and C apply with $h/d = 0.21$. The results are summarised in Figure 129.
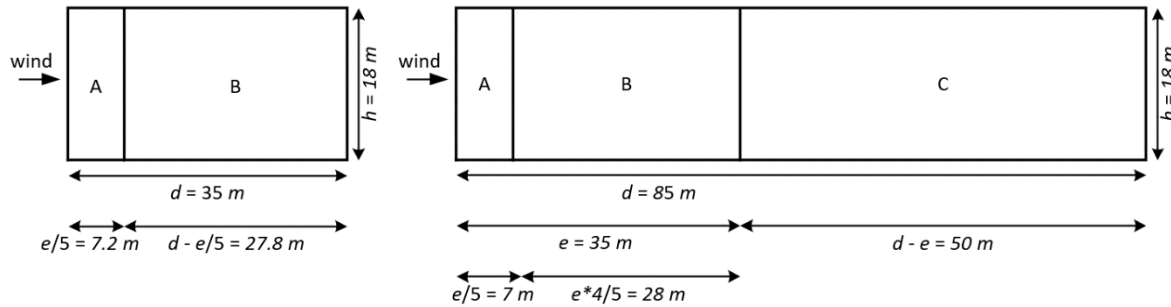
Figure 129 Distribution of wind pressure coefficients along the façade, with A: $c_{pe} = -1.2$, B: $c_{pe} = -0.8$ and C: $c_{pe} = -0.5$

With the factors determined, the maximum loads acting along the façade can be calculated. In Table 26 these are calculated for the service limit state and the two ultimate limit state combinations, using the formulas as defined in 3.1.3.1 Structural requirements.

Table 26 Echo building wind load combination (self-weight neglected) for Service Limit State and Ultimate Limit State

section	A	B	C
c_f [-]	1.2	0.8	0.5
$q_{wind} = F_w/A_{ref}$ [kN/m^2]	0.96	0.64	0.4
$E_{d,ULS1}$ [kN/m^2]	0.864	0.576	0.36
$E_{d,ULS2}$ [kN/m^2]	1.44	0.96	0.6
$E_{d,SLS}$ [kN/m^2]	0.96	0.64	0.4

5.2.3 Characteristics façade panels

The façade system used in Echo uses the outside canopies of the building to prevent solar heat from overheating the inside of the building. Additional climbing ivy is placed in front of the façade, blocking excessive solar heat. Furthermore, the glass is treated with a solar control coating, optimising the transparency in relation to solar protection.

The façade panels used in Echo span from floor to ceiling, with most panels only supported at the top and bottom. The largest panel is approximately 2.6x5 m^2, with a 12/14/12.12.4 (total 51 mm) structure of toughened/semi-toughened glass (Octotube, 2023). In most sections, the glass is placed in aluminium U-profiles at the top and bottom (Figure 130c). On the second floor, steel swords are used to span the additional height while allowing the glass to appear fully transparent (Figure 130d). Lastly, the section of the building where the façade spans two floor levels, the glass panes are supported with steel tubes (Figure 130b).
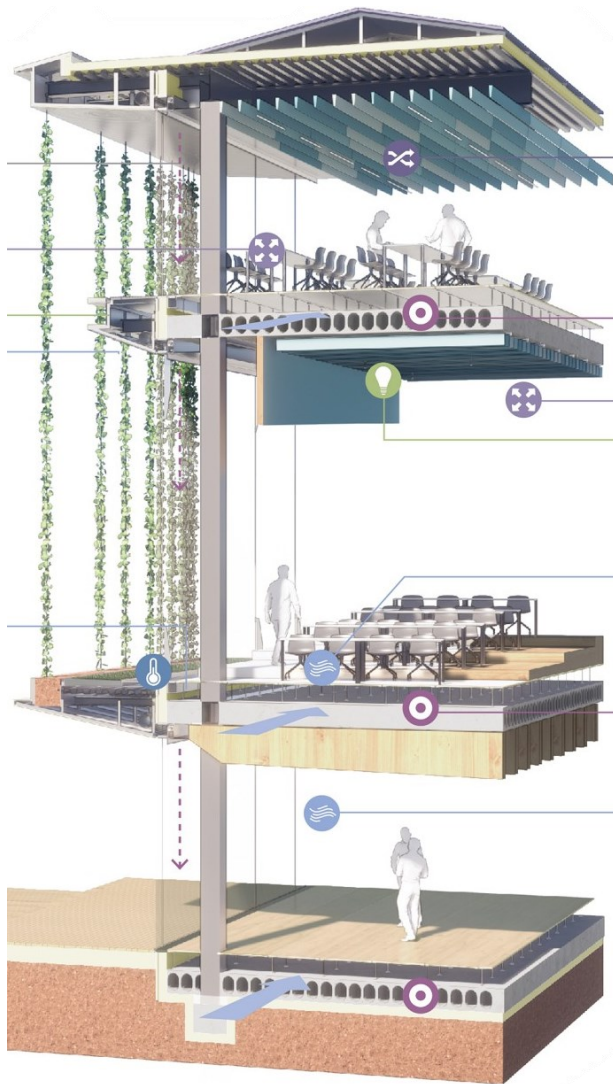
(a)

(b)
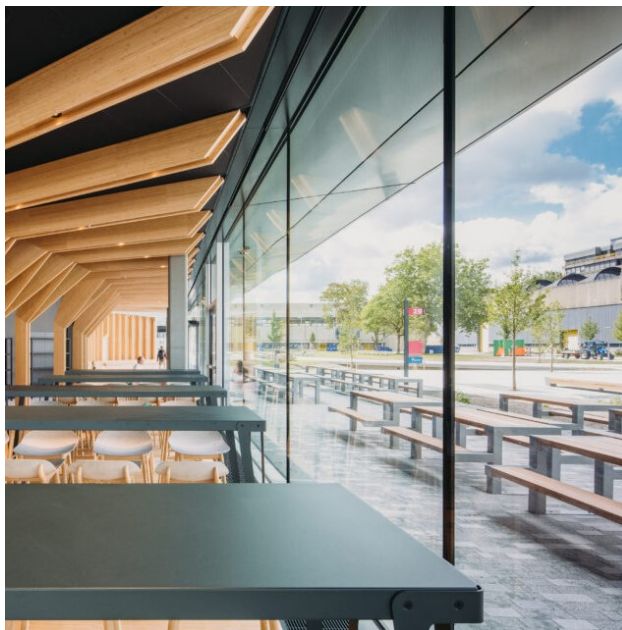
(c)

(d)

Figure 130 Impression façades used in Echo building ©Eva Bloem: (a) technical drawing façade; (b) steel tubes supported; (c) U-profile supported; (d) additional support with steel fins

5.3 Design process

5.3.1 Initial choices

For the design process, the full façade is split into two different types of panels. First, the panel of size 2.6x4.4 m^2, supported at the top and bottom (Figure 130c) is used for the majority of the building. For the section where the façade spans two levels, two panels supported at the sides with dimensions 2.6x5 m^2 are used (Figure 130b). The analyses executed in this case study are limited to the ground floor.

For the structural analyses, the normative wind load is taken, which is the load on wind section A as shown in Table 26; the SLS-load is 0.864 kN/m^2 and the ULS-load is 1.44 kN/m^2 (neglecting self-weight). The sensor grid used in the daylight analysis is determined as described in section 3.3.3 Grid. The maximum grid size is calculated as follows:

$$p = 0.2 * 5^{\log_{10}(35)} = 2.40 \ m$$

To be able to determine the views used for glare calculations, a direct sun hours analyses is executed, together with looking at the sun path in relation to the position of the building. For the floorplan of the ground floor, the debate room and lecture room are excluded, focusing only on the areas directly next to the façade.
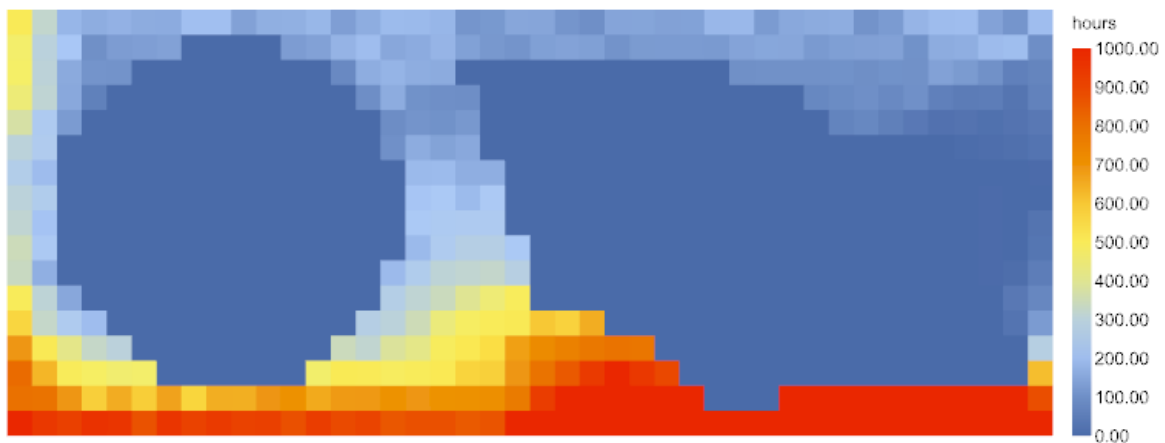
Figure 131 Direct Sun Hours in Echo building ground floor

As the results of the direct sun hours in Figure 131 show, it is mostly the west-side of the building which is exposed to direct daylight, increasing the risk of glare in those areas. The south-side of the building is located right next to a high-rise building, thereby preventing glare on this side. Using these results and the solar path, five views are selected to be analysed, see Figure 132.
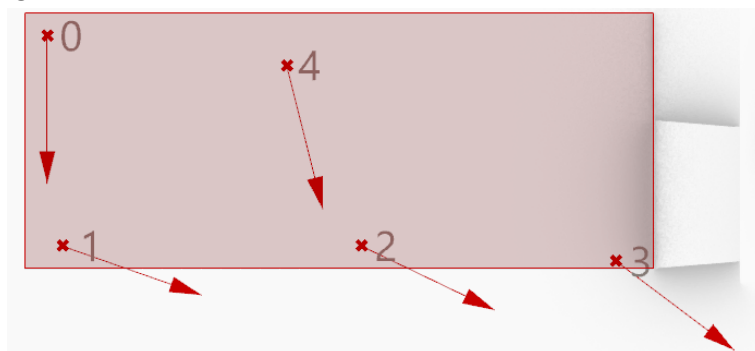
Figure 132 Point of views used for generating HDR-images to calculate DGP-value and read luminance levels
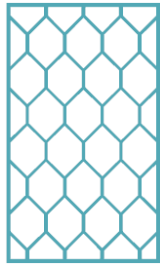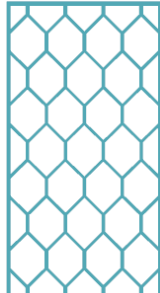
5.3.2 Structural optimisation core pattern

The main design objective of the original façade design of the Echo building is to create a transparent building, connecting the outside campus to the inside building. Therefore, for the design of the core pattern is partly focused on reducing the percentage of area covered by the pattern, allowing a clear view outside.

For the division parameters of the pattern, a matching combination is selected for the two different sized panels. This way, the full building has a uniform look. The thickness of the full pattern is chosen to be close to the original façade design, which is +-51 *mm*. Looking at the resulting deflection and stresses acting in the panel, a thickness of the glass of 1 *mm* and core pattern of 48 *mm* is chosen.

Following, an optimisation process is executed to determine the thickness of the pattern in both x and z direction, together with the factors determining how this thickness changes over the cross-section. The results for both panels are shown in Table 27. With the maximum allowed deflection at 50 *mm*, the 2.6x4.4 *mm²* panel is normative, with the equivalent stresses acting below the maximum allowed stress[1].

Table 27 Structural optimisation of core pattern

Parameters		
Width panel [*m*]	2.6	2.6
Height panel [*m*]	4.4	5.0
Location supports	Top and bottom	Vertical sides
Thickness glass [*mm*]	1.0	1.0
Thickness core [*mm*]	48	48
***U*-division**	8	8
***V*-division**	7	8
Thickness pattern *x* [*mm*]	40	40
Thickness pattern *z* [*mm*]	40	40
Factor *x* [-]	0.8	0.8
Factor *z* [-]	0.8	0.8
Results		
Number of cells	36	41
Mesh 20 *mm*: **Equivalent stress [*N/mm²*]**	144.40273	128.84478
Deflection [*mm*]	44.091413	24.005008
Mesh 14 mm: **Equivalent stress [*N/mm²*]**	147.42942	133.48416
Deflection [*mm*]	44.089101	23.972934

---

[1] Characteristic strength $f_{b,k}$ = 150 *N/mm²* used in this optimisation, should be corrected to the design strength $f_{g,d}$, see equation (20)

5.3.3 Inflatables design

With the structurally optimised pattern known, the properties of the inflatables can be determined. These are determined by finding the maximal transparency allowed to prevent disturbing glare, using the views as defined in Figure 132. To give an impression of these views, the resulting HDR-images are shown for 21st June 16:00 in Figure 133.

(a)   *(b)*   *(c)*

(d)   *(e)*
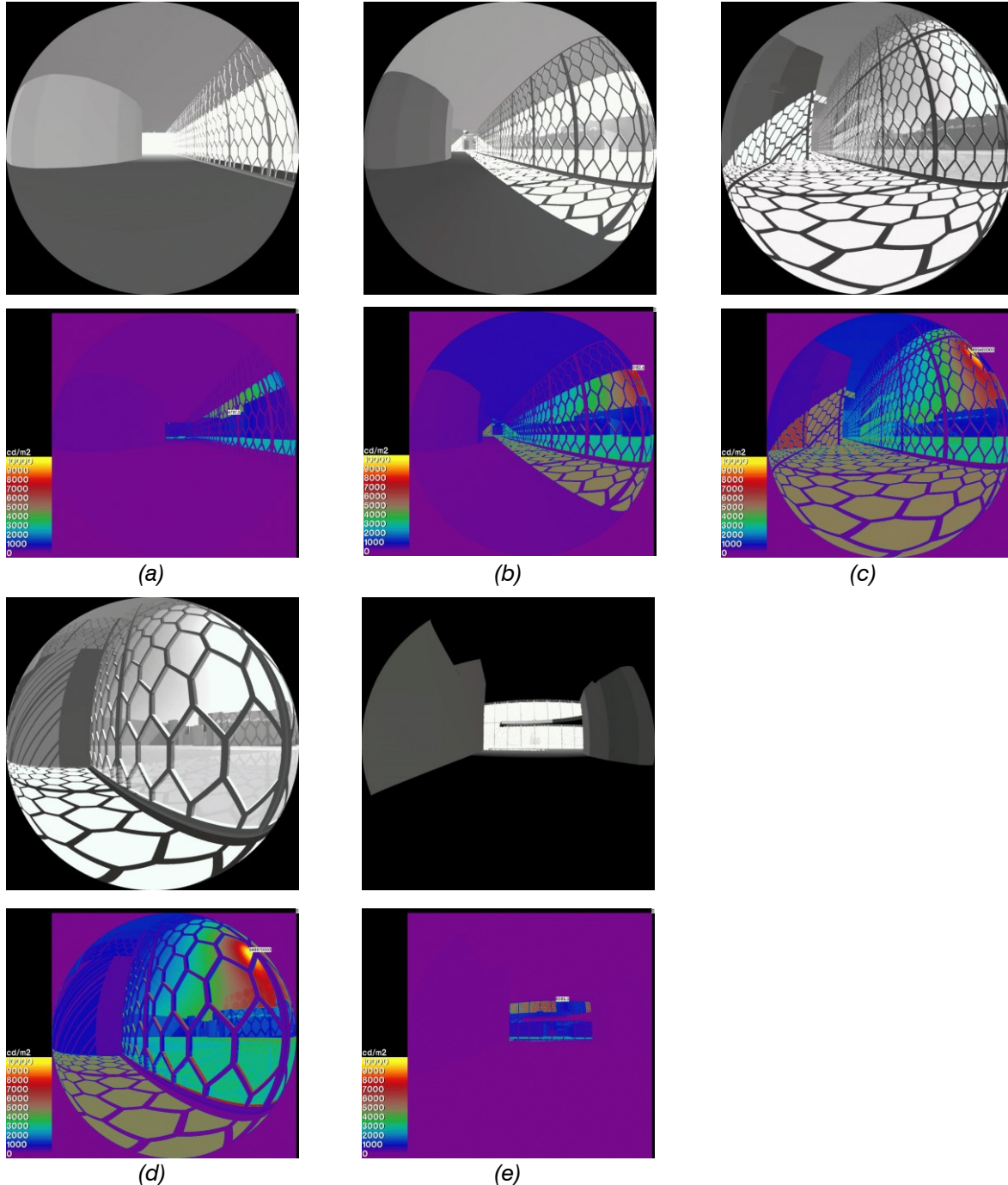
Figure 133 HDR-images views with corresponding False-colour image; (a) view 0, DGP=0.223484; (b) view 1, DGP=0.383299; (c) view 2, DGP=1.0; (d) view 3, DGP=0.248964; (e) view 4, DGP=1.0

First, the normative timeslots are determined by looking at the resulting *DGP*-values for both 21st December and 21st June. The results of the variant with only the core pattern is shown in Figure 134. Here it can be seen that view 2 and 4 experience disturbing glare in both summer and winter, while view 1 is mostly vulnerable to glare in winter.
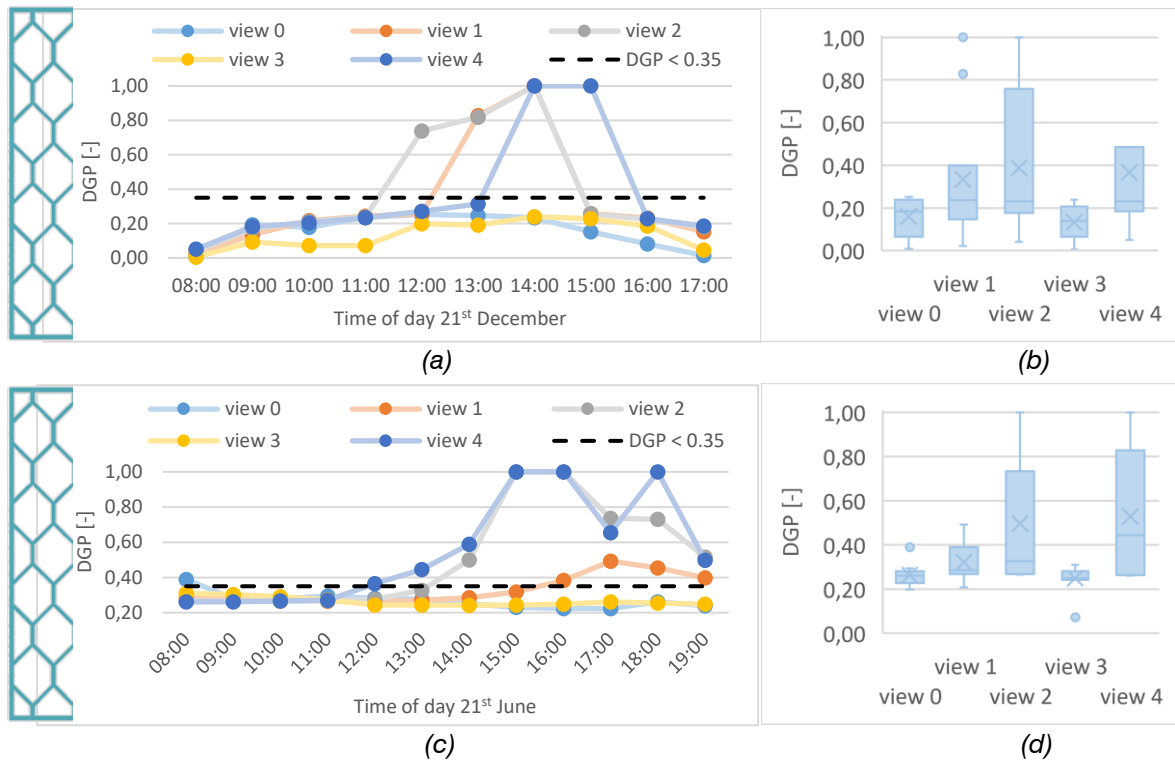
Figure 134 DGP-values for views as defined in Figure 132, for only core pattern, system deflated on (a, b) 21st December and (c, d) 21st June. Results depicted throughout the day and with a boxplot.

Using these view, at the timeslot of 15:00, various levels of transparency are evaluated to find the maximum transparency allowed to prevent disturbing glare, so with *DGP*-value < 0.35. The found transparency of the inflatables which meets this requirement is 0.14. For this value, the fully inflated system is evaluated for all the timeslots, see Figure 135.
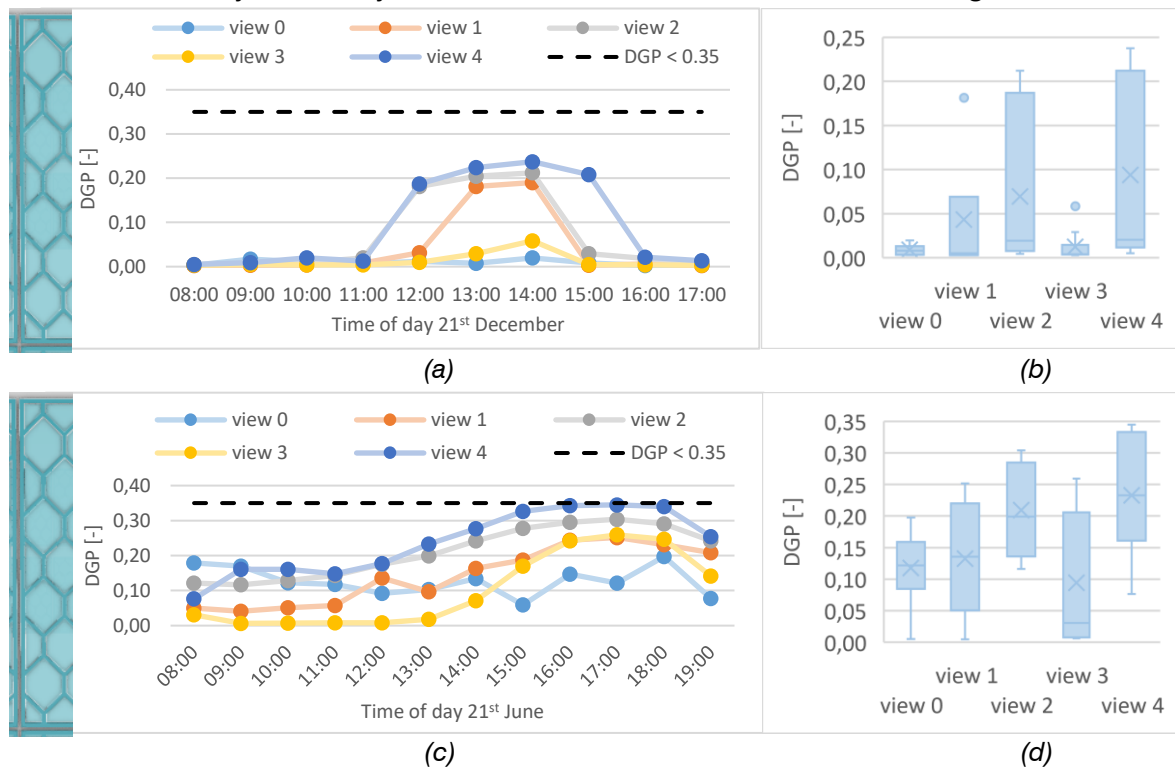
Figure 135 DGP-values for views as defined in Figure 132, for fully inflated system on (a, b) 21st December and (c, d) 21st June. Results depicted throughout the day and with a boxplot.

125

With the properties of the inflatables designed for glare control and the core pattern designed for structural efficiency, the daylight performance inside the building can be further improved by either changing the core pattern, or by defining a partly inflated option. The illuminance is determined using the point-in-time grid-based calculation. The grid points of the discussion room and lecture room are excluded from the results since these rooms are (mostly) closed off from direct daylight. For the remaining sensor points, the results are evaluated on whether they meet the minimal target illuminance E_{TM}, the target illuminance E_T, and the maximum illuminance to prevent over-lit sections E_{max}.
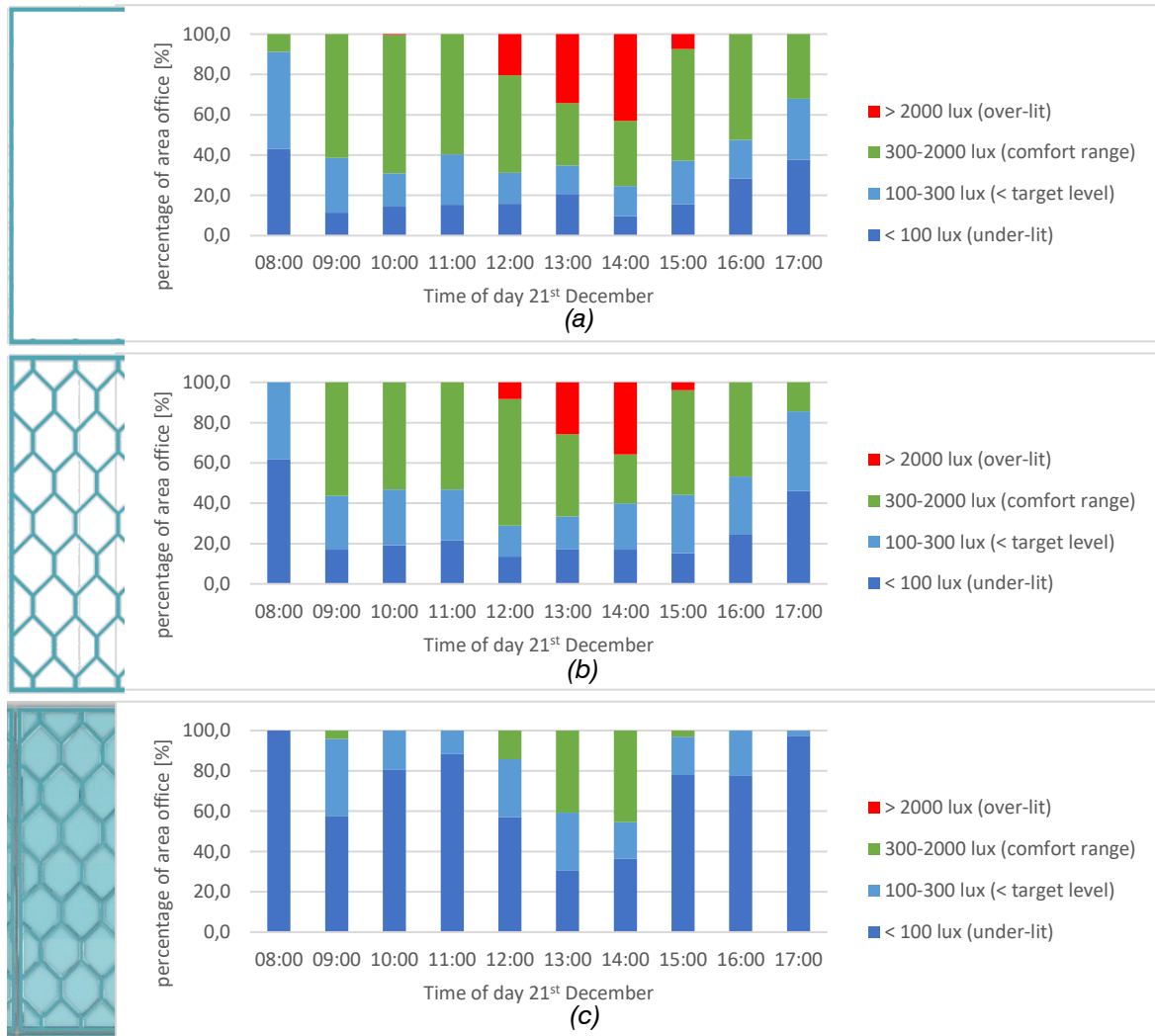
Figure 136 Percentage of area office which meets the target minimal illuminance E_{TM} (100 lux), target illuminance E_T (300 lux) and maximum illuminance E_{max} (2000 lux) on 21st December. Results for (a) only glass, (b) only core pattern and (c) fully inflated

Figure 136 shows the daylight performance on 21st December. The minimal target illuminance is not met, even for the option with only glass, which behaves similarly to the option with only the core pattern. This is due to certain sections not being exposed to direct sun light and this cannot be influenced by improving the façade. Artificial light will need to be placed in these sections.

The other results show that the option with only glass and only the core pattern behave similarly. The fully inflated option appears effective in preventing over-lit sections, but it no longer meets the target illuminance requirement. For this position of the sun, a more suitable solution should lie in between the option with only the pattern and the fully inflated

126

system. This can be achieved by either increasing the thickness of the core pattern, or by partly inflating the façade.
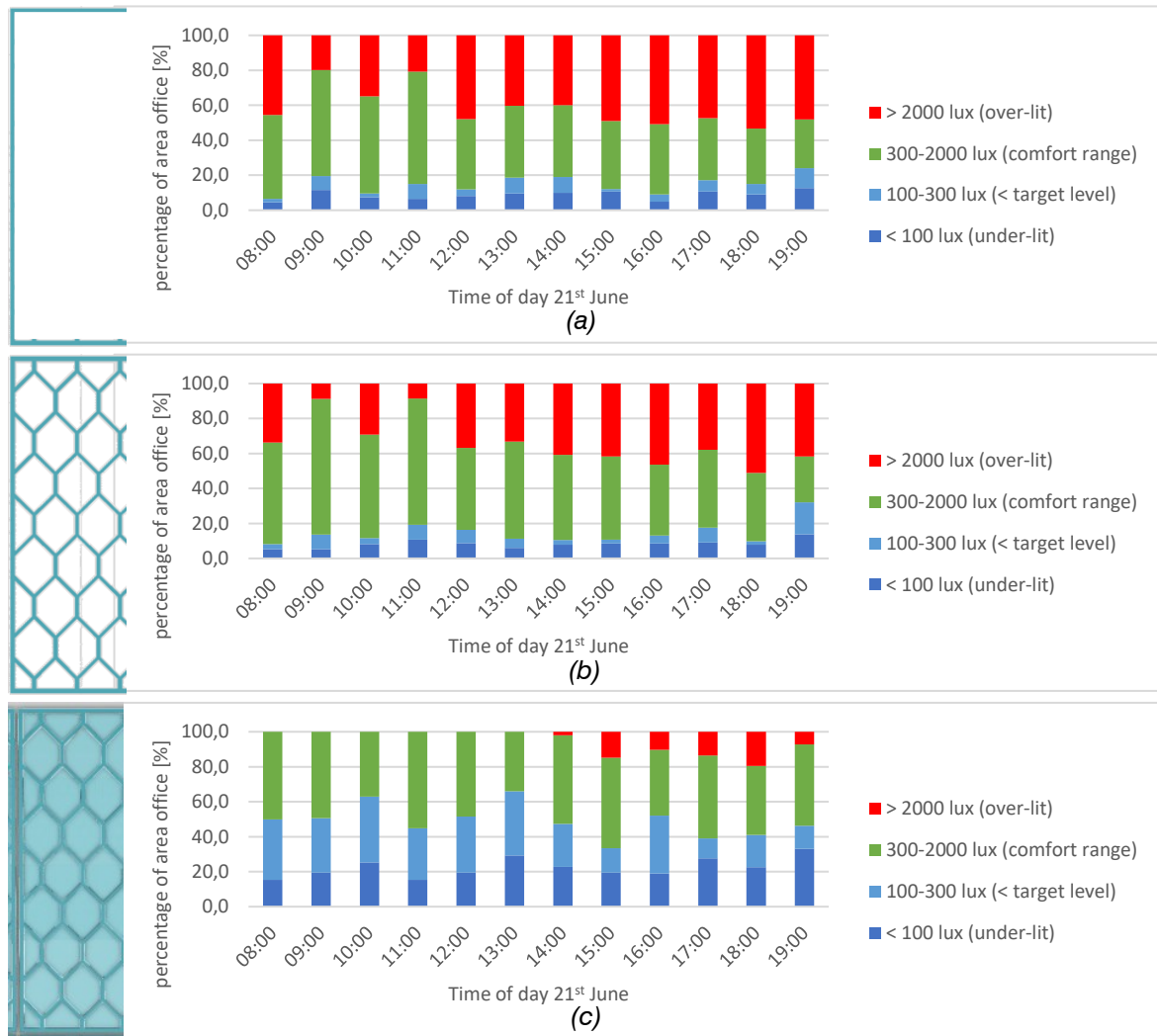
Figure 137 Percentage of area office which meets the target minimal illuminance E_{TM} (100 lux), target illuminance E_T (300 lux) and maximum illuminance E_{max} (2000 lux) on 21st June. results for (a) only glass, (b) only core pattern and (c) fully inflated

The results in summer on 21st June are shown in Figure 137. A significant increase in illuminance can be seen, with higher percentages reaching the target illuminance and exceeding the maximum illuminance resulting in over-lit sections. Since the façade design should be able to deal with the worst-case scenario, the fully inflated design should be adjusted to prevent over-lit sections from occurring.

To get an impression of how the illuminance varies over the total ground floor area and where over-lit sections occur, the heatmap for 21st June 18:00 is shown in Figure 138. The results of this analysis are in correspondence with the direct sun hours heatmap as shown in Figure 131. The sections which are under the minimal illuminance requirement are mostly located behind the lecture hall, which blocks the light. The over-lit sections are mostly located close to the façade, especially on the west-side of the building.

127

(a) Illuminance
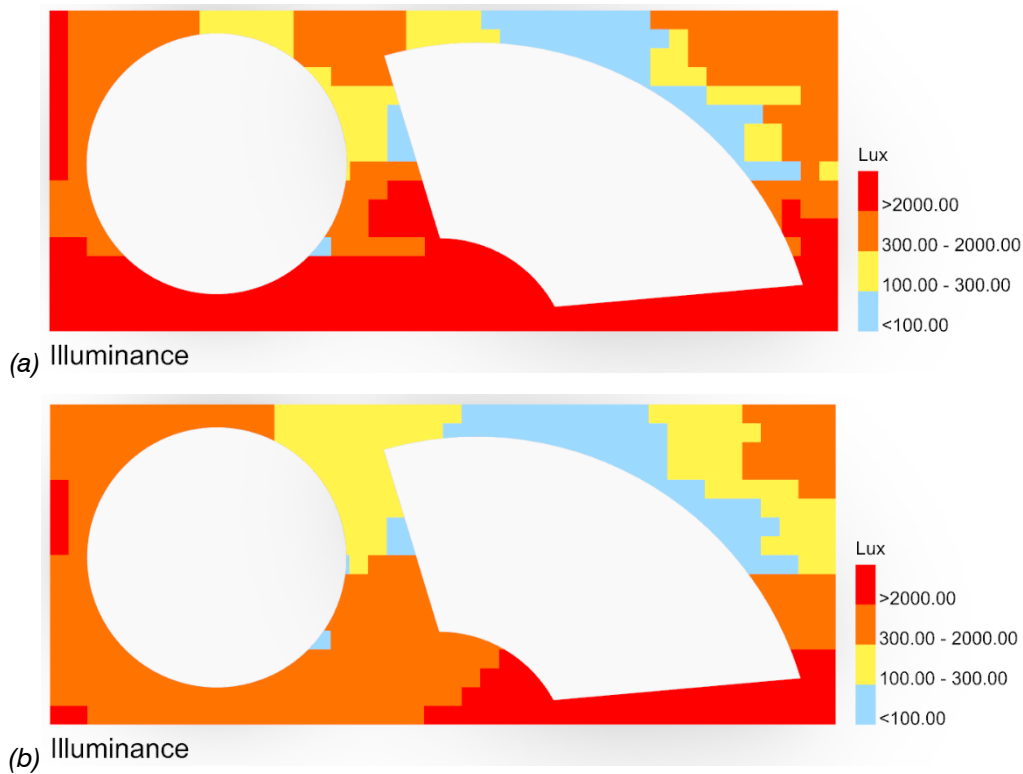
(b) Illuminance

Figure 138 Heatmap horizontal illuminance on 21st June 18:00 for (a) only the core pattern and (b) fully inflated with transparency=0.14

The under-lit sections are not exposed to direct daylight, thereby the illuminance here will have to be improved with the use of artificial lighting. The over-lit sections can be prevented or improved by decreasing the transparency of the façade system. This can be established by either increasing the thickness of the core pattern, or by decreasing the transparency of the inflatables. These measures only need to be applied to the west-side and north-west side of the building, since that is where over-lit sections occur.

The façade system is first improved by decreasing the transparency of a section of inflatables to a value of 0.05, see Figure 139. This placement is selected since the over-lit sections lie directly behind these parts. With the fully inflated adjusted option now being able to always prevent over-lit sections, changes to the core pattern and division of inflated cells can be explored.

(a)

128

(b)　　　　　　　　　　　　　　　　(c)
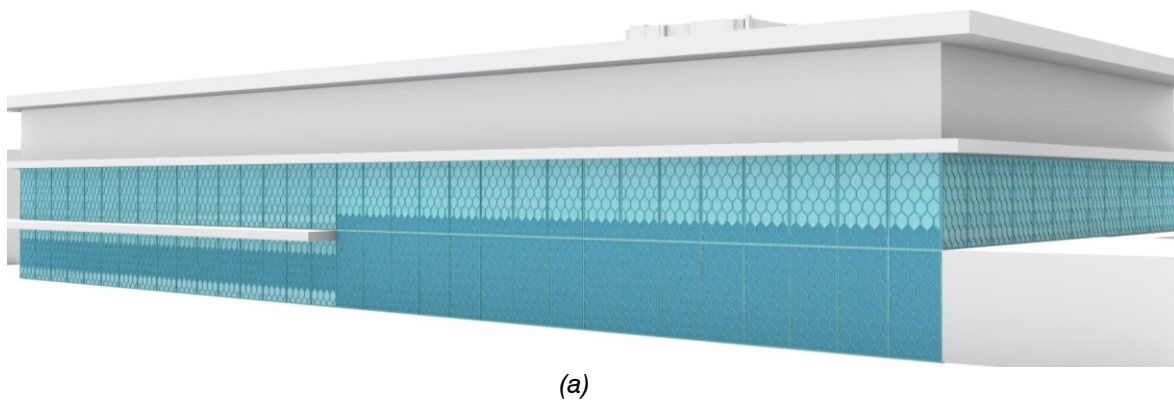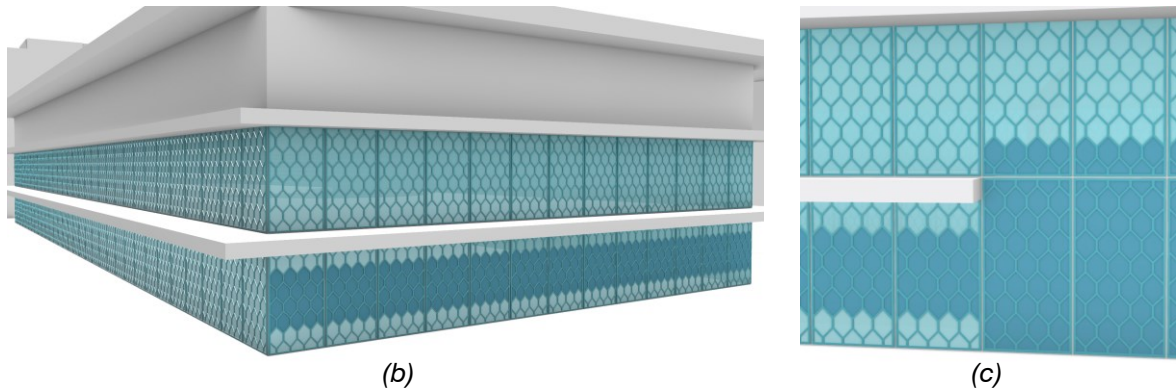
Figure 139 Fully inflated system with sections with transparency = 0.05 (dark blue) and transparency = 0.14 (light blue). (a) Full system south- and west-side; (b) full system north- and east-side; (c) zoomed in section

Next, the option of partly inflating the system is explored. The partly inflated option is designed based on which part of the façade cast a shadow directly onto the working plane. These are most likely to result in disturbing glare and therefore kept inflated. Opening up the bottom rows and top rows allows for more daylight to enter. The overhang on the right side protects the top rows from glare, therefore they can be opened. The resulting division of inflation is shown in Figure 140.

(a)　　　　　　　　　　　　　　　　(b)
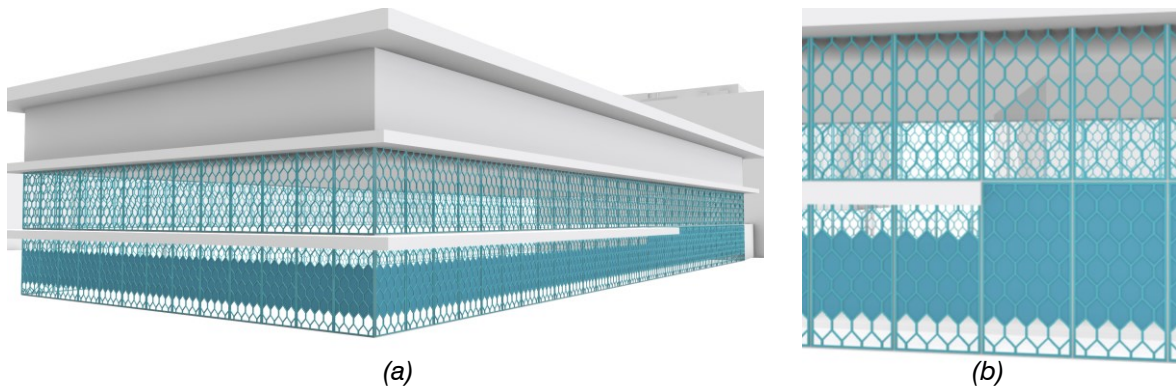
Figure 140 Partly inflated system. (a) Full system north- and west-side building; (b) zoomed in section

Lastly, the option of increasing the thickness of the core pattern is explored. This option slightly decreases illuminance levels, but this effect is limited. Since the core pattern was designed to be structural optimal, the original thickness of 35 *mm* is used in the final design and this option is not further explored. The two options, together with the previous option of only the core pattern are depicted in Figure 141 and Figure 142 for winter and summer, respectively. This shows the full reach of this system, being able to let in enough daylight to meet minimal requirements, but also able to be fully closed and effectively prevent over-lit sections and glare.

(a)
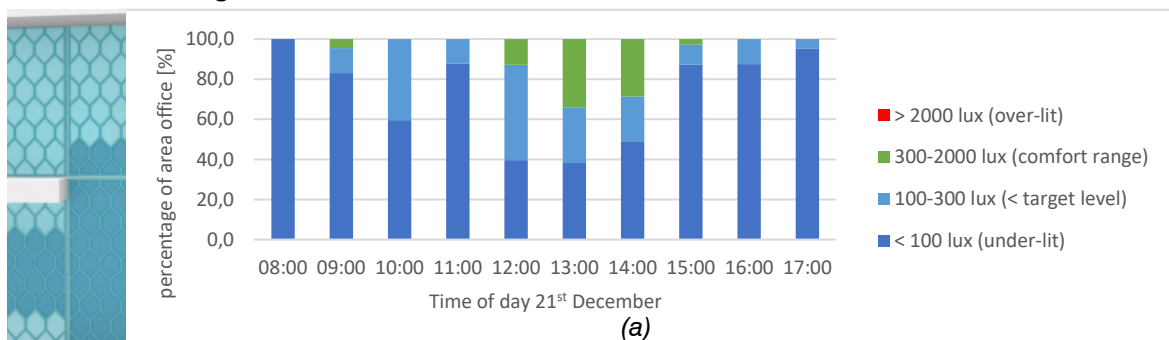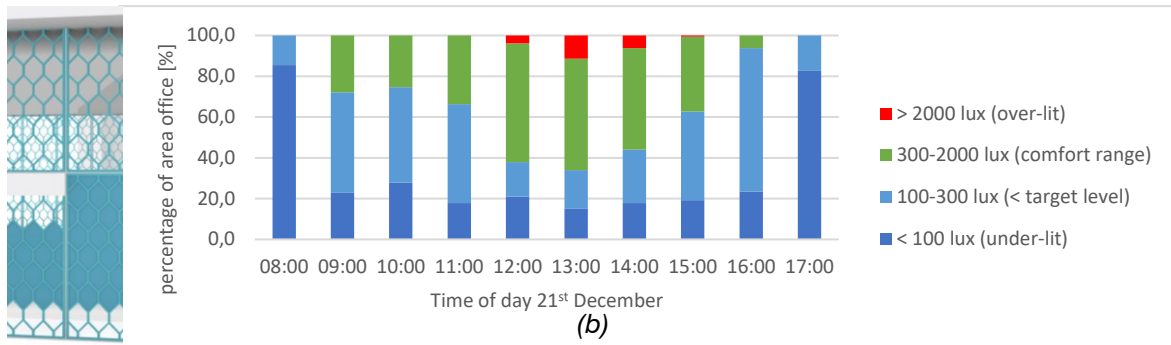
Figure 141 Percentage of area office which meets the target minimal illuminance E_{TM} (100 lux), target illuminance E_T (300 lux) and maximum illuminance E_{max} (2000 lux) on 21st December. Results for (a) fully inflated, adjusted and (b) partly inflated
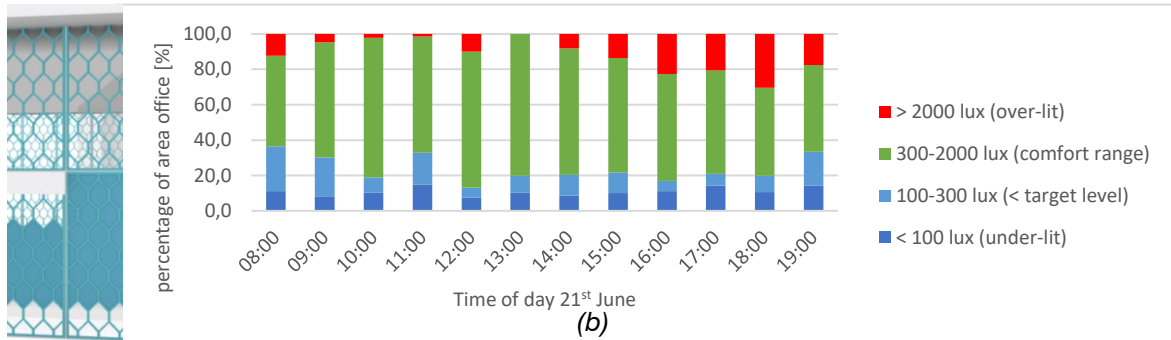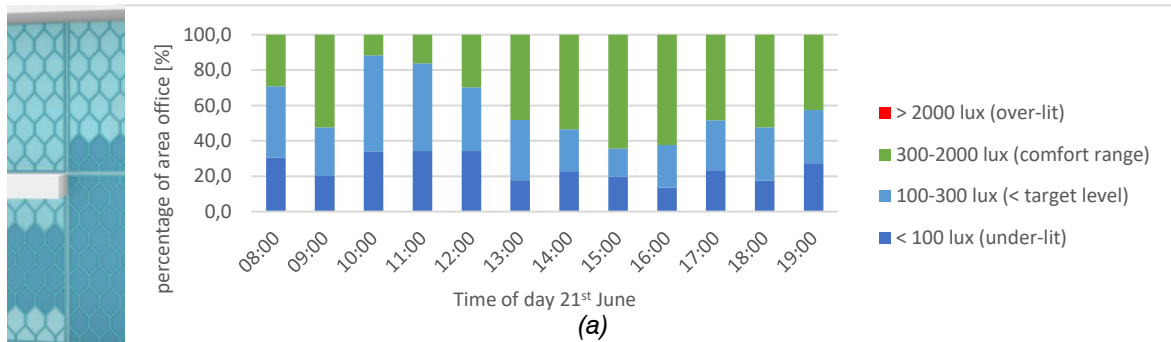

Figure 142 Percentage of area office which meets the target minimal illuminance E_{TM} (100 lux), target illuminance E_T (300 lux) and maximum illuminance E_{max} (2000 lux) on 21st June. Results for (a) fully inflated, adjusted and (b) partly inflated

Lastly, the resulting *DGP*-values of the partly inflated system are shown in Figure 143, showing that for most of the time, the partly inflated system is already effective in blocking glare. In summer, certain views do show disturbing glare, in which case the fully inflated system can be activated.

(c)   (d)
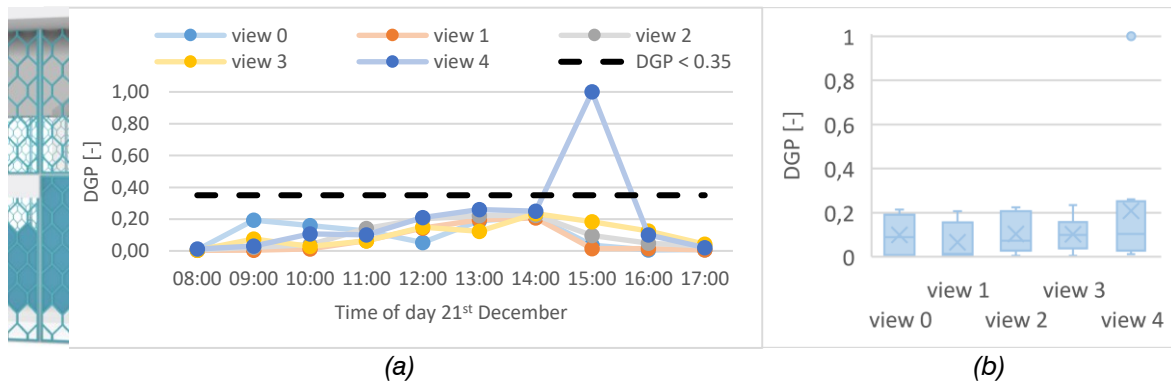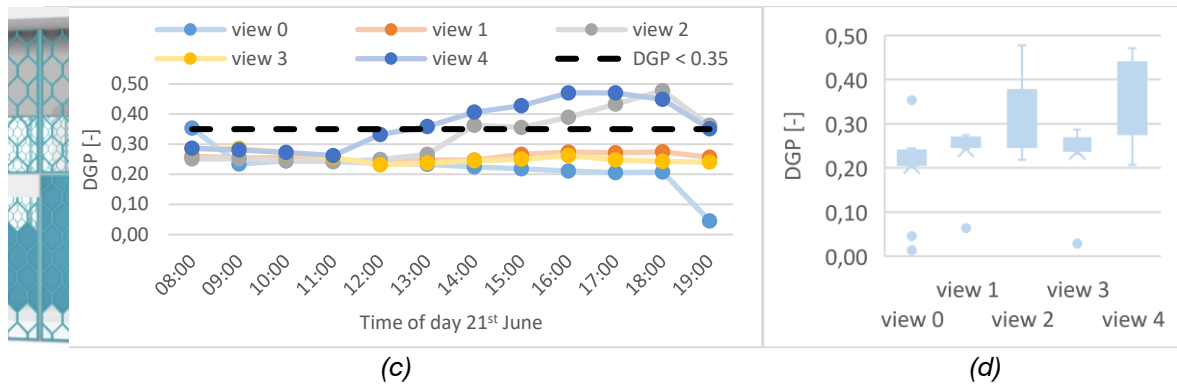
Figure 143 DGP-values for views as defined in Figure 132, for partly inflated system on (a, b) 21st December and (c, d) 21st June. Results depicted throughout the day and with a boxplot.

5.4 Evaluation

The resulting illuminances and *DGP*-values as depicted in 5.3 Design process, show that the inflatable façade system is effective in controlling glare and horizontal illuminance within the Echo building. The biggest difference is in the aesthetic of the façade, with the existing system being fully transparent, while the inflated system with core pattern is partly obstructing the view.

The façade system has an equal thickness compared to the original façade system used, only uses significantly less glass and introduces the core pattern. Figure 144a shows the section of the existing façade, with three 12 *mm* glass panes, with a 14 *mm* cavity and 1.52 *mm* for 4 x 0.38 *mm* lamination sheets. The design choice resulting from the optimisation process has two 1 *mm* glass panes with a 48 *mm* cavity originally. However, the additional safety from lamination can also be added to this design option. Therefore, on the inside the 1 *mm* glass pane is replaced by two glass panes and lamination sheets. Considering the thickness of the glass is much smaller, the option with 2 x 0.38 *mm* lamination is chosen.

For this laminated section, the calculations can use the equivalent thickness. This can be determined using the simplified method as defined in annex D of NEN-EN 16612 (2019). The two definitions for deflection and stresses are listed below:

$$h_{ef;w} = \sqrt[3]{\sum_k {h_k}^3 + 12\omega(\sum_i h_i h_{m.i}^2}} \qquad (30)$$

$$h_{ef;\sigma;j} = \sqrt{\frac{(h_{ef;w})^3}{(h_j + 2\omega h_{m;j})}} \qquad (31)$$

- $h_{ef;w}$ = equivalent thickness for calculating bending deflection [*mm*]
- $h_{ef;\sigma;j}$ = equivalent thickness for calculating stress of glass ply number *j*
- ω = shear transfer coefficient
- h = thickness glass pane
- h_m = distance centre glass ply to centre full laminated section

Considering the structural calculation showed a thickness of 1 *mm* is needed, these formulas can be solved to find the thickness of the laminated glass panes. The thickness of the laminated sheets is set at 0.76 *mm* with a shear transfer coefficient ω of 0.3. The resulting thickness should exceed 0.38 *mm*, as calculated in Appendix G. Determining laminated thickness panes. Therefore, two thin glass panes of 0.4 *mm* are chosen with the final section shown in Figure 144b.
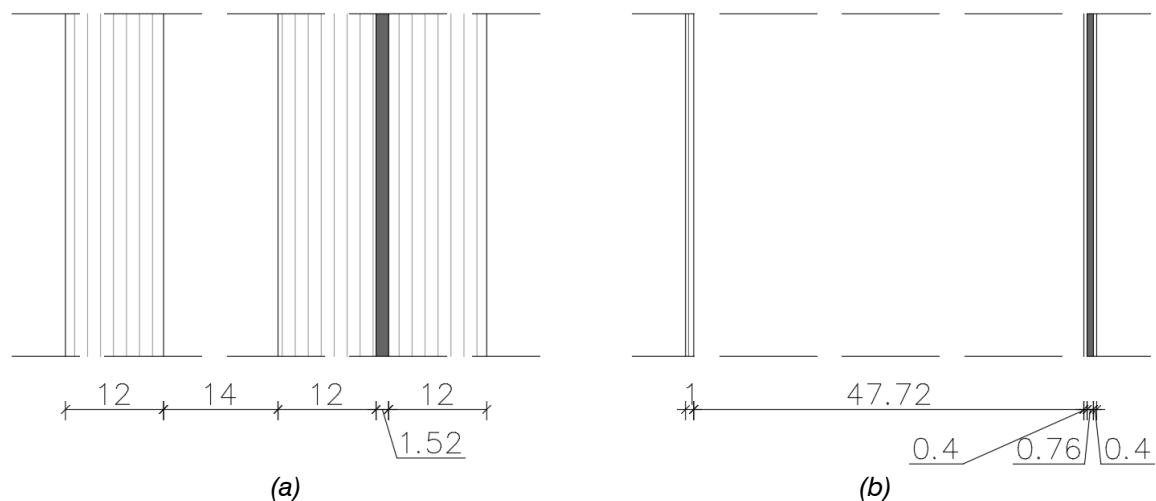
Figure 144 (a) Section existing façade 12/14/12.12.4; (b) section inflatable design façade 1/48/0,4.0,4.2

To make a comparison of the material used in both façades, first the volumes of the glass and core material are determined. For the existing design, the glass façade follows the 12/14/12.12.4 (total 51 *mm*) division. This translates to 12*3=36 *mm* total thickness of glass. For the 2.6x5 *m²* panel, this results in a total glass volume of 0.468 *m³*. The design with the inflatable system uses one glass pane of 1 *mm* and two of 0.4 *mm* thickness. Therefore, the total glass volume is equal to 0.0234 *m³*. This design also uses the core material, which has a total volume of 0.140 *m³*.

The volumes can be compared in terms of weight per panel and the environmental footprint. The weight of the existing façade is approximately the weight of the glass volume, which is 0.468 * 2480 = 1190.4 kg. The weight for the sandwich panel consists of both the glass and core material: 0.0234 * 2480 + 0.140 * 1270 = 235.8 kg. The weight of the façade panel designed in this thesis is approximately 1/5 of the existing façade, showing a significant reduction. The reduction in weight also contributes to reducing costs and emissions in relation to transportation.

5.5 Conclusion

In conclusion, the inflated façade system can function as an effective alternative to the existing façade of the Echo building. The system can prevent disturbing glare by blocking the incoming solar rays with the inflatables. It can also reduce over-lit sections in the building, using the inflatables with decreased transparency. The system can also be partly inflated, where disturbing glare and over-lit sections can still be preventing during certain timeslots in the day. This increases the benefit of natural light inside the building, reducing the need for artificial lighting.

The designed façade system weighs approximately 1/5 of the existing façade, thereby reducing its carbon footprint. The total thickness of the façade element remains the same compared to the existing façade, only the cavity space is increased from 14 *mm* to almost 48 *mm*. The final design solution is laminated similar to the existing façade, resulting in a safe façade design.

6 DISCUSSION

The main goal of this thesis was to develop a design and design strategy for an integrated solar control system within the thin glass sandwich panel. The design process was structured into four main phases: the literature review, the design of the façade system, the development of the design strategy and the application of the designed system in a case study. This approach aimed to systematically go through the initial concept to the realisation of a full design strategy, supported by a case study.

The literature review showed that the thin glass sandwich panel is a suitable option for façades, due to the high strength properties of the chemically strengthened thin glass and the use of the sandwich structure. For the core of this sandwich panel, various patterns are possible, but an open-cell pattern is preferred to create a see-through panel, limiting obstruction in the view through the façade panel. The honeycomb pattern in particular is efficient, providing both high stiffness and low density, resulting in a light-weight panel with high transparency. This reduction in materials compared to conventional façade solutions reduces the carbon footprint of the façade panel, thereby creating a more environmentally friendly panel.

Since the core pattern is partly obstructing the view, it can be used to influence the daylight performance of the panel. The core design was limited to patterns with uniform cell size, reducing the complexity of the design, but limiting the possibilities. In future research, more complex patterns could be explored to create more efficient designs that can respond more precisely to the incoming sunlight.

The literature review evaluated many existing façade systems and concluded that adding a dynamic aspect to the system is essential for optimising the visual comfort. Since the sandwich panel has an open cell core pattern, the dynamic system can be integrated within the panel itself, eliminating the need for additional internal or external systems. The two integrated dynamic systems explored in this thesis are the inflatable design and the folding design concept. After developing both these systems further and defining them in modelling software the main advantages and disadvantages of each system became clear.

The folding mechanism consisted of multiple parts within each cell, significantly increasing the complexity of the design. The limited space inside the cell also reduces the possible shapes of the folding curve, while also creating the risk of the material catching onto the glass and becoming defective. The inflatable system uses only a single inflatable per cell, which is made out of flexible material and can easily be adapted to fit different shapes. However, it does require a connecting pneumatic system, which introduces many connections which can be vulnerable to leakage.

Aside from complexity, the long-term functionality of the systems was also considered. Both systems can be vulnerable to fatigue, due to the repetitive motion in both the foldables and inflatables. Ensuring the material has a fully elastic deformation can prevent plastic deformations, thereby reducing the risk of failure. Ensuring the material is fully elastic and remains this during its lifetime is an important design aspect in both. Taking all this into account, the inflatable design was selected because of its repetitive design, reduced complexity and more manageable risks.

The inflatable design was further explored by parameterising the façade panel. By changing only one parameter, its effect was studied. This showed that the dimensions of the thin glass panes and the core pattern have a big influence on the resulting deflection of the panel and the maximum stresses acting in the glass and core. Using the defined requirements of the panel, an optimal design can be found for each panel design. For the 2x2 *m* façade panel used in the office room, on optimisation algorithm was used to quickly generate an efficient design.

Following, the daylight analyses were executed with a detail level determined with convergence tests with a limit of 10 % difference. This balances the precision with needed calculation time, but an increase in detail level may be necessary in further research. The design for the office was used to set up the various analyses, where three locations in the room were used to generate the views outside and parallel to the façade needed for glare analyses.

These analyses showed that changing the transparency of the inflatables is an effective way of controlling the amount of light able to enter through the façade. By adjusting this property, an optimal setting can be found to be able to prevent disturbing glare and over-lit sections in the room. This design strategy primarily addressed extreme scenarios, everyday conditions were excluded. The resulting illumination and glare control may perform differently, potentially needing different section divisions when partly inflating the façade. Aside from the inflatables, the core pattern itself also contributes to the daylight performance of the panel. Increasing the thickness of the core pattern reduced the likelihood of disturbing glare and reduced the horizontal illuminance in the room.

Using the properties of the inflatables and core material, disturbing glare and over-lit sections can be avoided fully with the inflatable façade panel. The design is further explored by looking at a larger scale of the system, either by partly inflating a single panel, or by designing a division to partly inflate multiple panels, forming a system together. For the office, leaving the top and bottom two rows of inflatables open greatly increased the inside illuminance levels, while the system still remained effective in blocking disturbing glare throughout most of the day. This showed that partly inflating the system allows for a more efficient use of natural light, avoiding unnecessary use of artificial light. In comparison to other systems which only have an on and off setting, this is a clear advantage.

To further show the effectiveness of the system, also on a full building scale, the system was applied in a case study on the Echo building on the TU Delft campus. The developed design strategy for the inflatable façade system is effectively applied to this case study. To reduce the complexity of the full-scale building, only the ground floor was analysed, together with limiting the number of views to five for the glare analysis. The full design is shown to be effective in preventing disturbing glare and over-lit sections. It also includes a partly inflated option, which increases the use of natural light while still being effective in preventing disturbing glare and over-lit sections.

The resulting design of the panel is structurally optimised, resulting in a light-weight panel with integrated dynamic solar control. In comparison, the inflatable façade panel weighs approximately 1/5 of the existing façade in the building, thereby also reducing its carbon footprint. The final design solution is laminated similar to the existing façade, resulting in a safe façade design.

7 CONCLUSION AND RECOMMENDATIONS

7.1 Conclusion

The main objective of this thesis is to develop a design for a thin glass façade panel with dynamic daylight control together with a suitable design strategy. The design is optimised for both its structural performance but also its daylight performance. The main research question is formulated as follows:

How can an optimal design be achieved for a thin glass façade sandwich panel that both meets the structural requirements and daylight requirements, finding the right balance between glare control and daylight performance?

The system designed in this thesis integrates inflatables within the honeycomb core pattern, placing an inflatable in each individual cell. Once inflated, the full cell is filled and able to prevent disturbing glare and influence the illuminance inside the room. By designing the transparency of the inflatables to prevent disturbing glare, a control system can be designed to (partly) inflate the full façade system. This allows for control over the horizontal illuminance within the room, preventing over-lit sections, while still meeting the minimal target illuminance values.

The core pattern can be designed to be structurally efficient, meeting both the requirement for maximum deflection (service limit state) and maximum stresses (ultimate limit state) within the glass panes and core material. The visual comfort resulting from the façade system can also be optimised. It is quantified in requirements for glare, illuminance and contrast.

Glare is measured in the Daylight Glare Probability, which should meet the threshold of $DGP < 0.35$ to prevent disturbing glare. For an office, the minimum illuminance of $E_{TM} = 100$ lux should be met for 95 % of the room, during 50 % of the workday. The target illuminance of $E_T = 300$ lux should be met for 50 % of the room, during 50 % of the workday. The maximum illuminance should not exceed 2000 lux, to prevent over-lit sections within the room. The horizontal contrast ratio between connecting sections should stay below 1:3.

The final design strategy combines all the requirements and wishes to find the optimal design solution for the façade system. The dynamic nature of the system allows for an accurate response to the incoming daylight, allowing for an optimal use of natural light inside the building, while providing visual comfort inside the building.

The resulting thin glass façade panel is significantly lighter compared to conventional façade systems. The panel designed for the Echo building in the case study is approximately 1/5 of the weight compared to the existing façade used in the building. The case study further showed that the façade system is effective in providing visual comfort to the building.

In closing, the inflatable design is an effective façade design with integrated dynamic solar control system, resulting in a compact façade solution. The design functions comparatively to existing façade solutions and shows potential to be explored further. It also expands on the possibilities of using thin glass in façade design, showing how the gained cavity space of a panel can be used to dynamically control the daylight performance.

7.2 Recommendations

This thesis was limited to structural and visual comfort related analyses. The thermal performance of this façade design should be evaluated. The inflatables making contact with the glass surface may influence the isolating ability of the panel, as well as the influence of the openings and tubes installed in the core pattern.

The design process of the façade system now only looks at the extreme situations, like the maximum chance of glare or creating over-lit sections in the room. The evaluation of the system should be expanded by including other sky conditions and other times in the year to provide a more extensive overview of the functionality of the system. In addition, multiple settings which can partly inflate the façade can be included as well, further showing the full range of abilities of the façade system.

For the design of the inflatables, the actual relation between material properties and how these are defined in the model should be defined. The relation between material choice, thickness of the material, colour and other properties should be matched with the properties as used in the models. The effect of the inflatables exerting pressure onto the thin glass should be researched as well, since it may affect the structural performance of the façade panel, potentially reducing over the long term as well.

8 APPENDICES

Appendix A. Grasshopper script geometry

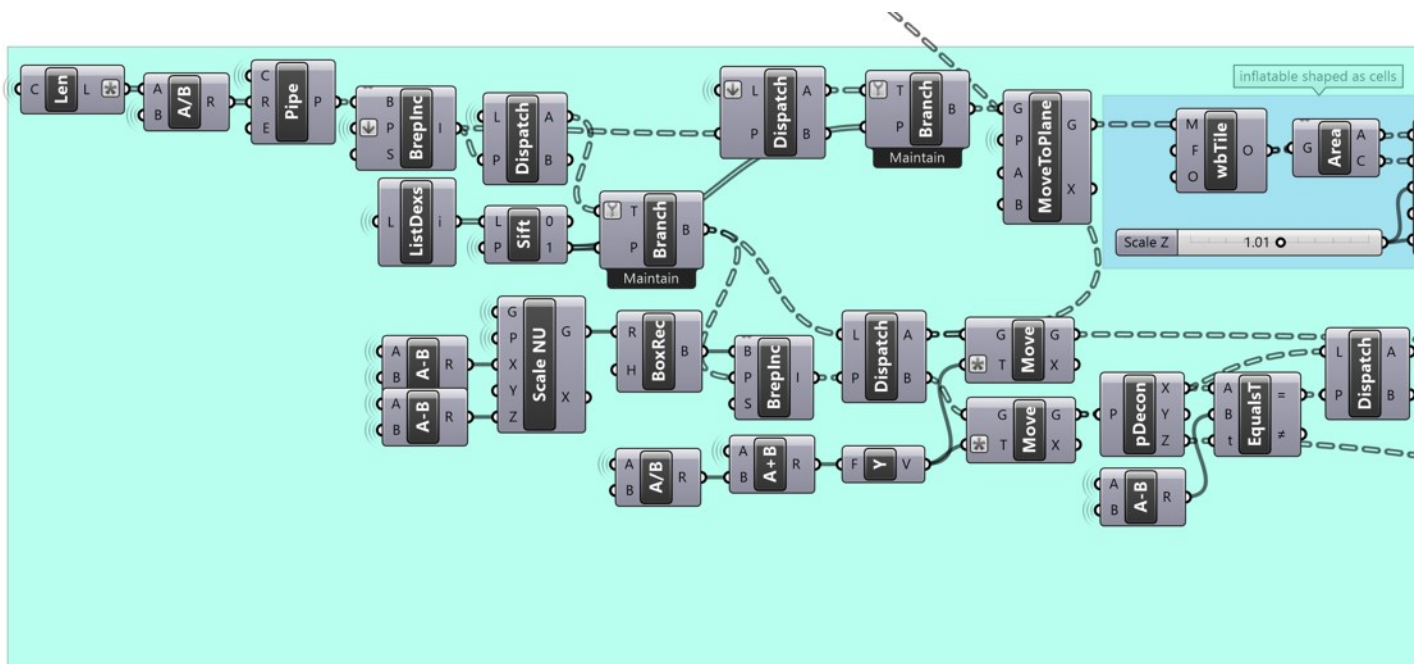A.1. Geometry standard office, thin glass panes and 3D-core for sandwich panel
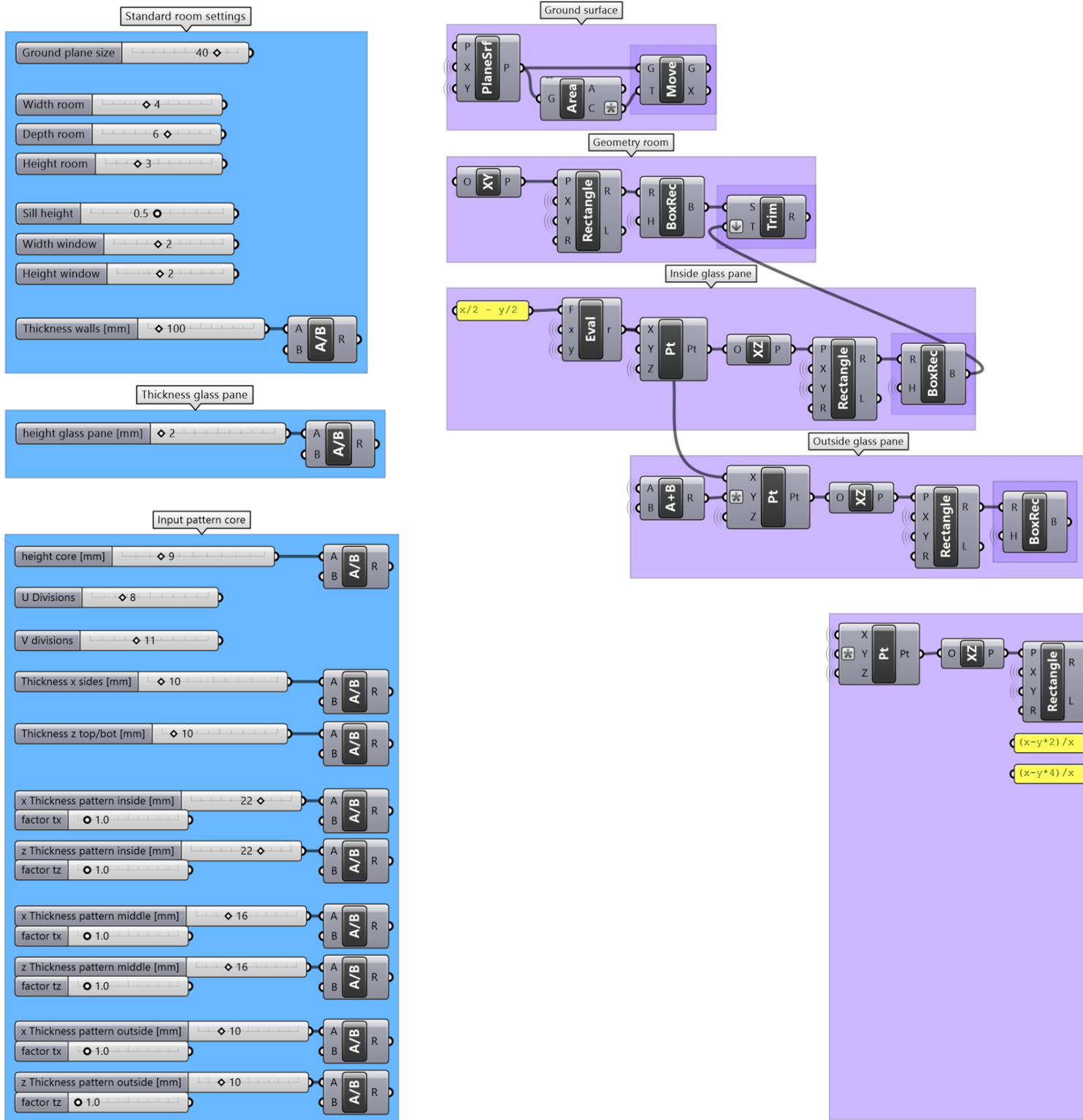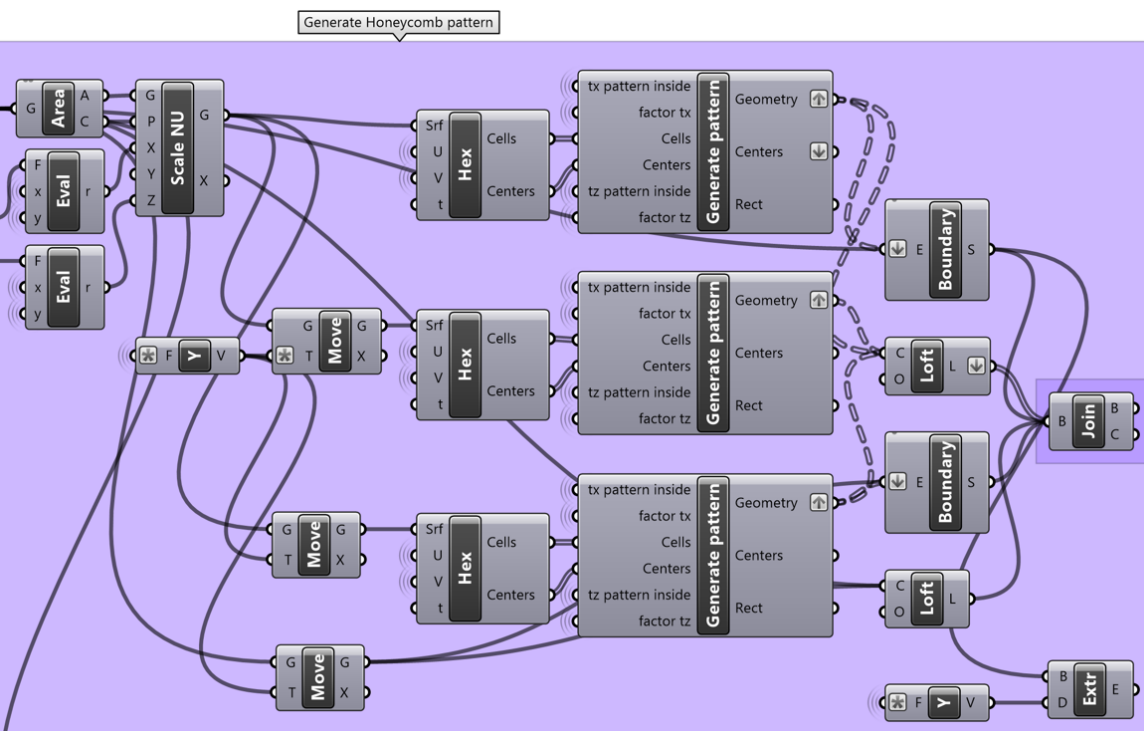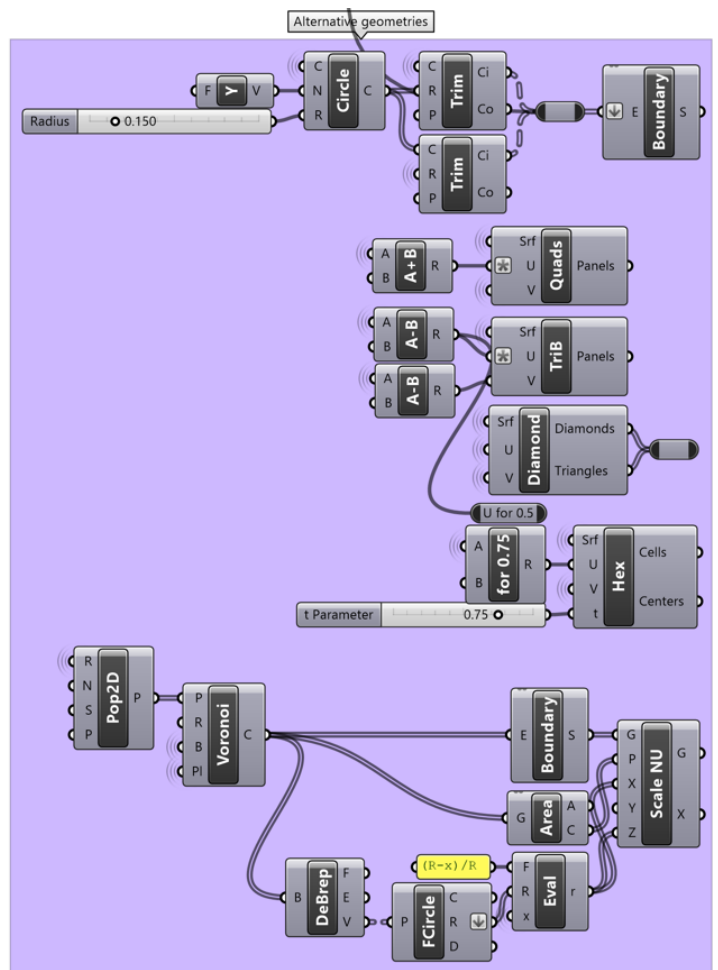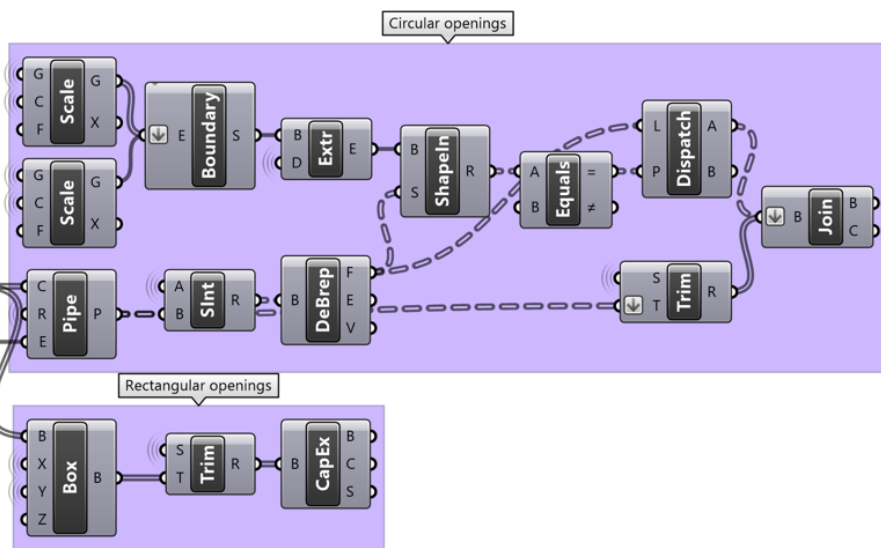
Cluster: Desk + Chair

Inflatable geometry core

Pressure strength — 4.00

Length factor edges — 1.15

1st row — True

2nd row — True

3rd row — True

4th row — True

Reset button

(Re)start calculation — True

Inflatable design

145
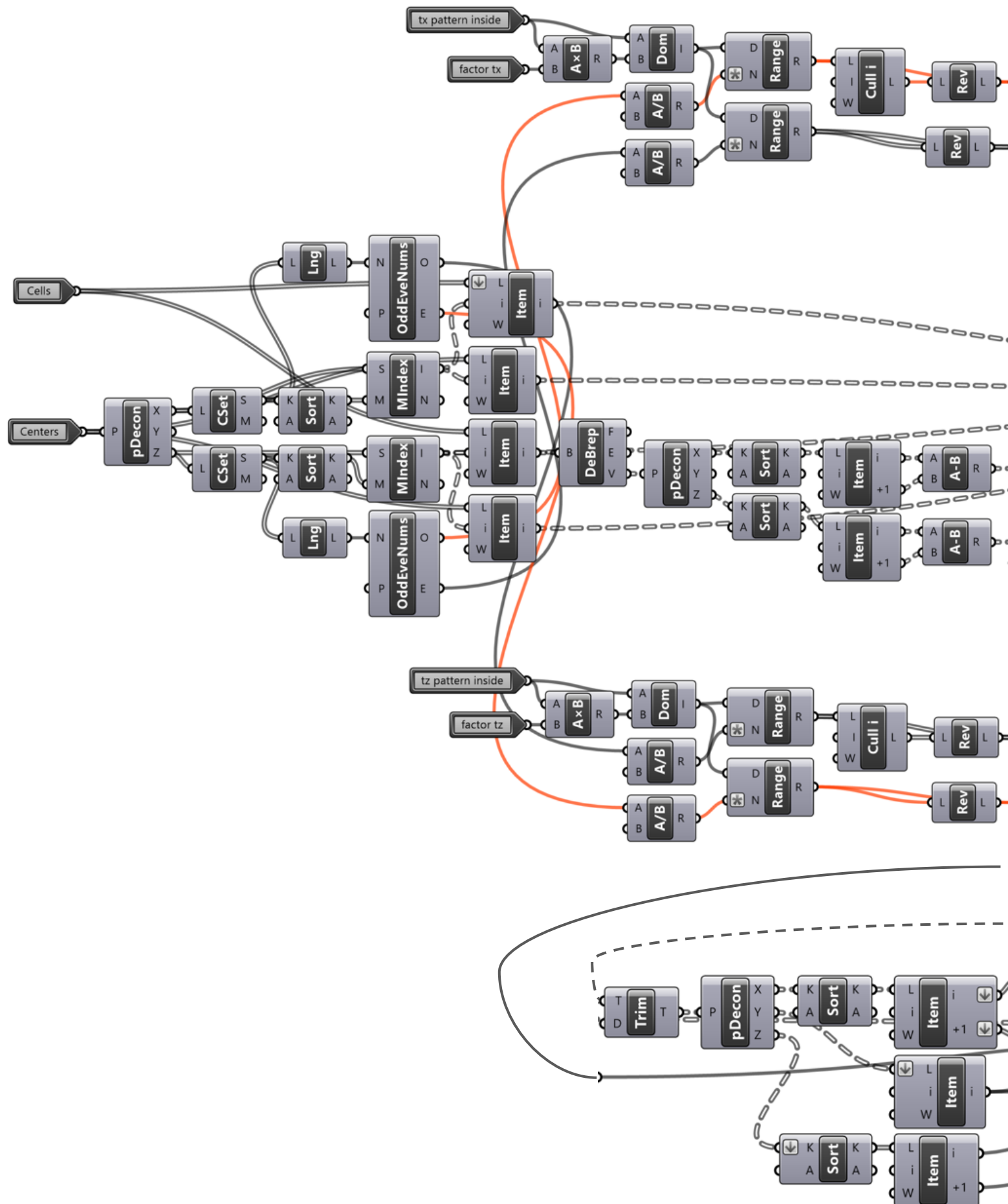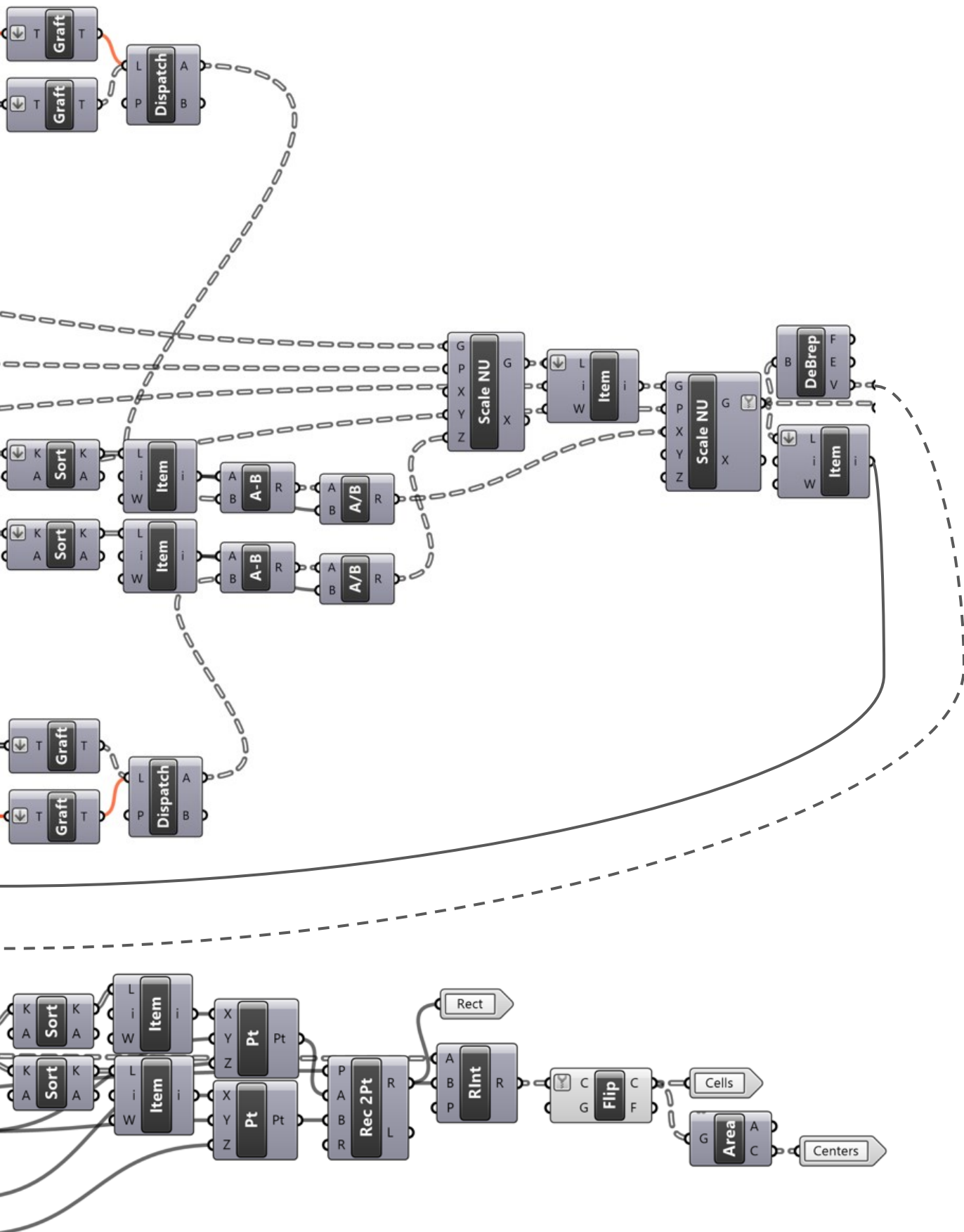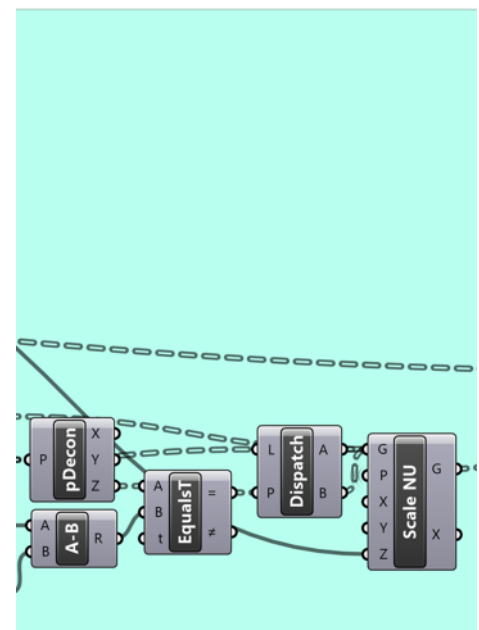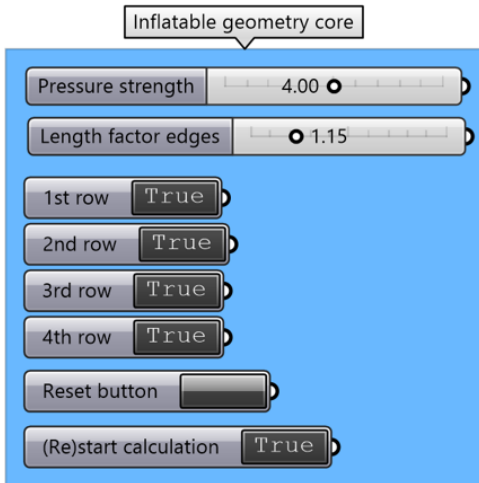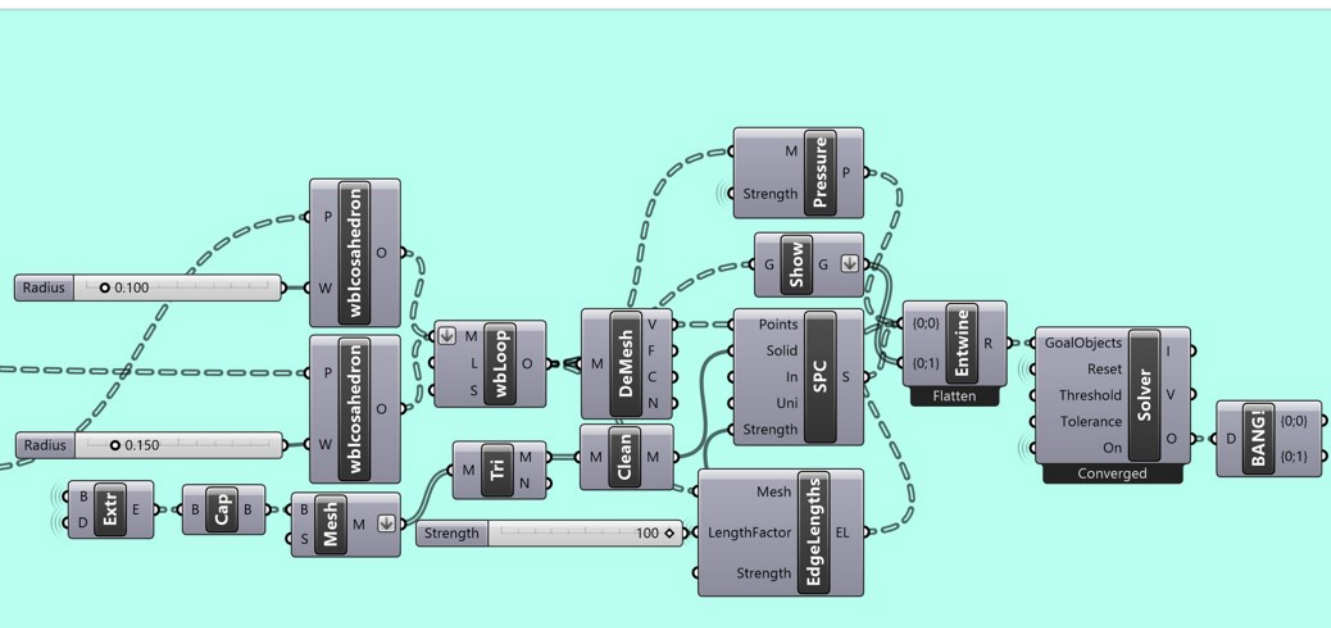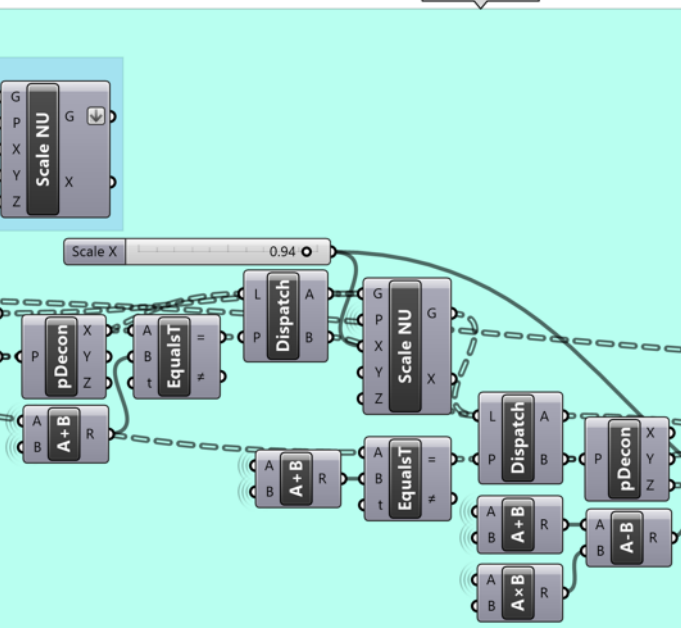
A.3. Grasshopper script Folding design

Opening system, no bending

| Angle | 45 ◇ |
| Visualize | False |

Openings system, with bending

Curve bending parameter 1	2.265
Curve bending parameter 2	2.156
Curve bending parameter 3	1.866
Curve bending parameter 4	0.430
Folding geometry simulation	False

Scale X   0.98

Scale Z   0.98

Folding following curve design
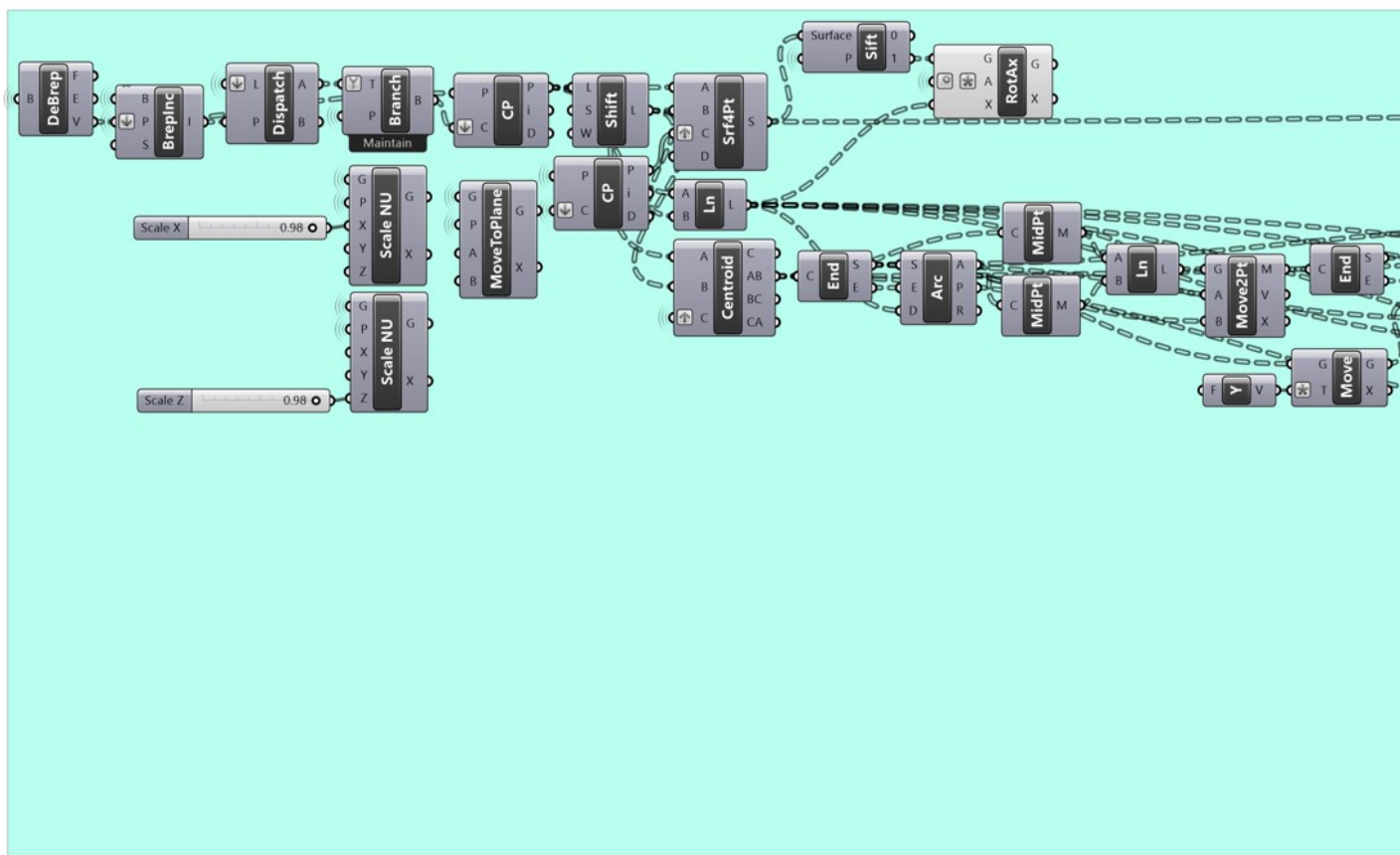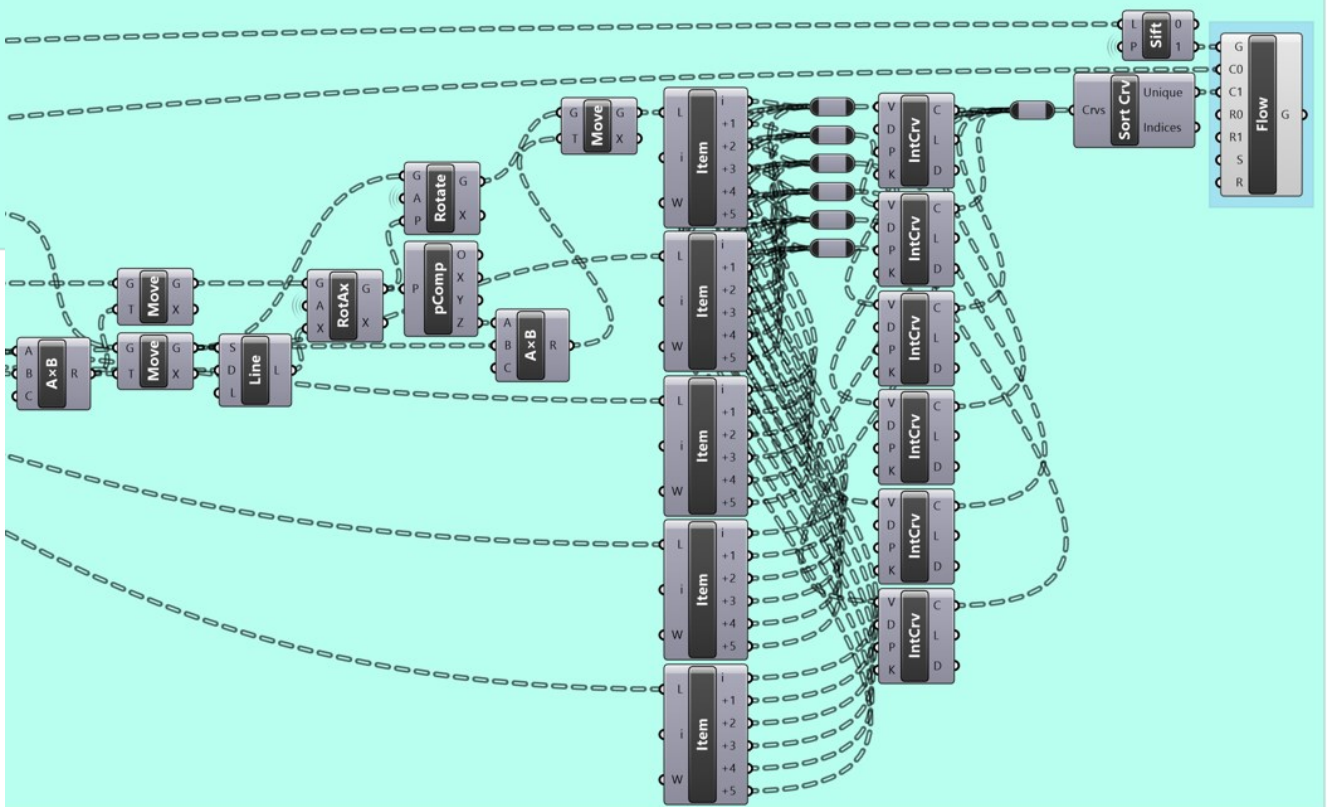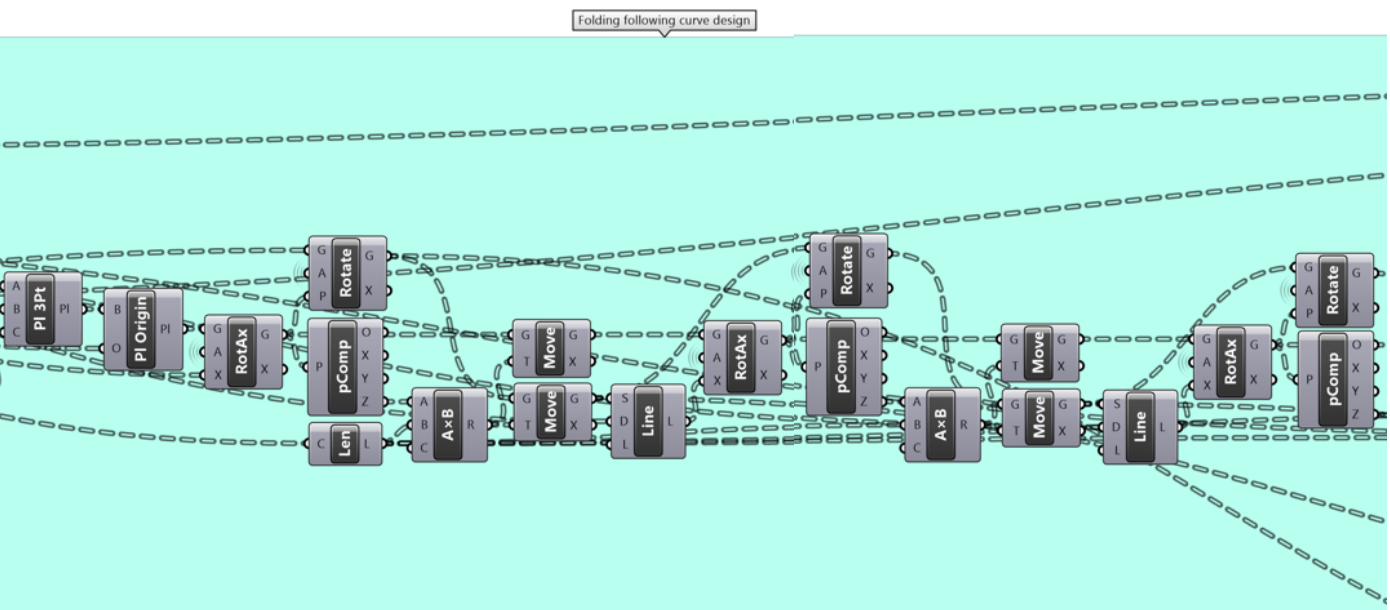
Appendix B. Grasshopper script for Karamba3D model

1

F Z V

Vec
Mesh
ElemIds
AddPos
LCase

Loads

Load

SLS

Orientation

Local to mesh ◉
Global ○
Global proj. ○

Generation

Point loads ◉
Line loads ○

Type of Load:

MeshLoad Const

1.5

F Z V

Vec
Mesh
ElemIds
AddPos
LCase

Loads

Load

ULS

Orientation

Local to mesh ◉
Global ○
Global proj. ○

Generation

Point loads ◉
Line loads ○

Type of Load:

MeshLoad Const

Glass

glass

E [GPa]
74

G12 [GPa]
30

G3 [GPa]
30

rho [kg/m3]
2480

ft [MPa]
260

fc [MPa]
260

A B A×B R

Family
Name
Elem|Id
Color
E
G12
G3
gamma
alphaT
ft
fc
S-Hypo

MatProps

Mat

Material Type:

Isotrop

glass inside

Family
Name
Elem|Id
Color
Material
Height

Cross Section

CroSec

Cross Section:

Shell Const

A B A×B R

glass outside

Mesh
Color
Id
CroSec

MeshToShell

Elem
Pts
Info

Options

Mesh
Color
Id
CroSec

MeshToShell

Elem
Pts
Info

Options

Core

core

core mat

E [GPa]
2.02

G12 [GPa]
0.90

G3 [GPa]
0.90

rho [kg/m3]
1270

ft [MPa]
50

fc [MPa]
50

A B A×B R

Family
Name
Elem|Id
Color
E
G12
G3
gamma
alphaT
ft
fc
S-Hypo

MatProps

Mat

Material Type:

Isotrop

A B A×B R

Family
Name
Elem|Id
Color
Material
Height

Cross Section

CroSec

Cross Section:

Shell Const

Mesh
Color
Id
CroSec

MeshToShell

Elem
Pts
Info

Options

149

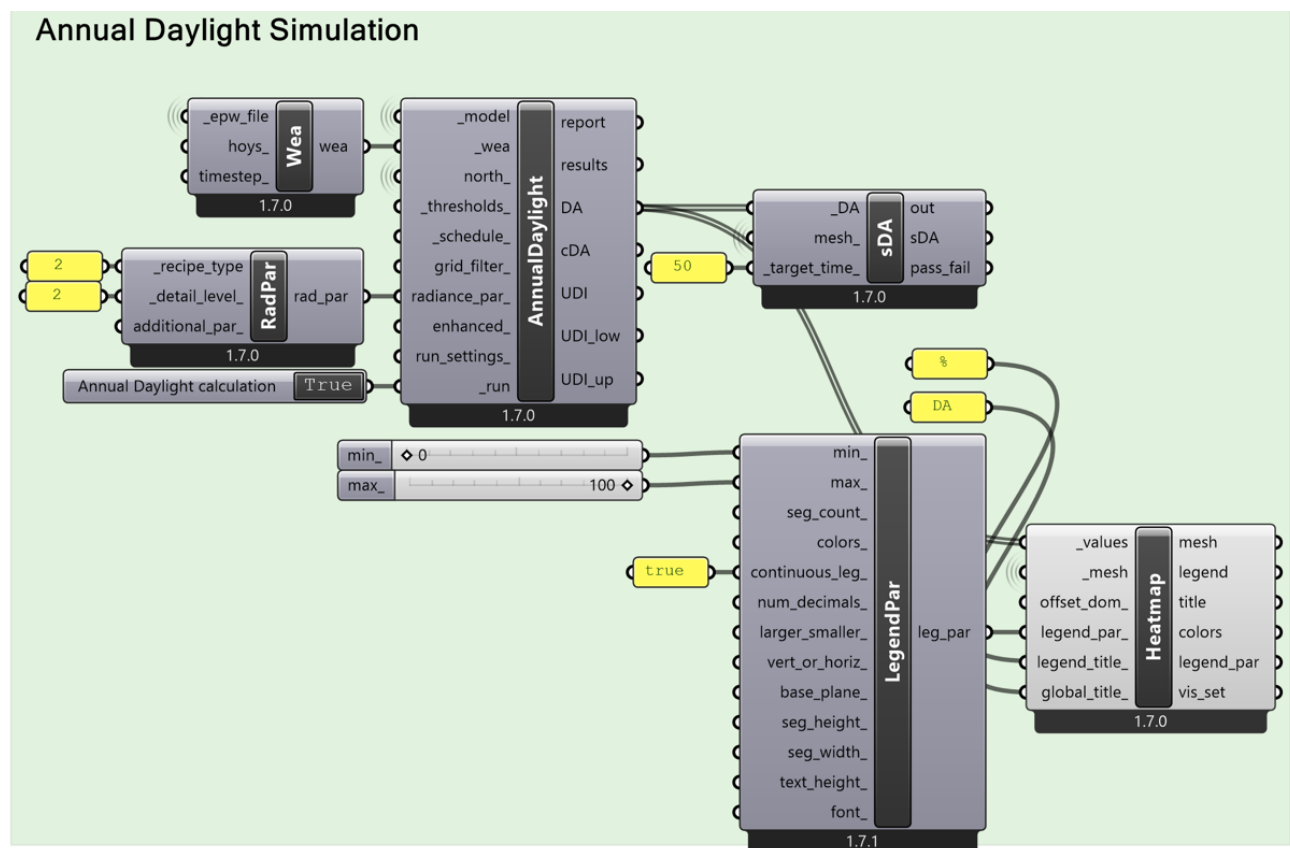# Appendix C. Grasshopper script for daylight simulation

C.1. Honeybee model

Point-in-Time Grid-Based simulation, Illuminance
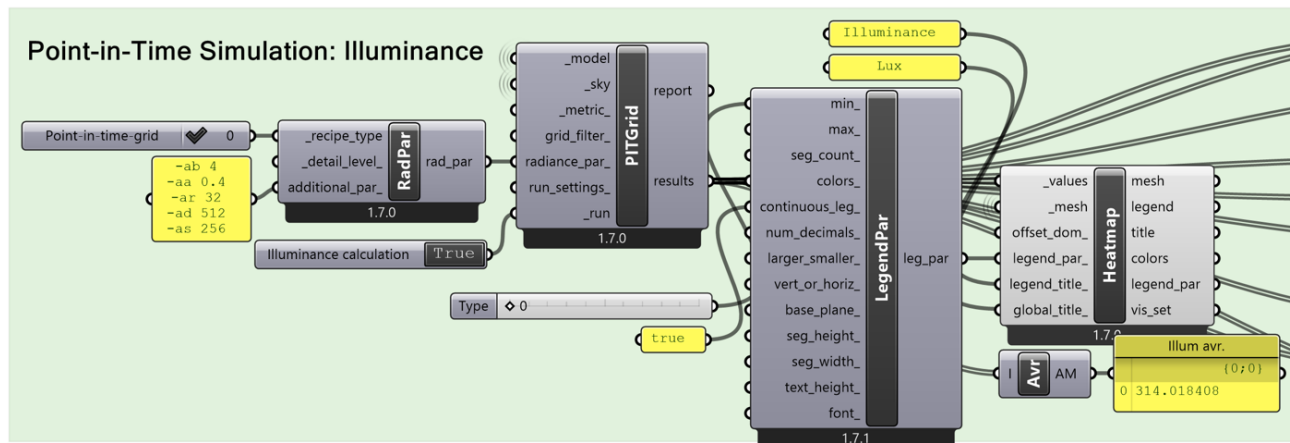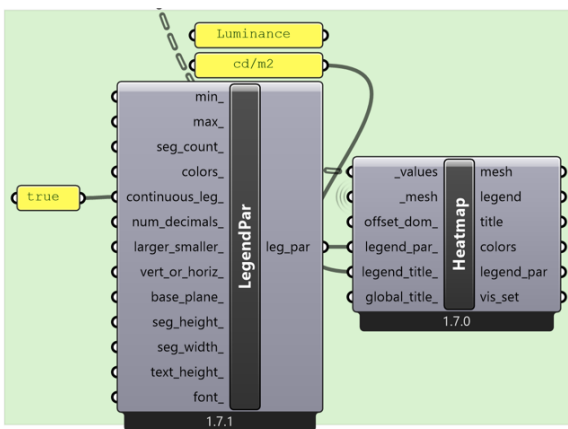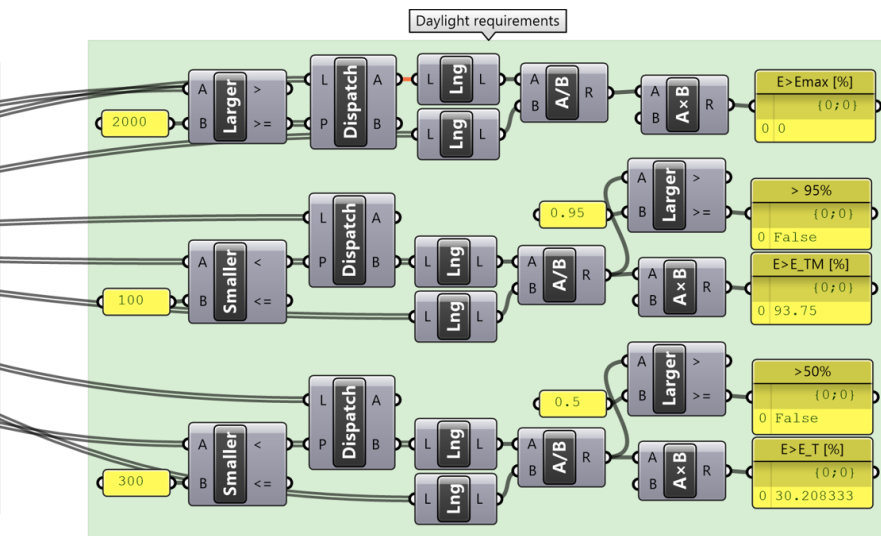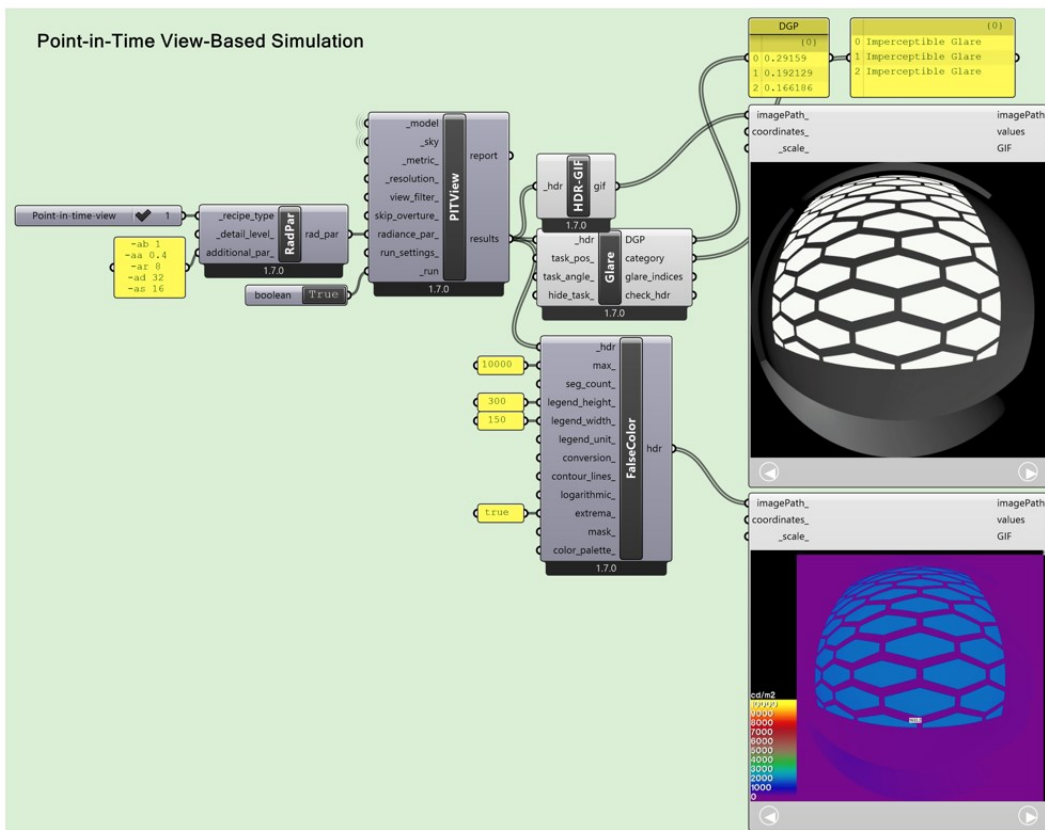

Point-in-Time Grid-Based simulation, Luminance
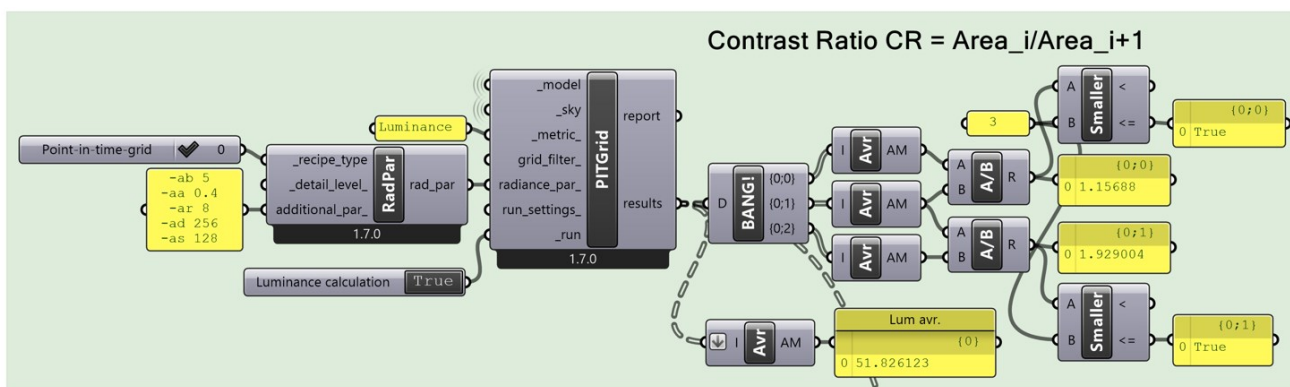
Annual daylight simulation

Point-in-Time View-Based simulation, Luminance

C.3.   Ambient parameters for Radiance

Convergence test to determine the ambient parameters for Radiance based calculations. After adjusting a parameter, the lowest value with an error less than 10 % is selected and those settings are used for selecting the following parameter.

Table C.1 Ambient parameters for point-in-time view-based: DGP calculation

-ab	-aa	-ar	-ad	-as	*DGP* [-]	Error (<10%)
Adjust -ad and -as						
1	**0.4**	**8**	**32**	**16**	0.29319	
1	0.4	8	64	32	0.2911	0.00715
1	0.4	8	128	64	0.29091	0.00066
1	0.4	8	256	128	0.28418	0.02311
Adjust -ar						
1	**0.4**	**8**	**32**	**16**	0.29319	
1	0.4	16	32	16	0.29407	-0.003
1	0.4	32	32	16	0.28924	0.01642
1	0.4	64	32	16	0.29295	-0.0128
Adjust -aa						
1	**0.4**	**8**	**32**	**16**	0.29319	
1	0.2	8	32	16	0.29169	0.00514
1	0.1	8	32	16	0.29186	-0.0006
1	0.05	8	32	16	0.29212	-0.0009
Adjust -ab						
1	**0.4**	**8**	**32**	**16**	0.29319	
2	0.4	8	32	16	0.30361	-0.0355
3	0.4	8	32	16	0.3075	-0.0128
4	0.4	8	32	16	0.29992	0.02467

Table C.2 Ambient parameters for point-in-time grid-based: illuminance calculation

-ab	-aa	-ar	-ad	-as	Average illuminance [lux]	Error (<10%)
Adjust -ad and -as						
1	0.4	8	32	16	118.477754	
1	0.4	8	64	32	171.361332	-0.4464
1	0.4	8	128	64	138.215501	0.19343
1	0.4	8	256	128	171.892352	-0.2437
1	**0.4**	**8**	**512**	**256**	169.812067	0.0121
1	0.4	8	1024	512	162.527472	0.0429
1	0.4	8	2048	1024	166.110931	-0.022
Adjust -ar						
1	0.4	8	512	256	169.812067	
1	0.4	16	512	256	135.048494	0.20472
1	**0.4**	**32**	**512**	**256**	143.995805	-0.0663
1	0.4	64	512	256	147.800254	-0.0264
1	0.4	128	512	256	149.131359	-0.009
Adjust -aa						
1	**0.4**	**32**	**512**	**256**	143.995805	
1	0.2	32	512	256	145.204485	-0.0084
1	0.1	32	512	256	143.121191	0.01435
1	0.05	32	512	256	145.337414	-0.0155

-ab	-aa	-ar	-ad	-as	Average luminance [cd/m²]	Error (<10%)
Adjust -ab						
1	0.4	32	512	256	143.995805	
2	0.4	32	512	256	243.77302	-0.6929
3	0.4	32	512	256	302.485607	-0.2408
4	**0.4**	**32**	**512**	**256**	332.358425	-0.0988
5	0.4	32	512	256	339.292102	-0.0209
6	0.4	32	512	256	333.251068	0.0178

Table C.3 Ambient parameters for point-in-time grid-based: luminance calculation

| -ab	-aa	-ar	-ad	-as	Average luminance [cd/m²]	Error (<10%)
Adjust -ad and -as						
1	0.4	8	32	16	32.714883	
1	0.4	8	64	32	20.970753	0.35898
1	0.4	8	128	64	29.327666	-0.3985
1	**0.4**	**8**	**256**	**128**	26.736123	0.08837
1	0.4	8	512	256	26.490137	0.0092
1	0.4	8	1024	512	24.634032	0.07007
Adjust -ar						
1	**0.4**	**8**	**256**	**128**	26.736123	
1	0.4	16	256	128	26.523068	0.00797
1	0.4	32	256	128	28.073289	-0.0584
1	0.4	64	256	128	26.646667	0.05082
Adjust -aa						
1	**0.4**	**8**	**256**	**128**	26.736123	
1	0.2	8	256	128	28.490886	-0.0656
1	0.1	8	256	128	28.275874	0.00755
1	0.05	8	256	128	29.816145	-0.0545
Adjust -ab						
1	0.4	8	256	128	26.736123	
2	0.4	8	256	128	39.467481	-0.4762
3	0.4	8	256	128	46.99806	-0.1908
4	**0.4**	**8**	**256**	**128**	56.503264	-0.2022
5	0.4	8	256	128	56.486705	0.00029
6	0.4	8	256	128	56.523104	-0.0006
7	0.4	8	256	128	57.560454	-0.0184

C.4. HDR images glare on 21st December (a) 10:00; (b) 12:00; (c) 16:00. Not inflated. Point in time fisheye view of view directly outside, fisheye view of view parallel to outside and the two corresponding false colour images
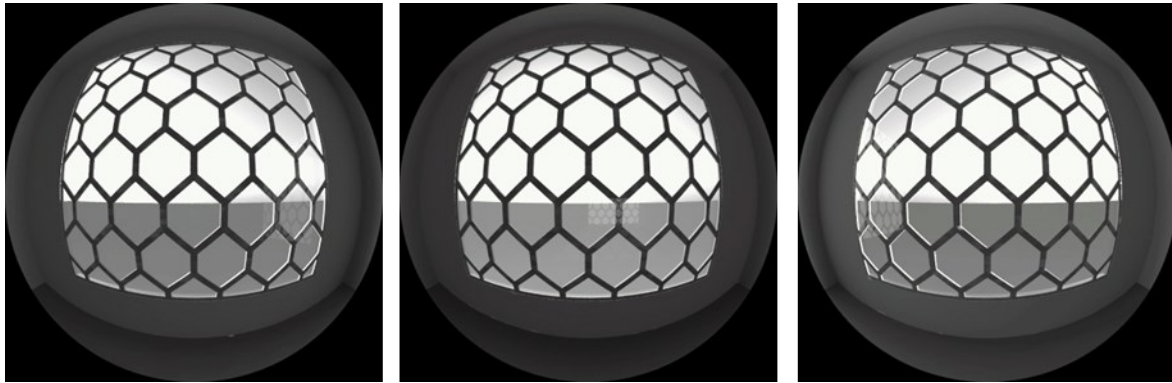
10:00 DGP=1.000 (intolerable); 12:00 DGP=1.000 (intolerable); 16:00 DGP=0.564 (intolerable)
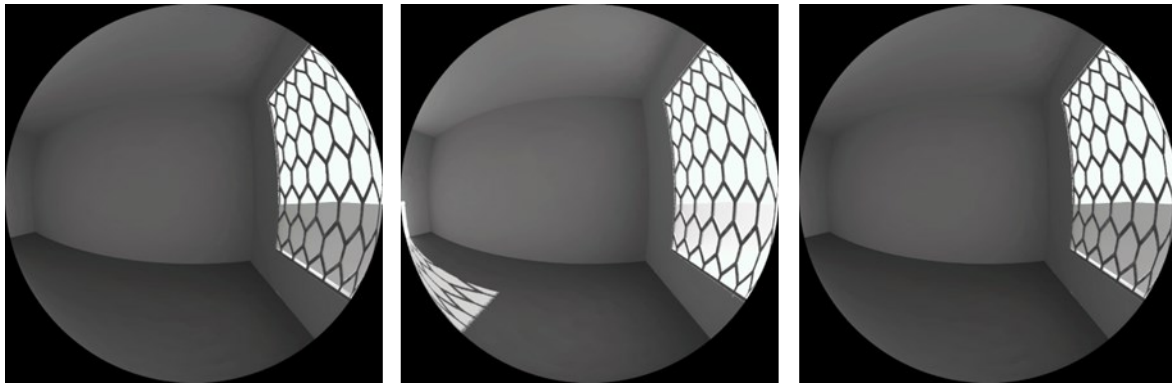
10:00 DGP=0.904 (intolerable); 12:00 DGP=0.722 (intolerable); 16:00 DGP=0.195 (imperceptible)
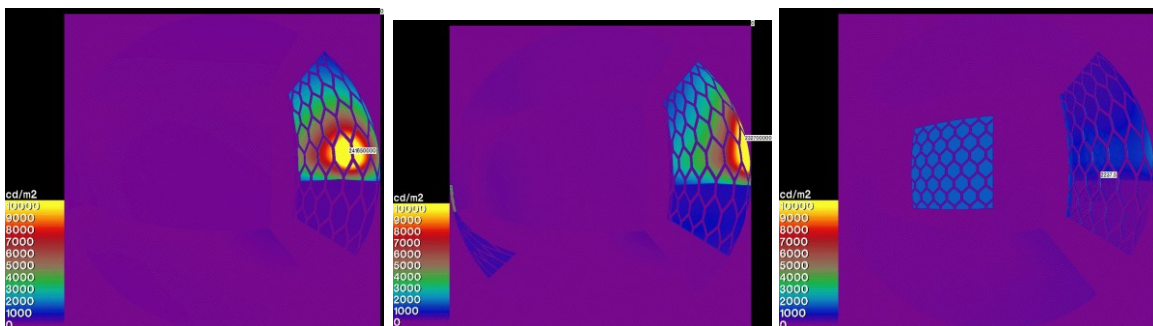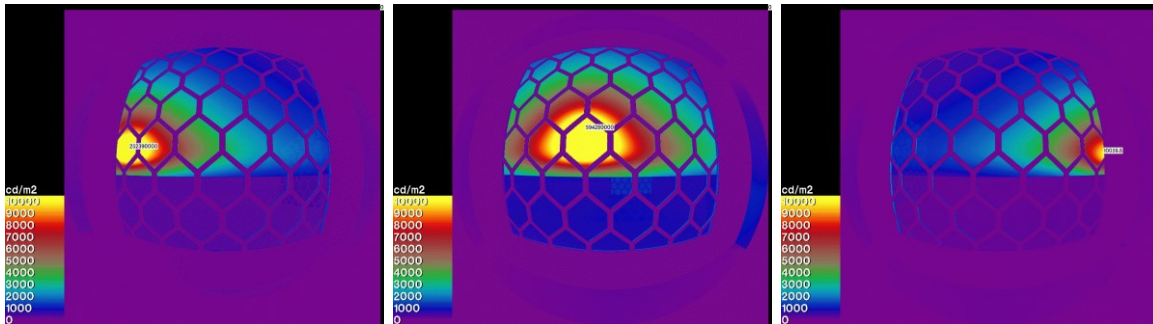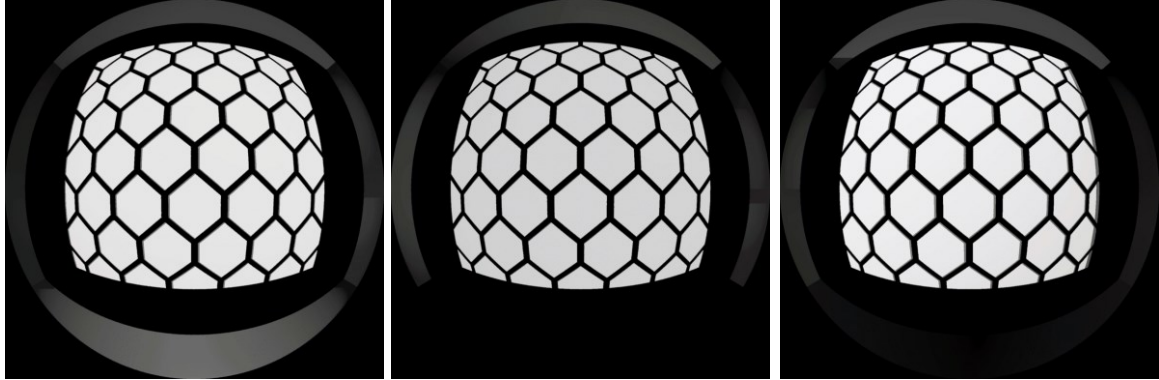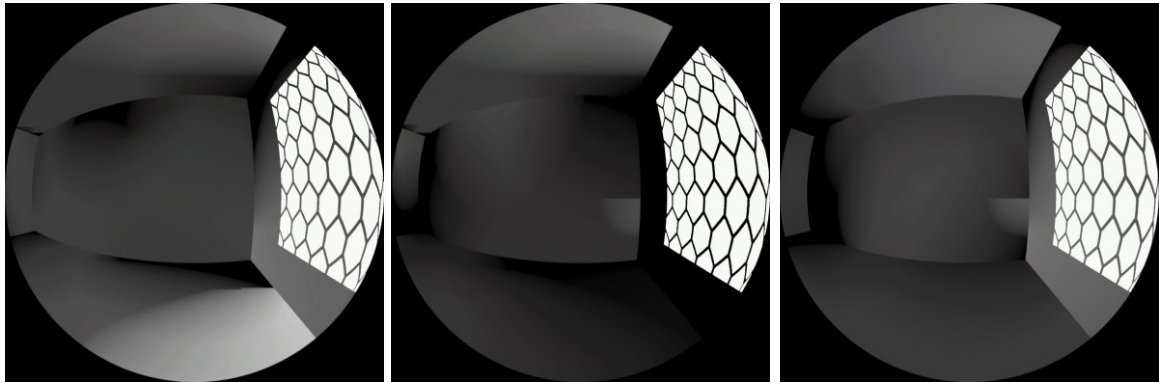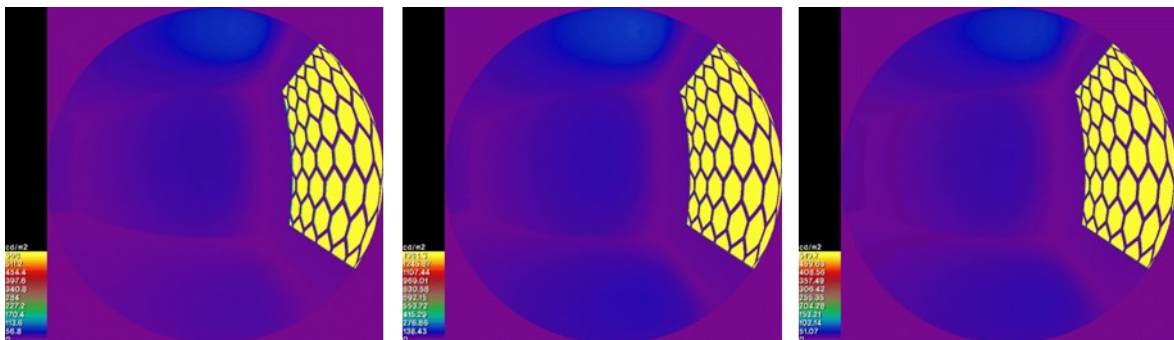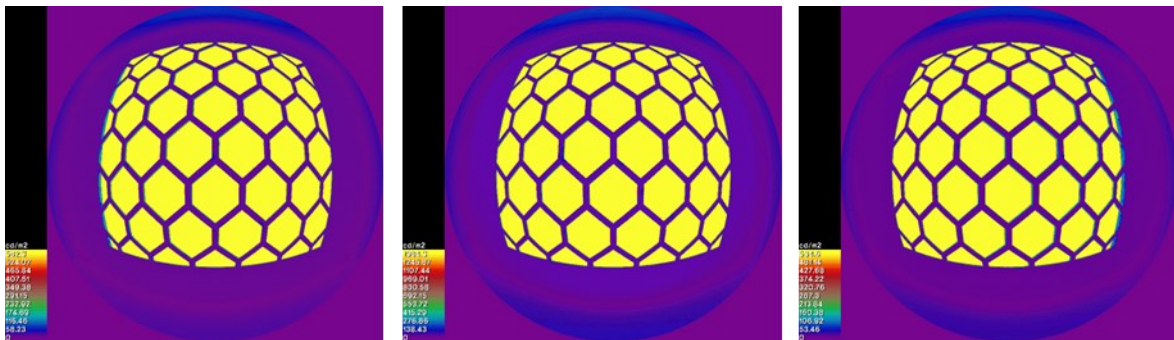
(a) *(b)* *(c)*

C.5. HDR images glare on 21st December (a) 10:00; (b) 12:00; (c) 16:00. Fully inflated, diff_ref=0.30, diff_trans=0.15, spec_trans=0. Point in time fisheye view of view directly outside, fisheye view of view parallel to outside and the two corresponding false colour images

10:00 DGP = 0.217;   12:00 DGP = 0.344;   16:00 DGP=0.207

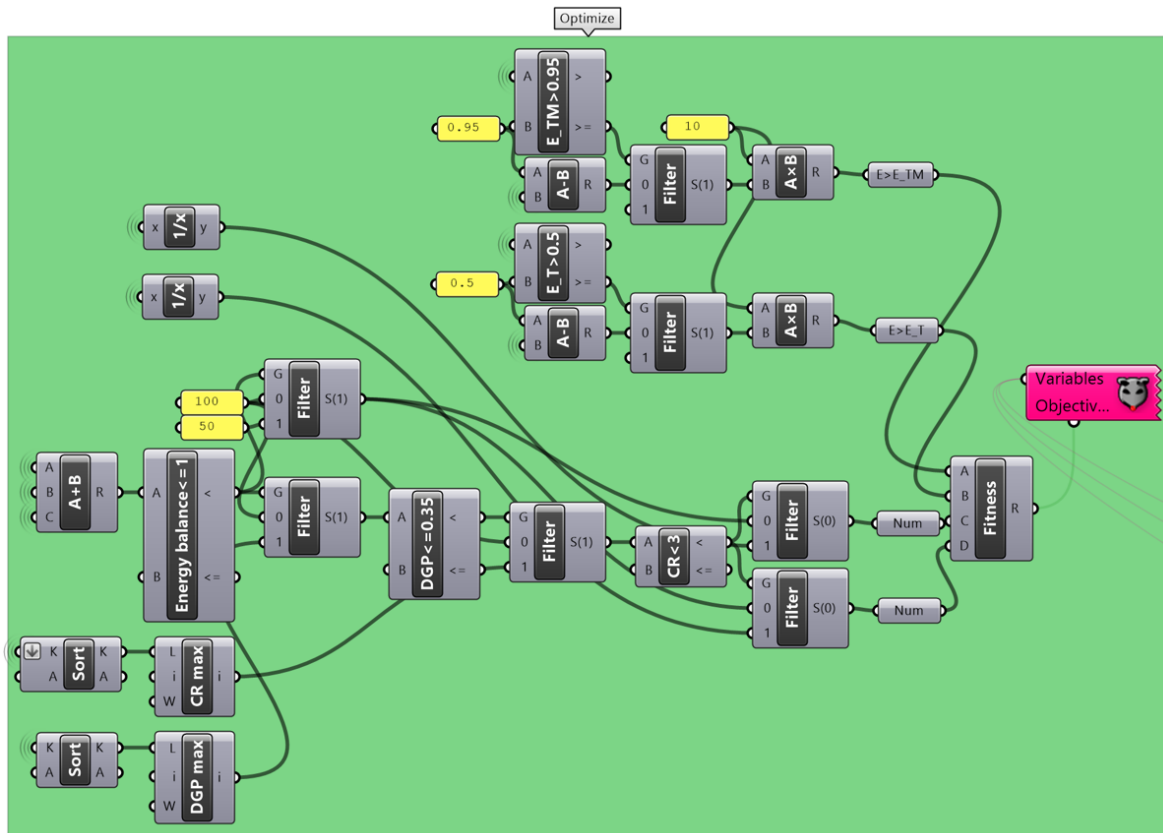10:00 DGP = 0.179;   12:00 DGP = 0.228;   16:00 DGP=0.174
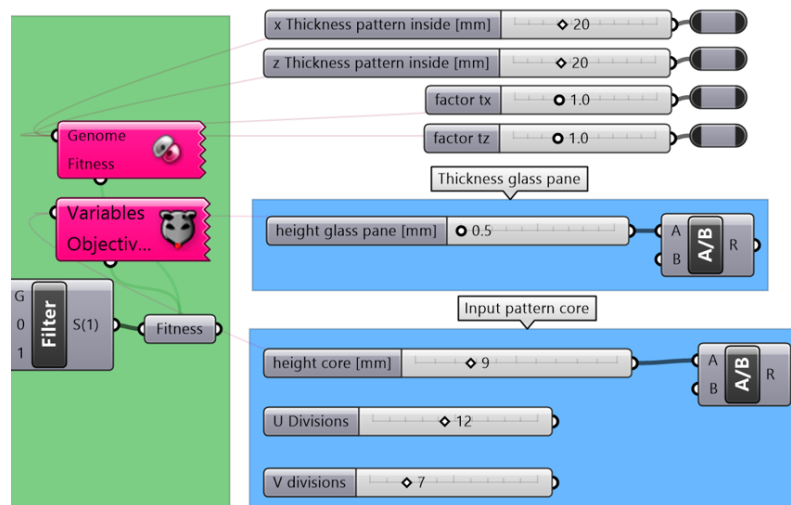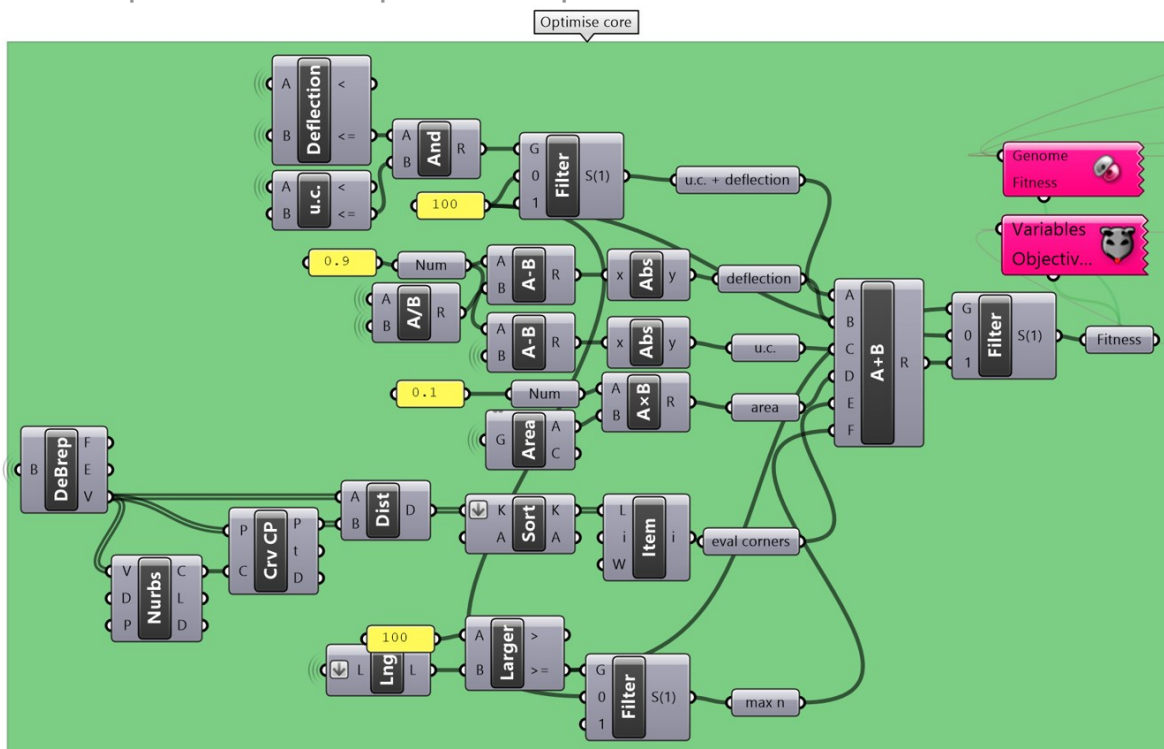
(a)   (b)   (c)

159

Appendix D. Optimisation process

D.1.   Optimisation script inflatable design
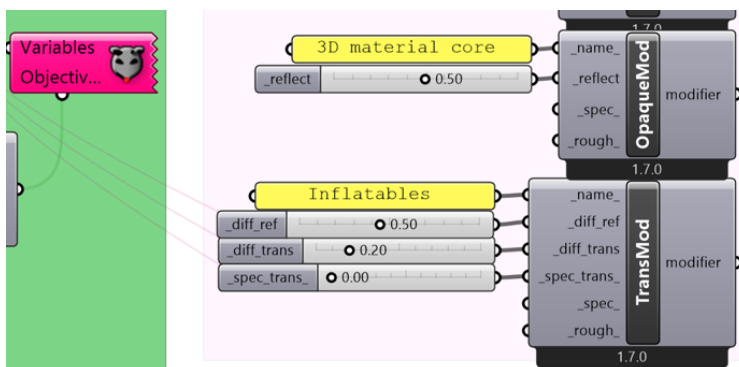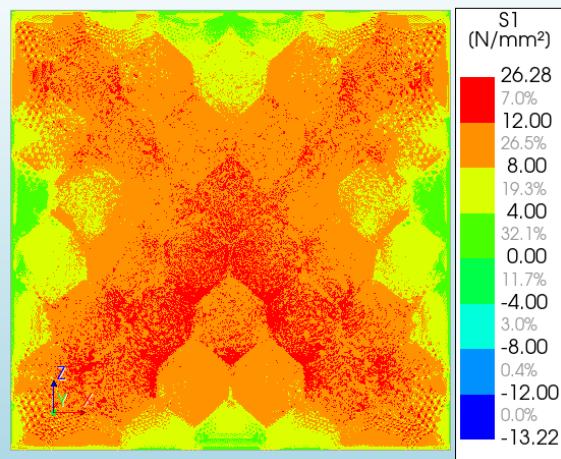
D.2.   Optimisation script for core pattern

Appendix E. Data of Diana FEA models
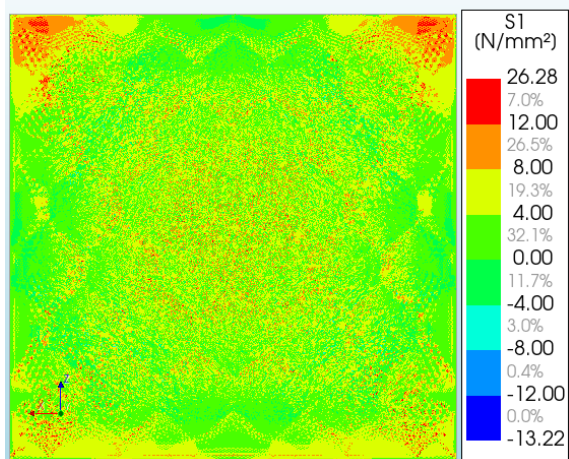
E.1.   Resulting principal stresses S1, S2 and S3

Panel used with the parameters of Table 17 and mesh element size of 6 *mm*. The results of the full panel are shown, one showing the side facing the outside and one facing inside the room.

(a) Principal stress S1 facing outside glass pane

(b) Principal stress S1 facing inside glass pane
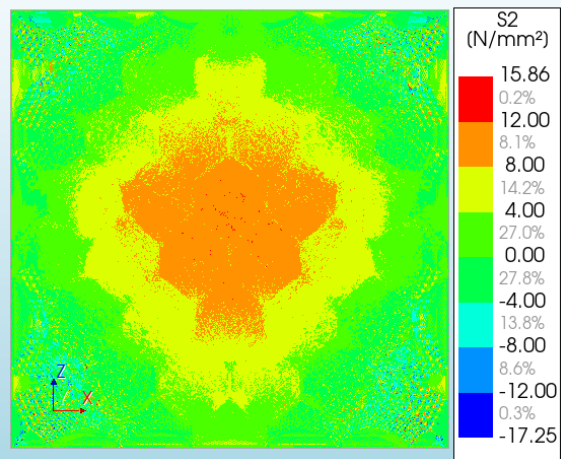
(c) Principal stress S2 facing outside glass pane
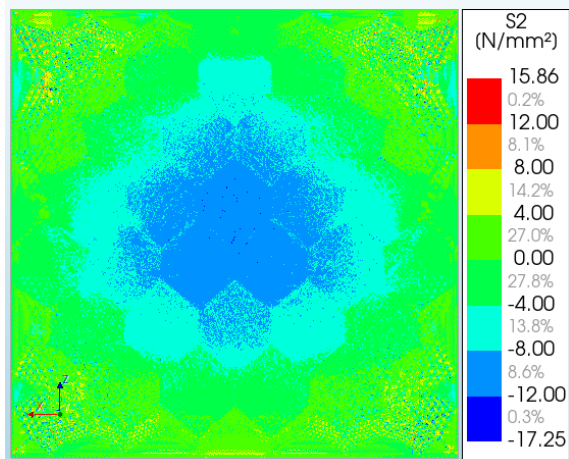
(d) Principal stress S2 facing inside glass pane
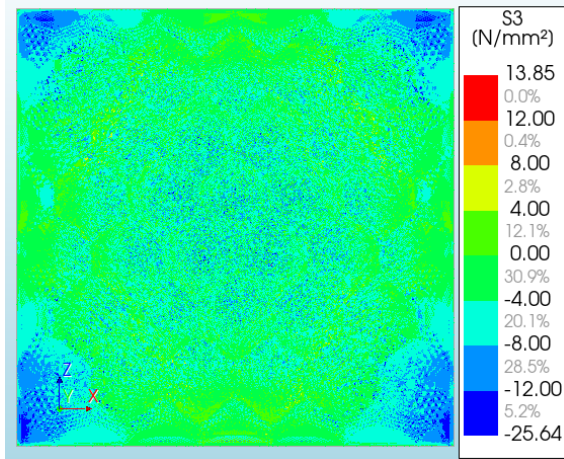
(e) Principal stress S3 facing outside glass pane *(f) Principal stress S3 facing inside glass pane*
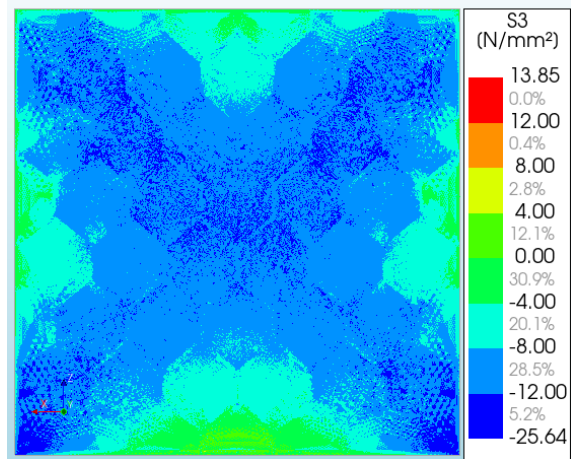
Appendix F. Wind calculation

F.1. Reference height, z_e, depending on h and b, and corresponding velocity pressure profile (NEN-EN 1991-1-4+A1+C2, 2011)
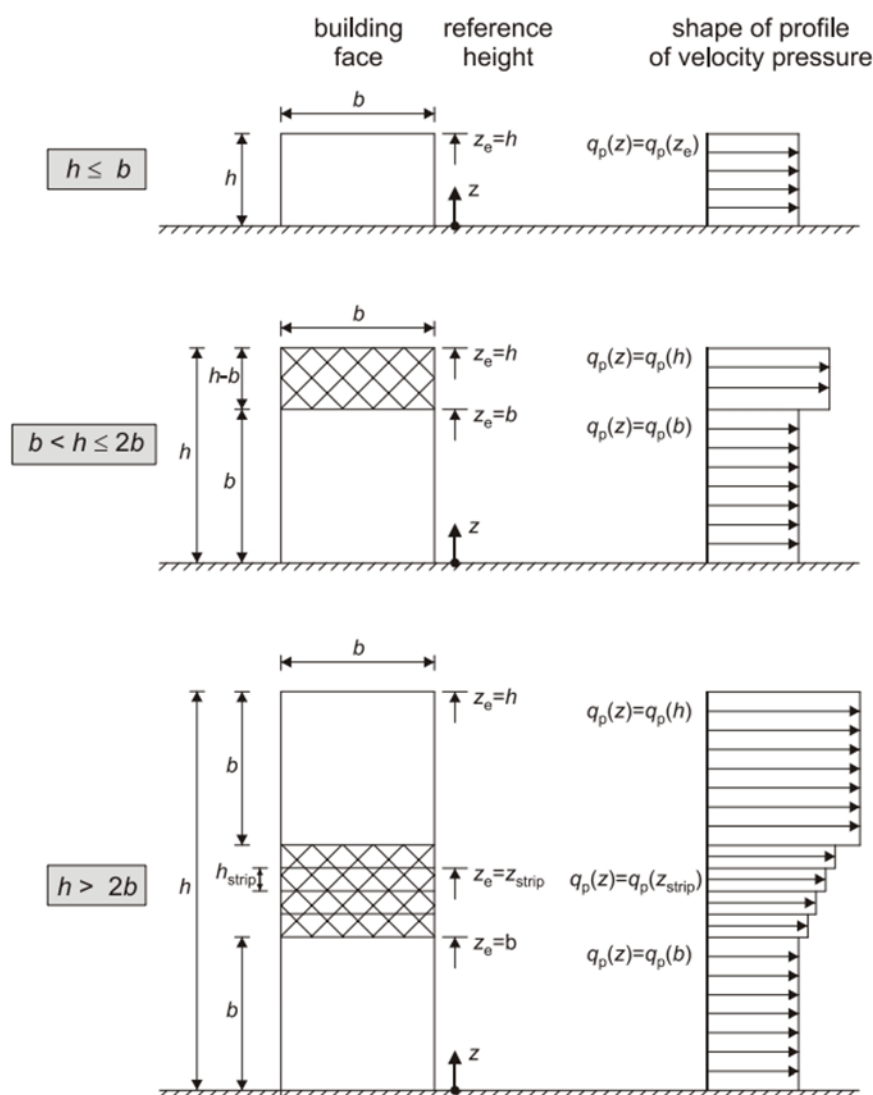
NOTE The velocity pressure should be assumed to be uniform over each horizontal strip considered.

F.2. Peak velocity pressure in kN/m^2 as function of the height (NEN-EN 1991-1-4+A1+C2/NB+C1, 2020)

| Hoogte	Gebied I			Gebied II			Gebied III	
m	Kust	Onbebouwd	Bebouwd	Kust	Onbebouwd	Bebouwd	Onbebouwd	Bebouwd
1	0,93	0,71	0,69	0,78	0,60	0,58	0,49	0,48
2	1,11	0,71	0,69	0,93	0,60	0,58	0,49	0,48
3	1,22	0,71	0,69	1,02	0,60	0,58	0,49	0,48
4	1,30	0,71	0,69	1,09	0,60	0,58	0,49	0,48
5	1,37	0,78	0,69	1,14	0,66	0,58	0,54	0,48
6	1,42	0,84	0,69	1,19	0,71	0,58	0,58	0,48
7	1,47	0,89	0,69	1,23	0,75	0,58	0,62	0,48
8	1,51	0,94	0,73	1,26	0,79	0,62	0,65	0,51
9	1,55	0,98	0,77	1,29	0,82	0,65	0,68	0,53
10	1,58	1,02	0,81	1,32	0,85	0,68	0,70	0,56
15	1,71	1,16	0,96	1,43	0,98	0,80	0,80	0,66
20	1,80	1,27	1,07	1,51	1,07	0,90	0,88	0,74

F.3. Recommended values of external pressure coefficient for vertical walls of rectangular plan buildings (NEN-EN 1991-1-4+A1+C2, 2011)
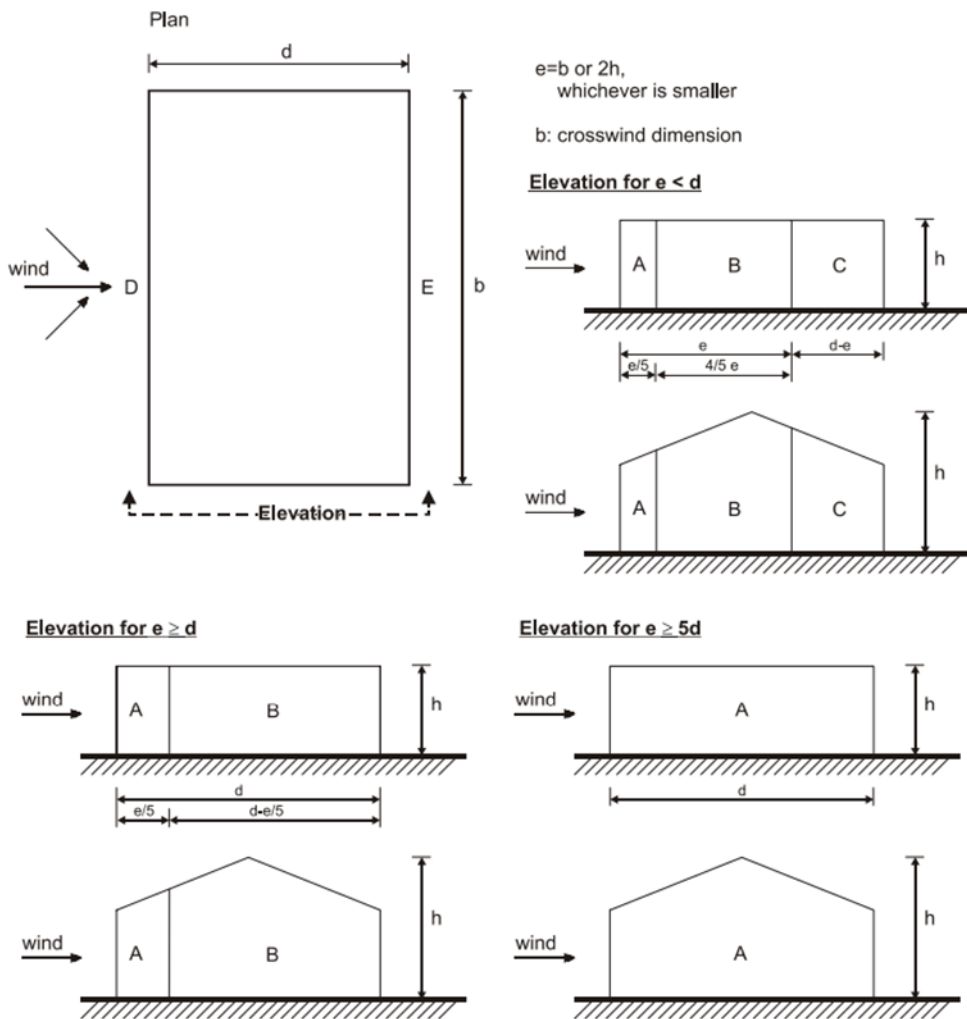
Zone	A		B		C		D		E	
h/d	$c_{pe,10}$	$c_{pe,1}$	$c_{pe,10}$	$c_{pe,1}$	$c_{pe,10}$	$c_{pe,1}$	$c_{pe,10}$	$c_{pe,1}$	$c_{pe,10}$	$c_{pe,1}$
5	-1,2	-1,4	-0,8	-1,1	-0,5		+0,8	+1,0	-0,7	
1	-1,2	-1,4	-0,8	-1,1	-0,5		+0,8	+1,0	-0,5	
≤ 0,25	-1,2	-1,4	-0,8	-1,1	-0,5		+0,7	+1,0	-0,3	

Appendix G. Determining laminated thickness panes

heq : $y = 1$

$w = 0.76$

-5   ●   5

$$hefw(x) = \left(2x^3 + 12 \cdot 0.3 \cdot 2x \left(\frac{w}{2} + \frac{x}{2}\right)^2\right)^{\frac{1}{3}}$$

$$= \left(2x^3 + 12 \cdot 0.3 \cdot 2x \left(\frac{0.76}{2} + \frac{x}{2}\right)^2\right)^{\frac{1}{3}}$$

$$hefsigmaj(x) = \left(\frac{(hefw(x))^3}{x + 2 \cdot 0.3 \left(\frac{w}{2} + \frac{x}{2}\right)}\right)^{\frac{1}{2}}$$

$$= \left(\frac{\left(\left(2x^3 + 12 \cdot 0.3 \cdot 2x \left(\frac{0.76}{2} + \frac{x}{2}\right)^2\right)^{\frac{1}{3}}\right)^3}{x + 2 \cdot 0.3 \left(\frac{0.76}{2} + \frac{x}{2}\right)}\right)^{\frac{1}{2}}$$

$A = $ Snijpunten(hefw, heq, (0.380278906645, 1))

$= (0.380278906645, 1)$

$B = $ Snijpunten(hefsigmaj, heq, (0.2813661463583, 1))

$= (0.2813661463583, 1)$

9 REFERENCES

Al-Yasiri, Q., & Szabo, M. (2021). A short review on passive strategies applied to minimise the building cooling loads in hot locations. *Analecta Technica Szegedinensia*, *15*, 20-30. https://doi.org/10.14232/analecta.2021.2.20-30

Albaugh, L., Hudson, S., & Yao, L. (2019). Digital Fabrication of Soft Actuated Objects by Machine Knitting. CHI Conference on Human Factors in Computing Systems Proceedings, Glasgow, Scotland UK.

ArchDaily. (2013). *Q1, ThyssenKrupp Quarter Essen / JSWD Architekten + Chaix & Morel et Associés*. Retrieved 8 October from https://www.archdaily.com/326747/q1-thyssenkrupp-quarter-essen-jswd-architekten-chaix-morel-et-associes

Ashby, M. F. (2013). Chapter 15 - Material profiles. In M. F. Ashby (Ed.), *Materials and the Environment (Second Edition)* (pp. 459-595). Butterworth-Heinemann. https://doi.org/https://doi.org/10.1016/B978-0-12-385971-6.00015-4

Auer, T., Knaack, U., & Schneider, J. (2019). Proceedings PowerSkin Conference 2019. Munich, Germany.

BASF 3D Printing Solutions GmbH. (2021). *Insert for Insulating Glass Units*. Retrieved 13 September from https://forward-am.com/use-cases-and-whitepapers/insert-for-insulating-glass-units/

Behl, M., & Lendlein, A. (2007). Shape-memory polymers. *Materials Today*, *10*(4), 20-28. https://doi.org/https://doi.org/10.1016/S1369-7021(07)70047-0

Belis, J., Louter, C., Nielsen, J. H., & Schneider, J. (2019). Architectural Glass. In (pp. 1781-1819). Springer International Publishing. https://doi.org/10.1007/978-3-319-93728-1_52

Cai, G., Ciou, J. H., Liu, Y., Jiang, Y., & Lee, P. S. (2019). Leaf-inspired multiresponsive MXene-based actuator for programmable smart devices [Article]. *Science Advances*, *5*(7), Article eaaw7956. https://doi.org/10.1126/sciadv.aaw7956

Coyle, S., Majidi, C., LeDuc, P., & Hsia, K. J. (2018). Bio-inspired soft robotics: Material selection, actuation, and design. *Extreme Mechanics Letters*, *22*, 51-59. https://doi.org/https://doi.org/10.1016/j.eml.2018.05.003

Cunico, M. W. M. (2019). *3D printers and additive manufacturing: the rise of the industry 4.0*. Concep3d.

CustomPartNet. (2008). *Addative Fabrication*. Retrieved 13 September from https://www.custompartnet.com/wu/additive-fabrication

Digumarti, K., Conn, A., & Rossiter, J. (2017). Euglenoid-Inspired Giant Shape Change for Highly Deformable Soft Robots. *IEEE Robotics and Automation Letters*, *PP*, 1-1. https://doi.org/10.1109/LRA.2017.2726113

Doroteo, J. (2016). *Let Your Building "Breathe" With This Pneumatic Facade Technology*. ArchDaily. Retrieved 10 October from https://www.archdaily.com/789230/let-your-building-to-breathe-with-this-pneumatic-facade-technology

Eisenbarth, C., Haase, W., Klett, Y., Blandini, L., & Sobek, W. (2021). PAOSS : Pneumatically Actuated Origami Sun Shading. *Journal of Facade Design and Engineering*, *9*(1), 147-162. https://doi.org/10.7480/jfde.2021.1.5535

FESTO. *Pneumatic connection technology*. Retrieved 19 February from https://www.festo.com/gb/en/c/products/industrial-automation/tubes-fittings-plugs-and-cables/pneumatic-connection-technology-id_pim209/

Flor, J.-F., Liu, X., Sun, Y., Beccarelli, P., Chilton, J., & Wu, Y. (2022). Switching daylight: Performance prediction of climate adaptive ETFE foil façades. *Building and Environment*, *209*, 108650. https://doi.org/https://doi.org/10.1016/j.buildenv.2021.108650

Fu, C., Xia, Z., Hurren, C., Nilghaz, A., & Wang, X. (2022). Textiles in soft robots: Current progress and future trends. *Biosensors and Bioelectronics*, *196*, 113690. https://doi.org/https://doi.org/10.1016/j.bios.2021.113690

Guidi, M. (2019). *Thin glass cold bent sandwich panel* Master thesis, TU Delft].

Hexcel Composites. (2000). *HexWebTM Honeycomb sandwich design technology*

Institut du Monde Arabe. (2016). *Architecture*. Retrieved 8 October from https://www.imarabe.org/en/architecture

JALOXA. (2021). *Radiance Colour Picker*. Retrieved 19 February from http://www.jaloxa.eu/resources/radiance/colour_picker/index.shtml

Kim, H., Ahn, S.-k., Mackie, D. M., Kwon, J., Kim, S. H., Choi, C., Moon, Y. H., Lee, H. B., & Ko, S. H. (2020). Shape morphing smart 3D actuator materials for micro soft robot. *Materials Today*, *41*, 243-269. https://doi.org/https://doi.org/10.1016/j.mattod.2020.06.005

Kim, M.-j., Kim, B.-g., Koh, J.-s., & Yi, H. (2023). Flexural biomimetic responsive building façade using a hybrid soft robot actuator and fabric membrane. *Automation in Construction*, *145*, 104660. https://doi.org/https://doi.org/10.1016/j.autcon.2022.104660

Kothe, C., Bodenko, A., Nicklisch, F., & Louter, C. (2021). Thin glass in façades: Adhesive joints for thin glass composite panels with 3D printed polymer cores. *Civil Engineering Design*, *3*(1-2), 35-42. https://doi.org/10.1002/cend.202100010

Kruisselbrink, T., Dangol, R., & Rosemann, A. (2018). Photometric measurements of lighting quality: An overview. *Building and Environment*, *138*, 42-52. https://doi.org/https://doi.org/10.1016/j.buildenv.2018.04.028

Laurent, O., Mantisi, B., & Micoulaut, M. (2014). Structure and Topology of Soda-Lime Silicate Glasses: Implications for Window Glass. *The Journal of Physical Chemistry B*, *118*(44), 12750-12762. https://doi.org/10.1021/jp506155p

Li, Q., Liu, C., Lin, Y.-H., Liu, L., Jiang, K., & Fan, S. (2015). Large-Strain, Multiform Movements from Designable Electrothermal Actuators Based on Large Highly Anisotropic Carbon Nanotube Sheets. *ACS Nano*, *9*(1), 409-418. https://doi.org/10.1021/nn505535k

Lin, H.-J., & Chang, W.-K. (2007). Influence of Isopipe Temperature on Glass Fusion for the Overflow Fusion Process. *Energy*, 159-163.

Livin Spaces. (2017). *Discussing the Design: An Indepth Look at the Design of the Al Bahar Towers in Abu Dhabi by Aedas*. Retrieved 8 October from https://livinspaces.net/ls-tv/discussing-the-design-an-indepth-look-at-the-design-of-the-al-bahar-towers-in-abu-dhabi-by-aedas-architects/

Louter, C. (2022). *Glass Properties [PowerPoint slides]*.

Ma, Q., Rejab, R., Siregar, J., & Guan, Z. (2021). A review of the recent trends on core structures and impact response of sandwich panels. *Journal of Composite Materials*, *55*. https://doi.org/10.1177/0021998321990734

Minner, K. (2011). *Moving Homeostatic Facade Preventing Solar Heat Gain*. ArchDaily. Retrieved 10 October from https://www.archdaily.com/101578/moving-homeostatic-facade-preventing-solar-heat-gain

Müeller, H. F. O. (2013). Chapter 9 - Daylighting. In A. Sayigh (Ed.), *Sustainability, Energy and Architecture* (pp. 227-255). Academic Press. https://doi.org/https://doi.org/10.1016/B978-0-12-397269-9.00009-8

Nabil, A., & Mardaljevic, J. (2006). Useful daylight illuminances: A replacement for daylight factors. *Energy and Buildings*, *38*(7), 905-913. https://doi.org/https://doi.org/10.1016/j.enbuild.2006.03.013

Neeskens, T. (2018). *Thin glass composites: based on a structural efficiency increasing design strategy* Master thesis, TU Delft].

NEN-EN 1990+A1+A1/C2. (2019). Basis of structural design. In: connect.nen.nl.

NEN-EN 1991-1-4+A1+C2. (2011). Actions on structures - Part 1-4: General actions - Wind actions. In.

NEN-EN 1991-1-4+A1+C2/NB+C1. (2020). National Annex to NEN-EN 1991-1-4+A1+C2: Eurocode 1: Actions on structures - Part 1-4: General actions - Wind actions. In.

NEN-EN 12464-1. (2021). Light and lighting - Lighting of work places - Part 1: Indoor work places. In: connect.nen.nl.

NEN-EN 16612. (2019). Glass in building - Determination of the lateral load resistance of glass panes by calculation. In: connect.nen.nl.

NEN-EN 17037+A1. (2022). Daylight in buildings. In: connect.nen.nl.

NEN 2608. (2014). Glass in building - Requirements and determination method. In: connect.nen.nl.

NVN-CEN/TS 19100-1. (2021). Design of glass structures - Part 1: Basis of design and materials. In.

Octotube. (2023). *Echo TU Delft*. Retrieved 26 February from https://www.octatube.nl/en_GB/project-item.html/projectitem/221-echo-tu-delft

Pfarr, D., & Louter, C. (2023). Prototyping of digitally manufactured thin glass composite façade panels. *Architecture, Structures and Construction*, *3*, 1-11. https://doi.org/10.1007/s44150-022-00080-7

Rus, D., & Tolley, M. T. (2015). Design, fabrication and control of soft robots. *Nature*, *521*(7553), 467-475. https://doi.org/10.1038/nature14543

Saleh, C. (2019). *Ultra thin composite panel: A research on the durability and stiffness of a composite panel of (thin) glass and recycled PET* Master thesis, TU Delft].

Sawyer, A., Navvab, M., Weissman, D., & Ji, G. (2022). Facade Photometry: Linking Annual Daylight Performance to Facade Design. *Buildings*, *12*, 1556. https://doi.org/10.3390/buildings12101556

Schaedler, T. A., & Carter, W. B. (2016). Architected cellular materials. *Annual Review of Materials Research*, *46*, 187-210.

Schittich, C., Staib, G., Balkow, D., Schuler, M., & Sobek, W. (2007). *Glass Construction Manual*. Birkhäuser. https://doi.org/doi:10.11129/detail.9783034615549

SCHOTT. (2020). *Technical Glasses: Physical and Technical Properties*.

Suk, J. Y. (2019). Luminance and vertical eye illuminance thresholds for occupants' visual comfort in daylit office environments. *Building and Environment*, *148*, 107-115. https://doi.org/https://doi.org/10.1016/j.buildenv.2018.10.058

Tabadkani, A., Roetzel, A., Li, H. X., & Tsangrassoulis, A. (2021). Design approaches and typologies of adaptive facades: A review. *Automation in Construction*, *121*, 103450. https://doi.org/https://doi.org/10.1016/j.autcon.2020.103450

Tahouni, Y., Krüger, F., Poppinga, S., Wood, D., Pfaff, M., Rühe, J., Speck, T., & Menges, A. (2021). Programming sequential motion steps in 4D-printed hygromorphs by architected mesostructure and differential hygro-responsiveness. *Bioinspiration & Biomimetics*, *16*(055002). https://doi.org/10.1088/1748-3190/ac0c8e

TNO. (2022). *Smart window with large energy savings potential shows promising results during first pilot field test*. Retrieved 10 October from https://www.tno.nl/en/newsroom/2022/06/smart-window-promising-results-in-pilot/

UNStudio. (2022). *Echo, TU Delft*. Retrieved 25 February from https://www.unstudio.com/en/page/13592/echo-tu-delft

van der Linden, A. C. E., P.; Kuijpers-van Gaalen; I.M., Zeegers, A. (2015). *Bouwfysica* (7 ed.). ThiemeMeulenhoff.

van der Weijde, I. (2017). *Ultra lightweight, insulating thin glass façade panel* Master thesis, TU Delft].

Vergauwen, A., De Temmerman, N., & Brancart, S. (2014). The design and physical modelling of deployable structures based on curved-line folding.

Wang, S.-Y. R. (2023). Framing responsive architecture with soft robots—the exploratory practice of soft pneumatic robotic architectural system. *Architectural Intelligence*, *2*(1), 17. https://doi.org/10.1007/s44223-023-00036-x

Zahner. (2016). *Simons Center*. Retrieved 10 October from https://www.azahner.com/works/stony-brook

Zarzycki, A. (2018). *Pneumatic Facade*. Retrieved 18 October from http://andrzejzarzycki.com/pneumatic-facade/

Zenkert, D. (1997). *The handbook of sandwich construction*. Engineering Materials Advisory Services.

Zhang, X., Yu, Z., Wang, C., Zarrouk, D., Seo, J.-W. T., Cheng, J. C., Buchan, A. D., Takei, K., Zhao, Y., Ager, J. W., Zhang, J., Hettick, M., Hersam, M. C., Pisano, A. P., Fearing, R. S., & Javey, A. (2014). Photoactuators and motors based on carbon nanotubes with selective chirality distributions. *Nature Communications*, *5*(1), 2983. https://doi.org/10.1038/ncomms3983